PHD

Functional Kinematic Study of Knee Replacement
The Effect of Implant Design and Alignment on the Patellofemoral Joint

Coles, Lisa

Award date:
2015

Awarding institution:
University of Bath

Functional Kinematic Study of Knee Replacement

The Effect of Implant Design and Alignment on the Patellofemoral Joint

Lisa Georgina Coles

A thesis submitted for the degree of Doctor of Philosophy

University of Bath

Department of Mechanical Engineering

Abstract

Total knee arthroplasty is a widely used and relatively successful procedure, designed to relieve pain and restore function to patients suffering from osteoarthritis. However, satisfaction following the procedure is low. One of the primary sources of pain and a cause of functional limitations following knee arthroplasty is the patellofemoral joint. Reasons for pain in the patellofemoral joint are not well understood but adverse patellofemoral biomechanics are thought to contribute.

Many *in vitro* methods exist for the investigation of patellofemoral joint biomechanics but there is no consistent standard protocol. It is therefore difficult to draw any general conclusions regarding the effect of specific design or alignment factors on the biomechanics of the patellofemoral joint. The present study aimed to improve current understanding of factors contributing to patellofemoral complications.

A knee simulator, which was based on the Oxford Knee Rig and included synthetic models for a number of soft tissue and bony structures, was developed. The simulator was demonstrated to provide a simplified but physiologically relevant model of the human knee, which allowed effective assessment of patellofemoral joint biomechanics under physiological loads. The system eliminated the need for cadaveric tissue and therefore demonstrated reduced variability, enabling the efficient assessment of a number of potentially influencing factors.

A number of investigations were carried out using the simulator to assess the effect of patella component design and position, and femoral component alignment on patellofemoral biomechanics using the Scorpio NRG system. The results of these studies indicate the benefit of medialisation of the apex of the patella component and warn against excessive femoral component sagittal plane malalignment. However, in general they indicated the relatively forgiving nature of the Scorpio system to malalignment and highlighted that irrespective of alignment and patella component design, pressures in excess of material limits are frequently achieved in deep flexion.

Acknowledgements

I would like to thank my supervisors, Tony Miles and Sabina Gheduzzi, whose advice, support and encouragement has been invaluable, and Tim Holsgrove for the photographs he took of the completed simulator. I would also like to acknowledge the support of Nick Waywell, who worked tirelessly in the lab to make the simulator, and the instrumentation department for helping with the electrical side of things. Finally, I would like to thank my family and friends, in particular my husband Jon, for all the support they have given me, in many different ways, while I have carried out this work.

Contents

Table of Figures

Table of Tables

List of Abbreviations

ACL	Anterior Cruciate Ligament
AHF	Anterior Horn Facet
AKP	Anterior Knee Pain
CAD	Computer Aided Design
COP	Centre of Pressure
CR	Cruciate Retaining
CS	Cruciate Sacrificing
CT	Computer Tomography
EF	Extension Facet
ER	External Rotation
IR	Internal Rotation
ITB	Iliotibial band
FF	Flexion Facet
LCL	Lateral Collateral Ligament
MCL	Medial Collateral Ligament
MPFL	Medial Patellofemoral Ligament
MRI	Magnetic Resonance Imaging
N	Sample Number
OA	Osteoarthritis
OKR	Oxford Knee Rig
PCL	Posterior Cruciate Ligament

PD	Proximodistal
PFJ	Patellofemoral Joint
PFL	Popliteofibular Ligament
PG	Patella Posterior Proximodistal Length
PHF	Posterior Horn Facet
PL	Physiological Loading
PS	Posterior Stabilised
PT	Patella Tendon Length
PTMA	Patella Tendon Moment Arm
QF	Quadriceps Force
RL	Reduced Loading
sMCL	Superficial Medial Collateral Ligament
SD	Standard Deviation
TAF	Tibial Articular Facet
TEA	Transepicondylar Axis
TFJ	Tibiofemoral Joint
TKA	Total Knee Arthroplasty
UHMWPE	Ultra High Molecular Weight Polyethylene

Chapter 1

Introduction

The human knee is a complex structure comprising multiple bones and soft tissue structures. It forms two articulations; the tibiofemoral joint (TFJ) and the patellofemoral joint (PFJ). Both articulations are subjected to significant forces during activities of daily living, but it is within the PFJ that joint reaction forces are highest, often exceeding seven times body weight [1]. The considerable demand placed on the human knee puts it at high risk of disabling osteoarthritis (OA) [2].

Total knee arthroplasty (TKA) is a surgical procedure which involves replacing the articulating surfaces of the knee, with the aim of relieving pain and restoring function to patients with OA [3,4]. Increases in life expectancy, patient expectations and rates of obesity are fuelling an unparalleled demand for TKA procedures [2]. Procedures in the USA alone are predicted to increase sevenfold from 400,000 in 2003 to 3.48 million in 2030 [5]. TKA is associated with good survival rates, but patient satisfaction is low [6]. Hip replacement patients are often said to forget they have had their hip replaced, but this is rarely the case for TKA patients [7].

There is no consensus regarding whether or not to resurface the patella during TKA [8-12]. However, in either case, the PFJ is a common source of pain and complications following TKA, which can contribute to substantial functional limitations [13-17]. In England and Wales in 2011, 27% of OA case revisions were carried out purely on the PFJ [18]. The PFJ is the most common, non-infectious, reason for pain after TKA [16] and up to 25% of patients report difficulties when carrying out everyday extension activities, which can imply a PFJ complication [15,17].

The reasons for pain in the PFJ are not fully understood [19]. The cartilage of the patella does not contain any nerve endings, but the synovium, the retinaculum, and the subchondral bone are highly innervated [20-22]. Changes in PFJ loading magnitudes and patterns may induce pain within these structures by causing inflammation and pain in the retinaculum, irritation in the synovium, and by stimulating intraosseous nerve cells [20-22].

The loading and contact situation within the PFJ may be influenced by a multitude of factors relating to the patient, component design, and alignment during surgery. The effect of these factors on the PFJ can probably be most accurately assessed using systematic *in vitro* methods. Multiple *in vitro* studies of the PFJ have been reported in the literature, but no consistent protocol has been used. Previous investigations have suggested that using a single femoral condylar radius and/or a posterior stabilised bearing may reduce pressures within the PFJ [23-27]; mal-rotation in the transverse plane or excessive flexion of the femoral component may increase joint pressures [28-30]; and lateralisation of the patella

component, patella alta or increased patella component thickness may contribute to increased PFJ forces [30-41]. However, the weight of evidence supporting any one of these trends is far from convincing, and there are many other factors which may contribute to PFJ complications that have never been studied.

The research presented in this thesis therefore aimed to improve understanding of the multitude of factors which influence changes in PFJ loading, and ultimately may contribute to the relatively high rate of PFJ pain, complications, and associated functional limitations following TKA. The research was structured around three investigations:

The first concerned the specification of the parameters and approaches most appropriate for the systematic assessment of PFJ biomechanics following TKA.

The second investigation involved the development of a robust, consistent and efficient protocol for the *in vitro* experimental assessment of the PFJ after TKA. This included the development of a reliable simulator and repeatable methods for assessing the specified parameters.

The third, and final, investigation involved the experimental assessment of the effect of a number of component design and alignment factors on the loading and contact situation within the PFJ. The scope of this experimental work was limited to the assessment of the PFJ following primary TKA with a single, posterior stabilised fixed bearing, implant system.

Many recent studies have focussed on improving the accuracy of the placement of the tibial and femoral TKA components during surgery [42]. Significant emphasis has also been placed on developing new tibial and femoral component designs [43]. Considerably less time and effort has been focussed on the design and alignment of patella resurfacing components [44,45]. This study therefore intended to inform how research could be better targeted, with regards to improving PFJ outcomes, by identifying design factors and alignment errors, which have a significant and detrimental effect on the PFJ. The research also aimed to highlight the importance of the design and placement of the patella component and produce an efficient *in vitro* simulator and protocol that could be used for future investigations into the multitude of factors which may influence PFJ biomechanics following TKA.

Chapter 2

Background, Literature Review & Project Aim

2.1. Introduction

The human knee is a complex structure which comprises multiple bone and soft tissue structures, and two complimentary articulations. Replacement of the joint surfaces to provide relief to arthritis sufferers is a very common, but not wholly successful procedure [5,46]. This chapter focuses on pertinent details relating to the anatomy and kinematics of the natural knee, and to the components and philosophies employed during total knee arthroplasty. The *in vitro* methods commonly used to assess the knee and specific details of the current understanding of the impact of total knee arthroplasty on the patellofemoral joint are also examined.

2.2. Anatomy of the Knee

The knee is an inherently unstable joint, comprising four bone structures, the femur, tibia, fibular and patella, which form two separate, but intrinsically linked, articulations: the tibiofemoral (TFJ) and patellofemoral joints (PFJ) (Figure 2-1). The knee is stabilised by a number of intrinsic and extrinsic muscles, and various soft tissue structures. This sub-section provides a brief introduction to the anatomy of the bone and soft tissue structures present in the human knee, which are relevant to this study.

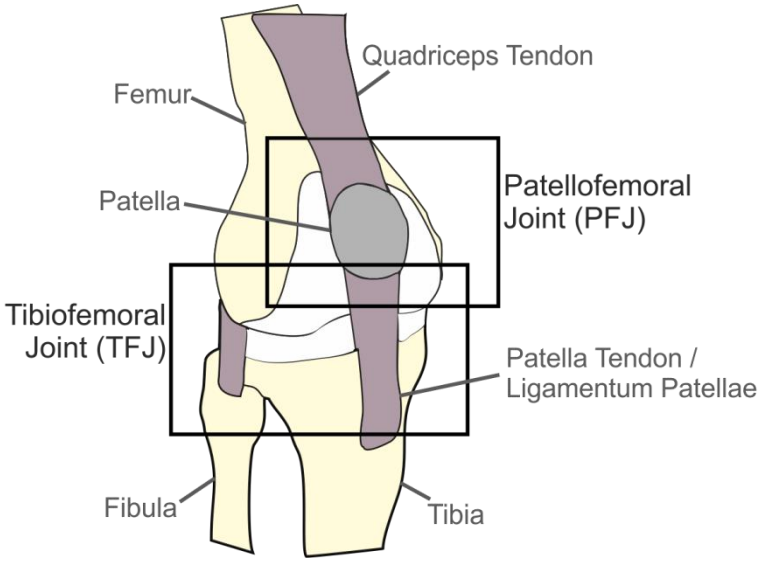

Figure 2-1: The two articulating joints of the knee

2.2.1. The Femur

The femur is the longest bone in the human body and connects the hip and knee providing insertion points for a number of muscles. The bone is often described as having two axes; a mechanical axis and an anatomical axis. The anatomical axis is defined as passing through the centre of the femoral shaft (Figure 2-2) [47]. The mechanical axis is defined as the line between the centre of the femoral head and the centre of the knee joint (Figure 2-2) [47].

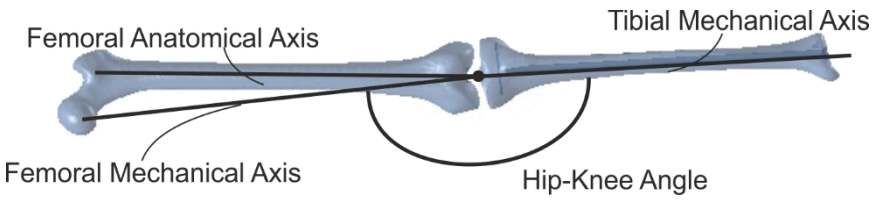

Figure 2-2: Tibial and femoral axes

The distal femur comprises medial and lateral condyles (Figure 2-3). These are separated inferiorly by the interchondylar notch, and superiorly by the trochlear groove [47]. The trochlear groove has a radius of approximately 24 mm and subtends an arc of 90° [48,49]. It articulates with the patella during active flexion and lies slightly lateral to the midplane of the distal femur [50]. The trochlear groove coincides with neither the mechanical, nor the anatomical axes of the knee [50,51].

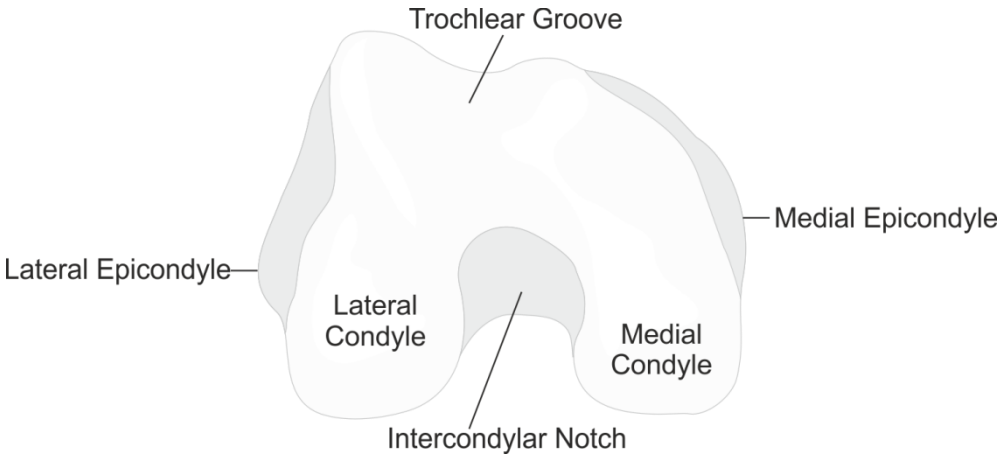

Figure 2-3: Distal femoral anatomy

The medial condyle is approximately 12.5% larger than the lateral condyle and is more spherical in shape [50,52]. The most prominent medial and lateral aspects of the distal femur are known as the medial and lateral epicondyles respectively (Figure 2-3). The line formed between these epicondyles is known as the transepicondylar axis (TEA) [50]. Weber and Weber, first described the functional anatomy of the distal femur as comprising three separate curves (Figure 2-4) [49,53]. The flexion facet (FF) is the largest; it has a 110 - 140° arc depending on the specimen and condylar side. It is the portion of the femur that articulates with the tibia during most activities of daily living [53].

The most anterior curve of the femoral condyle is the extension facet (EF), which articulates with the meniscus during full extension (Figure 2-4). The EF also has a constant radius, which is slightly larger than that of the FF. This radius is smaller on the lateral side [53,54]. The most posterior curve is the posterior horn facet (PHF). It is slightly larger on the lateral side, and only interacts with the tibia during passive deep flexion [49].

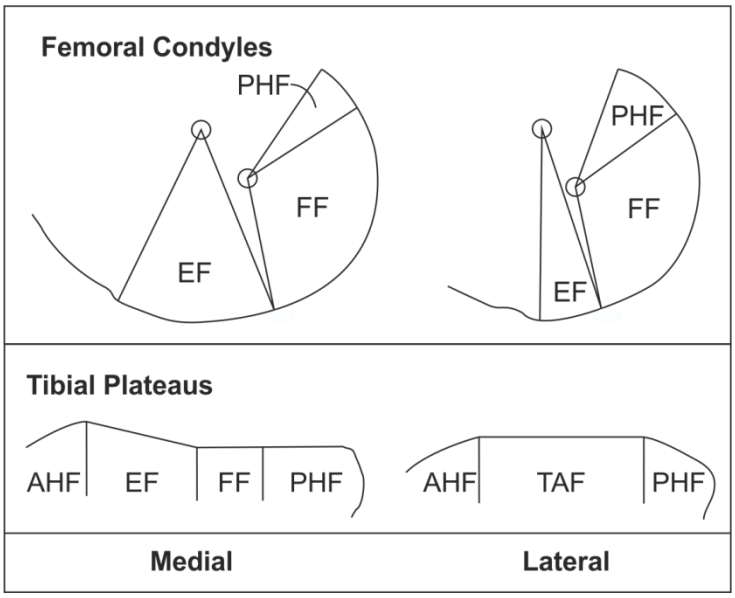

Figure 2-4: Sagittal plane sections of the femoral and tibial facets. Adapted with permission from Iwaki, et al. (2000) [53].

2.2.2. The Tibia

The tibia is one of the two long bones present in the lower human leg. It provides an attachment point, the tibial tuberosity, for the patella tendon [47] (Figure 2-5). The second bone, the fibula, runs laterally alongside the tibia, providing insertion points for some soft tissue structures in the knee. The fibular does not provide a proximal articulating surface [55]. The tibial mechanical axis is defined as the line joining the knee and ankle joint centres (Figure 2-2). The angle between the femoral and tibial mechanical axes, the hip-knee angle, is used to describe the mechanical alignment of the knee (Figure 2-2) [56].

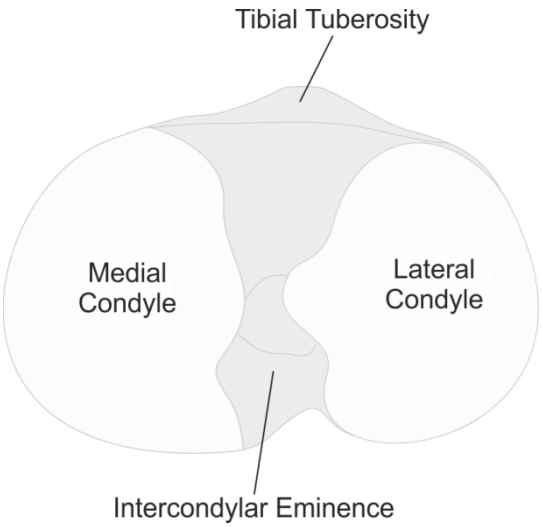

Figure 2-5: Proximal tibial anatomy

The proximal tibial surface, the site of articulation with the femur, also comprises a lateral and a medial condyle, separated by the intercondylar eminence (Figure 2-5) [47]. In a similar

manner to the femur, the proximal tibial surface is considered to comprise a number of facets (Figure 2-4) [53]. The anterior horn facet (AHF) accommodates the anterior horn of the meniscus, which articulates with the femoral EF in extension [53]. The central, and largest, section of the lateral tibial plateau is called the tibial articular facet (TAF) (Figure 2-4). The TAF is relatively flat, and contacts the femoral lateral FF during most activities of daily living [53]. On the medial tibial plateau this facet is split into two; the steep extension facet (EF) and the relatively flat flexion facet (FF) [53]. The most posterior tibial facet is the posterior horn facet (PHF) (Figure 2-4). The PHF is substantially more sloped on the lateral side than the medial. It articulates with the femoral PHF in deep flexion [53].

2.2.3. The Patella

The patella is a sesamoid bone located within the quadriceps tendon [51,57]. For reasons of clarity the soft tissue proximal to the patella is normally referred to as the quadriceps tendon, and that distal to it as the patella tendon, or ligamentum patellae (Figure 2-1) [47,57].The patella has an almost triangular shape when viewed from the posterior side, with the apex directed distally [55,57] (Figure 2-6). The posterior surface forms two concave facets split by a vertical ridge; the medial and the larger lateral [57] (Figure 2-6). The geometry of the two facets ensures high congruency with the femoral surface. This increases the PFJ contact area and reduces the joint contact pressure [44].

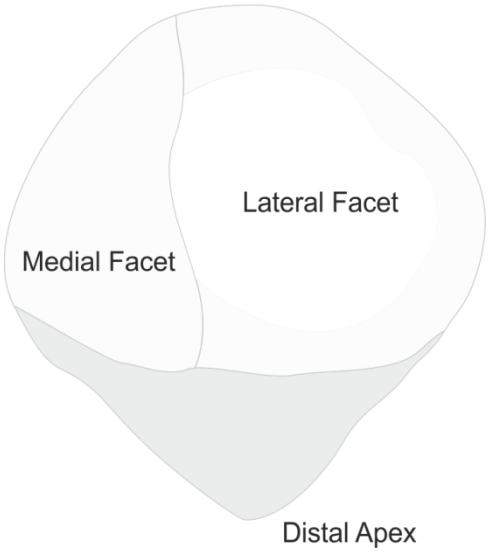

Figure 2-6: Posterior patella anatomy

The PFJ is subjected to significant joint reaction forces, which exceed those of the TFJ at flexion angles greater than 25° [44]. In high flexion activities, such as stair climb, peak flexion moments can exceed 40 Nm [1,58,59] which can induce PFJ reaction forces in excess of four times body weight [1]. Joint reaction forces during squatting can exceed seven times body

weight [1]. The posterior surface of the patella, which articulates with the femur, is therefore covered with a very thick layer of hyaline cartilage to protect the underlying bone [47,55].

The presence of the patella reduces the quadriceps force required for a given motion. It increases the patella tendon moment arm (PTMA), the moment arm of the quadriceps mechanism (Figure 2-7), relative to a situation where the tendon contacts directly with the femur and tibia [44,60,61].

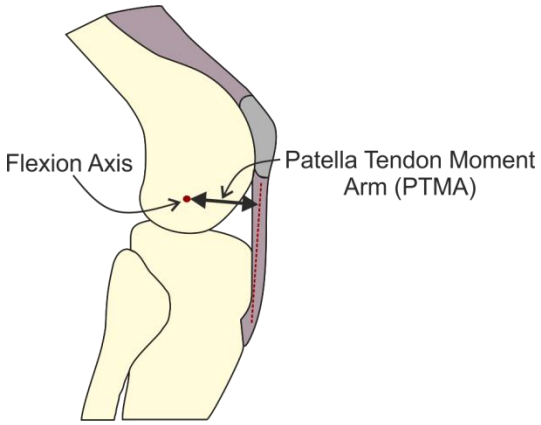

Figure 2-7: Patella tendon moment arm

2.2.4. Active Supporting Structures

The movement of the knee joint is primarily controlled by two muscle groups; the extensors and the flexors. These two muscle complexes work antagonistically to move and stabilise the knee joint [47].

The quadriceps complex dominates the extensor mechanism of the knee and comprises the rectus femoris, vastus lateralis, vastus medialis, and vastus intermedius muscles (Figure 2-8) [47]. These four muscles work together to facilitate knee extension, but are thought to activate at different loads and at different degrees of flexion [47].

The different muscles of the quadriceps complex merge, via the patella, to the same broad distal insertion point; the tibial tuberosity. The vastus medialis attaches distally on the base and medial border of the patella producing a medial restraining force. The larger, vastus lateralis mirrors this insertion on the lateral border of the patella [47,55].

Proximally, the separate quadriceps muscles have very different insertion points. Each muscle therefore has a distinctive line of action, and applies different forces and moments at the knee joint [47]. The rectus femoris inserts proximal to the hip joint, on the acetabulum and the inferior iliac spine. In contrast, the vastus lateralis has a broad insertion point, which begins on the lateral intertrochanteric line. This insertion is mirrored by the vastus medialis

on the medial side of the intertrochanteric line. The vastus intermedius is the deepest portion of the quadriceps complex, and arises from a long attachment point covering the proximal half of the femoral shaft [47,55].

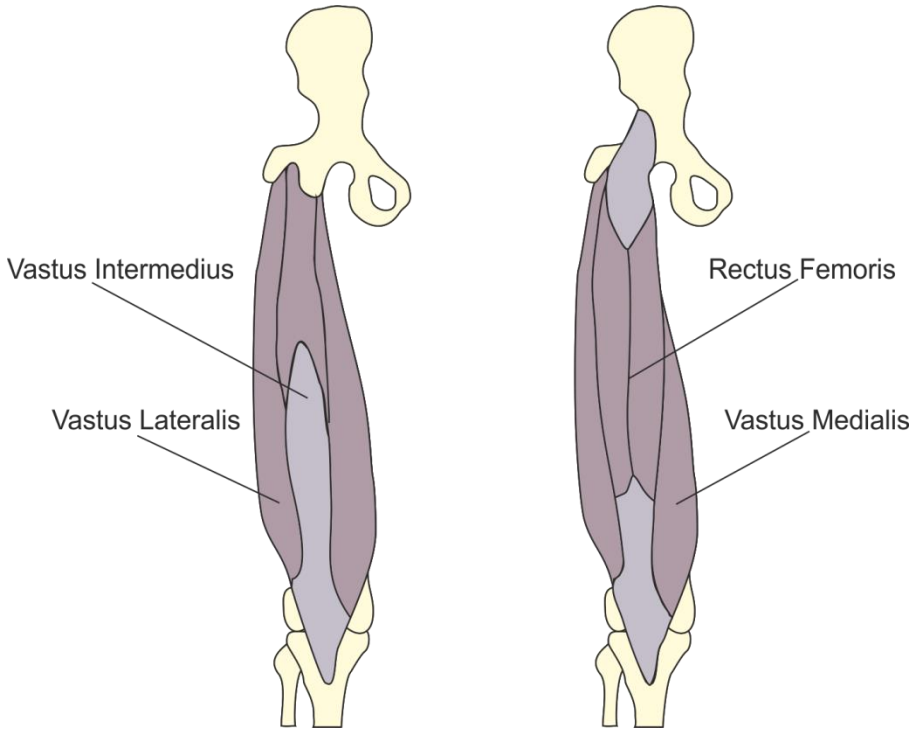

Figure 2-8: Quadriceps muscles

The seating of the patella in the trochlea groove of the distal femur, guides the extensor mechanism [44]. In full extension, the patella tendon is kept relatively parallel to the tibial axis in the coronal plane. In contrast, the quadriceps tendon maintains a lateral angle, relative to the patella tendon due to the location of the proximal insertions of the quadriceps muscles. This angular offset between the patella and quadriceps tendons is known as the Q-angle (Figure 2-9) [44,57]. In natural knees the Q-angle is approximately 15° in full extension [39,44,51,62]. As a consequence of the Q-angle a lateral force acts on the patella [44,63]. In order to prevent subluxations, the anterior surface of the lateral femoral condyle is therefore more pronounced, and the vastus medialis is stronger than the vastus lateralis [44].

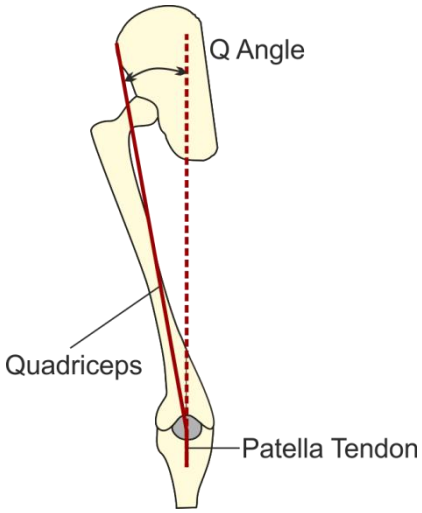

Figure 2-9: Q-angle

The hamstrings complex maintains trunk stability and is the primary knee flexor. The hamstrings also regulate the effect of inertial forces when the leg is extended and stabilise the tibia in terms of both anterioposterior and rotational movement [47]. The hamstrings complex comprises the semitendinosus, semimembranosus and biceps femoris muscles (Figure 2-10) [47].

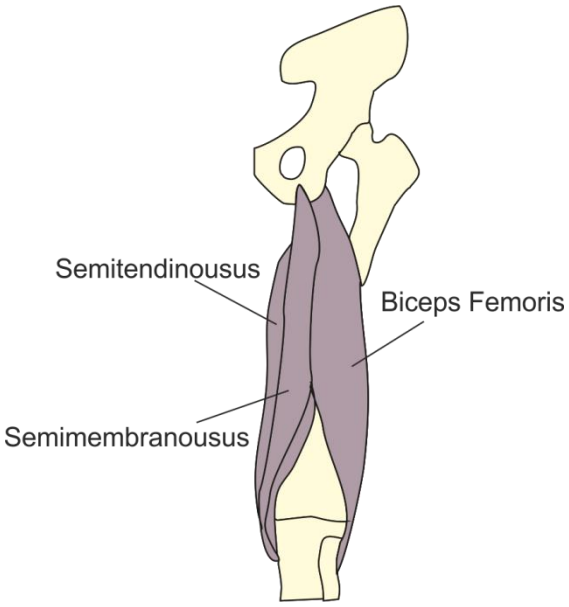

Figure 2-10: Hamstrings

The semitendinosus muscle, and one arm of the biceps femoris, attach to the pelvis via a combined tendon, proximal to the ischial tuberosity. The semimembranosus muscle inserts just above this combined insertion point. The shorter arm of the biceps femoris inserts proximally over a large area of the femoral shaft [47].

The semitendinosus is a relatively short muscle which develops into a tendon proximal to the knee joint. This long tendon passes behind the femoral medial condyle, alongside the medial collateral ligament, and inserts onto the tibial medial condyle. The semimembranosus muscle forms a shorter tendon, and inserts distally into a horizontal groove just proximal to the semitendinosus muscle [47]. The two arms of the biceps femoris combine together proximal to the patella. The muscle then becomes tendinous and passes over the lateral femoral condyle inserting distally onto the head of the fibular [47].

2.2.5. Passive Supporting Structures

The TFJ is a complex structure comprising multiple ligaments, cartilaginous constructions and an all-encompassing joint capsule. The major structures, which are commonly considered to support the TFJ, are the meniscus, the collateral ligaments, and the cruciate ligaments (Figure 2-11).

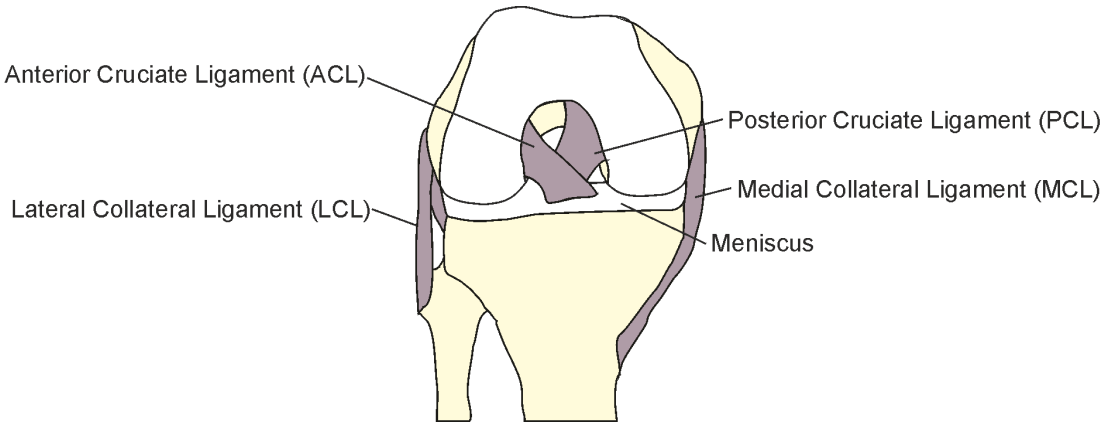

Figure 2-11: Soft tissue structures of the TFJ

The medial collateral ligament (MCL) resists valgus motion of the knee, and limits tibial anterioposterior motion and rotation [64]. The MCL is able to provide this varied pattern of restraint because it comprises three separate structures: the superficial MCL (sMCL), the deep MCL, and the posteriomedial capsule [65].

The sMCL is comprised of relatively parallel fibres. They strain as one if the joint is in valgus, but are recruited progressively during tibial rotation and anterioposterior motion [64]. As the primary restraint to tibial internal rotation and valgus motion [64], the sMCL is the strongest component of the MCL [65]. Unlike other ligaments in the body, the sMCL does not commonly operate within its toe region. It remains relatively taut throughout flexion, providing a fairly isometric restraining force [64,66]. It undergoes less than a 2% change in length during flexion of the knee [66].

The lateral collateral ligament (LCL) inserts proximally on the femur and distally on to the fibula (Figure 2-11). The LCL resists tibial internal rotation in flexion, and external rotation in extension [67]. The ligament also provides the primary restraint to varus motion of the knee [68]. Unlike the MCL, the LCL is not taut throughout flexion; it slackens by approximately 12% as the knee flexes from 0-120° [66-68].

The popliteofibular ligament (PFL) is an additional primary stabilising structure located in the posterolateral corner of the knee (Figure 2-12). The PFL originates proximally from the tendinous junction of the popliteous tendon femoral attachment. It inserts distally on to the fibular head [69].

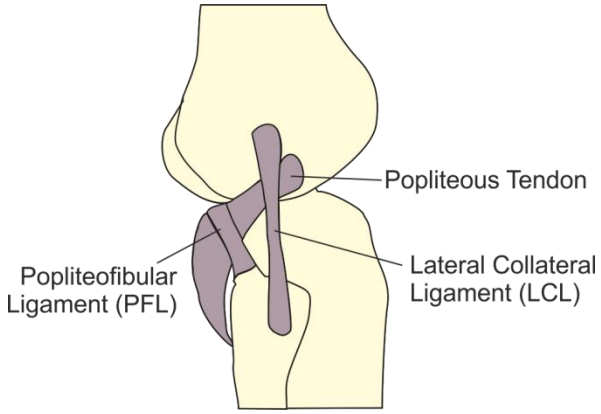

Figure 2-12: Posterolateral corner of the knee

Multiple studies have assessed the posterolateral corner of the knee by sequentially sectioning the various structures on cadaveric specimens. Differences in the cutting sequence and the position of the popliteus tendon resection between different investigators has influenced the conclusions drawn. However, all studies concur that the PFL contributes to constraint of tibial posterior translation, and varus and external rotational [70-75].

The PFJ is mainly stabilised by the action of the quadriceps muscle components. However, the medial and lateral retinacula provide additional passive support [55]. The patella retinaculae are the portions of the overall knee joint capsule directly attached to the patella. They constrain the patella to the femur [47,51] and have been termed the collateral ligaments of the PFJ [47,49,76].

The medial retinaculum comprises the medial patellofemoral ligament (MPFL), the medial meniscopatellar ligament and a number of other fibrous tissue bands [77,78]. The MPFL varies in size considerably between specimens, but is considered to be the primary constraint to lateral patella motion during early flexion of the TFJ [77-79]. The MPFL remains relatively taut in early flexion of the TFJ providing a resistance to the lateral quadriceps force on the

patella [77-79]. As the knee continues to flex the ligament slackens as the patella enters the trochlear groove and bone geometry offers the primary resistance to lateral patella motion [77-79].

The lateral retinaculum is considered to comprise iliotibial band-patella fibres, the lateral patellofemoral ligament and the lateral meniscopatellar ligament [80]. These structures are essentially characterised by a thickening of the retinaculum [80]. Their kinematic roles are therefore difficult to define [77,80].

2.3. Kinematics of the Knee

The seemingly simple act of flexing and extending the knee results in complex interactions between the three bones that form the knee. Although the kinematics of the human knee have been investigated for over 150 years, this complexity was not appreciated until relatively recently. The periods of development that have led to the current understanding of knee kinematics can be broadly split into three; early understanding of knee kinematics, classical theory of knee kinematics, and a modern interpretation of knee kinematics.

2.3.1. Early Understanding of Knee Kinematics

The anatomy, shape and kinematics of the bones within the TFJ have been studied for centuries. In 1836 the Weber brothers [81] dissected a human cadaver and examined the shapes and relative movements of the bones within various lower limb joints. They demonstrated the circular nature of the posterior femoral condyles, and that longitudinal rotation, around a medial pivot, occurs alongside flexion. Further early work, using primitive motion capture systems, supported the assertion that the knee joint experiences longitudinal rotation coupled to any flexion movement [82].

The first radiographic study to be carried out on the knee led to the suggestion that it could be modelled as a linkage mechanism. Zuppinger assumed that the cruciate ligaments remain taut throughout the flexion range and, along with the tibia and femur, formed a rigid four bar linkage. Other early work disputed the assumption that the posterior cruciate ligament (PCL) was taut throughout the range of flexion. However, it was only the four bar linkage image that persisted and was incorporated into classical theory in the 1970's [82].

Many other early studies, carried out largely by anatomists, were in German and largely forgotten as English became the primary language of science [82]. The PFJ was largely ignored in these early investigations of the knee as it was considered to act as a simple two dimensional pulley [51,83].

2.3.2. Classical Interpretations of Knee Kinematics

Little work to evolve understanding of knee joint kinematics was carried out in the period from 1917 to 1970. However, in the 1970's, scientists and engineers, unaware of much of the early work published in German and French, utilised x-rays and other imaging techniques to understand and describe knee kinematics [82].

Sagittal plane x-rays were taken of cadaveric and *in vivo* knees. The axis of tibiofemoral flexion was assessed using the Rouleaux method, making the assumption that the two axes

of the joint are planar. This assumption results in significant errors if images are not taken in the plane of motion. These analyses indicated that the femoral FF was elliptical or egg shaped [84], and that the instantaneous centre of rotation of the knee moves in a semi-circle or J shaped curve during flexion [52,85-87].

The four bar linkage mechanism, originally proposed by Zuppinger, and reprinted by Kapandji, has classically been used to describe the complex motion inferred by the moving centre of rotation. This model was demonstrated to describe not only flexion-extension of the knee joint, but also the femoral posterior translation and rotation known to occur with flexion [86,88].

During this period the PFJ was again rarely studied. Sagittal plane x-rays resulted in the continued pursuit of simple pulley models of the PFJ. Such models assume that the tension in the patella tendon and the quadriceps tendon remain the same throughout the flexion range [89]. In 1977 Bishop demonstrated, empirically and experimentally, that this was not the case. This caused researchers to reconsider the PFJ model, and ultimately led to the development of modern understanding of the PFJ [57].

2.3.3. Modern Interpretations of Knee Kinematics

In the 1980's there was renewed interest in the anatomy of the distal femur, and how this may inform understanding of knee kinematics. Kurosawa *et al.* [90], used x-ray images and calliper measurements of cadaveric knees to demonstrate, in line with the work of the Weber brothers [81], that the posterior femoral condyles can be modelled as spheres. The circular nature of the distal femoral condyles was further demonstrated by Elias *et al*. [49], who indicated that the centre of the lateral and medial spheres corresponded with the insertion points of the collateral ligaments.

In 1993, Hollister *et al.* [91] demonstrated, using cadaveric specimens, that knee motion can be described as rotations around two non-orthogonal axes: the flexion axis and the longitudinal axis (Figure 2-13). These axes are not related to normal planes of motion and can be difficult to interpret anatomically and surgically [91].

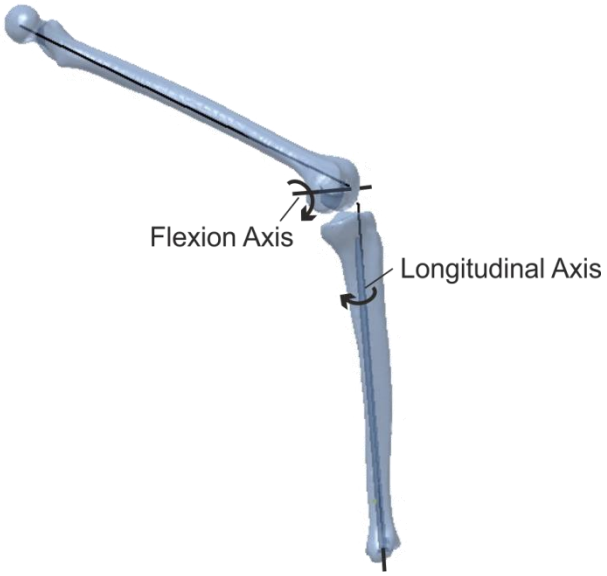

Figure 2-13: Axes of rotation

It has been demonstrated, using techniques such as MRI, CT, and fluoroscopy, that the posterior section of the femoral condyles can be modelled as cylinders with a coincident axis (Figure 2-14) [50,53,91-94]. This is the flexion axis (or cylindrical axis) of the knee. It does not correspond with the surgical TEA [95], but does coincide with the circular centres described by Elias *et al*. [49]. The longitudinal axis of the knee passes though the medial plateau of the tibia and is not in the same plane as the flexion axis [91].

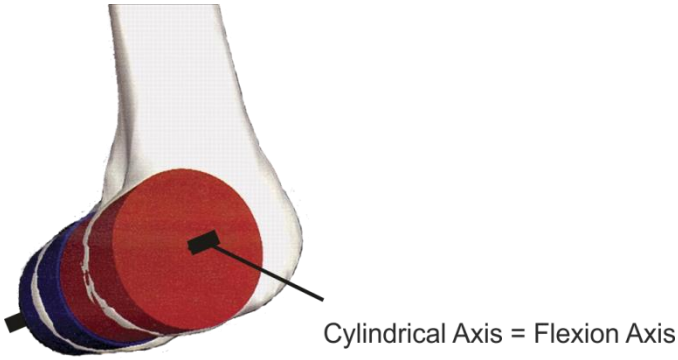

Figure 2-14: Cylindrical posterior femoral condyles. Adapted with permission from: Eckhoff, et al. (2005) [92]

In 1980 Ellis *et al.* [89] continued the work of Bishop and others [57,61] and demonstrated, using a geometric model, that the simple pulley model of the PFJ was inconsistent with radiographic images. Ellis *et al*. and others [57,89], demonstrated that the patella acts as an amplifying lever during dynamic motion (Figure 2-15).

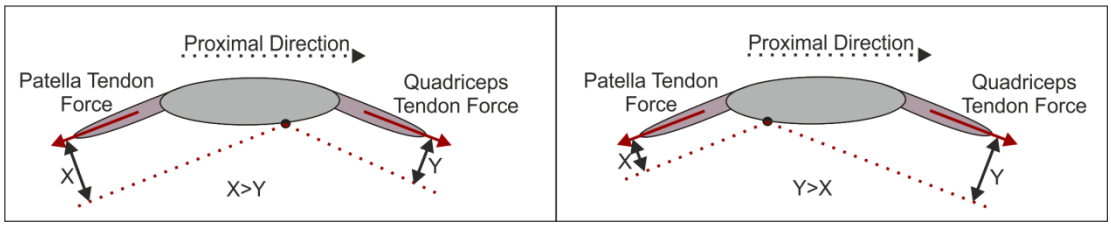

Figure 2-15: PFJ soft tissue moment arms (LHS: Flexion of the TFJ; RHS: Extension of the TFJ) [89]

The patellofemoral contact point is not located at the centre of the proximodistal axis of the patella [96]. When positioned distally of the patella centre, as is the case in extension of the TFJ, the moment arm of the quadriceps tendon is larger than that of the patella tendon. As the contact point moves proximally with flexion of the TFJ this difference reduces [48]. Therefore, in early flexion, less quadriceps force will be required to move the tibia and flex the knee [96]. In order to maintain a constant patella tendon force, the required quadriceps force increases with flexion as the moment arm ratio decreases [57].

The work of Hollister, Freeman, Ellis, and others has led to the formulation of modern knee kinematic theory [54,57,89,91,97]. Modern kinematic theory is based around the notion that knee motion occurs in three distinct phases, as depicted by Figure 2-16.

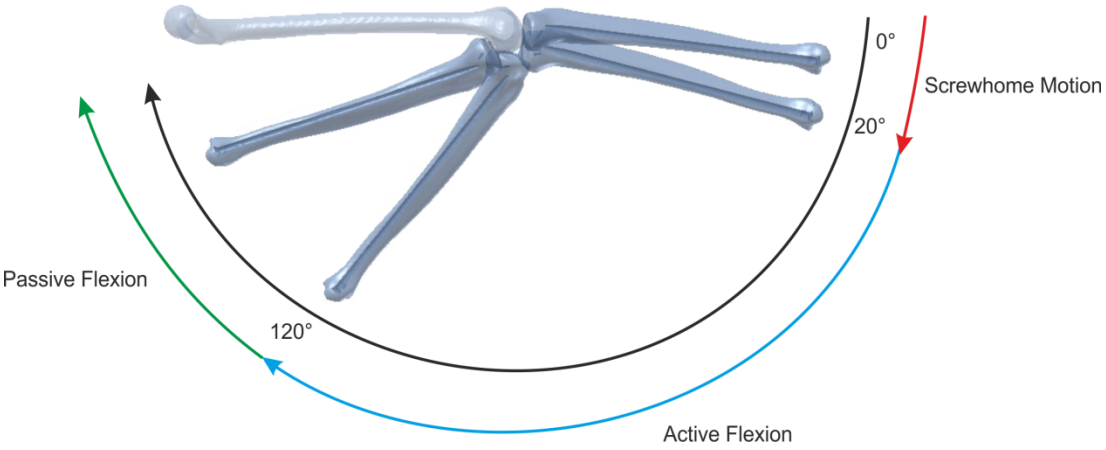

Figure 2-16: Phases of knee motion

The Screwhome arc of motion describes flexion-extension of the TFJ from full extension to approximately 20° of flexion. In full extension both the collateral and cruciate ligaments are taut [98]. During an extension motion, at approximately 20° of flexion, the knee appears to rock as the femoral condyles shift from the femoral FFs to the femoral EFs. The medial condyle rolls up on to the tibial EF causing its centre to move approximately 1.2 mm posteriorly. The lateral condyle rolls down the tibial AHF moving up to 2 mm distally as the LCL relaxes. This results in posterior roll back and a net internal tibial rotation, relative to the femur, in the order of 1° axial rotation for every 2° of flexion [54,97-100].

At, and near, full extension of the TFJ, the patella is located proximal to the trochlear groove of the femur [44]. During this phase of motion, the Q-angle is at its largest and puts the patella under a significant lateral force [44]. Femoral geometry offers little lateral constraint to patella movement in full extension. The lateral pull of the quadriceps is therefore, restricted largely by soft tissues, namely the retinaculum [101].

During the active flexion arc, approximately 20-120° of flexion, the femur rotates about the flexion axis [54,91,97]. During this range of flexion, the femoral medial condyle moves very little anterioposteriorly, whereas the lateral condyle moves consistently posteriorly. This equates to a small amount of posterior roll back, and tibial internal rotation (approximately 10-20°) around a medial pivot [54,97,99,102-106]. There are multiple theories as to the cause of this tibial rotation which is reduced under active flexion [103]. It has been suggested that tibial rotation may be a result of the lack of symmetry in the collateral ligaments: throughout flexion the medial collateral ligament (MCL) remains isometric, but the LCL slackens slightly with flexion [66,98]. The posterior distal insertion point of the LCL also acts to force the lateral femoral condyle posteriorly and hence induce rotation [66]. Alternatively, it may be due to the difference in constraint and conformity provided by the lateral and medial menisci [54,107]. Tibial rotation is undoubtedly necessary in deeper flexion, to facilitate the femur and tibia moving in relation to each other [108]. However, its role in early flexion is less clear. Although tibial rotation is passively coupled to flexion, it can be reversed or prevented, and may be an evolutionary hangover [53,97,103,104,108]. The accompanying posterior rollback is largely driven by the action of the cruciate ligaments and stabilised by the MCL in the natural knee [64,98,109].

During active flexion, the patella rotates around the femoral condyles with an axis of rotation that is parallel to the femoral flexion axis [60,110-113]. Patella flexion is proportional to tibiofemoral flexion, but lags by approximately 30% [114]. The patella contacts the trochlear groove at approximately 10-20° of tibiofemoral flexion [44,101]. From this point until approximately 90° of flexion of the TFJ, the patella runs deep within the congruent trochlear grove. Throughout this range of motion, femoral geometry forms the primary constraint to patella subluxation [101].

From approximately 30° of tibiofemoral flexion onwards, the patella initially translates medially and then laterally (Figure 2-17) [39,44,57,110-112,115-117]. This lateral translation, coupled with rotation of the tibia, reduces the Q-angle, and hence the lateral pull of the quadriceps [51]. With increased flexion of the TFJ, the patella also rotates medially to a

maximum of approximately 15° at 50° of tibiofemoral flexion [44]. This pattern is highly variable, even within the healthy population, and is greatly affected by foot orientation [110,115,118].

The reported patterns of patella tilt also vary widely. Many studies report a medial tilt during early flexion of the TFJ, which becomes lateral from approximately 30-90° of flexion of the TFJ [110,115,118]. Conversely, other studies have indicated an entirely lateral tilt, often demonstrating a medial lean in deep flexion of the TFJ [110-112,117,119,120].

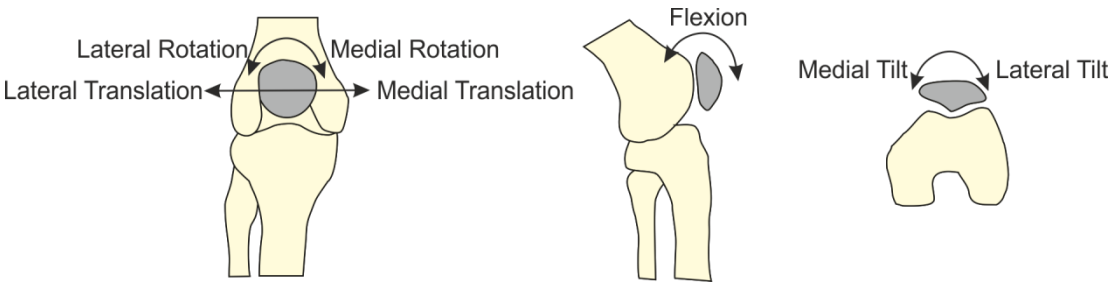

Figure 2-17: Patella degrees of freedom

Flexion of the TFJ in excess of approximately 120° (deep flexion) is a passive motion as the muscles have insufficient moment arms to actively move the limb. Deep flexion is, therefore, only possible with additional external forces, such as body weight [54]. During the passive flexion arc of motion the femur as a whole begins to move posteriorly as the femoral condyle PHFs articulate with the tibial PHFs [54]. During this range of motion the patella sits deep within the intercondylar notch [51].

2.4. Total Knee Arthroplasty

Total knee arthroplasty (TKA) or total knee replacement is a major surgical procedure. It involves resurfacing the articular surfaces of the TFJ, and in some cases the patella. It is generally indicated for patients suffering with severe disability as a result of arthritis, which is causing pain, deformity or is significantly limiting function [3,4].

TKA primarily aims to relieve pain and restore acceptable function [4,84,121]. As patient expectations rise however, there is also a drive to improve function, enable high flexion, and restore the knee to a natural, pre-disease state. Osteoarthritis (OA), the primary indicator for TKA, is the most prevalent joint condition in the USA, affecting 11.5% of over 50s [2]. As the baby boomer population ages, and life expectancies increase, a greater proportion of the population will suffer from arthritis [2]. This will increase the demand on TKA procedures. The increasing rate of obesity in the developing world is also causing an increase in traumatic joint injuries; a risk factor for TKA [2].

In 2011, in England and Wales alone, more than 84,000 primary knee replacements were carried out [122]. This was greater than the number of total hip arthroplasties carried out and represented an increase on the preceding year, continuing the exponential rise seen throughout the developed world [123,124]. In 2003 approximately 400,000 primary TKAs were carried out in the USA [5]. The number of procedures carried out each year rose to more than 600,000 in 2008 and is predicted to reach 3.48 million by 2030 [5,125].

TKA is a very successful procedure in terms of surgical outcomes and is characterised by high survival rates. Most studies report survival rates of approximately 83-94% at 15 years and 77-91% at 21+ years [3,6,126,127]. Multiple indications for revision are recorded in the 2012 National Joint Registry for England and Wales [122]. The reasons for many indications are unclear but, with the exception infection and progressive arthritis, they could be attributed to surgical error, the choice of surgical technique, or the implant design.

Sharkey *et al*., 2002 [126] carried out a comprehensive review of 212 revisions carried out by a number of surgeons. The authors indicated that 55.6% of revisions occurred within two years, with 25.4% of them due to infection. Of the revisions that occurred after two years, 44.4% were due primarily to wear. No early failures, within two years of implantation, were due to wear but there was evidence of polyethylene damage in 11.8% of cases. The data also indicated that malalignment, a purely surgical factor, was the primary cause of revision in 11.8% of cases.

In England and Wales in 2011, revision operations in 27% of OA and 15% of rheumatoid arthritis cases were carried out purely on the PFJ [18]. There is some debate as to whether this was due to inappropriate patella resurfacing. However, it does highlight the substantial number of failures that are related to PFJ complications. The prominent role PFJ complications play in the need for revision was also highlighted by Sharkey *et al*. [126]. Extensor deficiency, avascular necrosis and resurfacing of the patella were the primary indications for revision in 6.6%, 4.2% and 0.9% of cases respectively and were reported in approximately 20% of all revision cases.

In terms of patient satisfaction, TKA is noticeably less successful than THA. Even when adjusted for age, TKA patients report significantly lower satisfaction, pain, and function scores than contemporary THA patients [46,128]. Satisfaction with the procedure, something which is difficult to define, is only reported in 80-95% of cases [17,123,126,127,129]. Hip replacement patients are often said to forget they have had their hip replaced, but this is rarely the case for TKA patients, who commonly suffer from pain or, more commonly, abnormal or restricted knee motion [7,128]. Only 66% of young active patients report that their joint felt "normal" after TKA and nearly a third of patients report pain within the joint [17].

Various studies have highlighted the significant role of the PFJ in the development of constant pain after surgery which can cause substantial functional limitations [13-17]. The PFJ is the most important non-infectious reason for pain following TKA [16]. Anterior knee pain (AKP), which is often associated with complications relating to the PFJ or localised around the patella, is suffered by 8-10% of patients after TKA [13-15]. Similarly, up to 25% of patients report difficulties in carrying out extension activities such as stair ascent and descent or rising from a chair, which indicates PFJ pain or an extensor mechanism deficiency [15,17].

Similar to the native knee, the likely sources of AKP in the replaced knee are not fully understood [19]. AKP is often associated with an imbalance in the quadriceps mechanism, possibly as a result of pre-existing vastus medialis weakness; hip abductor insufficiencies due to hip osteoarthritis; or component malpositioning. Such problems can be treated by physiotherapy, hip replacement and knee joint revision respectively [19]. Other sources of AKP are less well understood [19].

The cartilage of the patella does not contain any nerve endings but the synovium, retinaculum and subchondral bone have many [20-22]. Excessive loading of the cartilage, either due to an unexpected impact, or repetitive loading below the material yield stress,

may damage the structure causing a localised tissue response. This may induce inflammation and pain in the retinaculum, irritation in the synovium, or a reduction in cartilage thickness [20,21]. Excessive loading, or simply an alteration in the loading pattern, with or without cartilage present, may also stimulate intraosseous nerve cells within the patella bone [20-22].

2.4.1. Tibiofemoral Implant Designs

The concept of knee arthroplasty has been around for over a century [130,131]. However, it was not until the 1950's and 1960's that modern TKA really took shape. Two distinct philosophies were developed; constrained or hinged prostheses, and total condylar knees [130]. Hinged prostheses are still widely available and used where a patient's soft tissues are severely compromised. Hinged prostheses are rarely required for primary surgery and will not be considered within the scope of this study [18,121]. The present report will concentrate on total condylar knee systems, which resurface the femoral and tibial articulating surfaces with two separate, unlinked components [131].

Modern total condylar knee replacements comprise three parts, a femoral component, a tibial component and a polyethylene bearing (Figure 2-18). Various materials have been used historically, but most commonly available implants have metallic femoral and tibial components and polyethylene bearings [18]. In some cases the patella may also be resurfaced.

The design of the femoral component varies widely (Figure 2-18) [4]. The vast majority of traditional implant designs were based on the classical J curve theory of TFJ kinematics. They exhibit a range of radii (multiradius TKA designs) in the functional range of motion, and have been reported to suffer from mid-range instability [23,24,132]. The remaining implant systems, and the majority of most recently introduced designs, take modern theory of knee kinematics into account and have only one condylar radius in the functional arc (single radius TKA designs).

In vitro and *in vivo* studies comparing single radius and multiradius designs have demonstrated that single radius TKAs have a reduced quadriceps force requirement, and hence an improved extensor mechanism efficiency [23,24,133,134]. This may be due to the perceived increase in PTMA as a result of the posterior single axis of rotation, or may be a consequence of the deeper trochlear groove present in all single radius designs which may alter the patella flexion angle [24].

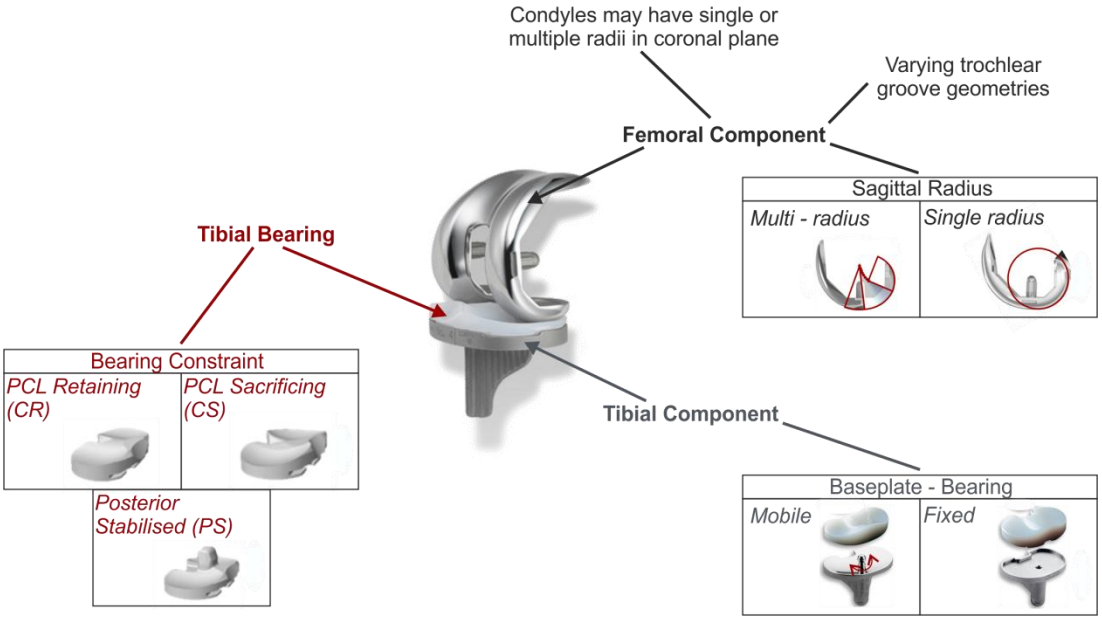

Figure 2-18: Modern TKA prosthesis design (Adapted from: [135-139])

In the majority of commercially available designs the polyethylene bearing and tibial base plate are separate components to allow ease of manufacture, flexibility within surgery and, if required, the ability to replace the bearing without requiring a full revision [43]. The bearing can either be fixed or mobile (Figure 2-18). In the fixed configuration the bearing insert is permanently locked to the tibial base plate to prevent micromotion. In the mobile bearing configuration, the bearing is allowed to rotate and/or translate with respect to the tibial base plate [121].

The level of constraint provided by the proximal geometry of the bearing is commonly defined as Cruciate Retaining (CR), Cruciate Sacrificing (CS) or Posterior Stabilised (PS) (Figure 2-18) [18,140]. As well as the level of constraint, bearing geometries are also described in terms of conformity [140]. A higher degree of conformity will increase the joint surface area. However, it may also increase the joint constraint, cause increased shear forces, higher forces at the implant fixation surfaces, and a reduction in the range of motion [140].

Most modern total condylar implants require the removal of the ACL to enable placement of the prosthesis. CR bearings have anterior cut outs to allow retention of the PCL. They provide little constraint to axial rotation or anterioposterior motion, instead relying on the PCL to resist excessively anterior contact positions and rotations [4,84].

Studies have indicated that the PCL may be unable to provide sufficient anterioposterior constraint without the ACL [141]. Some surgeons therefore routinely resect it. It may also be

necessary to resect the PCL due to damage or degeneration. In these cases the surgeon may choose to use a CS or PS bearing.

CS bearings are similar in design to CR bearings, but are all highly conforming [4]. They often have high anterior lips to prevent excessive anterior motion and guide femoral roll back [121]. PS bearings have a cam-post system, which provides additional anterioposterior, but not mediolateral constraint [121]. The interaction of the post and cam guides joint motion, often inducing posterior roll back of the femur, and preventing excessive anterioposterior motion and rotation [84].

2.4.2. Patella Resurfacing

The percentage of patellae, which are resurfaced during primary TKA procedures varies widely by country (Figure 2-19). The National Joint Registry for England & Wales, indicated that 34% of primary TKA operations carried out in 2011 included the implantation of a patella component [122]. This is a significant fall from the 65.2% reported in 2007 [142], but shows a slight increase from the 33.5% recorded in 2010 [18]. In Australia and New Zealand there has been a trend in recent years towards a higher proportion of patella resurfacing [143,144]. In contrast, the Swedish Knee Register Annual Report for 2011 indicates that only 3% of primary TKAs carried out in 2010 included a patella resurfacing procedure. The number of patellae resurfaced in Sweden, Canada and Denmark is diminishing year on year [6,144,145].

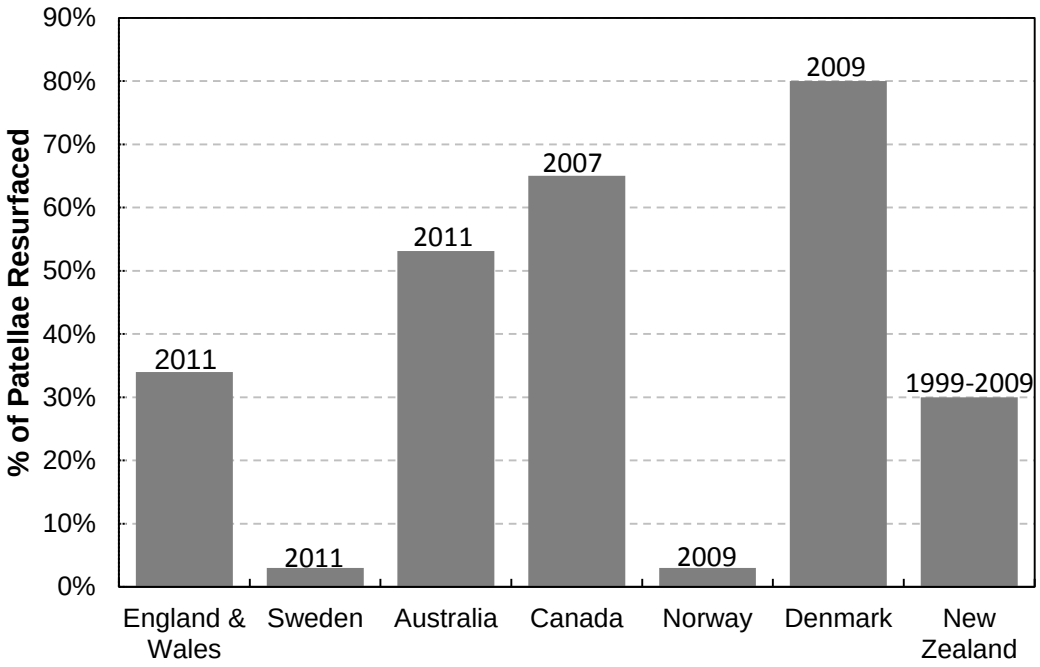

Figure 2-19: Percentage of primary total condylar knee procedures carried out with patella resurfacing [122,124,144-148]

The complex effect of patella resurfacing on implant failure has been investigated by registries in Australia and Sweden, which suggest a slightly increased risk of failure for non-resurfaced patellae [124]. Recent reviews and retrospective registry studies have also highlighted the increased risk of failure in non-resurfaced joints. However, they note the lack of reliable evidence to support or explain this and disagree as to its significance [8-12]. There is no consistent evidence regarding the effect of resurfacing on pain and function following TKA.

Lygre *et al*. 2011 [8] demonstrated that resurfacing led to a significant reduction in the risk of revision due to pain, but a significant increase in the risk due to osteolysis or polyethylene failure. Evidence such as this has led some to suggest that patella resurfacing should be reserved for use in minor revisions, when patellofemoral pain has become an issue. However, data from the Australian registry indicates that secondary resurfacing (i.e. resurfacing at a later date following primary TKA) is associated with a 15% chance of revision compared to 3.1% for patients resurfaced during a primary procedure [9].

2.4.3. Patella Component Design

A variety of patella component designs are used in modern TKA, reflecting a lack of convergence in the design philosophies (Figure 2-20) [44,45]. The components are either inset within the patella bone remnant, or simply resurface it, the latter being more common. Almost all commonly used TKA systems include a dome patella component option [149-156]. Dome shaped components, which may have a simple dome profile or a sombrero shaped periphery (Figure 2-20), are relatively forgiving to mal-placement and soft tissue changes within the joint [44]. A few systems also provide asymmetric components [151,154], or anatomical designs [155]. Asymmetrical and anatomical designs (Figure 2-20) are believed to facilitate more congruent tracking in the femoral trochlea. They are designed to increase contact area within the PFJ and hence reduce wear [44]. However, the maximum contact area achieved with these designs is still reported to be only 40% of that seen in the native joint [44].

Figure 2-20: Patella component designs (Adapted from: [157,158])

The majority of modern TKA systems only provide all polyethylene patella components as opposed to metal backed patella components [149-156]. This is probably due to a number of

historical failings associated with metal backed components. These failures were considered to be a consequence of substantially reduced patella bone stock following the introduction of metal backed polyethylene components [159]. However, there are a few modern mobile bearing patella components which have demonstrated good clinical results [44,155].

2.4.4. Surgical Techniques

The current gold standard for TKA involves the restoration of the knee joint to a 0°, or neutral, mechanical alignment; a straight line from the hip to the ankle passing through the centre of the knee. This method aims to promote approximately equal loading in the medial and lateral joint compartments, and hence a lower wear rate. In order to achieve this surgically, the femoral component is aligned with the femoral TEA, the posterior condyles or Whiteside's line [56,92].

A neutral mechanical alignment, and correct component position in other planes of motion, is most commonly achieved using intra and extra-medullary guides and jigs [56]. Guides are relatively user-friendly [56], but associated with significant placement errors due to issues of poor resolution, surgeon errors, and patient factors such as obesity [84]. Computer navigation was developed as a method to more accurately place implants. Computer navigation has a steep learning curve, and causes a substantial increase in theatre time and procedure cost [160]. It reduces alignment variability [42], but has not been demonstrated to have any effect on functional outcomes or satisfaction [160-162].

Early wear and failure studies, using now redundant implants, indicated a failure rate of 24% in knees aligned with a mechanical axis in more than 3° varus or valgus. Knee replacements aligned closer to neutral (<± 3°) only failed in 3% of cases [159,163]. These studies led to the conclusion that aiming for neutral (0°) is the ideal joint alignment following TKA [42]. Perhaps, a more appropriate interpretation of the findings was that there was a range of ± 3° from a neutral mechanical axis for safe placement.

Studies using modern implants have failed to identify a relationship between alignment and early failure [164-168]. This suggests that modern designs and materials can support the loading patterns associated with small variations in varus or valgus knee alignment [164-168]. Recent *in vivo* studies have also shown that the normal, healthy knee does not, on average, display a neutral alignment [92,169,170]; only 2% have a neutral joint alignment and only 63-80% of healthy individuals fall within a range of ± 3° from a neutral mechanical axis [92,169,171].

This has led to a debate about whether the drive to achieve neutral mechanical alignment is leaving patients with unnatural anatomy, predisposing them to pain and poor functional outcomes. The theory of kinematic alignment advocates the need to replicate the patient's natural, pre-disease, alignment rather than a general correction to a 0° mechanical alignment. Kinematic alignment can be achieved by aligning the femoral component with the knees natural flexion axis, using surgical pre-planning and/or patient specific cutting guides [56].

2.4.5. Surgical Accuracy

Whichever method or technique is used to align the components during a TKA procedure, errors will be made due to human error, surgical inaccuracies, cement fixation issues and bone cutting errors [172,173]. Poor component alignment, in the coronal and other planes, does not always correlate with patient dissatisfaction, but has been linked to poor functional outcomes [174]. Table 2-1 details the levels of surgical malalignment commonly reported in the literature. Translational tibiofemoral errors and many patella errors are rarely reported.

Due to widespread concern regarding coronal joint alignment, surgical methods have been developed to reduce the risk of malalignment in this plane. As a consequence a high percentage of tibial and femoral components are reported to be within ± 3° of neutral mechanical alignment (Table 2-1) [162,175-179]. Less effort has been concentrated on improving sagittal plane alignment. A significant proportion of patients therefore continue to demonstrate errors in the placement of tibial and femoral components of more than 3° of flexion or extension (Table 2-1) [162,172,177,179,180].

Internal and external rotational alignment of the femoral component is relatively accurate using both conventional and computer navigation methods (Table 2-1) [162,179]. In contrast, tibial internal and external rotational alignment is very variable (Table 2-1) [162]. There is a lack of well-defined landmarks available on the tibial side of the joint to guide component rotational alignment [181-183].

Surgical error during patella resection is a major cause of early revision [184]. However, despite implant systems being supplied with patella resection guides, patella resection is most commonly carried out by hand without the use of templates [3,184]. Surgeons simply use vernier callipers to measure the resection depth and place the patella component by eye. Unlike femoral and tibial resection, there is little consensus as to which landmarks are most appropriate to use, and most reliable, when defining the patella resection plane [185].

Table 2-1: Literature reported values of surgical error

	Computer Navigation	Traditional Methods	
Femoral Component			
Coronal Plane	93% within ±3° 68% 0° error	82-89% within ±3° Maximum errors 3° varus - 4° valgus	[162,176,177,179]
Sagittal Plane	84% 0° error Maximum error of 3.5°	Significant number not within ±3° Maximum error 7°	[172,177,179,180]
Transverse Plane	97% within ±3° Maximum errors 4.7°IR – 2.2°ER	89% within ±3° Maximum error of 5°	[162,179]
Tibial Component			
Coronal Plane	93% within ±3° 82% 0° error	81-82% within ±3° Maximum error 6°	[162,175-178]
Sagittal Plane	62% within ±3° 66% 0° error	Significant number not within ±3° Maximum error 4.7°	[162,172,177,180]
Transverse Plane	Maximum errors 27.1°IR – 15°ER	Maximum errors 21.2°IR – 19.6°ER	[162]
Patella Component			
Mediolateral Rotation	-	4.6±10° medial average placement	[185-187]
Flexion - Extension	-	4.2±10.7° flexion average placement	[187]
Thickness	-	1.4±1.9mm	[187]

2.5. *In Vitro* Investigation Methods

In vitro testing of knee replacement systems is routinely carried out to assess implant wear as part of pre-clinical evaluation tests (for example ISO 14243). However, kinematic testing of implants is largely confined to research. Within this sub-section, common methods of *in vitro* testing and the factors which need to be considered when developing protocols, such as specimen type and loading levels, will be discussed. The anatomical and biomechanical elements of the knee joint that must be considered when developing a knee simulator are also reviewed.

2.5.1. Simulators

The majority of modern biomechanical studies are carried out using derivatives of the Oxford Knee Rig (OKR) [38,96,188-192]. Other methods employ systems which fix the tibia or more commonly the femur [25,26,193,194], are adaptations of wear test rigs, or make use of simple surgical leg holders.

2.5.1.1. Oxford Knee Rig & Derivatives

In 1975 Perry *et al.* [195] published a study carried out using a static, table-top, knee rig, which was the precursor to the OKR. This rig fixed the tibia to a single plane hinge, which only allowed flexion. The femur could be flexed to position the knee at a specific degree of tibiofemoral flexion, whilst maintaining the hip position vertically above the ankle. The quadriceps mechanism was then loaded via a cable until the knee was balanced. A variable compressive force was also applied at the hip joint. Bourne *et al*., 1978 first described the modern OKR [196]. Bourne developed Perry's rig to include ankle and hip gimbal joints, facilitating rotation around the tibial axis. This rig only allowed static testing.

In order to evaluate dynamic movements such as squatting, stair climbing, or gait many authors have modified the original OKR [96,196-200] (Figure 2-21), or used standard materials testing machines adapted to produce similar motions [188,190]. Such rigs either dynamically move the hip or ankle joint vertically against a quadriceps force [96] or use a quadriceps force to move the knee joint against a simulated body weight [196].

OKRs allow repeatable testing of a knee joint in a dynamic manner, under a range of simulated body weights, up to and including physiological levels of loading. However, the dynamic range of knee motion is often limited to 20-120° or less, due to inertial forces induced by movement, and frequent dislocations in full extension [96,197-200]. OKRs are also limited by the structural (but not physiological) requirement for the hip and ankle to remain vertically aligned. This prevents the replication of physiological loading profiles for

activities such as gait, or rising from a chair. When carrying out such a motion naturally, the effect of body weight would be moderated by trunk anterioposterior motion [196].

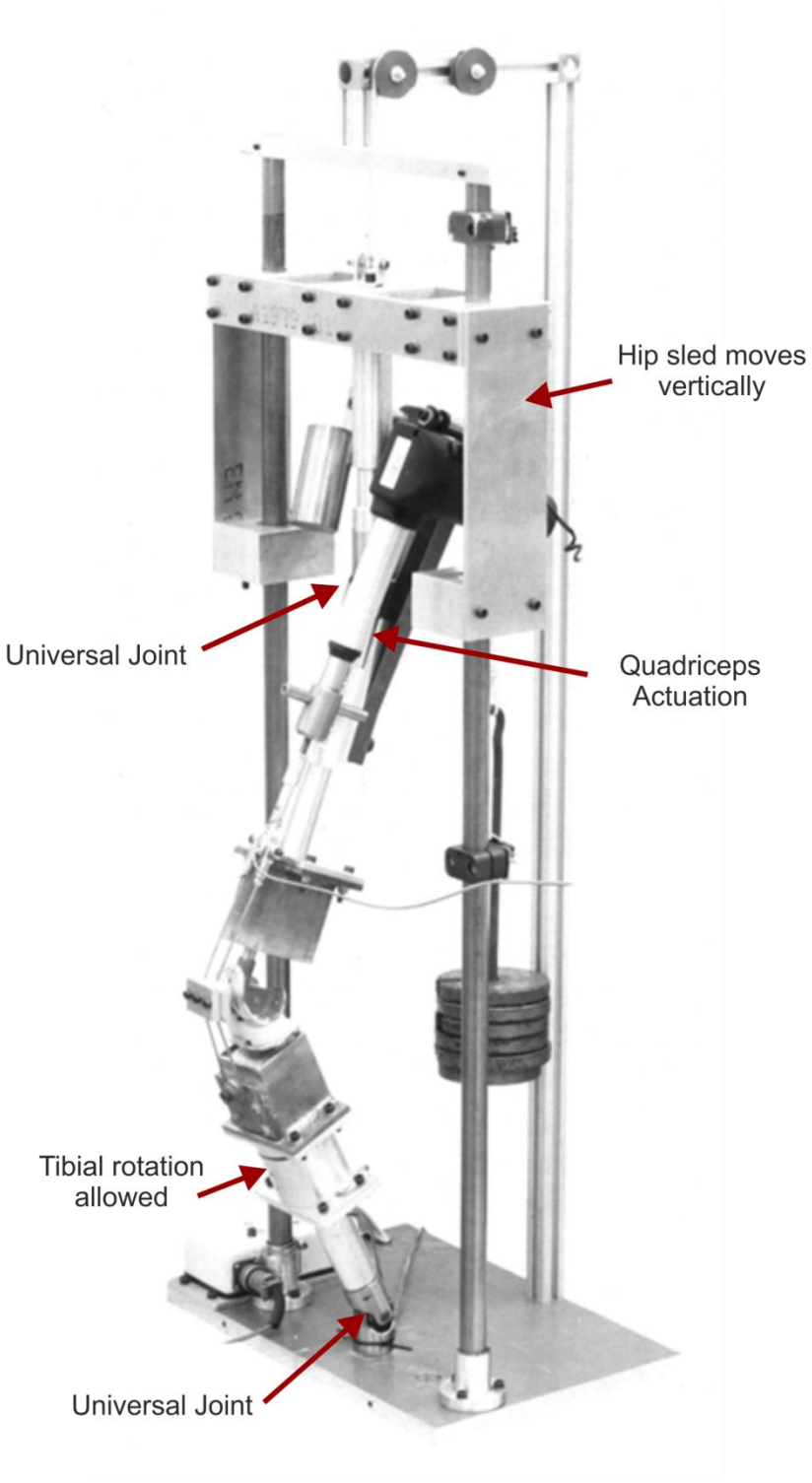

Figure 2-21: Example of an Oxford Knee Rig. Adapted with permission from: Long (2011) [196].

Different authors have used varying ankle and hip attachment methods to allow the knee to be tested with a full six degrees of freedom. Many rigs, including the traditional OKR, force the tibia to rotate longitudinally around the tibial mechanical axis [196]. However, naturally

tibial rotation occurs around a more medial axis [91]. Some studies therefore use ball joints at the ankle, or relocate the bearing which allows tibial rotation from the tibial shaft to below the ankle [201]. The latter of these configurations is employed in the Kansas Knee Simulator, which has been reported in a number of studies [96,192,199,200]. The Kansas Knee Simulator actuates the knee in a different way to the traditional OKR. This will be discussed later in this chapter.

2.5.1.2. Fixed Femur Rigs

A second common simulator design involves fixing the tibia [194] or, more frequently, the femur [23,25,26,202-204]. The knee is then allowed to move freely in all degrees of freedom with the exception of flexion and extension, which is constrained to a fixed arc (Figure 2-22). In most cases the flexion and extension motion is actuated via the quadriceps against a constant extension moment. Fixed femur rigs allow relatively natural motion of the knee joint under any level of loading up to and including physiological levels and facilitate testing up to 120° of flexion. However, they are limited to use with cadaveric specimens as they rely heavily on natural joint integrity.

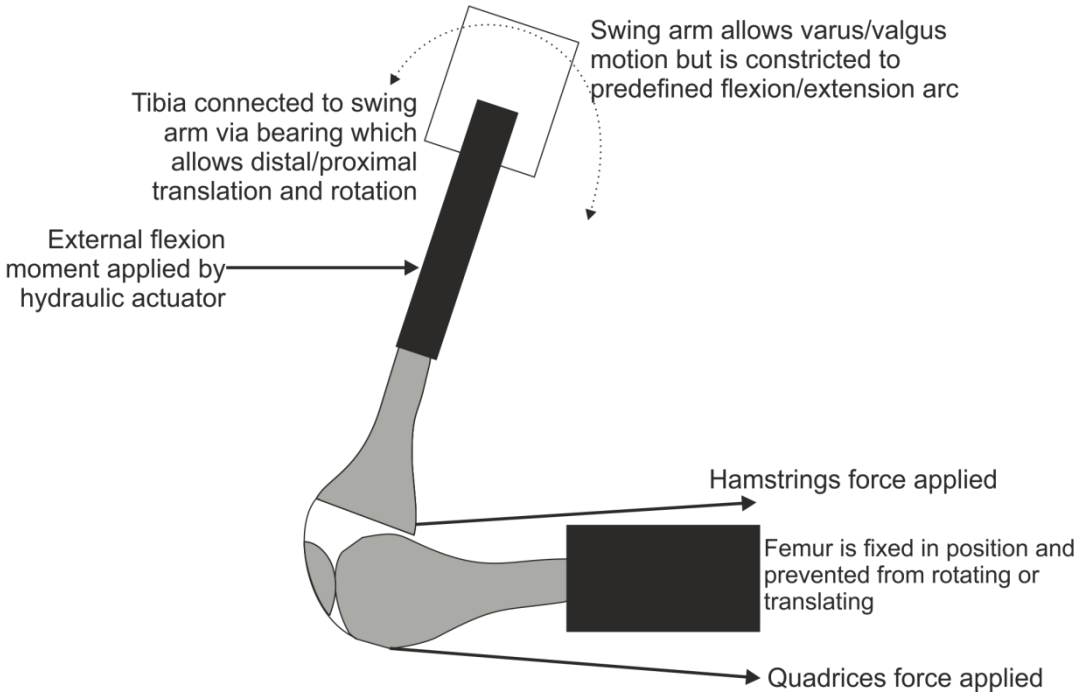

Figure 2-22: Example of a fixed femur rig

Fixed femur rigs do not facilitate the simulation of body weight. They model the isokinetic extension carried out by patients during rehab rather than activities of daily living. Similar to many OKRs the bearing, which allows longitudinal rotation of the tibia, is located along the tibial axis. Once again tibial rotation is therefore constrained to a central axis, which is not

physiological [91]. In contrast to the OKR design this cannot be changed as there is no scope to alter the bearing configuration.

2.5.1.3. Other Simulators

Verlinden, *et al.* [28] carried out kinematic testing of the PFJ using a wear test rig. A standard knee wear test rig was modified to accept femoral and patella components. Soft tissue constraints of the PFJ were modelled with springs. Flexion-extension and tilt of the patella component and the PFJ reaction force were continuously controlled to model gait. This method applies unnatural levels of constraint to the joint, and does not allow for tibiofemoral interactions, or the simulation of any muscular structures.

Other studies have included investigations carried out under simulated intra-operative conditions [63,119]. A full cadaveric leg is typically placed in a surgical leg holder and either moved by hand, or using a passive motion machine. These methods have no provision for the actuation of any muscles, and can suffer from a lack of repeatability.

2.5.2. Specimens

In vitro studies are most commonly carried out using cadaveric specimens and most computational models are also based on cadaveric data. Cadaveric models have high physiological relevance. They are also the only way to feasibly assess the effect of resurfacing of the patella; comparing the native and resurfaced patella. The majority of studies are carried out using cadavers, which have been fresh frozen following harvesting [37,38,188,189,205], but embalmed cadavers have also been used [194,206]. The authors of these studies specify that the embalming process did not affect the tissue properties of the specimen. However, work with cadaveric spines has indicated that embalming affects soft tissue laxity, and hence joint range of motion [207].

Human tissue properties depend on the conditions under which samples are stored and tested [208,209]. Specimens may also deteriorate over time and suffer damage each time prostheses are implanted or modified. This limits the number of conditions that can be tested on a single specimen [31]. The susceptibility of cadaveric samples to deterioration may also result in a systematic bias in experimental data, if the order of the conditions to be tested is not randomised. Human tissue properties vary greatly between individuals, resulting in high inter-specimen variability. However, cost, ethical, and time implications prevent the testing of large numbers of cadaveric samples [37,38,63,188-190,205,210], which can substantially restrict the ability of studies to detect statistically relevant effects.

Investigations have also been carried out without using cadaveric tissues. For instance during wear testing implants are mounted directly into the wear rig [28]. In these cases the constraints normally provided by the soft tissues within the knee are provided by springs and actuators. In other studies components have been implanted in to synthetic bones [211,212] or metal fixtures [192,196]. The resulting construct is then treated in a similar manner to a cadaveric specimen. Synthetic bones are considered to provide a good anatomical representation of natural bones and have comparable physical properties [211-213]. The quadriceps mechanism has generally been modelled and used to apply force using these methods. However, other soft tissues are not modelled, and instead joint stability is maintained through the application of a compressive joint force [211,212].

2.5.3. Loading Conditions

In vitro and computational investigations can be classed as either static or dynamic. The majority of daily living activities, such as walking, climbing stairs or rising from a chair are however, dynamic. Standing, with the knee joint in approximately full extension puts the PFJ under relatively little stress [1], and few other activities involve static loading of the joint. However, limitations associated with some measurement techniques, which mean they must occur in a static environment, has frequently resulted in static measurements at a range of tibiofemoral flexion angles being carried out [29,38,188-190,194,206]. This is normally achieved either by positioning the joint at a chosen flexion angle and applying a constant quadriceps force, or by controlling the applied quadriceps force so as to achieve a specific ground reaction force [29,38,188-190,194,206]. The results of such studies can provide an insight into the biomechanics of the PFJ, but often do not provide information which is directly relevant to activities of daily living.

OKRs are generally used to simulate dynamic motion at the knee, during activities such as stair climbing or squatting, by altering the distance between the hip and ankle. This is achieved either by actuating the quadriceps against a simulated body weight and allowing the hip or ankle complex to move vertically [31,61,197,214-219], or through a combined actuation of the quadriceps and hip position to maintain a constant ground reaction force [96,191,192,220].

OKRs can only fully represent activities such as squatting against a wall, where the hip remains vertically above the ankle. In other motions, such as stair climbing or gait, patients will also move their upper body to reduce the body weight moment arm and thus the joint reaction forces [1]. OKRs are able to model the peak flexion moment applied to the knee

during an activity such as stair climbing. However, they cannot model more complex changes in the flexion moment induced by trunk motion *in vivo*, as the hip, and the associated body weight component, is fixed vertically above the ankle.

OKRs are also unable to model other external forces such as mediolateral ankle forces. The Kansas knee simulator [199,200] has a similar outward appearance to the OKR. However, it has actuators, which not only act vertically at the hip and replace the quadriceps, but also drive tibial rotation and mediolateral ankle translation. All of these actuators are force or displacement controlled with profiles designed to replicate daily living activities such as gait. The Kansas knee simulator has the potential to provide a more physiological dynamic loading envelope than an OKR. However, the replication of human movement by the Kanas knee simulator is only as good as the underlying, experimentally measured, loading profiles. Measuring joint forces during activity *in vivo* is a complex process and can result in highly variable results [221,222].

Fixed femur rigs are also unable to replicate complex activities of daily living. They are not able to model body weight and instead apply a constant flexion moment, modelling dynamic isokinetic flexion-extension [23,203,204,223].

Fixed femur rigs are commonly designed to maintain a constant flexion moment of 31 Nm [23,25,26,193,202-204,223]. In contrast, studies using the OKR quote peak moments of approximately 40 Nm [61,196]. Mason's review of patella joint forces [1], indicates that the maximum knee joint moment experienced during stair climbing, a relatively high force activity, can be approximated as 0.04 times the multiple of a patient's body weight and height. This relationship was also confirmed through experimental work by Andriacchi *et al.* [58] and equates to an approximate peak moment of 40 Nm for an average woman [59].

It is important to carry out experiments at physiological levels of loading [215]. However, the quadriceps forces during high-flexion activities such as squatting can easily exceed 2 kN [1]. Such high forces can damage cadaveric specimens [215]. Many studies are therefore carried out with reduced quadriceps loading or the simulation of a reduced body weight [29,38,63,188,191,194,206,210].

In addition to the forces which are applied, the speed of joint movement must also be considered. Testing speeds have been reported in the range of 3-8°/sec [26,192,196,202,215,224]. During preliminary work Long [196], measured the quadriceps forces required to flex and extend hinged knee replacements at 3, 6 and 12°/sec and

indicated that, within this range, speed had no statistically significant effect on the quadriceps force at any flexion angle.

2.5.4. Musculature Modelling

Motion of the human knee is primarily controlled by the quadriceps and the hamstring mechanisms [47]. Although these are not the only muscles which act at the knee, for reasons of simplicity, they are the only ones considered during *in vitro* testing.

2.5.4.1. Quadriceps

The quadriceps complex is almost always simulated as part of the joint actuation. The quadriceps mechanism is generally modelled as either multiple muscles loaded with constant forces [39,101,116,194,206,225] or a single muscle dynamically actuated against a constant flexion moment or to maintain a constant ground reaction force [23-26,61,190,192,193,201-204,217,218,223,225] (Figure 2-23). However, two more recent investigations have involved the dynamic actuation of three separate muscles to maintain a constant ground reaction force [191,198].

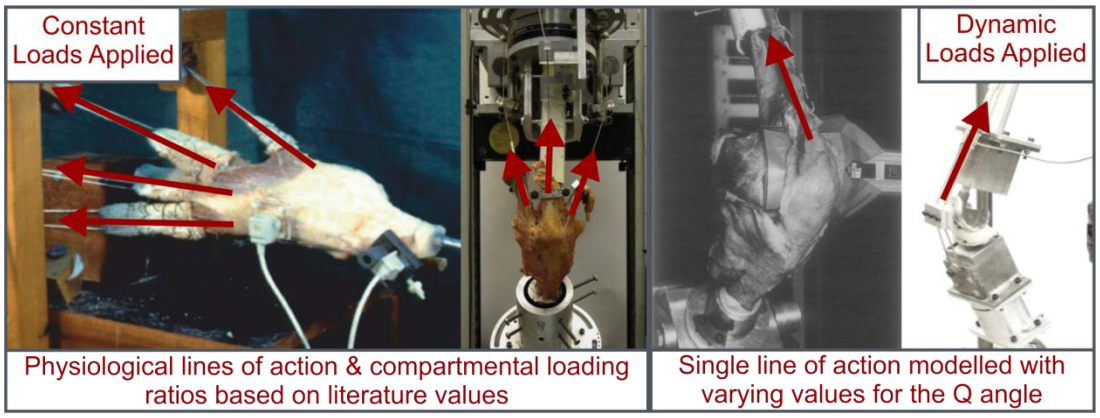

Figure 2-23: Alternative methods of *in vitro* quadriceps actuation Adapted with permission from: [37,114,189,196].

Studies which have loaded multiple quadriceps muscles have all used cadaveric specimens [39,101,116,191,194,198]. The isolated activation of different muscles of the quadriceps, and changes in the relative loading levels of the individual muscles, has been demonstrated to alter knee joint kinematics and internal joint loading [198,220,226,227]. For instance, cadaveric work has indicated that asymmetrical quadriceps loading has a significant effect on patella rotation and tilt [228]. The lack of information regarding the exact activation pattern of the different muscles, and the complexity associated with multiple actuators, has meant that most models only apply a constant load to each muscle [39,101,116,194]. This is a simplification of the actual loading naturally experienced by the knee [1].

Cadaveric specimens are normally supplied without the pelvis [39,101,116,191,194,198], the primary proximal attachment point for the quadriceps muscles [47]. The lines of action used in *in vitro* testing are therefore based on general literature values and may not directly resemble the anatomy of the specimen being used [39,194]. Approximating the different muscles of the quadriceps by applying load through a single line of action undoubtedly simplifies the natural system. However, it requires the estimation of fewer anatomical points, and can also be employed when using models which do not include cadaveric tissue.

Models which only represent a single line of action of the quadriceps complex generally simulate the rectus femoris [196]. This can be achieved by locating an actuator parallel to the femur [31,189]. However, it is more physiological to replicate the natural Q-angle, so as to preserve the natural lateral force applied at the PFJ [196].

2.5.4.2. Hamstrings

Many studies do not simulate the hamstrings, choosing instead to concentrate on the larger extension forces of the quadriceps [24,96,101,110,111,199,200,211,214,229-232]. It has been demonstrated however, that co-contraction of the hamstrings during flexion and extension significantly affects the required quadriceps force, the patellofemoral and tibiofemoral contact forces, and tibial stability, by reducing tibial anterior shift [193,204,233-235].

The accurate, physiological, modelling of the hamstrings is hindered by the paucity of data available in the literature relating to the anatomy or loading of the hamstrings. The semitendinous and the semimembranous muscles have lines of action that can be grossly approximated [47]. The biceps femoris however, follows a distinctly different path, producing a significantly more lateral force than the other muscles [47,236]. Loading of the medial and lateral muscles of the hamstring complex have distinctly different effects on tibial anterioposterior position and rotation [236]. Therefore, in order to provide a physiologically relevant model of the hamstrings, it is appropriate to at least model the hamstrings as two muscles as achieved by a number of studies [25,26,201,202,204,218,225]. Other studies however, simply attach a spring or actuator to one or all of the hamstring tendons [23,194,223].

The variable nature of the flexion force produced by the hamstrings has been modelled in previous studies, using extension springs [197] or actuators [237], with little evidence provided to support the chosen loading patterns [197,237]. The majority of studies have represented the hamstrings with constant forces throughout the flexion range, using

constant force springs, pulleys or actuators [23,25,26,194,202,204,218,223,225]. This simplifies the natural hamstrings action and does not allow for the differences between the muscle's role in extension and flexion to be modelled [47]. The magnitude of hamstring force modelled *in vitro* varies widely; from 20 N to 200 N [23,25,26,42,197,198,201,202,236]. These relatively small loads reflect the relatively low activation levels of the hamstring complex during squat activities [238]. Where more than one compartment has been loaded most studies have split the total load evenly between the compartments [201,204,218,225].

All studies, which have to date modelled the hamstrings, have made use of cadaveric specimens [23,25,26,194,197,201,202,204,218,223,225,237]. Such studies model a physiological distal insertion point by attaching to the tendon(s) of the muscles to be loaded. As the cadaveric specimens used are normally dissected distal to the hip joint, the proximal insertion points are harder to accurately model. Most authors fail to state how the hamstrings line of action has been modelled [23,25,26,197,201,202,204,218,223,225,237].

2.5.5. Ligamentous Modelling

The knee is constrained by the complimentary action of a multitude of ligamentous structures. These are inherently accounted for when cadaveric specimens are used, but mechanical replacements are required when cadaveric material is not included.

The ACL is removed in the majority of TKA procedures to prevent impingement of the tibial tray and in many cases the PCL may also be resected. It is therefore only the action of the collaterals, which is generally considered [212]. The PFL has not been considered in previous *in vitro* simulators.

Many models which do not include cadaveric tissue neglect to specifically model the collaterals, simply applying a constant compressive force to the joint to prevent dislocation [212]. This does not take into account the changing restraint supplied by the ligaments through the range of motion of the joint and therefore may not simulate the physiological kinematics of the knee [65,67].

There is little data in the literature relating to LCL and PFL properties and, due to differences in loading rates, inconsistent data regarding MCL properties. However, the human MCL has been demonstrated to have a stiffness of, on average, 67 N/mm [65,67,209,239,240]. The LCL is slightly less stiff (approximate stiffness of 58 N/mm) [67,209].

2.6. The Patellofemoral Joint after Total Knee Arthroplasty

Issues associated with the PFJ have been implicated as a contributing factor in around 20% of TKA revisions, most commonly due to pain, instability, fracture or wear [126]. The PFJ, and associated AKP, are also commonly cited as reasons for dissatisfaction by TKA patients who have not had a revision, but suffer with functional limitations [15]. The reasons for AKP and PFJ complications are not fully understood, but are thought to be related to the biomechanics and loading within the PFJ of the replaced knee [19-22].

There are a variety of surgical and implant factors which can affect the PFJ after TKA. Different design geometries, material properties of the articulating surfaces, soft tissue damage during surgery, and malalignment of components can all contribute to mal-tracking, alter the kinematics of the PFJ and change the patterns of joint loading [25,60,116]. Changes in the kinematics of the PFJ are important to understand, however, it is most appropriate in the first instance to assess changes to the biomechanics and loading of the PFJ.

PFJ biomechanical and contact characteristics can be assessed using various methods. Joint loading directly relates to stress in the components and is closely linked to pain, and component wear and failure [20,21,241]. Assessment therefore, generally involves the measurement of the contact pressure distribution between the patella and distal femur, compressive joint forces and joint contact areas. This sub-section will discuss what is currently understood regarding the effect of TKA, patella resurfacing, implant design and surgical mal-alignment on the biomechanics of the PFJ.

2.6.1. The Effect of Arthroplasty

Numerous *in vitro* and computational studies have investigated the biomechanics, contact characteristics and loading within the PFJ, before and after TKA [29,63,189,191,193,194,205,206,210,242]. The peak and mean pressures, and the mean contact areas that have been reported before and after TKA are summarised in Figure 2-24, Figure 2-25 and Figure 2-26. Previous studies use a variety of experimental methods and a wide range of implant systems (Figure 2-24, Figure 2-25 and Figure 2-26).

Most studies are carried out using fresh frozen cadaveric specimens [63,189,191,193,205,210]. However, two studies have used embalmed cadavers [194,206], one a subject specific computational model [242], and one a mathematical computational model [29]. Some of the studies were carried out under dynamic loading, driven by the quadriceps either in an OKR [191,242] or using fixed femur configurations [193]. Other

authors have used static OKR methods [189,194,205,206], and a few have moved the joint passively by hand [63,210].

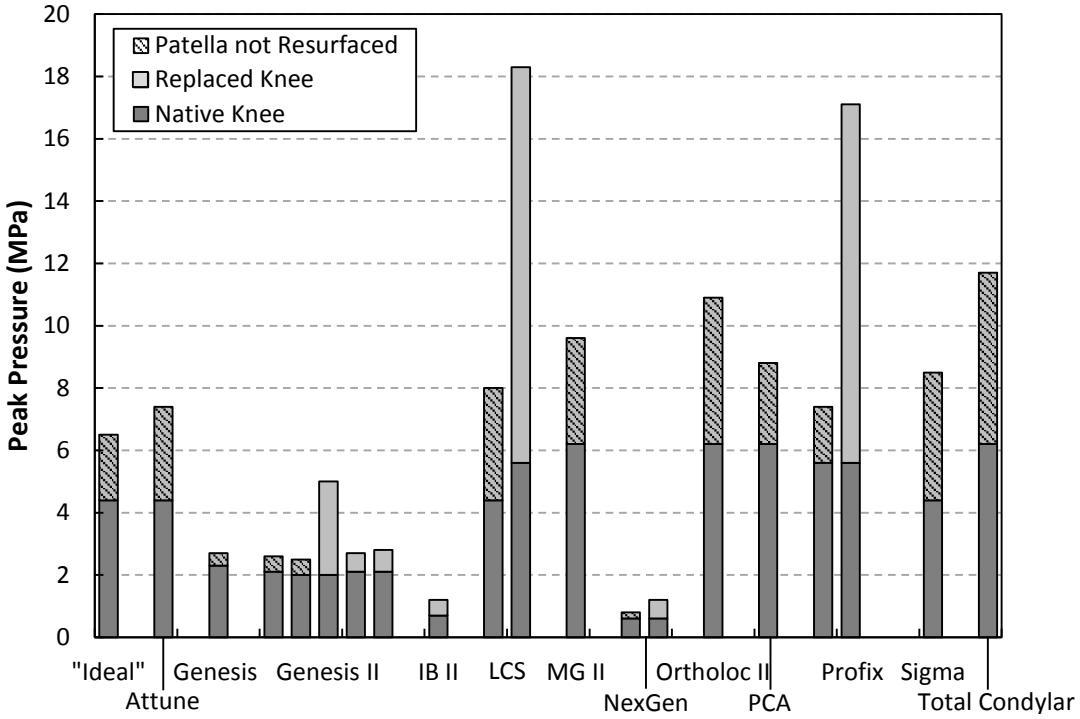

Figure 2-24: PFJ peak pressure values recorded in peer reviewed literature during *in vitro* biomechanical testing [29,63,189,191,193,205,206,210,242]

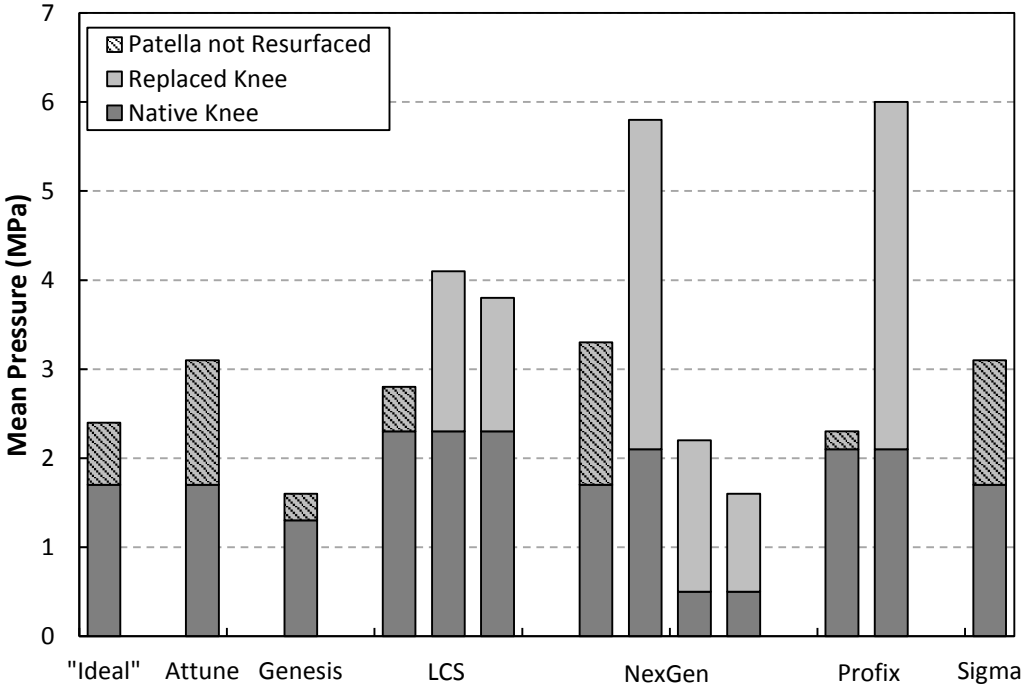

Figure 2-25: PFJ mean pressure values recorded in peer reviewed literature during *in vitro* biomechanical testing [189,193,194,206,242]

Previous studies of the PFJ have also differed with regards to measurement techniques. Some have assessed contact pressures and areas using the relatively thin Prescale pressure film (Fujifilm Europe GmbH, Dusseldorf, Germany) [206]. This is only possible under static loading conditions. Other authors have therefore made use of pressure arrays, which can assess joint contact pressures under dynamic loading conditions. Most studies use the less flexible, but more accurate Tekscan system (Tekscan, Boston, USA) [189,191,193,205,243], but a few have used the Pliance system (Novel, Munich, Germany) [63,194,210,243].

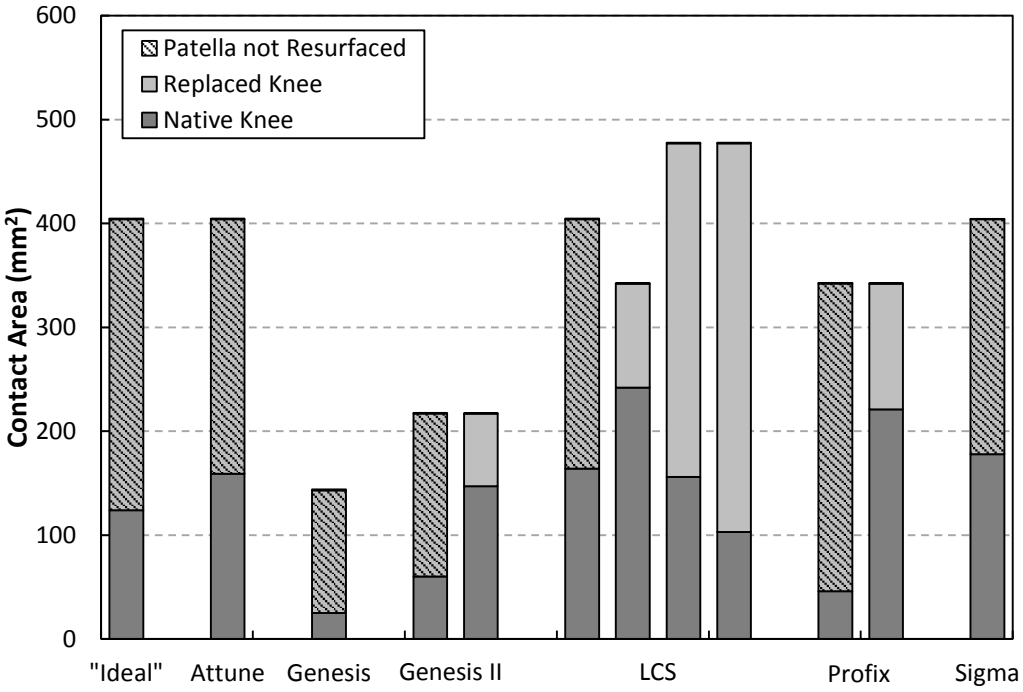

Figure 2-26: PFJ mean contact area values recorded in peer reviewed literature during *in vitro* biomechanical testing [189,191,193,194,206,242]

All reported studies which have taken measurements under physiological levels of loading report peak pressures less than 6 MPa for the native knee [193,242]. This is well below the threshold of healthy human cartilage with regards to fatigue or impact damage (10-15 MPa [244]), and explains why the majority of the population carry out everyday tasks without pain or injury.

The peak contact pressure within the PFJ increases after TKA by 105-531%, and the mean contact pressure by 120-308% compared to the native joint (Figure 2-24 and Figure 2-25) [29,63,189,191,193,194,205,206,210,242]. Similarly, the PFJ contact area reduces after TKA (Figure 2-26) to between 30 and 87% of the pre-TKA value [189,191,193,194,206,242]. These results highlight that modern knee replacement designs do not provide the same levels of

congruency as the native PFJ. Such increases in the PFJ force may lead to cartilage damage and/or bone remodelling, which may initiate a pain response [19-22].

The wide variability between the published results, both for native and replaced knees (Figure 2-24, Figure 2-25 and Figure 2-26) highlights how the results are affected by variations in experimental protocols and how different implant designs may affect the biomechanics of the PFJ. The inconsistent nature of the protocols used by different studies, and the different implant systems employed, limit the number of general conclusions that can be drawn with regards to the effect of TKA on the PFJ.

2.6.2. The Effect of Patella Resurfacing

Resurfacing of the patella generally results in an increase in peak and mean PFJ contact pressures, and a reduction in the contact area in comparison to the un-resurfaced state (Figure 2-24, Figure 2-25 and Figure 2-26) [29,63,189,191,193,194,205,206,210,242]. Figure 2-27 summarises the peak pressure measurements previously reported over a full range of flexion of the TFJ. There is a clear trend towards a greater peak pressure throughout the flexion range after patella resurfacing. Patella resurfacing also appears to cause a spike in PFJ contact pressure in mid flexion, which is not present when the patella is not resurfaced [29,189,205,242].

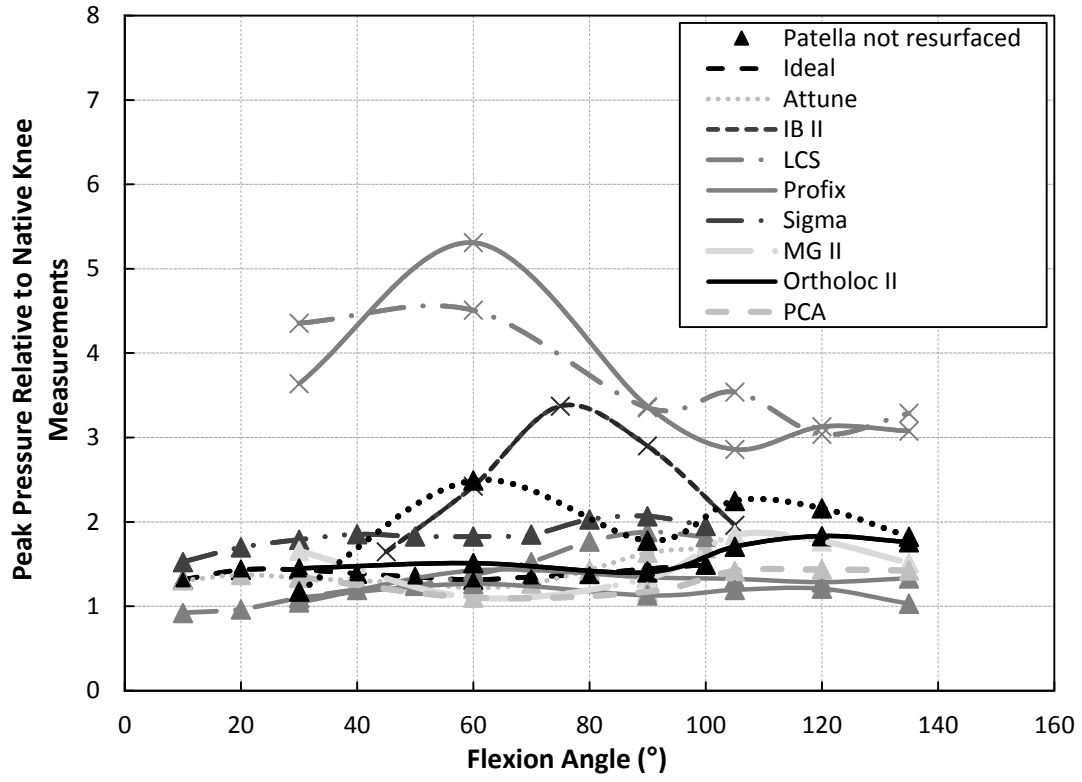

Figure 2-27: Relative PFJ peak pressure measurements over flexion cycle recorded in peer reviewed literature during *in vitro* biomechanical testing [29,189,205,242]

The geometry of commercially available patella components is different to that of the native patella [44,45]. This may lead to an alteration in the tracking of the patella within the trochlear groove, as has been observed in *in vitro* tests [194,245]. This in turn may lead to a shift in the contact characteristics of the PFJ due to changes in PFJ contact area, and quadriceps forces arising from alterations in the PTMA. The change of patella articulating material from compliant cartilage, to less compliant UHMWPE, will also reduce the PFJ contact area, which will increase the contact pressures within the joint [190].

The degree to which the PFJ contact pressure is greater after resurfacing of the patella, compared to a joint in which only the tibiofemoral surfaces have been replaced, appears to be dependent, to some degree, on the prosthesis design. Cadaveric investigations, using static OKR protocols and simulating passive flexion, have indicated that the Profix (Smith & Nephew, Memphis, USA) and NexGen (Zimmer, Warsaw, USA) systems demonstrate significant increases in contact pressures after patella resurfacing [63,189,190,210]. In contrast, the Genesis 2 implant (Smith & Nephew, Memphis, USA) has been reported, using a dynamic fixed femur protocol, to demonstrate similar peak PFJ contact pressures whether the patella is, or is not, resurfaced [193].

A domed patella component and a natural patella are geometrically very different. Femoral component geometry cannot be fully optimised for both situations. The literature suggests that the Profix and NexGen femoral components, which have deepened trochlear grooves and are described as *"patella friendly"* [63,210], are better suited to an unresurfaced patella than the dome components which are available for these implants [63,189,190,210]. Conversely, the Genesis 2 femoral component has a lateralised, deepened, trochlear groove [246], which appears to be equally well suited, in terms of absolute pressures, for the oval patella component design that is used with this implant and with the native patella [193]. This may suggest that the Genesis 2 patella component design is more anatomical.

Due to the increased pressure the patella is subjected to, and the consequent increased activation of intraosseous nerve cells, resurfaced patellae may be considered to be at a greater risk of AKP. However, little is understood about the thresholds of force or pressure that will induce such responses.

Knowledge of the forces and associated stresses that occur at the patella contact surfaces also allows an analysis of the likelihood of fracture or wear of the articulating surfaces. Human articular cartilage and UHMWPE respond differently to loading and contact stresses. UHMWPE can be approximated as an elastic material with an offset yield strength of

approximately 13 MPa and a fatigue limit, for 1 million cycles, of less than this [190,247,248]. The viscoelastic, time-dependent, nature of hyaline cartilage renders the quotation of a yield strength redundant. However, cartilage, which has little propensity for repair, does exhibit a fatigue response, if sufficient time for relaxation (approximately 90 min) is not allowed, under repetitive loading, as experienced in daily life. Cyclic loading of as little as 10 MPa can initiate fatigue failure after less than 100 cycles [244]. Human cartilage can also be damaged by excessive static or impact loads [244]. It has been suggested that a static load for as little as 500 ms or impact loads at levels greater than 15 MPa can initiate damage in the cartilage layer [244]. These values are likely to over-estimate the thresholds in the case of elderly, osteoarthritic, cartilage [190,249]. Increased levels of static or dynamic loading on articular cartilage, which is articulating with a metal surface, will also result in increases in the coefficient of friction between the articulating surfaces [249-251]. This occurs because the non-physiological bearing coupling prevents efficient rehydration of the cartilage. This trend is exacerbated by increased joint loading time. It may also increase the rate of wear and surface damage within the joint associated with a given loading level [249].

In vitro investigations, which have assessed the pressures within the PFJ under physiological levels of loading, indicate that the cartilage surface of an unresurfaced patella is subjected to peak pressures of 9-12 MPa during activities of daily living [190,242]. This level of loading, even if only carried out intermittently when stair climbing, rising from a chair or carrying out sport or exercise, is likely to initiate damage in the cartilage layer of an elderly TKA patient [244]. Similar investigations with resurfaced patellae indicate peak pressures greater than 25 MPa occur within the PFJ in high flexion activities. Once again, this suggests fatigue or yield damage of the UHMWPE patellae used during the investigations would be likely during extended clinical use [96,190,192].

Randomised control trials have so far failed to provide sufficient evidence to support whether the patella should or should not be resurfaced at the time of primary TKA [12]. The *in vitro* biomechanical studies available in the literature do not provide any further insight. However, they do indicate that both resurfacing and non-resurfacing results in levels of contact stress that may cause damage to the patella articulating surface over time.

2.6.3. Design Factors

Whether the patella is resurfaced or not during TKA, the femoral articulating surface will have been changed from natural, compliant, cartilage to a much stiffer metal. Computational work has indicated that this material change alone, independent of geometric alterations, gives

rise to a 50% increases in pressure values within the joint and a reduction of up to 35% in the joint contact area [252]. Cartilage is much less stiff than cobalt chrome or titanium, and will therefore undergo significantly more deformation under load. This will result in an increase in the contact area, and hence a reduction in the contact pressure within the PFJ.

Traditionally, femoral implant design paid little attention to the PFJ, as the importance of the role it plays was poorly understood. Older designs, which are no longer used in the UK, have been demonstrated to result in significantly higher peak pressures after TKA without patella resurfacing, compared to more modern implants [205]. As the importance of the PFJ became more apparent, and AKP and PFJ complications were more widely reported, the design of the trochlear groove and patella component has become more important. This has culminated in a recent trend towards more anatomical, laterally orientated or asymmetrical trochlear grooves [101]. This has significantly reduced pressures in the PFJ after TKA [205].

Analysis of the PFJ following TKA with a variety of modern prostheses, without resurfacing of the patella, indicates that all of the implants demonstrated statistically increased pressures compared to a design with a component whose geometry exactly matched the natural knee [242]. All of the implants tested were produced by the same manufacture and therefore these results do not apply to the market as a whole. However, they do support the suggestion that knee replacement femoral geometries are not good replications of the natural joint surface [253].

Modern kinematic theory has led to the development of prostheses characterised by a single femoral sagittal radius in the functional arc. *In vitro* work comparing the single radius Scorpio (Stryker, Rutherford, NJ) implant with the traditional multi radius Series 7000 (Stryker, Rutherford, NJ) prosthesis, using the same patella component for both, has indicated that the single radius design resulted in statistically lower compressive forces behind the patella component at flexion angles greater than 60° [61]. This may reduce the risk of AKP. The reduction in forces experienced in the PFJ after TKA with a single radius knee may be a result of the increased and more stable PTMA associated with the designs, which reduces the force required by the quadriceps for a given motion [23,24]. Femoral roll back has also been hypothesised to reduce the hamstring moment arm, reducing the applied strength of the flexor mechanism [61]. However, there is analytical evidence that the force reduction may, at least in part, be due to the deepened trochlear groove associated with most single radius designs [24].

Presently, there are no studies assessing whether a reduction in force behind the patella component is mirrored at the contact surfaces of the PFJ, and therefore to what degree it may reduce the risk of wear or failure. Experimental work, focussing on the pressures and contact areas within the PFJ, but not the forces, indicates that the changes in the two variables are not necessarily correlated [242]. This would suggest that variations in pressure and force may also not always follow the same pattern, possibly due to the additional effect of changes in the PFJ contact area.

Tibial component design and bearing type will also affect the PFJ. Many studies do not report what type of bearing, whether CR or PS, fixed or mobile, has been used. This not only makes comparisons difficult, but also adds an additional uncertainty to other trends highlighted in this section and in review papers on the topic.

There is limited evidence that the use of a mobile, as opposed to a fixed, tibial bearing may cause a slight, but not significant, reduction in PFJ contact pressures [193]. The only study available which assesses this directly, has been performed on cadaveric specimens using a single implant without randomisation of the order of implantation for each test. Given that in this study the mobile bearing variant was consistently tested last, there is uncertainty as to the true cause of the observed reduction in compressive contact force.

Due to the increased bone and soft tissue removal required for the implantation of PS bearings as opposed to CR bearings, studies assessing the effect of bearing constraint on the PFJ suffer from similar issues relating to non-randomised experimental sequences. There is however, evidence that the use of a PS bearing significantly reduces the peak and mean pressures within the PFJ compared to CR bearings [25,26,119]. This may indicate that the post-cam system of PS designs induces posterior roll back of the femoral component. This would increase the PTMA, reducing the required quadriceps force, and hence the force within the PFJ. While contact force measurements are not available to fully evaluate this hypothesis, a reduction in the required quadriceps force for PS compared to CR knees has been established [31,202]. In addition it has been reported that larger quadriceps forces result from use of a highly conforming CS implant compared to a PS design [202]. This supports the assertion that it is the post-cam geometry and not the absence of a PCL, which affects the PTMA.

Despite significant geometric differences between the various commercially available patella components, and the substantial forces the PFJ is subjected to during activities of daily living [44], little research has been carried out to investigate the relative merits or effects of

different patella component design philosophies [16]. Few studies even specify the patella component type used during testing. Many studies purporting to investigate the effect of patella component design alter the femoral component as well as the patella component between trials, which does not allow comparisons of patella component designs [189,254].

Symmetric domed patellae are frequently reported to be easier to implant. Dome implants demonstrate less kinematic variability when subjected to malalignments than anatomic implants, but maintain significantly reduced contact areas, often displaying little more than point contacts [44,255,256]. Dome implants have therefore been shown to suffer from increased wear, compared to anatomic or medialised components due to higher contact forces and stresses [61]. This is supported by evidence from retrieval studies, which demonstrate that domed patella are often worn down to sombrero or medialised geometries [257].

2.6.4. Surgical Factors

Different philosophies are used in clinical practice to align prostheses during TKA surgery. Multiple studies have demonstrated that errors in the placement of the components occur irrespective of alignment philosophy due to human error, bone resection inaccuracies, and the effects of variations in the cement mantle [162,172,175-180,185-187].

Probabilistic analyses using a subject specific computational PFJ model have indicated that femoral transverse plane rotation of the femoral component, which has been linked to increased incidences of AKP [258], has a significant effect on PFJ mediolateral shear forces and kinematics [256]. It has been suggested that these affects are substantially larger than any seen following mal-placement of the patella component. However, the values of mal-placement modelled are relatively optimistic [256].

Investigations have demonstrated that internal rotation (IR) of the femoral component affects the flexion gap [259], causes lateral shifts of the centre of pressure, increased joint forces and induces an overall increase in patellofemoral contact pressures [28-30,260]. Conversely, femoral component external rotation (ER) has been shown to effect rotational laxity, cause joint opening [259] and again an overall increase in patellofemoral contact pressures [28-30]. The increases in pressures caused by rotation may be due to altered tibiofemoral angles, which alter the Q-angle, and hence the PFJ reaction forces [33,261,262]. However, the degree to which femoral rotation affects forces within the PFJ and the required quadriceps force is debated [216,261,263].

Peak pressures in the PFJ have been demonstrated to rise by up to a factor of 1.3 following 5° femoral ER and a factor of 1.7 following 5° IR and appear to be affected significantly by as little as 2.5° mal-rotations [29,264]. However, the studies carried out to date assess the effect of femoral rotation on the PFJ contact characteristics using sub-physiological loads and/or rigs which excessively constrain the knee joint [28-30,260]. It is therefore not possible to assess the degree to which commonly observed femoral rotation values will cause pressure within the joint to exceed acceptable levels during activities of daily living.

Alignment of the femoral component in the sagittal plane is harder to achieve (even with navigated surgery) than coronal or transverse plane alignment, and is therefore often the source of more substantial errors [172,177,179,180]. The effect of femoral component flexion or extension has been sparsely investigated. However, there is evidence to suggest that increased femoral flexion contributes to significant PFJ contact pressure increases. This is possibly a result of overstuffing of the PFJ [29].

Attaining appropriate tibial component rotation is challenging, with errors in excess of 25° frequently reported [162]. Excessive internal rotation has been clinically linked to increased incidences of AKP [258]. However, in contrast, *in vitro* studies have demonstrated that tibial rotations up to 15-20° have little effect on the PFJ and have significantly fewer effects on PFJ kinematics than comparable levels of femoral flexion [261,265].

Anterior mal-placement of the tibial prosthesis has also been demonstrated to cause relatively small increases in PFJ contact forces, pressures and patella bone strains. This is possibly a result of the anterior shift of the tibial component causing an alteration of the PTMA, and overstuffing of the PFJ [192,219].

The patella component can be malaligned mediolaterally due to surgical inaccuracy, or may be deliberately medialised by the surgeon in an attempt to better replicate natural patella geometry [31,266,267]. Several studies have reported reductions in the PFJ contact force and pressure in deeper flexion, following medialisation of as little as 4 mm [31,35]. The same studies reported an alteration in the location of the centre of pressure with medialisation [31,35]. In contrast, alternative studies have demonstrated little effect on PFJ and quadriceps forces of up to 5 mm of medialisation [33,38]. In terms of forces on the patella, a lateral shift of the patella by as little as 5 mm, has been reported to double shear forces on the patella when compared to a neutral placement [36]. The effect of mediolateral alignment of the patella may therefore be dependent on the implant design and possibly the approach used in the investigation.

The patella resection angle, or tilt, is a term which generally relates to the mediolateral angle formed by the resection cut and is likely to be fairly inaccurate as surgeons frequently choose not to use a template or jig to perform the resection. Patella tilt has been correlated to changes in PFJ kinematics [187]. Lateral tilt of the patella component has been shown to cause a modest increase in shear forces of 6.4% per 1° of tilt and have a corresponding impact on PFJ contact pressures, whereas medial tilting of the component appears to have a substantially reduced effect [35]. The greater effect of lateral titling may be, at least partially, explained by the natural tendency of the patella to contact more with the lateral shoulder of the trochlear grove due to the lateral force on the patella induced by the Q-angle of the quadriceps mechanism.

Changes to the patella thickness have been demonstrated to lead to reductions in joint contact area and increases in patella compressive forces [39-41]. A 2 mm increased thickness of the patella post-implantation may result in as much as a 174% increase in the PFJ compression force [39], which may result in increased levels of pain and/or wear. From a biomechanical perspective, a thicker patella could be considered beneficial due to the associated increase in the PTMA. This is however, only a benefit in early flexion, beyond which, the effects of changes in the patellofemoral contact point dominate. Throughout the flexion cycle the increased patella thickness causes an overstuffing of the joint, which over stretches the soft tissues and potentially leads to increased pressures and forces within the PFJ.

The superioinferior position of the patella relative to the TFJ is in part defined by the natural height of the patient's patella, which may naturally sit in an infera/baja (distal) or alta (proximal) position. However, it may also be artificially altered by a shift in the joint line due to incorrect levels of tibial and/or femoral resection or a proximodistal error in the placement of the patella component. Different methodologies and implants have been used to model patella height using alterations in different components; the patella position on the quadriceps tendon, the tibial bearing thickness and the patella component proximodistal position [37,38,96]. There is some evidence that an increasingly superior position of the patella relative to the tibia results in increased contact pressures and reduced contact areas [30] and an increase in the required quadriceps force, potentially, because it causes a reduction in the PTMA [268]. The increase in pressure and forces demonstrated with patella alta may also be a result of the increased patella height delaying the contact of the quadriceps tendon with the femur and hence the load sharing this provides. Conversely, inferior

placement has been shown to result in an 8% reduction in contact area for each 1 mm of mal-placement [35].

2.7. Summary of Main Literature Findings

The human knee is a complex structure comprising two intrinsically linked joints; the TFJ and the PFJ. The joints are restricted and guided by bony geometry and constrained by a complex array of soft tissue structures. Of the numerous structures which stabilise and control the joint, some of the most important are commonly considered to be the quadriceps and hamstring muscle complexes, and the cruciate, collateral and popliteofibular ligaments [47].

The patella affords a biomechanical advantage to the human knee; acting as a pulley to guide the quadriceps mechanism across the TFJ with minimal friction. It increases the moment arm of the quadriceps complex, reducing the amount of force required to achieve a given movement [44,60,61]. The patella also acts as a lever amplifying the quadriceps force, hence further reducing the required muscle force [61,96].

The PFJ is subjected to significant compressive joint forces. These are in part mitigated by high joint contact areas, and load sharing with the quadriceps tendon in deeper flexion, but can still result in significant contact pressures, often exceeding seven times body weight [1]. The PFJ is also subjected to shear forces and moments due to the bony geometry of the trochlear groove and the Q-angle of the quadriceps mechanism [44,57].

Modern kinematic theory proposes that, during the functional flexion arc, the TFJ flexes and extends about an axis coincident with the femoral cylindrical axis. The tibia simultaneously rotates longitudinally around a medial pivot point during active flexion with respect to the femur [50,92,93,95]. During the majority of the flexion arc, the patella flexes around an axis parallel to the tibiofemoral flexion axis with a lag of approximately 30° [114]. The patella also tilts and shifts during the flexion cycle as it tracks within the trochlear groove, and then into the intercondylar notch [44]. The exact patterns of patella motion are debated. The high variability in reported patella kinematics may be a result of the inherent joint instability, but may also be due to the wide range of methodologies and the assumptions that have to be made when assessing bone kinematics [118,221,222].

In the USA 11.5% of over 50's suffer from OA of the articulating surfaces of the TFJ and/or the PFJ [2]. TKA is a high volume surgical procedure aimed at reliving pain and restoring function for patients with severe knee disability as a result of arthritis [5]. TKA implant systems comprise tibial baseplate, polyethylene bearing, femoral and patella components. The tibiofemoral components of modern TKA prosthesis systems each have distinctly different design philosophies, but also many common design features and a shared general

structure. Patella component design is much more varied. The need, or appropriateness, for resurfacing the patella in TKA is also widely debated. Studies report increased incidences of AKP in patients who do not have the patella resurfaced, and increased rates of implant failure when it is replaced [8-12]. Randomised control trials and meta-analyses have however, so far failed to define standard guidelines [8-12].

Satisfaction following TKA is poor [46]; 32% of patients report pain and only 66% class themselves as "satisfied" [17]. Whether the patella is or is not resurfaced, the PFJ is a significant cause of pain, discomfort, instability, and failure following TKA. Patellofemoral complications are a primary indication in 20% of revision cases, [126] and more than 25% of patients, who have not had a full revision, have issues with high flexion activities of daily living, or report AKP [15].

AKP is poorly understood, but it is thought, in part, to be a consequence of excessive magnitudes or altered patterns of loading within the PFJ. This can cause cartilage deterioration in unresurfaced knees, synovial inflammation, and the stimulation of intraosseous nerves within the patella whether it has or has not been resurfaced [20-22]. It is therefore important to assess the changes in PFJ forces and pressures caused by TKA, in order to better understand the reasons for pain and functional limitations following TKA.

The pressures and forces within a joint are best assessed using *in vitro* methods. Fixed femur simulators can be used to assess the knee joint [23,25,26,202-204]. However, only OKRs allow the dynamic application of physiological forces and the simulation of body weight, whilst giving both joints in the knee full kinematic freedom [96,196-200]. The Kansas knee simulator may simulate more physiological knee joint loading patterns than OKRs, but it is significantly more complex and dependent on potentially unreliable input data [221,222].

OKRs are most commonly used with cadaveric specimens. Cadaveric specimens are good representations of the *in vivo* situation, but they demonstrate high inter-specimen variability and are often damaged by testing at physiological loads [31]. Synthetic bones are considered to be a good anatomical representations of human bone, have similar mechanical properties, and have been used previously in place of cadaveric specimens for biomechanical testing [211-213]. No previous study, using synthetic bones, has however attempted to model the passive soft tissue structures within the knee, such as the collateral ligaments, with anything more than a simple compressive force [211,212]. Using synthetic bone and tissue analogues, rather than cadaveric specimens, can reduce the inter-specimen variability and limit the introduction of multiple compounding factors. This may allow a more accurate and efficient

assessment of the effect of a single factor on the PFJ. However, any synthetic joint model will be substantially simpler than the human knee due to the absence or simplification of many important soft tissue structures. This must be borne in mind when extrapolating results to the *in vivo* situation.

Multiple quadriceps muscles of cadaveric specimens have been simultaneously loaded during *in vitro* investigations [39,101,116,194,206,225]. However, the dynamic actuation of the quadriceps mechanism as a single muscle is more common [23-26,61,190,192,193,201-204,217,218,223,225] and is more adaptable to studies which do not utilise cadaveric tissue [212]. The second major muscle complex, the hamstrings, is most commonly actuated with a constant tensioning force as two compartments because the natural muscle activation patterns are poorly understood [25,26,201,202,204,218,225].

It is well documented in previous *in vitro* studies that TKA results in an increase in PFJ contact pressure, and a reduction in the joint contact area independent of whether the patella is resurfaced or not [29,63,189,191,193,194,205,206,210,242]. This is likely to be a result of the PFJ kinematic changes induced by the alterations in surface geometry and materials associated with TKA. Patellar resurfacing is also widely reported to cause an increase in PFJ pressures, and a reduction in joint contact area, and may therefore increase the risk of pain within the patella bone remnant [29,63,189,191,193,194,205,206,210,242]. Following patella resurfacing, PFJ pressures in excess of 13 MPa, the offset yield stress of UHMWPE, have been reported [190,247,248]. Similarly, without resurfacing, the patella is subjected to peak pressures in the range of 9-12 MPa. This level of stress is sufficient to cause damage to the patella cartilage layer [244]. Patella resurfacing does not therefore appear to increase the risk of surface damage or wear within the PFJ. In line with survival and outcome studies [8-12], there is currently insufficient biomechanical evidence to guide best surgical practice regarding management of the patella.

Irrespective of the choice of patella treatment, the degree to which TKA affects the pressures and forces within the PFJ is highly variable [29,63,189,191,193,194,205,206,210,242]. This is in part due to the use of inconsistent investigative protocols, but also suggests that component design variations may have a significant impact. Modern implant designs allow for smoother patella tracking and as such are associated with reduced joint loading and pressures [205]. However, they are not true replicas of the natural situation [242]. The use of a single femoral condylar radius and/or a PS bearing has been demonstrated to result in reduced PFJ contact pressures [23-27]. It has also been suggested that anatomically shaped

patella components suffer from less wear than dome shaped components [44]. However, few other attributes of TKA component design have previously been studied.

Whichever implant design is used, there are a number of alignment philosophies that surgeons may choose to utilise during a TKA procedure. Each philosophy is open to error; surgical mal-placement of up to 6° in a number of orientations is commonly reported for each component [162,172,175-180,185-187]. Femoral internal and external rotation, of as little as 2.5°, has been demonstrated, in overly constrained and insufficiently loaded studies, to cause a significant increase in PFJ pressures [28-30]. Conversely, tibial internal and external rotation has been shown to have little effect on PFJ biomechanics [261,265]. Excessive femoral flexion has also been suggested to increase PFJ pressures, but an insufficient number of studies are available for review [29].

Patella component lateralisation has been linked to PFJ force and pressure increases, whereas medialisation may be linked to a reduction in joint forces and contact pressures [31,35,36]. Similarly, patella alta and increased patella thickness are associated with increased joint reaction forces [30,37-41]. The effect of other femoral, tibial and patella component mal-alignmentss has not been systematically investigated with respect to the biomechanics of the PFJ.

2.8. Literature Review Conclusions

The PFJ is a significant source of pain, a potential reason for persistent functional limitations, and a primary cause of revision following TKA. TKA alters the TFJ and PFJ surface materials and surface geometries, causes an increase in PFJ pressures, and is susceptible to errors in surgical component placement. Multiple *in vitro* methods exist for the investigation of the PFJ after TKA, but there is no consistent, standard protocol. Multiple investigations have therefore been carried out, using a variety of implants and a number of different protocols, making general conclusions hard to draw.

It can be concluded that the use of a CR bearing, a multi-radius femoral condylar design, femoral component internal and external rotation, patella component lateralisation, femoral component flexion and an increased patella thickness may increase the risk of PFJ complications, but the weight of evidence is far from compelling. Inferences regarding the effect of many other factors, such as patella implant design, cannot be made as the investigations simply have not been carried out. The systematic analysis of factors that may potentially influence PFJ biomechanics is needed to increase the general understanding of the effect of TKA on the PFJ so as to inform future implant designs and surgical protocols.

Traditionally PFJ biomechanics have been investigated using *in vitro* cadaveric investigations, but issues of high inter-specimen variability and tissue degradation may make the systematic assessment of such a large number of factors costly and impractical. Methods which do not include cadaveric tissue but utilise the well validated OKR and an appropriate number of soft tissue models may provide an efficient alternative for initial investigations into the factors which affect PFJ biomechanics after TKA.

2.9. Project Aim and Objectives

The overall aim of this research study was to gain a better understanding of the biomechanics of the PFJ and factors that may contribute to the high reported rates of PFJ complications following TKA. The risk of PFJ complications and AKP is hypothesised to be associated with changes in the biomechanics of the PFJ after TKA, which may originate from a multitude of factors related to the design and alignment of the implant components used in TKA procedures. In order to understand these complex issues fully, a large number of factors must be assessed. The development of a reliable standardised experimental protocol for the efficient analysis of the biomechanics of the PFJ was therefore a primary component of the research.

The overall project aim was addressed through completion of the following objectives:

1. Develop an *in vitro* human knee simulator, which enables the dynamic assessment of the PFJ after primary TKA.
2. Develop *in vitro* test methods to measure pressures, contact areas, and forces in the PFJ, as well as the quadriceps force and patella tendon moment arm during a dynamic knee movement.
3. Evaluate the effect of design and component alignment on the variables detailed in Objective 2.
    3.1. Evaluate the effect of patella component design.
    3.2. Evaluate the effect of patella component mediolateral placement.
    3.3. Evaluate the effect of femoral component transverse plane rotation.
    3.4. Evaluate the effect of femoral component sagittal plane rotation.

Chapter 3

Methods & Materials

3.1. Introduction

In order to achieve the primary study aim, and specifically fulfil objectives 1 and 2, it was necessary to develop a dynamic *in vitro* knee simulator and methods to accurately measure pressures, contact areas, and forces in the PFJ, as well as the quadriceps force and PTMA. Using cadaveric specimens within the knee simulator would have provided the most physiological test set up. However, cadaveric specimens suffer from a high inter-specimen variability and are commonly damaged under physiological loads [31]. Therefore a system, which allowed implant testing without the use of a cadaveric knee, was developed. The objective was to provide a structured testing system with good repeatability and reduced variability, which permits extended periods of testing under physiological loads [269].

This chapter details the development of the knee simulator and the associated measurement techniques to facilitate the physiological assessment of PFJ biomechanics. The results of preliminary studies carried out to enable the development of a soft tissue analogue to replicate natural soft tissue structures and assess the suitability of various measurement options are also discussed.

3.2. Dynamic Knee Simulator

The first objective of the research project was to develop an *in vitro* knee simulator to enable the dynamic assessment of the PFJ after primary TKA. Previous work within the Centre for Orthopaedics at the University of Bath, resulted in the development of a table top knee simulator designed for the assessment of hinged knee replacement systems. The axes of motion of this simulator were largely dictated by the mechanism of the hinged knee replacement. It did not require the simulation of any soft tissue structures other than the quadriceps.

The Scorpio NRG (Stryker, NJ, USA) primary PS fixed bearing TKR which is commonly implanted in the UK [122], was used for all investigations carried out as part of this study as it represents the first of an increasing generation of knee designs with a single radius femoral component. Further investigations must be carried out using alternative systems as well to facilitate the assessment of the effect of factors such as femoral component geometry, and assess the generality of the results but this is not an insignificant piece of work and was outside the scope of the present study. The assessment of the effect of alignment factors and patella geometry was prioritised over a comparison of a number of implant systems as such factors have rarely been systematically studied before. The Scorpio system is s supplied with

central and asymmetrical dome patella components. In order to incorporate this primary total knee replacement system, the original knee simulator required further development.

This sub-section discusses the pertinent features of the original simulator design and details the modifications which were required to facilitate repeatable and physiologically relevant testing of the Scorpio system. The necessary modifications included, but were not limited to, incorporating elements of the soft tissue envelope, simulating the flexor mechanism, and altering the ankle model.

3.2.1. Previously Developed Simulator

As part of a previous study carried out at the university [196,270], a knee simulator, based on the design of the OKR, was developed and built at the Centre for Orthopaedics at the University of Bath. Figure 3-1 highlights the principal details of the simulator design.

The hip and ankle joints were replicated by universal joints and axial rotation was allowed around the central longitudinal tibial axis. The action of a single actuator, which represented the quadriceps mechanism, dynamically cycled the knee joint through 20-90° flexion and extension of the TFJ. Each cycle took approximately 30 seconds. The simulator was designed to replicate an average UK female and a peak flexion moment of 40 Nm [196,270].

The simulator was designed for the testing of hinged total knee replacements, and facilitated testing of implants without any additional bone or soft tissue models, except those required for actuation. The patella and quadriceps tendons were modelled by a looped length of 3 mm steel cable attached to the tibial block via a pulley. The patella assembly, which secured the patella component, was clamped on to the steel cable. The femoral and tibial component stems were accurately placed using a bespoke alignment jig and secured using a low melting point alloy [196,270].

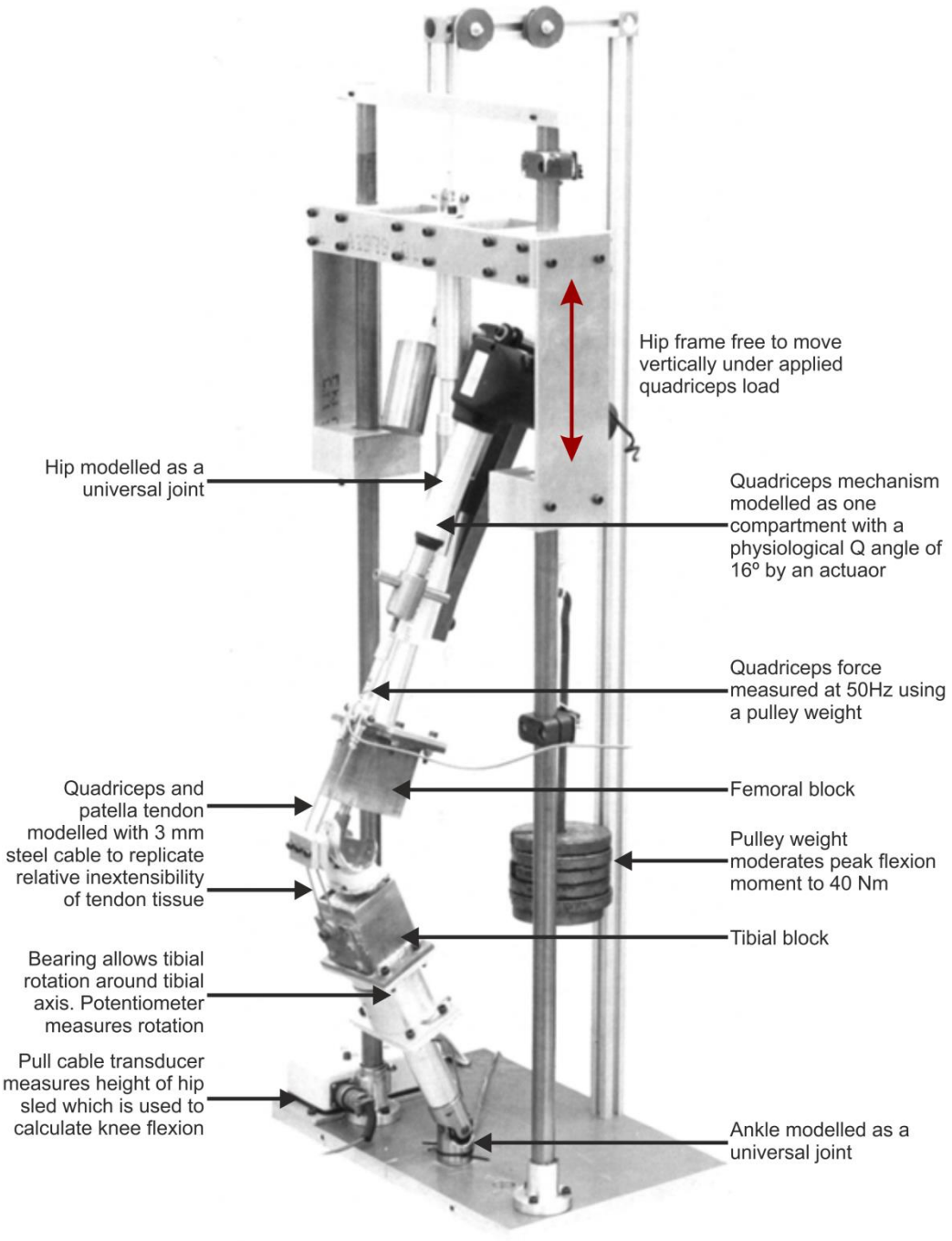

Figure 3-1: Previous Oxford Knee Rig developed at the University of Bath. Adapted with permission from: [196,270].

3.2.2. Structural Modifications

Initial analysis and testing indicated that two modifications were required to the structure of the simulator to provide a physiological and repeatable motion for this study.

The original ankle joint constrained tibial rotation around the central tibial longitudinal axis. In order to allow for the longitudinal axis of rotation to be defined by the prosthesis

geometry, the rotational bearing was relocated from the tibial shaft to below the simulated ankle joint. In this new configuration the tibial rotation could no longer be measured using the potentiometer which was employed in the previous study.

The original rig used brass bushings as a linear bearing surface for the hip frame assembly, which required constant application of lubrication to the shafts. This process was deemed to be inadequate for the purposes of the present study. The bearings and shafts were therefore replaced with linear ball bearings, and bearing grade steel respectively. The hip frame was also stiffened.

These modifications added weight to the structure and altered the frictional properties. The counter weight was therefore reassessed to ensure physiological loading levels were simulated. The final set up modelled a peak flexion moment of 43 Nm, which corresponds with the peak moment reported to be associated with an average UK adult female [1,59].

3.2.3. Component Mounting

Hinged total knee replacements are indicated for patients with severe soft tissue deficiencies. Their design incorporates a mechanical link between the femoral and tibial components [270]. The original rig therefore required no soft tissue restraints and relied on the mechanical link between the implant components to facilitate repeatable positioning.

Implantation of the tibial and femoral components on to synthetic bone models, which are fair representations of natural bones [211-213], provides anatomical reference points for the location of soft tissue structures. Therefore, for the present study, the size 7 Scorpio tibial and femoral components were implanted onto Sawbone (Sawbones Europe AB, Malmo, Sweden) medium composite tibia and femur replicas. The implanted Sawbone femur and tibia were then mounted onto the rig. The implantation process, which followed standard surgical practice, is detailed in Appendix B.

The femoral and tibial components of a primary total knee system are not mechanically linked. The existing method of alignment was therefore not appropriate for the present study. A new alignment jig (protocol for use detailed in Appendix C) was developed to facilitate the accurate location of the implanted tibial and femoral Sawbones within the simulator independently of each other (Figure 3-2).

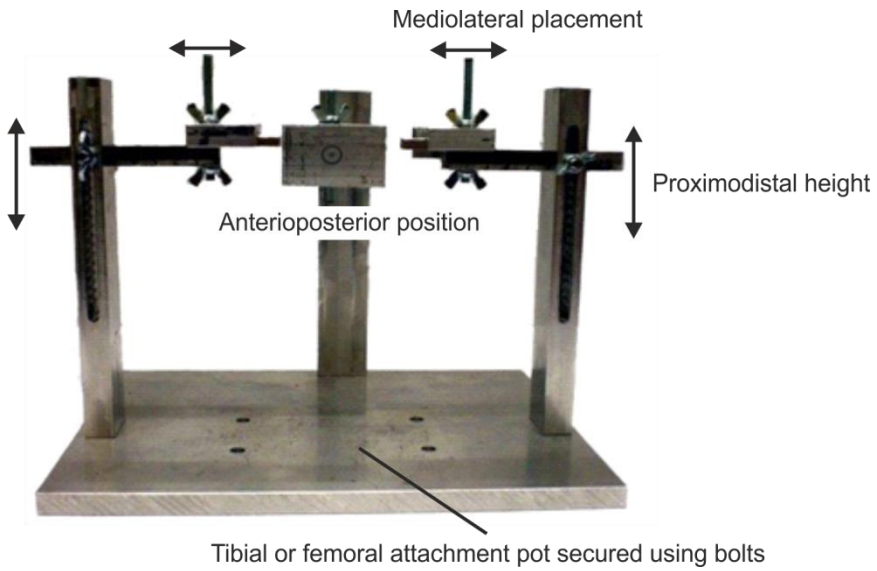

Figure 3-2: Alignment rig

Holes were drilled into the synthetic bone surfaces at known locations, which would not interfere with the joint articulation (Appendix B). Rapid prototype jigs were used to secure the synthetic bones so that the holes could be accurately drilled using a milling machine. Metal pegs were screwed into the holes and used as reference surfaces for the alignment of the tibial and femoral components within the alignment rig in terms of coronal plane rotation, sagittal plane rotation, proximodistal height, and mediolateral position. The remaining rotational and translational degrees of freedom were referenced using the posterior surfaces of the femoral and tibial components. The implanted synthetic femur and tibia were aligned to maintain a mechanical axis and comply with the standard operating procedures detailed by the manufacture.

This new alignment method was compared to the system used previously by Long *et al* [196,270] (Appendix D), and demonstrated to reduce quadriceps force and PTMA variability for the placement of a hinged implant (Quadriceps Force Standard Deviation (SD) (average over flexion range) 2.34 N for the new method compared to 2.78 N for the previous set up; patella tendon moment arm SD 0.2 mm for the new method compared to 1 mm for the previous set up). The new method was therefore considered sufficient to facilitate the repeatable placement of the implanted tibial and femoral components.

Given the focus on the PFJ of the present study, a method was also required to repeatably define the patella tendon length and hence the clamping position of the patella assembly on the steel cable which simulated the patella and quadriceps tendons. This is clearly not an issue of concern for cadaveric studies reported in the literature [37,38,188,189,205] and

previous studies which have not used cadaveric specimens do not report the method of location [211,212].

In the clinical setting, patella height, i.e. its proximodistal location in relation to the TFJ, is assessed radiographically. In order to allow comparisons and assessment across populations, various indices have been established. The most applicable method for this application is the Modified Insall-Salvati Index (Figure 3-3) [271,272].

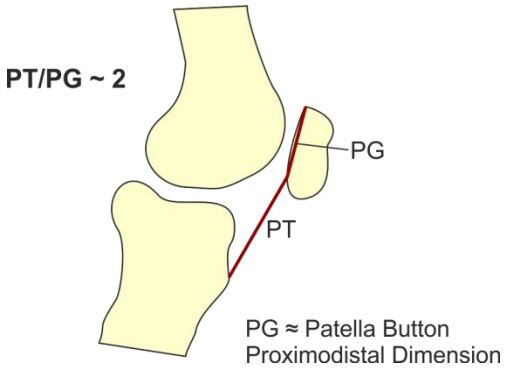

Figure 3-3: Modified Insall-Salvati Index [271,272]

The patella posterior proximodistal length (PG) can be approximated as the proximodistal measurement of each patella implant, which is known accurately. The patella tendon length (PT), the distance from the most distal point of the patella component to the centre of the distal pulley attachment, measured parallel to the steel cable which represents the patella tendon, can be assessed accurately using Vernier callipers. The patella tendon length (PT) should be maintained as twice the patella length (PG) to replicate a "normal" height patella. This can be measured at any tibiofemoral flexion angle.

3.2.4. Musculature Simulation

Motion of the human knee joint is driven and stabilised by a number of muscles. The most important are considered to be the quadriceps and hamstring complexes [47]. The majority of *in vitro* studies reported in the literature replicate the quadriceps mechanism but the hamstrings are commonly overlooked [24,96,101,110,111,199,200,211,214,229-232].

3.2.4.1. Quadriceps

The quadriceps mechanism used by the previous set up [196,270] was maintained. A webbing construct was added to the quadriceps tendon, to better distribute load when the tendon contacted the femoral component in deeper flexion. In line with Long's work, [196,270] the patella tendon was modelled with a loop of 3 mm steel cable attached, via a pulley, to the tibial tuberosity of the Sawbone tibia (Appendix B). Modelling the quadriceps as a single

compartment simplified the forces exerted by the extensor mechanism [47], but was comparable to multiple previous studies [23-26,61,190,192,193,201-204,217,218,223,225].

3.2.4.2. Hamstrings

The action of the hamstrings significantly affects the forces experienced by the knee joint during active motion [57]. It was therefore considered important to simulate their action in the present study. In line with previously reported studies, the muscle group was modelled using two constant force springs, each producing 50 N; one spring was designed to simulate the semi-membranous and the semi-tendinous muscles, and one the biceps femoris [201,204,218,223,225].

The available literature was collated to allow estimated ideal proximal mounting positions of the hamstrings to be defined (Table 3-1, Figure 3-4).

The actual mounting positions were adapted within the physical constraints of the simulator to ensure smooth operation. In line with previous work [201,204,218,223,225], and in the interest of simplicity, the proximal insertion of the short head of the biceps femoris was ignored. The final mounting dimensions, assessed using CAD software, are detailed in Table 3-1.

Table 3-1: Ideal and modelled hamstring proximal mounting locations (Angles relate to reference frame in Figure 20)

	Ideal		Actual
Biceps Femoris			
Proximal	29 mm medial, 44 mm distal and 61 mm posterior to the centre of the femoral head	[273]	49.36 mm medial, 43.5 mm distal and 61mm posterior to the centre of the femoral head
Frontal Plane Moment Arm	46.1 mm	[274]	47.86 mm
Sagittal Line of Action	-85° @ 0° Flexion	[275]	-84° @ 0° Flexion
Semi-tendinous and Semi-membranous			
Proximal	Same anterioposterior and proximodistal positioning and medial to Biceps Femoris	[273,276] [276]	89.36 mm medial, 43.5 mm distal and 61mm posterior to the centre of the femoral head
Frontal Plane Distal Moment Arm	28.2 mm	[274]	32.53 mm
Sagittal Line of Action	-102.5 @ 0° Flexion	[275]	-78° @ 0° Flexion

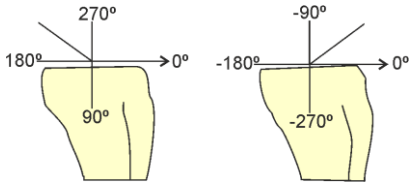

Figure 3-4: Reference frame used by Herzog *et al*. Adapted with permission from: [275]

Data on the precise location of the distal insertion points of the three compartments has not previously been published. The distal insertion points were therefore defined using anatomical descriptions in the literature [47] and anatomical landmarks on the Sawbone tibia (Table 3-2).

Table 3-2: Hamstring distal attachment point locations [47]

	Anterioposterior Positioning	Proximodistal Positioning	Mediolateral Positioning
Biceps Femoris	As close to the PFL as possible.		20 mm from the tibial lateral surface to simulate the fibula. (Bone cement was used to strengthen the structure)
Semi-tendinous & Semi-membranous	Posterior to the MCL attachment	As proximal as possible	As close to the bone surface as possible.

A preliminary study was carried out to assess the effect of the addition of the hamstring simulation on the measured quadriceps force. Tests were carried out using the Zimmer NexGen hinge prosthesis, which was positioned using the new alignment rig detailed in Section 3.2.3. The knee simulator was cycled against a peak flexion moment of 43 Nm and the quadriceps force measured for the third extension cycle. Two conditions were tested: Group 1: hamstring model not engaged; and Group 2: hamstring model engaged. Five repeats were carried out for each group, repositioning the components each time. Normality was demonstrated therefore the difference between the sample means was assessed using an independent 't' test ($\alpha = 0.05$). All statistical tests carried out as part of this research project were completed using SPSS (IBM, NY, USA).

The results indicated that extension required substantially greater quadriceps forces than flexion (Figure 3-5). In extension, the quadriceps actuator was working against the rig weight, the body weight simulation, and the friction of the bearings as they traversed along the shafts. The extension cycle can therefore be considered the worst case.

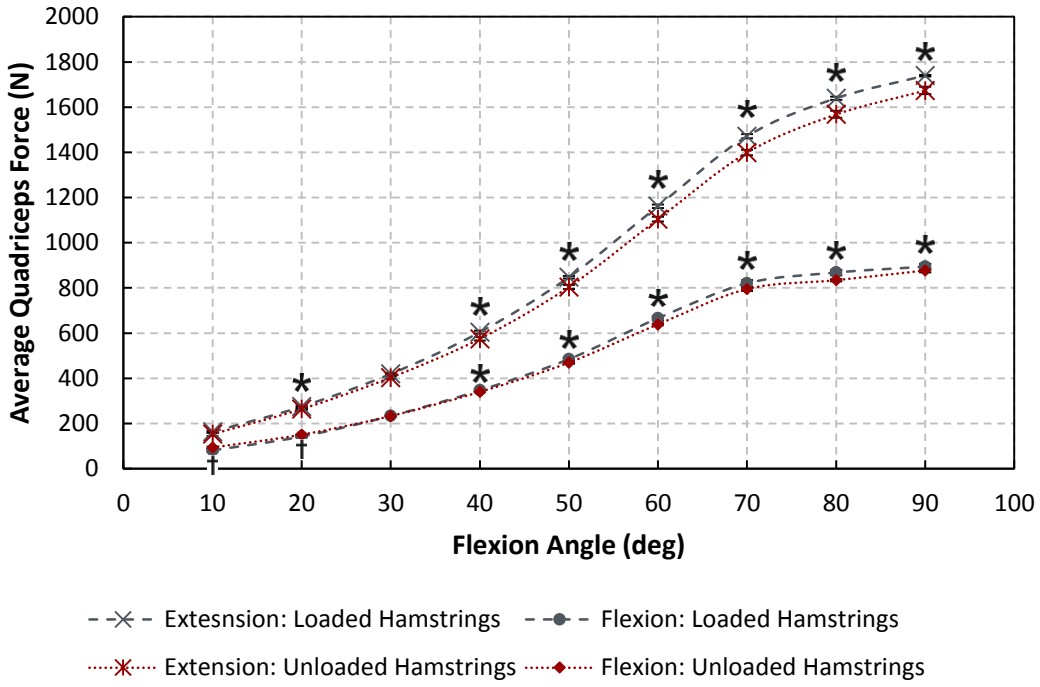

Figure 3-5: Comparison of average quadriceps force required to extend and flex the knee at a constant rate in a simulated squat. Error bars demonstrate standard error in measurement of the mean values. $p < 0.05$: * loaded force significantly greater, † unloaded force significantly greater.

In early flexion a greater quadriceps force was required when the hamstrings were not loaded (Figure 3-5). However, at all flexion angles greater than 30°, the quadriceps force required to extend the knee was significantly larger when the hamstrings were loaded (Figure 3-5). This corresponded with the results of cadaveric studies reported in the literature [204,218], and demonstrated that the simulated hamstrings were providing a flexion moment about the knee joint in a similar manner to the *in vivo* situation. The significant increase in measured quadriceps force could be hypothesised to equate to increased PFJ forces. This preliminary study therefore confirmed the importance of including a hamstring model when assessing PFJ biomechanics *in vitro*.

3.2.5. Ligamentous Simulation

The kinematics of the human knee are influenced by the action of a number of soft tissue structures. Following TKA, with a PS implant, the primary constraining structures are considered to be the MCL, LCL and PFL [212]. In order to maintain joint integrity, and ensure the replication of physiological knee kinematics, it was therefore important to simulate these structures. Previous models which do not include cadaveric tissue have simply replaced the action of the collateral ligaments with a compressive spring to prevent dislocation [212]. In order to simulate physiological kinematics of the knee joint [65,67,277], a ligament model

which better replicated the action of the MCL, LCL and PFL was developed for the present study.

3.2.5.1. Model Material

The LCL is slightly weaker than the MCL [67,209]. However, given the paucity of data relating to LCL and PFL properties in the literature, and the need for relative simplicity, a single synthetic model was developed [277]. Porcine MCL specimens have similar properties to human collateral ligaments [278]. Six porcine knees were therefore sourced from a local butcher. The porcine MCLs were dissected by an orthopaedic registrar and their mechanical properties assessed to provide a baseline for comparison with potential synthetic substitutes.

Testing of the porcine ligaments followed similar protocols to those reported in the literature so as to facilitate comparisons [65,278]. It is customary to assess cyclic creep, static creep and pure tensile loading. Given the dynamic nature of the rig, static creep was not considered to be relevant. A test protocol was therefore developed (Figure 3-6) to include cyclic creep and tensile testing to failure using an Instron Materials Testing Machine (Instron, High Wycombe, UK).

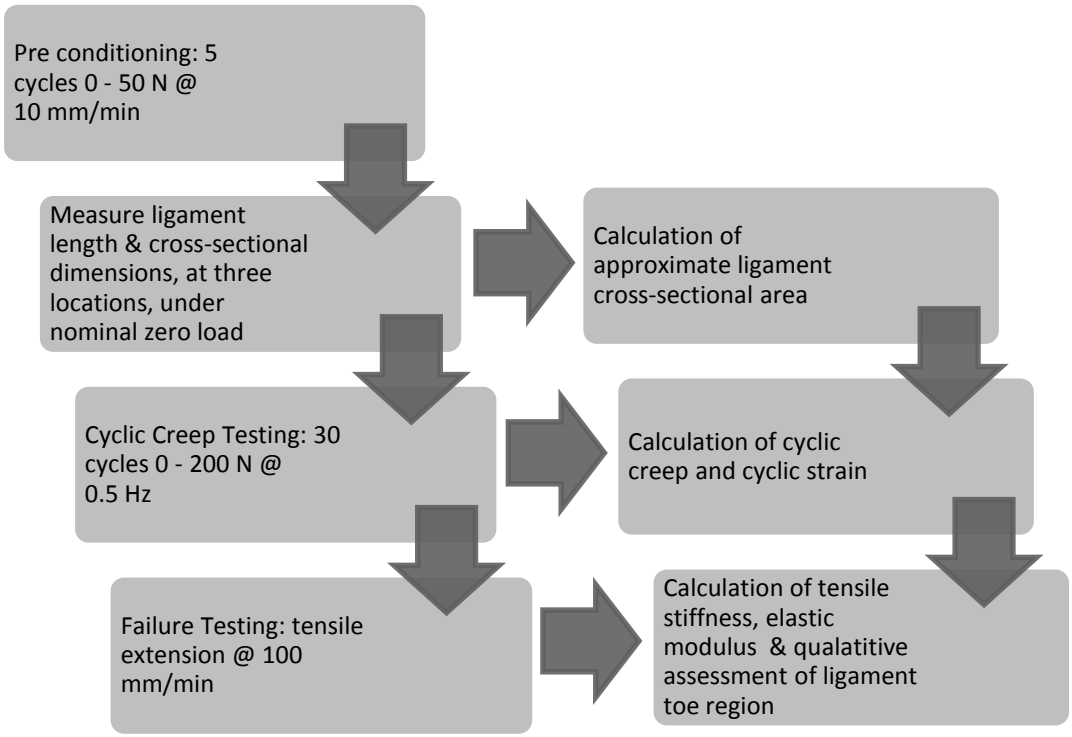

Figure 3-6: Ligament assessment protocol

In addition to porcine specimens, the LARS 80 (Corin Ltd, Cirencester, UK) synthetic ligament replacement system, designed for use as an ACL replacement, and eight cords and braids

sourced from local hardware stores were tested. Non-parametric Mann-Whitney U tests were carried out to compare each synthetic construct to the porcine control. No Bonferri correction was used as these were planned comparisons.

The synthetic materials were secured using standard hand tightened clamps (5 kN). However, purely hand tightening or using hydraulically tightened clamps around biological specimens has been reported to result in excessive damage at the clamp location [279]. Cryogenic clams, which had previously been developed at the university [279,280], were therefore used to minimise the risk of damage to the ligament (Figure 3-7).

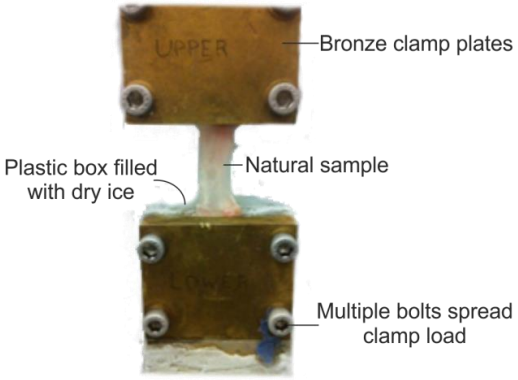

Figure 3-7: Cryogenic clamping of porcine MCL

The porcine specimens demonstrated 2.2 ± 0.6 mm (mean ± standard error) extension after 30 cycles of loading up to 200 N, which equates to 7% ± 1% strain. Tensile extension tests indicated that the porcine specimens had a tensile stiffness of 100 Nmm^{-1} ± 8.9 Nmm^{-1}. This value was comparable, in terms of order of magnitude, to literature values for both porcine and human specimens (Figure 3-8) [65,278].

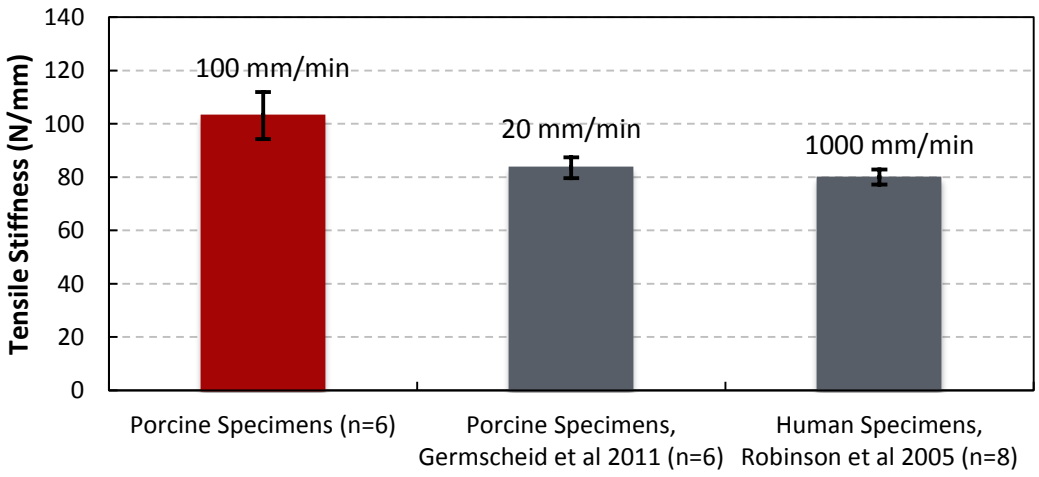

Figure 3-8: Tensile stiffness (Mean ± 1 standard error) of the porcine specimens shown alongside results of cadaveric human specimens [65] and porcine specimens [278]. The loading rates the tests were carried out at are also shown.

The porcine specimens had a toe region of approximately 3 mm (Figure 3-9). This was again comparable to that reported in the literature for human specimens [65].

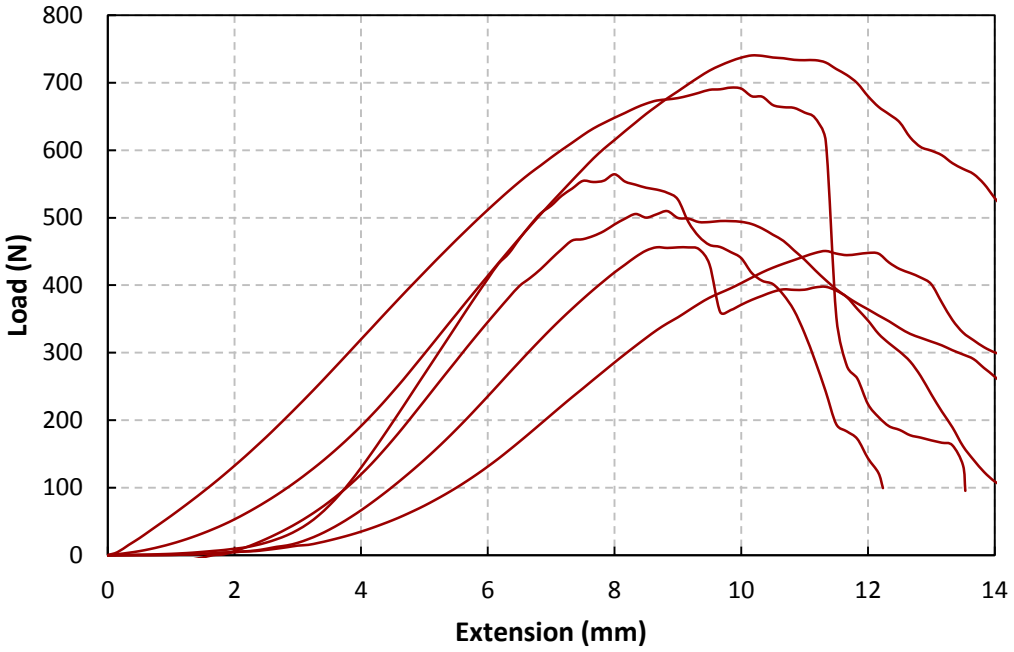

Figure 3-9: Load deformation curves generated from failure testing for pocine specimens.

The LARS analogue had a tensile stiffness nearly nine times that of the porcine specimens. It was not suitable for use as a kinematic model. Of the eight synthetic materials which were tested, three had tensile stiffnesses which were not statistically significantly different to the porcine samples ($p > 0.05$) (Figure 3-10): polyester braid, cotton cord and nylon cord.

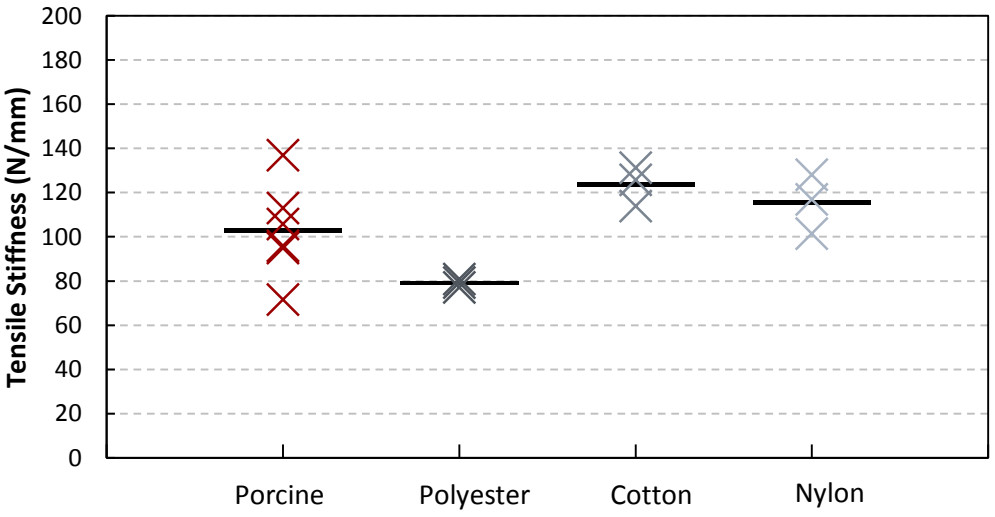

Figure 3-10: Tensile stiffness values for each porcine specimen and each synthetic material which did not show a statistically significant difference to porcine ($p>0.05$). Average values also shown.

An appropriate tensile stiffness is vital, therefore these three potential analogues were analysed further and the others discarded. None of the synthetic materials replicated the cyclic strain behaviour exhibited by the porcine specimens (Figure 3-11). Generally, kinematic test rigs are used for relatively few cycles and therefore replication of cyclic creep behaviour was not a high priority. The low recorded creep after 30 cycles for the synthetic materials may be beneficial, as it indicated that the properties of the material will not change greatly over multiple tests.

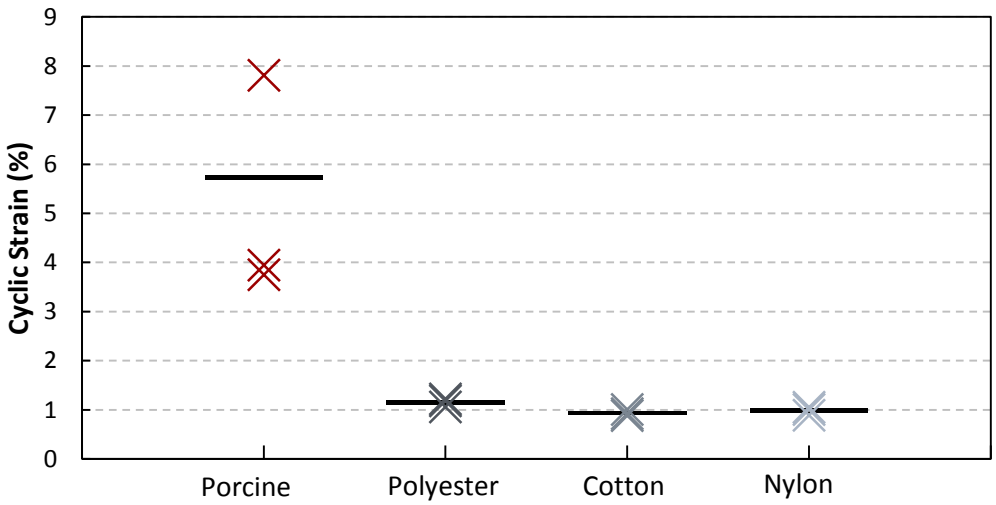

Figure 3-11: Cyclic strain values for each porcine specimen and each synthetic material which did not show a statistically significantly different tensile stiffness to porcine (p>0.05). Average values also shown.

The polyester braid demonstrated the most physiologically relevant toe region, falling completely within the range of porcine data (Figure 3-12). The polyester braid was therefore considered an appropriate synthetic ligament analogue for use in the present study.

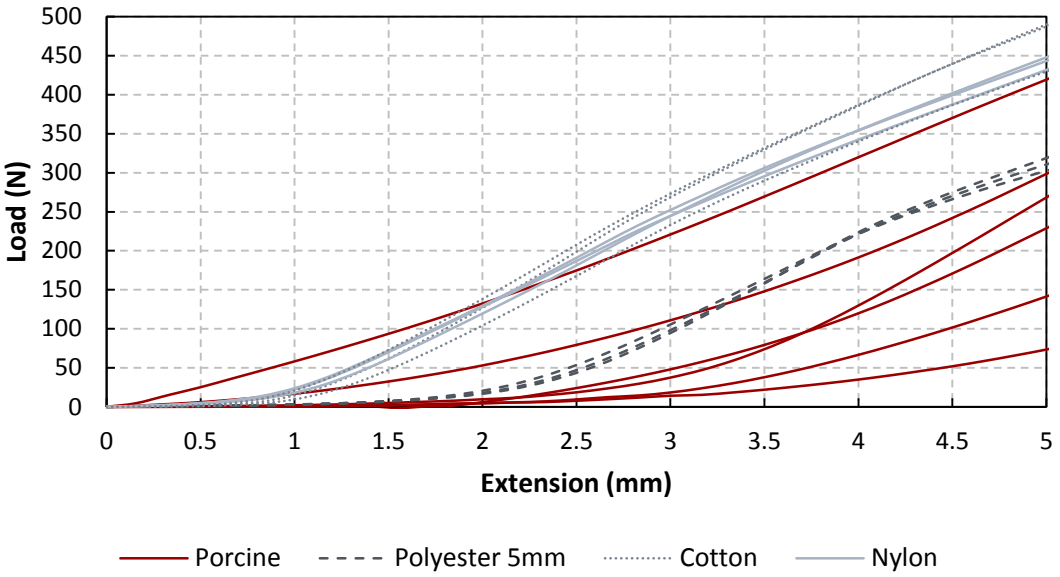

Figure 3-12: Load deformation curves generated from failure testing of each porcine specimen and each synthetic material which did not show a statistically significantly different tensile stiffness to porcine (p>0.05)

The synthetic ligaments were attached to the Sawbone tibia and femur using the method depicted in Figure 3-13.

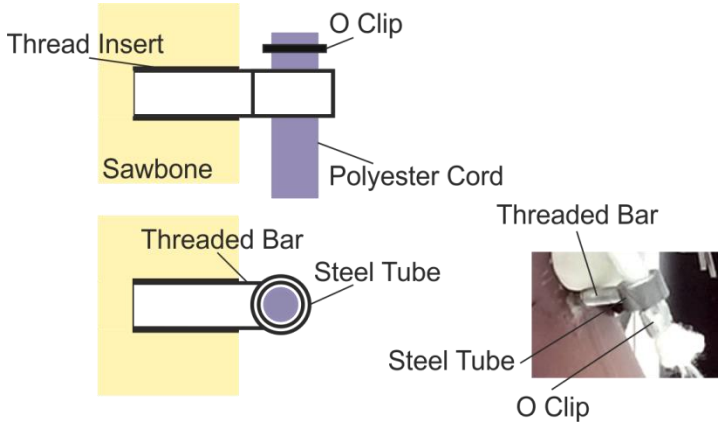

Figure 3-13: Ligament model attachment method

3.2.5.2. *Medial Collateral Ligament*

Measurements of the proximal sMCL attachment point relative to anatomical femoral landmarks have been reported in the literature [281,282]. These landmarks were not palpable on the Sawbone femur. Given that the MCL is isometric throughout normal ranges of motion of the knee, in line with the work of Colwell *et al* [216], it was therefore concluded that the axis of rotation of the ideally placed single radius knee joint would be an appropriate attachment point for the simulated MCL. Placement relative to the cylindrical axis of the femoral prosthesis negated some surgical placement errors and replicated a well-balanced resurfaced knee. Placement relative to the implant was achieved using a rapid prototype jig

produced using known implant dimensions. Proximally, the sMCL inserts directly onto the femoral surface. The ligament attachment was therefore screwed into the bone so that the steel tube locating the synthetic substitute was flush with the synthetic bone surface.

On the tibia, the sMCL inserts approximately 62 mm distal to the TFJ line [281,282], over a large surface area just anterior to the posteromedial tibial crest [55]. There is little other data available in the literature relating to the sMCL distal insertion point. During active flexion, the MCL has been shown to be isometric [66]. Given that the proximal insertion point of the MCL is modelled to coincide with the centre of rotation of the knee joint it was therefore considered appropriate to position the distal MCL attachment vertically below the proximal attachment when viewed in the sagittal plane with the knee at 0° flexion. This was achieved using a rapid prototyped guide to mark the Sawbone tibia an appropriate depth, based on anatomical studies in the literature [281,282], below the tibial plate top edge (34.7 mm). The mediolateral position was then determined using a plumb line, with the knee positioned within the rig at 0° of flexion. The ligament attachment was positioned flush with the tibial surface of the synthetic tibia.

3.2.5.3. Lateral Collateral Ligament

LaPrade *et al.* [69], indicated that the centre of the femoral insertion of the LCL is 1.4 mm proximal and 3.1 mm posterior to the lateral epicondyle. However, due to a lack of palpable landmarks on the Sawbone femur, dimensions referenced to the surgical epicondyle were difficult to replicate. It was therefore more repeatable, again in line with Colwell *et al.* [216], to link the LCL proximal insertion point to the centre of rotation of the single radius knee replacement. This was achieved using the method detailed for the MCL. The LCL proximal attachment was also positioned flush to the surface of the synthetic femur.

Distally, the LCL inserts on the fibula approximately 28.4 mm distal to the proximal tip and 8.2 mm posterior to the anterior margin of the head of the fibula [69]. The LCL has a 12° posterior line of action in the sagittal plane, when the knee is in 0° of flexion [68]. A rapid prototyped guide was again used to mark the Sawbone tibia an appropriate depth below the tibial plate top edge (44.35 mm) [69]. A 12° posterior line of action could not be fully realised due to the geometry of the Sawbone model. Instead, the attachment was placed as posterior as possible. The LCL inserts on the fibula rather than the tibia. The attachment screw was therefore positioned such that the steel tube location was 20 mm from the Sawbone tibia surface, to simulate the presence of the fibula. Bone cement was used to strengthen the structure.

3.2.5.4. Popliteofibular Ligament

Proximally the PFL does not have a bony insertion point, but rather forms a connection between the muscle-tendinous junction of the popliteus tendon and the proximal fibula [69]. It was not feasible to replicate this complex geometry on a synthetic model.

Surgeons also struggle to replicate this complex geometry when repairing it, and have therefore proposed many alternative methods. The modified Larson method (Figure 3-14) [73], involves reconstructing the static stabilisers of the knee, the PFL and LCL, but not the dynamic stabilisers such as the popliteus tendon. This method has been demonstrated, in cadaveric studies, to result in the recreation of a knee joint with appropriate laxity [73]. The modified Larson technique models the PFL proximal attachment as the popliteus tendon femoral insertion point.

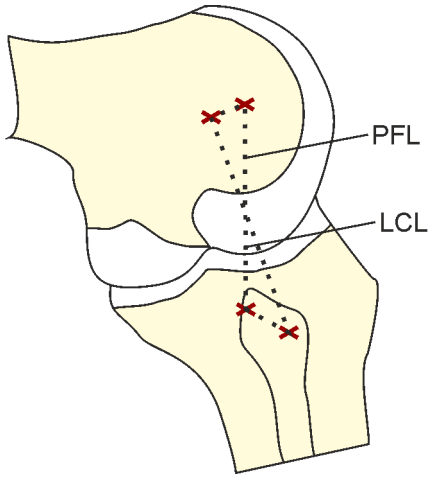

Figure 3-14: Modified Larson method of posterolateral corner reconstruction

A replication of the modified Larson technique is the most appropriate way to position the PFL and LCL on the model. However, given the space limitations on the synthetic model, this was modified slightly (Figure 3-15). The LCL proximal attachment point previously detailed was used for both ligaments, acting as a loop point. To model the natural attachment of the PFL to the tip of the posterior fibula, the attachment was placed as proximally and as posteriorly as possible and screwed in so that the steel tube location was 10 mm from the surface of the Sawbone tibia, to simulate the presence of the fibula.

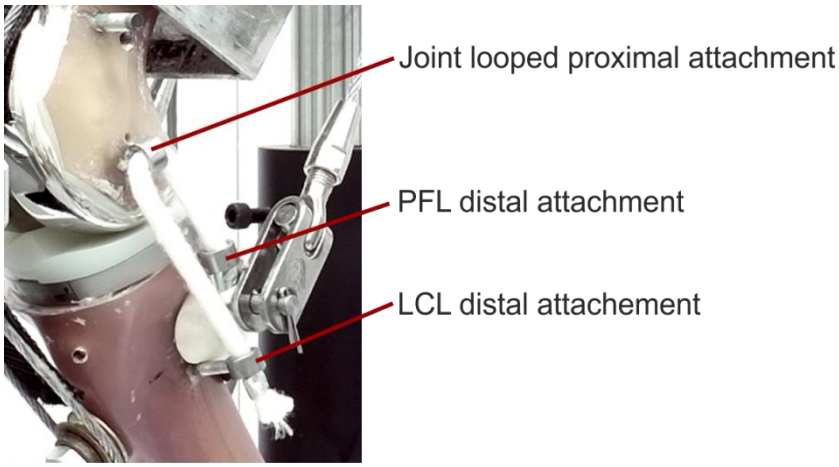

Figure 3-15: Modified Larson method employed on the rig

3.2.6. Allowances for Design and Position Variations

In order to fulfil objective 3 of the study a number of design and alignment factors which were hypothesised to effect PFJ biomechanics were investigated. The simulator was therefore adapted to allow the assessment of a number factors, specifically: patella component design, patella component medialisation, femoral component rotation and femoral component flexion and extension.

The patella components to be tested were placed on plates and located using the three polyethylene pegs on the back of the patella components which are used in normal practice to locate the patella during cement fixation. Multiple plates were produced to allow the assessment of different patella component designs. Each plate was designed to ensure that when placed optimally the centre of the polyethylene component coincided with the centre of the quadriceps tendon. Additional patella plates were produced to allow positioning of the symmetric dome component 5 mm medial of the centre of the quadriceps tendon.

The attachment of the femoral mounting box to the femoral shaft was designed with three locating screw positions to allow femoral transverse plane alignment to be altered from neutral to ± 5° rotation (Figure 3-16). Wedges were also designed, which modelled ± 5° flexion and extension of the femoral component. These could be placed between the femoral mounting box and the femoral shaft without altering the leg length.

3.2.7. Final Simulator Design

The knee joint simulator used for the present study and a summary of key details of its design, are depicted in Figure 3-16.

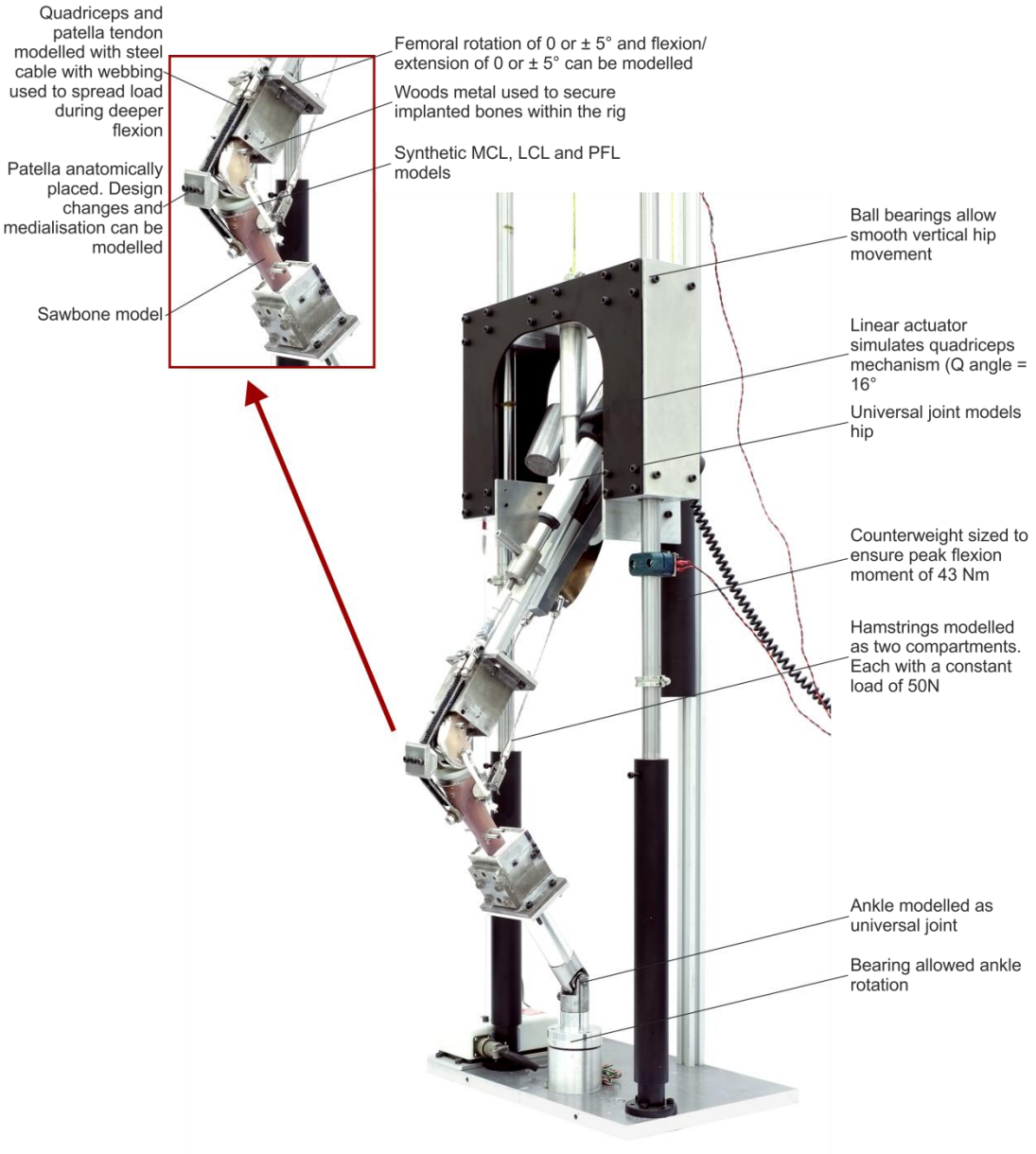

Figure 3-16: Final simulator

3.3. Outcome Measures

There are multiple variables that could be measured using the knee simulator (Figure 3-16) to assess the PFJ biomechanics. This sub-section will detail the measurement systems, which were re-used, modified or developed for use in the current protocol to measure the variables which were considered most important.

3.3.1. Flexion Angle

Flexion of the TFJ was important to monitor as it was against this parameter that all other variables were evaluated. The method employed by Long to monitor the flexion of the TFJ was maintained for this study [196,270]. The height of the hip joint relative to the ankle was measured using a pull cable transducer (VPA-40, UniMeasure, Oregon, USA). The transducer was connected, via an analogue-to-digital converter card, to a computer running Labview (version 11.0.1, NI, Newbury, UK), which allowed data collection at a rate of 100 Hz. The voltage output of the sensor was converted to length values (mm) using a calibration factor. Flexion angles were calculated using known implant dimensions and Matlab (Mathworks, Natick, Massachusetts) during post-processing of the data (Appendix E).

The calibration factor for the pull cable transducer was assessed by using an Instron Materials Testing Machine to extend the cable in steps of 75 mm from 0 mm to 375 mm five times. At each step the voltage generated by the sensor was recorded for a minimum of 5 seconds and then averaged. The method of least squares and the calculation of a weighted average was then used to calculate the gradient of the calibration slope and the uncertainty in this measurement [196]. The calculated calibration factor for the pull cable transducer was 106.8 ± 0.2 mm/V.

3.3.2. Quadriceps Force

The quadriceps force required by a patient to achieve a certain movement gives an indication of the extensor mechanism efficiency. It determines whether a patient will be able to carry out a motion or activity after surgery, as significant muscle strengthening, to levels exceeding those seen pre-operatively or in the healthy population, is unlikely [283,284].

Multiple studies have measured the quadriceps load using a load cell placed in series with the cable loading the quadriceps mechanism [23,24,61,96,199,202,236]. Long's work was no exception, and showed comparable accuracy to published studies [196]. The quadriceps force was therefore measured using the same method for this study.

The bespoke quadriceps load cell was connected, via an analogue-to-digital converter card, to a computer running Labview. This allowed data collection at a rate of 100 Hz in conjunction with the pull cable transducer.

The quadriceps load cell calibration factor was assessed using the same method as previously described for the pull cable transducer, with known loads applied using an Instron Materials Testing Machine. The calculated calibration factor was 520.8 ± 0.2 N/V for all tests reported here with the exception of the last two repeats for which it was 475.0 ± 0.2 N/V.

3.3.3. Patella Tendon Moment Arm

A greater PTMA may suggest the need for a reduced quadriceps force and may therefore be associated with improved patient function [44,60,61]. The PTMA also gives an indication of the seating of the patella component within the trochlear groove.

Long made use of a static 2D method for measuring the PTMA at 10° intervals using a single camera [196]. This method was used successfully, but is limited by the camera resolution, is highly sensitive to human errors in positioning the camera, and is not dynamic. It is also based on the assumption of a planar hinge joint. This assumption is not true of the natural knee, but following TKA, tibial rotation of less than 15° [285] is commonly reported. When considered mathematically, it can be shown that out of plane rotations of this magnitude (< 15°) will have minimal effect on the recorded 2D planar measurements.

Optical marker tracking is a method which has been used widely in a variety of disciplines to assess 2D and 3D motion [221]. 3D measurements require complex programming and multiple cameras [221,222]. Dynamic 2D measurements can be achieved with a single high speed camera, a series of black on white dots to act as markers, and a Matlab script.

A method to capture and analyse the movement of dots attached to the knee and calculate the required lengths and angles dynamically was developed (Figure 3-17). It was hypothesised that the new method, as well as being dynamic, was less prone to user error than Long's method [196]. Two preliminary experiments were carried out to test this hypothesis and assess the errors associated with the method.

Firstly, the PTMA of the Zimmer NexGen hinged knee system, mounted without bone or ligament models, was measured using Longs' static measurement method [196], and the new dynamic protocol. The measurements were repeated five times, repositioning the tibial and femoral components each time. Secondly, the knee was positioned statically at 10° intervals and the flexion angle and a known length measured using both methods. These values were

compared to those generated by the pull cord transducer and the use of Vernier callipers respectively. At each angle, ten images taken were taken with the high speed camera and five using the static method.

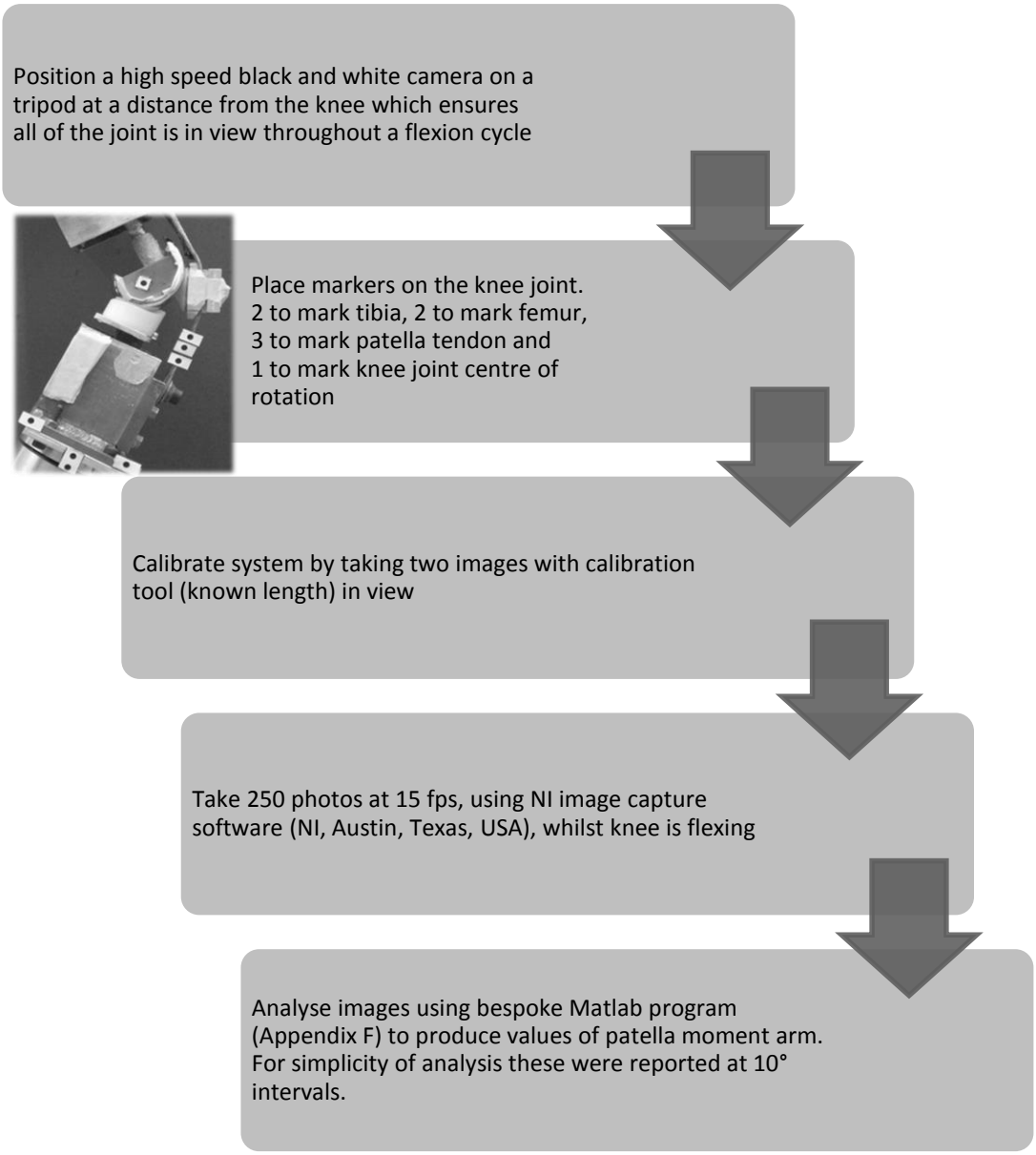

Figure 3-17: Patella tendon moment arm measurement protocol

The two protocols resulted in distinctly different absolute values for the PTMA, but followed similar patterns of change with flexion (Figure 3-18). Both methods demonstrated similar variability of approximately 2% of the measured value (SD: 0.75 mm (range: 0.48-1.63) for the new, dynamic, method and 0.79 mm (range: 0.37-1.17) for the original, static, method). In contrast, when assessing a known value the new method was substantially more repeatable (average SD of 0.07 mm and 0.78° verses 0.45 mm and 1.2°). The original, static

camera, method also consistently showed greater systematic errors than the new dynamic method (Figure 3-19).

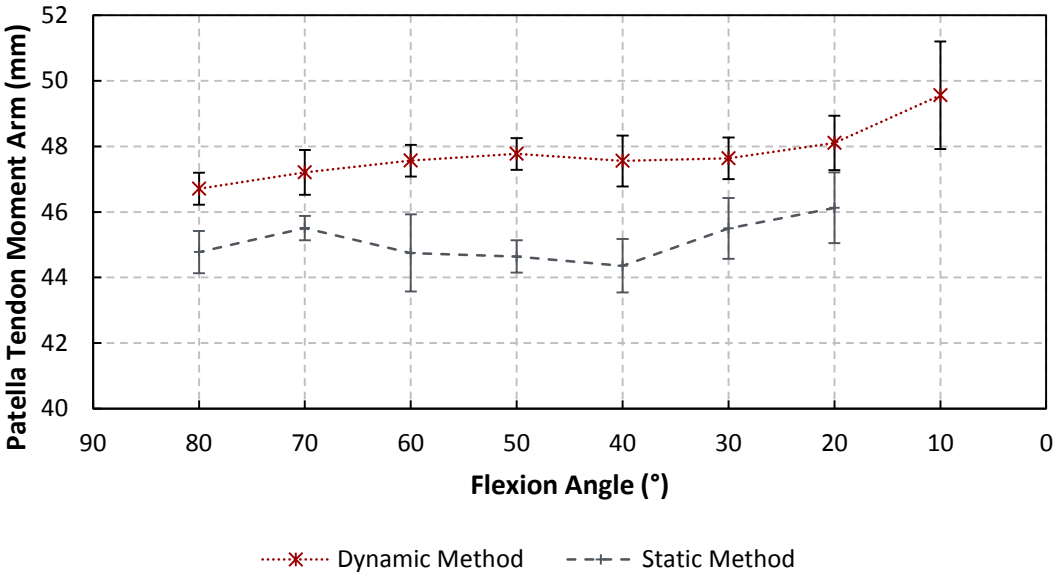

Figure 3-18: Average moment arm values over the flexion range (mean± SD).

Both protocols demonstrated varying magnitudes of error with flexion. As the systematic errors associated with the out of plane motions vary with tibial rotation it was difficult to assess the true error, the combination of the random and systematic, in the new system. For this study the true error was estimated by combining the random error and the systematic error (the average deviation from the absolute value) in quadrature. An estimation of the true random error was achieved by combining, in quadrature, the standard deviations from the two preliminary experiments [286]:

$$Random\ Error\ Distance = \sqrt{0.07^2 + 0.75^2} = 0.75mm$$

$$Random\ Error\ Angle = \sqrt{0.8^2 + 1.2^2} = 1.44°$$

$$Total\ Error\ Distance = \sqrt{0.75^2 + 0.03^2} = 0.75mm$$

$$Total\ Error\ Angle = \sqrt{1.44^2 + 0.45^2} = 1.5°$$

At any given flexion angle this may be a slight over or underestimate. However, it is sufficient to demonstrate that, in line with the camera resolution (0.5 mm), the method can be used to measure distances and angles with a resolution in the order of 1 mm or 1°.

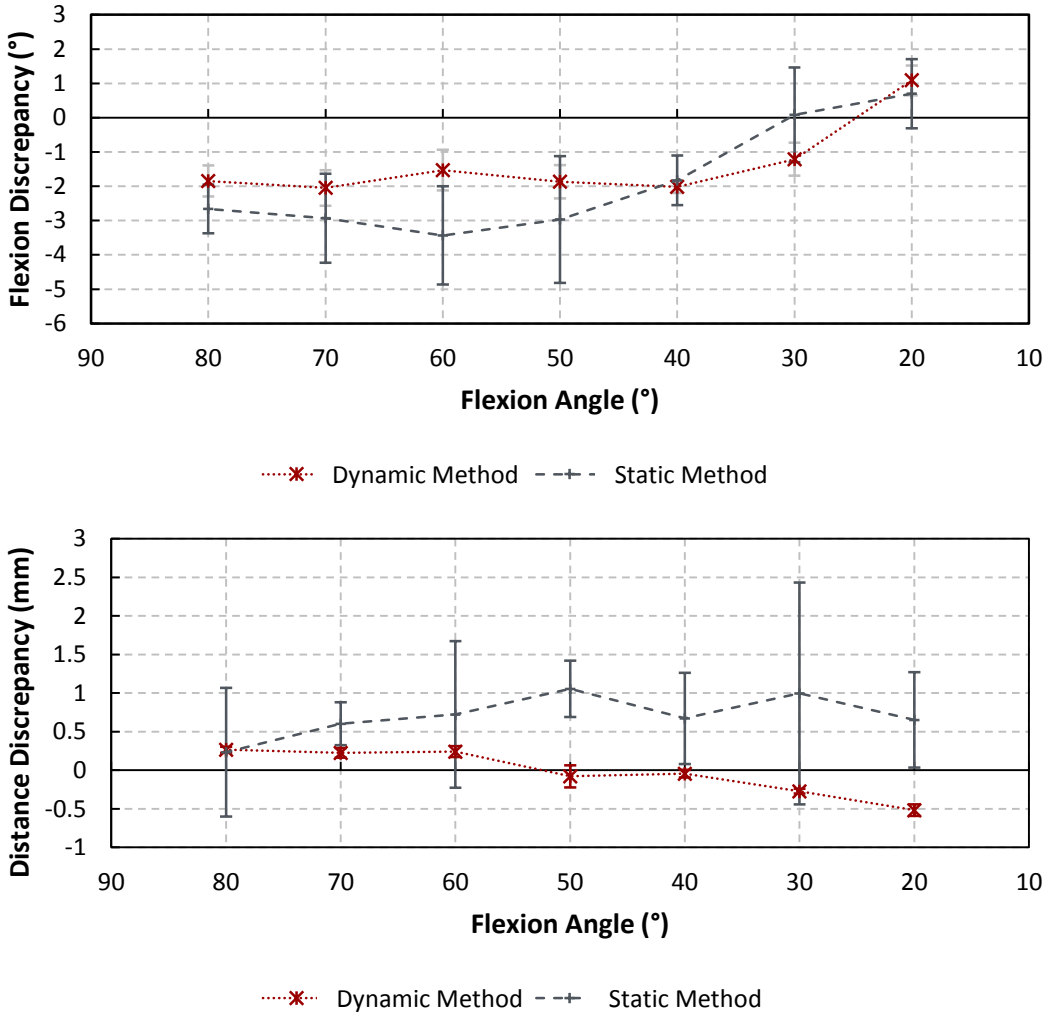

Figure 3-19: Top: Average flexion angle discrepancies. Bottom: Average distance discrepancies (mean ± SD).

3.3.4. Patellofemoral Joint Contact Area

The contact area within the PFJ is important to measure as it is intrinsically linked to the pressure within the joint and gives an indication of the PFJ congruency. The pattern of contact area also indicates the areas which are most at risk of deformation and long term failure and can be used to infer elements of the PFJ kinematics.

The contact area within articulating joints can be measured using a variety of methods. Early studies made use of dyes and rubber to statically assess the contact area within a joint [287]. In the 1980's Fujifilm (Europe GmbH, Düsseldorf, Germany) developed pressure-sensitive film, Prescale [287]. Prescale film comes in a range of grades each designed for a different pressure range. When subjected to pressure above a threshold, microcapsules within the film break down causing a colour change. The intensity of the colour change is related to the magnitude of the pressure applied. The film is less than 200 µm thick and can be cut to allow

a consistent, and compliant, placement over a curved surface, such as a patella. Prescale film is flexible and relatively cheap. However, it is limited to static measurements only [206].

The developed Prescale films can be scanned using a standard flatbed scanner [288]. The images can then be converted to greyscale and the number of pixels with an intensity above a certain threshold counted. Using a scale factor the number of pixels can be converted into an area value. This process was automated for this study (Appendix G).

In order to dynamically record contact pressures and areas, electronic pressure arrays must be used. These may be resistive in nature, such as the K-scan sensor system (Tekscan, Boston, USA) [189,191,193,205,243], or capacitive, such as the Pliance sensors (Novel GmbH, Munich, Germany) [63,194,210,243]. There are advantages and disadvantages associated with both types of sensors as assessed by Martinelli, et al. (2006) [243]. The K-scan system has a greater sensor density and is thinner, but is substantially less flexible than the Pliance system. This prevents the measurement of curved surface contacts without substantial buckling of the sensor [243]. The Tekscan system is also more expensive and less hard wearing. In situations where high shear forces may occur, such as the PFJ, the sensors may be damaged by as few as 16 cycles [287,289].

Although the Pliance sensor (Figure 3-20) is less accurate that the Tekscan system, and only functional at levels of loading substantially below those which are physiological (maximum pressure 2400 KPa), for reasons of cost, durability and pliability it was chosen as the most appropriate sensor which could be used within the present system.

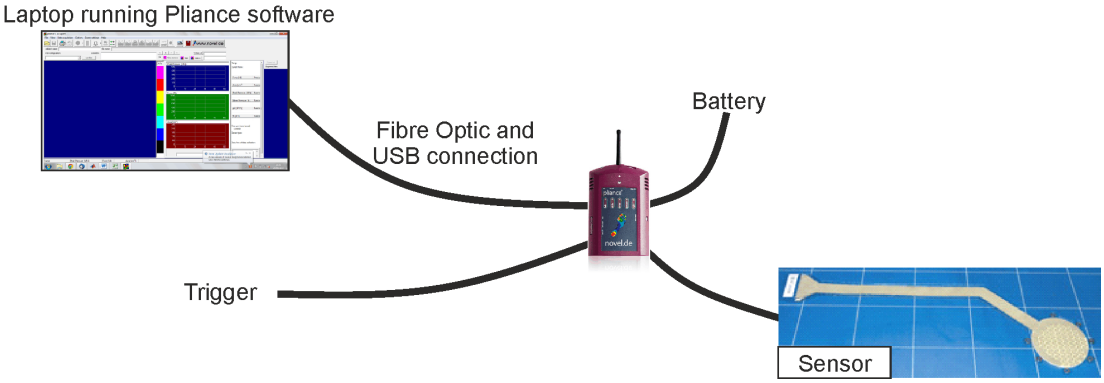

Figure 3-20: Novel Pliance sensor system

The 1.2 mm thickness and relatively low sensor density of the Novel system was hypothesised to result in measurements which over-estimated the contact areas within the PFJ. Fujifilm has been demonstrated in the literature to measure contact areas with an error of less than 7% [287]. In order to assess the accuracy of the contact area measurements generated by

the Pliance system a preliminary study was therefore carried out to compare static measurements of the PFJ contact area measured using the Pliance sensor and Fujifilm Super Low Pressure film. As a second objective, the contact area measurements achieved using the Pliance system under static and dynamic loads were compared.

The investigation was carried out using the model detailed in Section 4.2.7, Scorpio NRG PS components, and a concentric dome patella. Due to the reduced working loads of the Pliance system the tests were carried out at a significantly reduced load (peak flexion moment approximately 19 Nm). This was achieved by replacing the physiologically sized counterweight with a larger one. Protocols for the use of the sensors are detailed in Section 3.5. The quadriceps force and the PTMA were also measured. Six repeats were carried out repotting the tibial and femoral components between the tests. Wilcoxon signed ranked tests were used to assess differences between the results measured using different sensors, and under static and dynamic loads ($\alpha = 0.05$). Due to issues positioning the knee accurately at a given flexion angle, the sample number ranged from 3 – 6.

No statistical differences were reported between the quadriceps force and PTMA magnitudes or patterns measured under static loading using the Novel and Prescale systems (Figure 3-21 and Figure 3-22). This suggests that the insertion of the thicker Pliance sensor (1.2 v 0.2 mm) did not result in a significant change in the PFJ biomechanical environment.

The Pliance system appeared to measure the pattern of contact area changes with flexion appropriately, but overestimated the contact area magnitude by a factor of 10-15 (Figure 3-23). The Pliance system also demonstrated substantially larger measurement variability than the Prescale system (average S.D. 0.64 mm^2 v 0.07 mm^2). This was most likely a result of the poor sensor density associated with the system: each sensor segment has an area of 25 mm^2. For the purposes of this study, the Pliance system was therefore not considered suitable for contact area measurements within the PFJ.

The measured quadriceps force was substantially higher in deeper flexion under dynamic rather than static loading (Figure 3-21). The PTMA measurements did not however show any differences between the two loading situations (Figure 3-22). The contact area measurements recorded dynamically and statically also demonstrated no notable differences (Figure 3-23) indicating, as reported in the literature, that the presence or lack thereof of motion does not affect the PFJ kinematics [290], if the knee is allowed sufficient time to settle. Static contact area measurements can therefore be used as a surrogate for dynamic contact area measurements for investigations utilising this simulator.

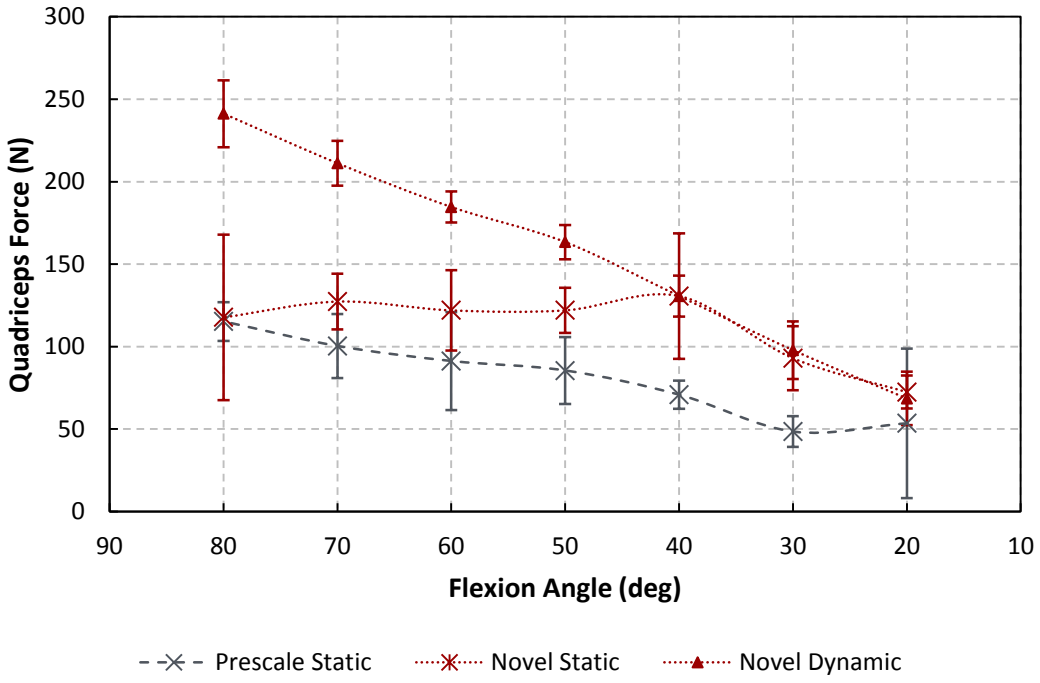

Figure 3-21: Quadriceps force measurements at 10° intervals of extension measured using different systems under static and dynamic conditions (mean ± SD).

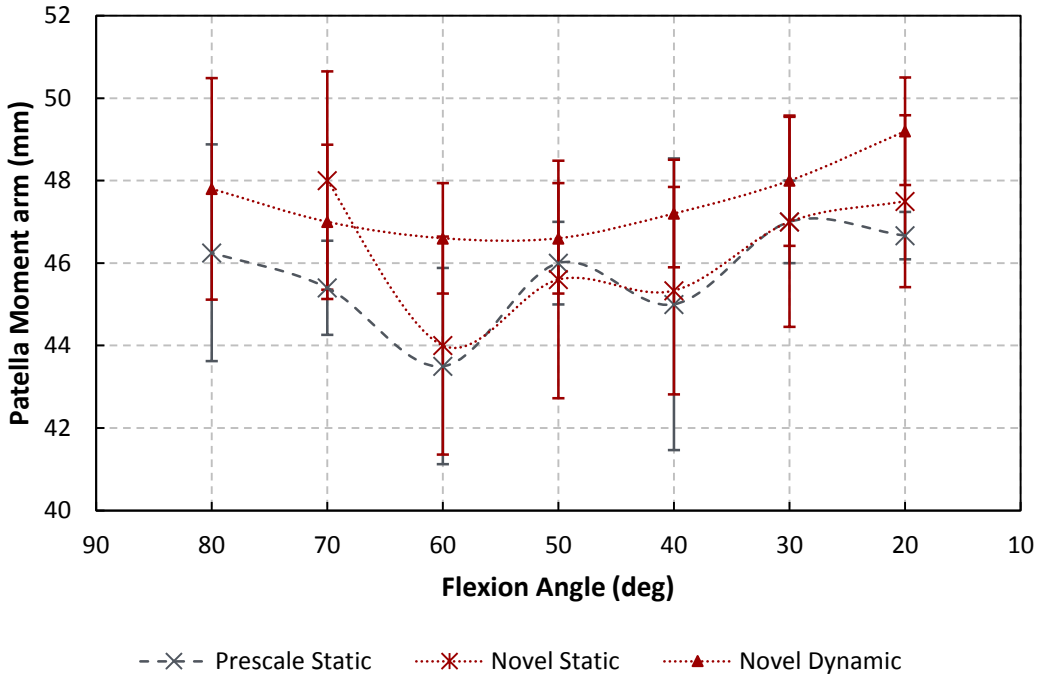

Figure 3-22: Patella moment arm measurements at 10° intervals of extension measured using different systems and under static and dynamic conditions (mean ± SD).

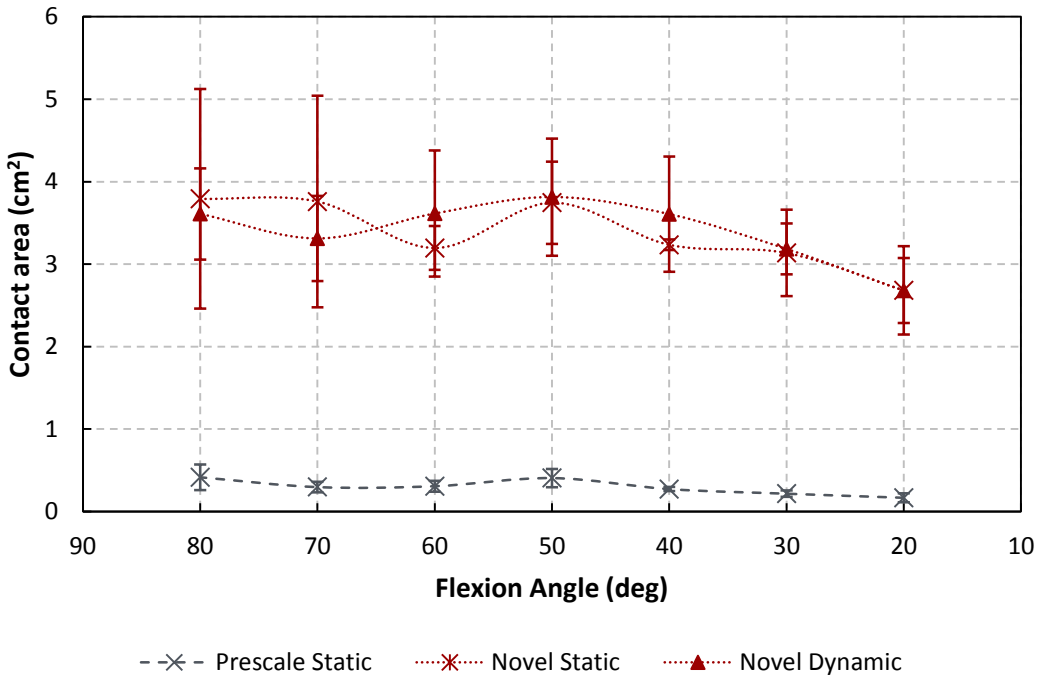

Figure 3-23: Contact area measurements at 10° intervals of extension measured using different systems under static and dynamic conditions (mean ± SD).

Based on this preliminary work it was concluded that Prescale measurements of the static contact area would provide the most accurate value for the dynamic PFJ contact area at 10° intervals. The Super Low Pressure film (measurement range of 0.5-2.5 MPa) selected for use at the levels of loading appropriate for the Pliance sensor can also be used to measure the contact area at physiological levels of loading. Excessive loading results in saturation of the pressured cells, but has been demonstrated in the literature to not distort contact area measurements [287].

3.3.5. Patellofemoral Joint Compressive Force

The magnitude of force that the patella component is subjected to is important to measure as it is intrinsically linked to the pressure within the joint and, when combined with the measured quadriceps force, gives an indication of the patella lever effect.

A load cell located behind the patella component has been used by multiple authors to dynamically measure the resultant force on the patella component and remaining bone [40,41,61,62]. Measurement of the forces in multiple axes would give the greatest understanding of the resultant load on the patella component and remaining bone. However, miniature three axis loads cells were expensive and too bulky to incorporate in the patella assembly. As, based on literature results, the major force component was expected to be

perpendicular to the patella component anterior surface [62], a single axis load cell was selected to measure the compression force.

The single axis load cell (Omegadyne INC, Ohio, USA), which was specified to allow up to 2.2 kN of load, was mounted in the configuration detailed in Figure 3-24. The load cell was connected, via an analogue-to-digital converter card, to a computer running Labview, which allowed data collection at a rate of 100 Hz in conjunction with the quadriceps load cell and pull cable transducer. The calibration factor was assessed using the same method as previously described for the quadriceps load cell. This factor was 207.0 ± 0.1 N/V for the first two investigations carried out as part of this study. For the third it was 218.3 ±0.1 N/V.

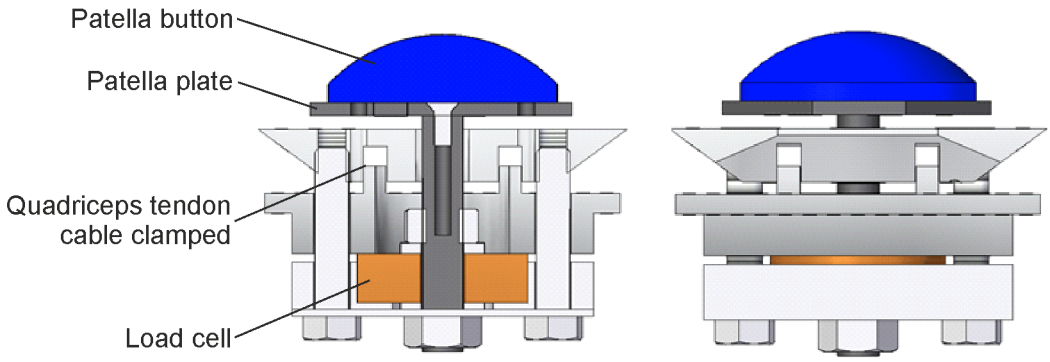

Figure 3-24: Patella configuration

3.3.6. Patellofemoral Joint Contact Pressure

The magnitude of contact pressure within the PFJ indicates the potential risk of the development of functional limitations relating to the PFJ as a result of excessive pain [20-22]. PFJ contact pressures in excess of the yield strength of the component material can also indicate the potential risk of long term plastic deformation and failure due to instability or patella component delamination [16,248].

The Prescale and Pliance systems have been used by multiple studies in the literature to measure the contact pressure within the PFJ [63,194,206,210,243]. The Prescale system can only be used statically, but the Pliance system can take dynamic measurements. Both systems can be used to assess peak and mean values and produce surface pressure maps. The Pliance system can also measure the centre of pressure.

Given the inaccuracies in the contact area measurements achieved using the Pliance system it was expected that the pressure measurements, in terms of magnitude, would also be erroneous and could not therefore be reported in good faith. In order to assess if the Prescale system was a credible alternative, the preliminary work discussed in the previous sub-section was re-analysed and the contact pressures recorded for each test calculated.

The Prescale system appeared to have been saturated throughout the flexion cycle (Figure 3-25). This may indicate that the film was inappropriately specified. However, based on visual observation it was concluded that surface imperfections and the relative stiffness of the articulating surfaces, caused localised stress peaks. The Prescale system was therefore also inappropriate for use as a system to measure the PFJ contact pressures in the present study.

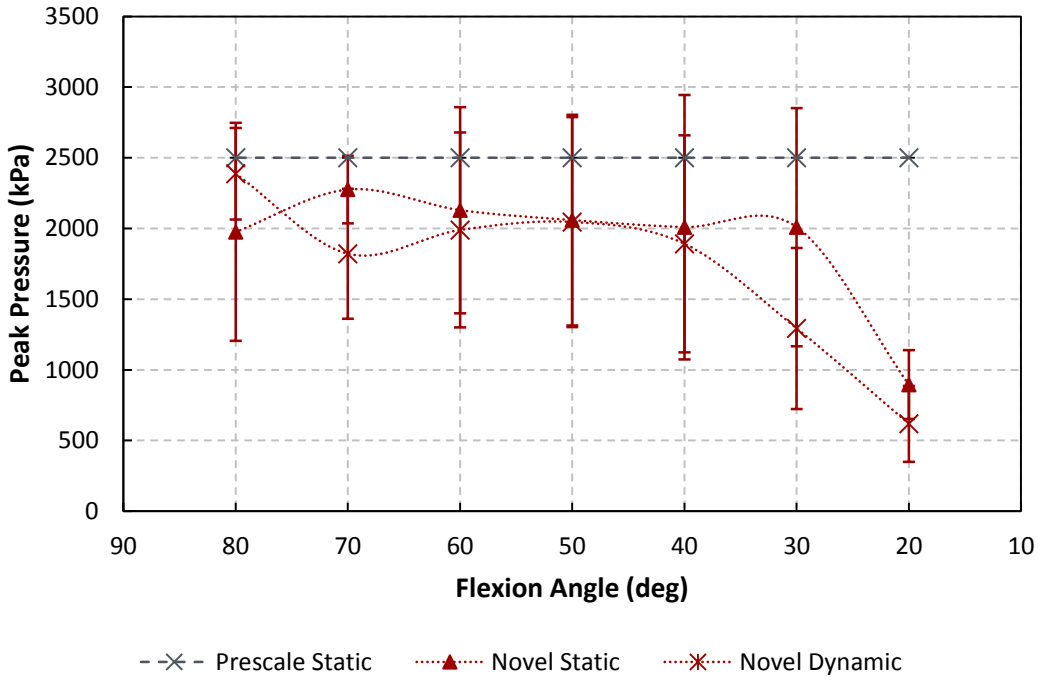

Figure 3-25: PFJ peak pressure measurements at 10° intervals of extension measured using different systems under static and dynamic conditions (mean ± SD).

If the patella component was assumed to be a rigid body and the compressive force assumed to be the largest component of force acting on it, the force measurements taken using the single axis load cell could be used as a surrogate for the contact force. It was therefore concluded that the most reliable, available, method to assess PFJ pressures in the present study was a calculation based on the measurement of the compressive force acting on the PFJ and the Prescale film contact area measurements.

The PFJ pressure values calculated using this method are not absolute values, as the resultant force vector on the patella component was unlikely to correspond directly with the measurement axis of the single-axis load cell. However, they could be expected to give a good indication of the magnitude of pressure the patella component and remaining bone were subjected to during the modelled activity.

The Pliance and Prescale systems demonstrated similar pressure distribution patterns (Figure 3-26). The Pliance system was therefore considered sufficient for use to explore pressure

distributions within the PFJ. The centre of pressure (COP) values produced by the system, were used to understand the transfer of load across different areas of the patella surface during the dynamic loading.

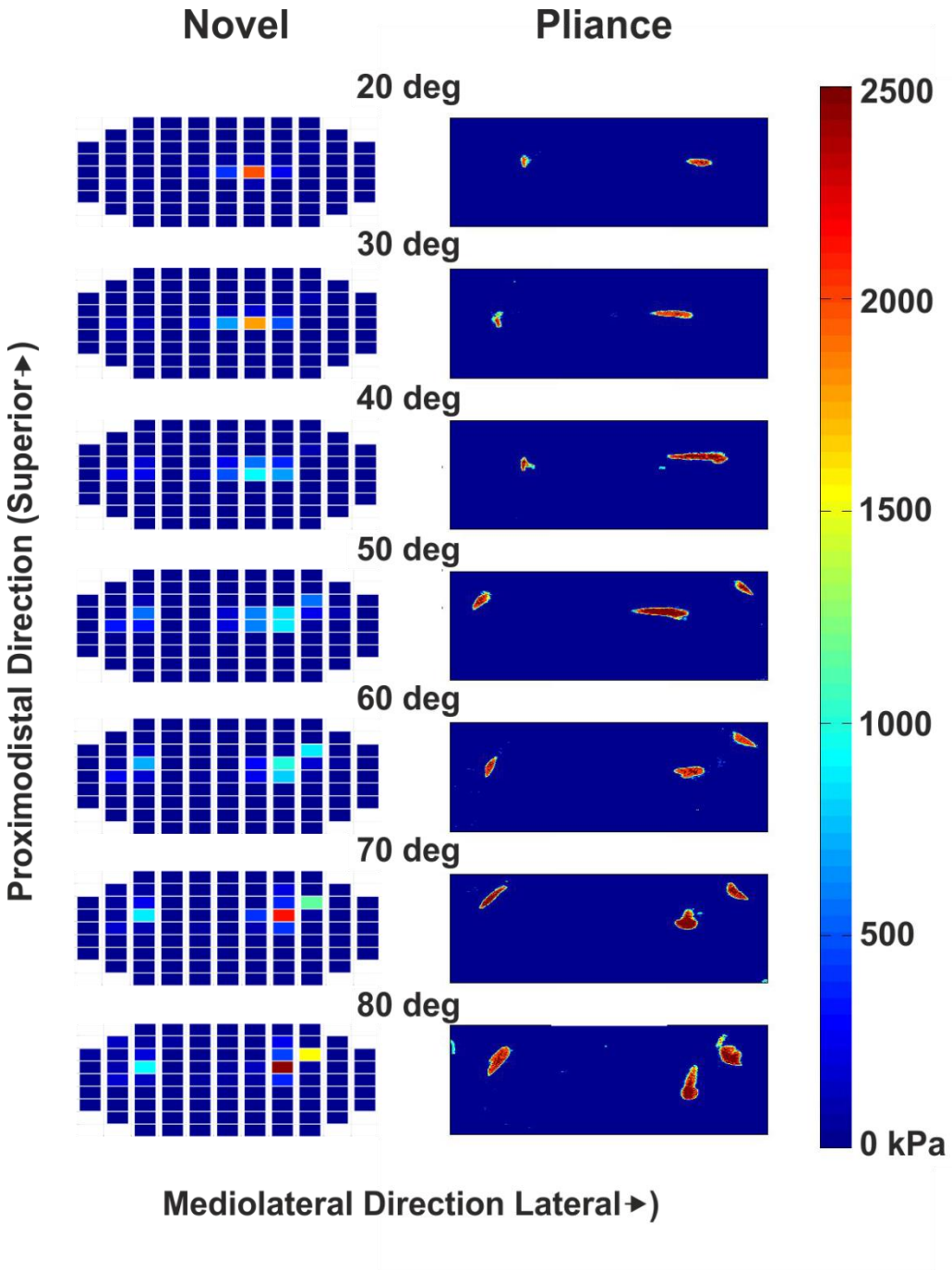

Figure 3-26: Example pressure maps produced using Prescale and Pliance systems

3.3.7. Surface Digitisation

During preliminary testing, anecdotal observations suggested that the UHMWPE patella components were subjected to a degree of plastic deformation during the testing process. It was not clear whether this deformation was occurring gradually, or was part of a bedding in

process. In order to assess this, a method was developed to measure how the surface geometry of each component varied during the study.

A desktop digitizer, Incise (Renishaw PLC, Wotton-under-edge, UK), which can produce surface maps of a variety of small geometries was used. Renishaw PLC developed a regime which allowed the progressive deformation of the patella components to be assessed during the study (Figure 3-27). This method involved digitisation of the surface profile of each patella component, and the production of a point cloud, before any use. The point cloud was converted into a surface profile. After each repetition of testing, the surface was again digitised and a surface profile generated. The different surface profiles were compared computationally and any differences represented graphically as areas of high or low surface deformation.

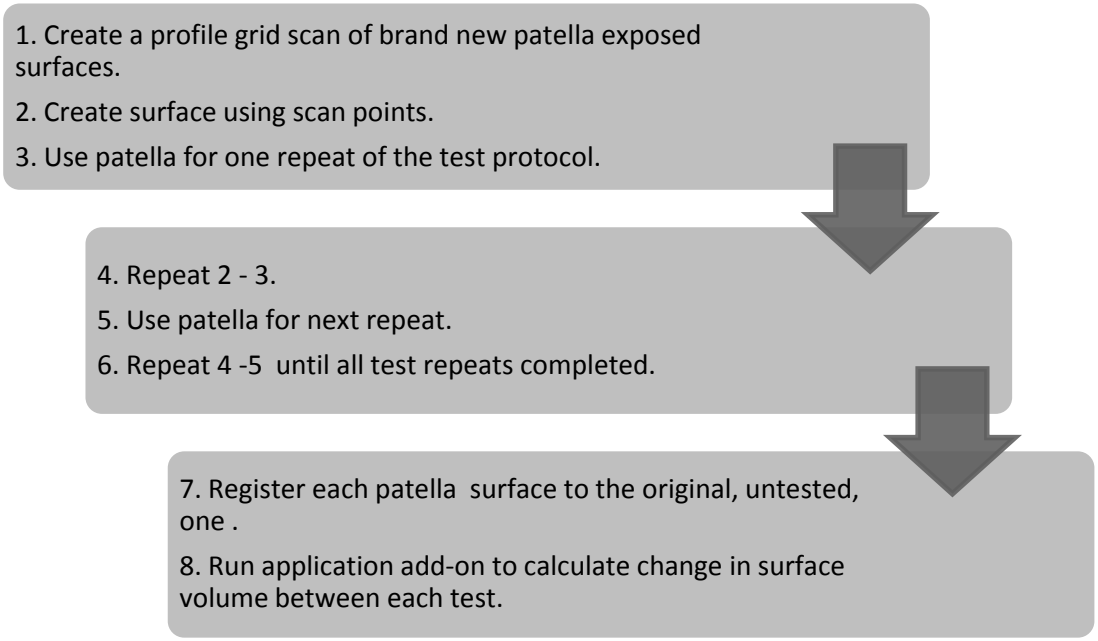

Figure 3-27: Digitization protocol

3.3.8. Summary of Study Outcome Measures

The output measures, which were assessed in the present study, are summarised in Table 3-3.

Table 3-3: Output variables for present study

Output Variable	Equipment/Method	Notes
Flexion Angle	Hip joint height relative to ankle height measured using Pull Cable Transducer. Distance values converted to flexion angle using Matlab protocol	
Quadriceps Force	Single axis load cell in series with the quadriceps actuator	
Patella Moment Arm	Dynamic measurement using single camera and marker recognition routine	Accurate to ± 1 mm & ± 1°
Patellofemoral Joint Contact Area	Prescale Film	Measured statically and assumed to be equal to dynamic contact area
Patellofemoral Joint Contact Pressure	$Calculated\ as\ \frac{Force: measured\ using\ Load\ Cell}{Contact\ Area: measured\ using\ Prescale}$	Calculated estimate
Patellofemoral Joint Pressure Map	Prescale Film	
Patellofemoral Joint Centre of Pressure	Novel Pliance System	
Patella Compressive Force	Single axis load cell	

3.4.Consecutive Cycle Assessment

Long's previous work carried out on the original knee simulator (Figure 3-1) only reported the results of a single motion cycle [196,270]. A small preliminary study was therefore carried out to confirm that there was no variation between the results of consecutive cycles and that therefore the measurement of one cycle was also sufficient when using the final, modified, simulator (Figure 3-16).

The quadriceps load for six consecutive dynamic load cycles was assessed using the Scorpio NRG PS system and a concentric dome patella component. In order to protect the patella component, the tests were carried out at a reduced level of quadriceps loading (peak flexion moment of approximately 19 Nm). Six repeated measurements were carried out repotting the joint between each repeat. A Friedman paired samples test was used to assess if there were any differences between the quadriceps forces for each consecutive cycle.

There were no statistical differences between the quadriceps forces recorded over six consecutive cycles (Figure 3-28). It was therefore acceptable to measure and report results of only one extension cycle.

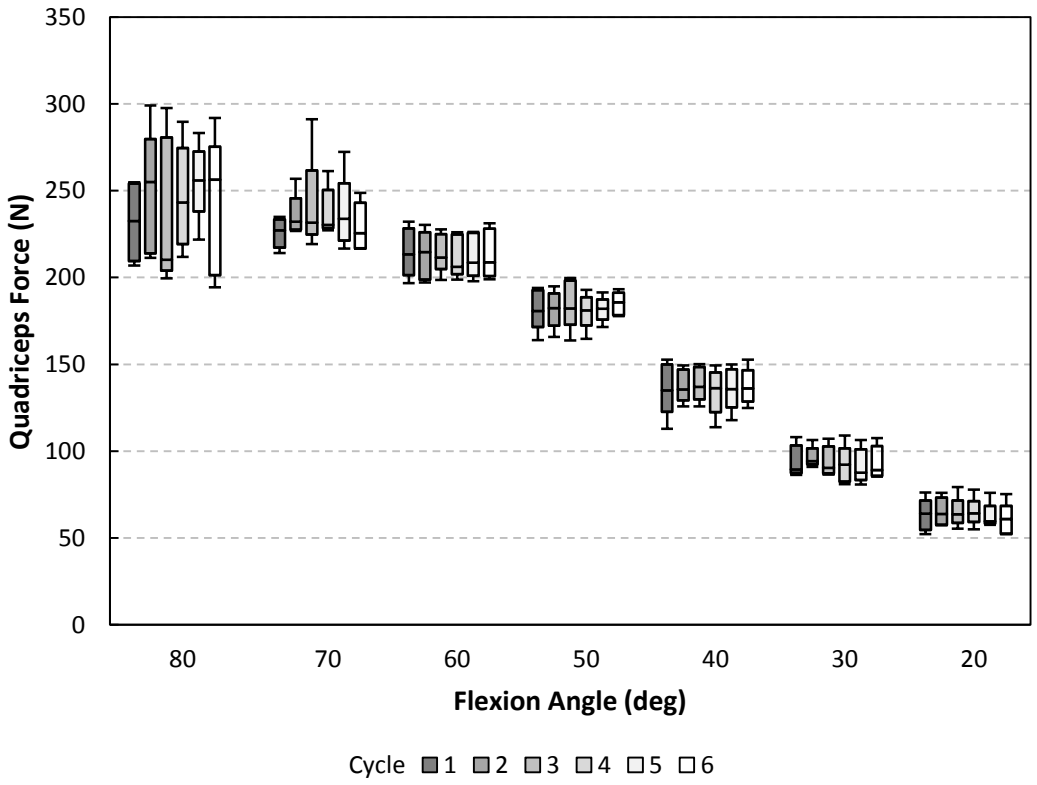

Figure 3-28: Average quadriceps force variation with flexion angle over six consecutive dynamic cycles

3.5.Final Protocol

Based on preliminary work the following protocol was developed to allow the accurate measurement of the variables detailed in Table 3-3. The protocol was used to carry out each repeat of all of the experiments detailed in the following chapters. The protocol assumes the two load cells and the pull cable transducer had previously been calibrated.

1. Prosthesis Mounting (See Appendix C for further details)

1.1. Set up mounting jigs

1.2. Position implanted tibia and femur

1.3. Secure tibial and femoral models with Wood's metal

2. Rig Set-up

2.1. Ensure patella plate matches patella component and patella mediolateral position to be tested

2.2. Ensure larger counterweight, which equates to 19 Nm peak flexion moment is attached

2.3. Bolt femoral and tibial mounting blocks to mounting plates. Attach ligaments with knee positioned at 90° flexion and no tibial bearing in place. When tibial bearing is then inserted a preload is applied to the ligaments to ensure they are operating within their linear region

2.4. Ensure femoral mounting block is at desired internal/external rotation and flexion position

2.5. Set quadriceps actuator and limit switch power supply to appropriate values for physiological testing speed [196,270]

2.6. Start Labview data capture program and set scale values (calibration factors) for the two load cells and the pull cable transducer

2.7. Position rig at 0° of flexion and ensure no load is transferring through the patella or quadriceps load cells. Set offsets in Labview program

3. Reduced Load Assessment Protocol

3.1. Apply adhesive to reverse of Pliance sensor surface. Place Pliance sensor onto patella component and affix firmly

3.2. Start Pliance X software program and record data for approximately 5 seconds while no load is applied to the sensor. Set this pressure map as "Zero" and subtract from future measurements to eliminate effects of the curved patella surface

3.3. Place rapid prototype centre marker on to patella and apply pressure. Record data for approximately 5 seconds and save as "COP reference". This will provide a COP

measurement, which can be used during the data analysis to recalculate all the test COP measurements in reference to the centre of the modelled patella

3.4. Apply grease to PFJ & TFJ articulating surfaces

3.5. Set up camera system and calibrate as detailed in Figure 3-17

3.6. Ensure limit switches are in the correct position to achieve desired flexion range

3.7. Carry out dynamic extension test. Position joint at 90° flexion and then record images, load cell data and Pliance data for one dynamic extension cycle

3.8. Remove Pliance sensor and clean grease from the PFJ

3.9. Reduce actuator power supply voltage to allow fine position control and position joint at a flexion angle of 90°

3.10. Carefully insert Prescale film into joint space and allow application of force for 5 sec before removing the film. Note the pull cable transducer reading. Repeat at 10° increments to 20° of flexion

3.11. Repeat dynamic and static tests as required for each test condition altering the patella condition, femoral rotation or femoral flexion as required

4. Physiological Loading Investigations

4.1. Use a jubilee clip to secure the hip sled and replace the large counterweight with the counterweight sized to ensure physiological loading

4.2. Grease the PFJ and ensure the patella condition, femoral rotation and femoral flexion are as required

4.3. Set quadriceps actuator power supply to appropriate voltage

4.4. Carry out dynamic extension test. Turn on actuator to begin cycling and then record images and load cell data for the third extension cycle

4.5. Clean grease from PFJ and reduce the actuator power supply voltage to allow fine position control and position joint at a flexion angle of 90°

4.6. Position joint at a flexion angle of 20° and carefully insert Prescale film into joint space and allow application of force for 5 sec. Note the pull cable transducer reading. Repeat at 10° increments to 90° of flexion

4.7. Repeat dynamic tests as required for each test condition altering the patella condition, femoral rotation or femoral flexion as required

Chapter 4

Experimental Investigations

4.1. Introduction

The primary objectives of the research set out in Chapter 3 (Objectives 1 and 2) and discussed in Chapter 4 were to develop an *in vitro* test methodology to efficiently assess a number of parameters influencing the PFJ during dynamic knee movement. These parameters included; quadriceps force, PTMA, patellofemoral compressive force, PFJ contact area and PFJ pressure.

To address the remaining objectives set out in Chapter 3 (Objectives 3-5), three separate studies were carried out, using the protocols developed, to determine the effect of; patella component design, patella component position, and the influence of femoral and sagittal plane rotations on the measured parameters.

Study (i) - The effect of Patella Component Design and Position

Three patella component design configurations were compared: two involved symmetric patella components, one placed in a central and one in a medialised position, and the third a centrally placed asymmetric patella component. Comparisons of the PFJ biomechanics measured for each scenario addressed Objectives 3.1 and 3.2. The results of this study were also analysed to assess the effect of applied load on PFJ biomechanics, the physiological relevance of the simulator and the variability in the measured parameters.

Study (ii) - The effect of Femoral Rotational Alignment Errors

Three femoral rotational alignment errors were compared to address Objective 3.4: 5° internal rotation (IR), optimal placement (as defined by the surgical protocol), and 5° external rotation (ER). A centrally placed asymmetric patella component was used for all of the tests.

Study (iii) - The effect of Femoral Sagittal Plane Alignment Errors

Three femoral sagittal plane rotations were compared to address Objective 3.5: 5° flexion, optimal placement, and 5° extension. A centrally placed asymmetric patella component was used for all of the tests.

All three studies included one comparable configuration; a centrally placed asymmetric patella component articulating against an optimally placed femoral component. The long term repeatability of the system was therefore also assessed by comparing these results from the three studies.

4.2.Study (i) - The effect of Patella Component Design and Position

4.2.1. Aims

This study focussed on the effect of patella implant design and patella component medialisation on the biomechanics of the PFJ during dynamic knee movements. The investigation aimed to assess the potential influence of patella component design and the effect of component medialisation on the risk of the development of patellofemoral issues and pain after TKA. An additional aim was to evaluate the influence of the level of loading applied to the knee during dynamic knee movements on the PFJ biomechanics.

4.2.2. Methods & Materials

This investigation was carried out with a Scorpio NRG PS fixed bearing implant using the simulator and protocol detailed in the previous chapter. The quadriceps force, PTMA, and patellofemoral compressive force were measured during dynamic knee motion under physiological (43 Nm peak flexion moment) and reduced (approximately 19 Nm peak moment) levels of loading. The PFJ COP was also monitored during the reduced loading tests. In addition, the PFJ contact area was measured during static loading at 10° intervals of tibiofemoral flexion under both levels of loading.

Three patella configurations were assessed; a centrally placed concentric dome patella component (*Concentric*), a centrally placed asymmetric patella component (*Asymmetric*), and a concentric dome patella component medialised 5 mm relative to the quadriceps tendon (*Medialised*) (Figure 4-1). Medialisation of 5 mm was chosen to replicate common surgical practice [31,266,267].

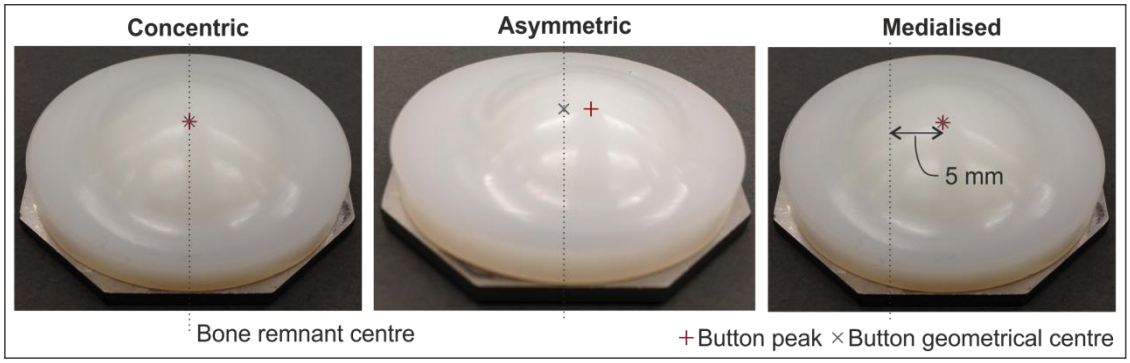

Figure 4-1: Tested patella configurations

Each configuration was assessed six times, repositioning the Sawbone tibia and femur between each experimental repeat. The order of the tests for the three patella configurations was altered for each repeat.

Only one new patella component was available for each of the patella configurations, each component was therefore subjected to six test sequences. In order to assess the effect of repeated testing the digitising protocol detailed in the previous chapter was used to map the surface profile before the testing began and following each experimental repeat.

4.2.2.1. Statistical Methods

A sample size of six was used for all configurations with the exception of the *Asymmetric* configuration under a physiological hip load, for which, due to a data collection error, only five samples were available. Data has been reported using mean ± standard deviation (SD) to give an indication of the variability. The standard deviation values for the reported percentage of lateral contact area were capped at 100% as this variable could not physically exceed 100%.

All data was assessed for statistical differences. The p values are not reported but when a difference was significant it has been highlighted on the appropriate graph. Non-parametric tests were used to assess differences between the configurations to reduce the threat of outliers within the relatively small sample. A paired Friedman test and, where appropriate, Wilcoxon signed rank post hoc tests, were used to assess any differences for each variable between the three patella configurations ($\alpha = 0.05$).

Where appropriate, the results were also normalised relative to the results at 20° flexion of the TFJ. Differences between the normalised results at the two levels of loading (43 Nm and 19 Nm peak) were assessed using Wilcoxon signed rank tests ($\alpha = 0.05$).

4.2.3. Results

4.2.3.1. Quadriceps Force

Quadriceps force is commonly measured when assessing TKA implant systems in *in vitro* studies as it directly impacts the patient's ability to carry out activities of daily living. An increase in the required quadriceps force to complete a task at a given speed, or under a specified load, implies an increased requirement in terms of quadriceps strength requirement. Elderly patients are unlikely to be able to complete extensive muscle strengthening exercises and thus any increased muscle strength requirement may result in them being unable to complete a task [283].

Measurements during this study were taken during extension of the knee joint from 90 to 20° of flexion. All of the graphs presented in this thesis are therefore reported with a reversed x-axis to indicate the direction of motion. The measured quadriceps force (QF) for all of the

patella configurations decreased non-linearly with extension under both levels of loading (Figure 4-2). Medialisation and the assessed difference in patella component symmetry had few statistically relevant effects on the measured QF.

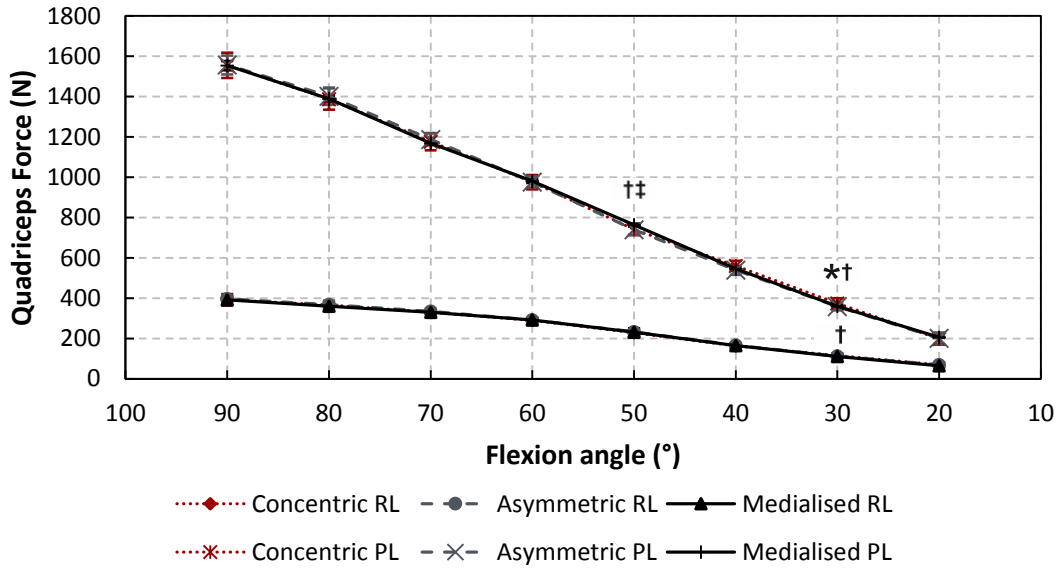

Figure 4-2: Variation in quadriceps force with flexion angle for each patella configuration (mean ± SD). RL: Reduced Load; PL: Physiological Load. $p < 0.05$: * Concentric vs Asymmetric; † Concentric vs Medialised; ‡ Asymmetric vs Medialised

Irrespective of the patella configuration, the decrease in measured QF with extension was more pronounced under the physiological load. Between 90° and 20° of flexion, the QF decreased from 1555.2 ± 51.5 N to 201.7 ± 25.1 N under physiological loading and from 393.3 ± 20.7 N to 67.5 ± 10.5 N under reduced loading. This equated to a reduction by a factor of 7.8 ± 0.9 under physiological loading compared to only 5.9 ± 0.7 under reduced loading (Figure 4-3).

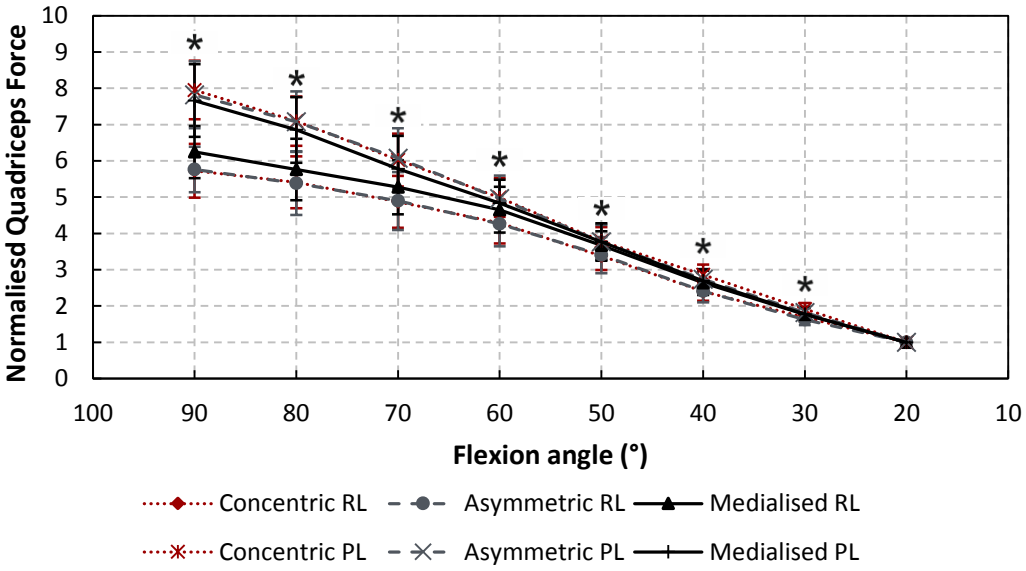

Figure 4-3: Variation in quadriceps force normalised relative to the force at 20° of flexion angle for each patella configuration (mean ± SD). RL: Reduced Load; PL: Physiological Load. $p < 0.05$: * Reduced Load vs Physiological Load for the Concentric configuration

The normalised QF for the *Concentric* configuration was statistically lower, throughout the extension cycle, under the reduced loading compared to the physiological loading. For the other patella configurations there was only a trend towards a reduction in the normalised QF under the reduced loading in deep flexion.

4.2.3.2. Patella Tendon Moment Arm

The PTMA is commonly measured in *in vivo*, but not *in vitro* studies [224]. Changes in the PTMA can imply alterations to the extensor mechanism efficiency, PFJ kinematics, or the anterioposterior position of the femur. For all of the tested patella configurations, under both levels of loading, the PTMA increased non-linearly with extension (Figure 4-4). Measurements were not possible at 20° of flexion under the reduced loading because of issues relating to measurements when the joint was close to full extension. The PTMA was therefore normalised with reference to the data at 30° rather than 20° of flexion. Data collection issues also resulted in some data sets being unattainable in deeper flexion (*Concentric*: 90° N = 4; *Medialised*: 90° N = 4, 80° N = 5).

For both the physiological and reduced loading conditions the PTMA increased, on average, by 6 mm during the extension cycle. The PTMA was also, on average, 3 mm larger throughout the extension movement under the reduced loading. The different patella configurations demonstrated few statistical differences with respect to PTMA.

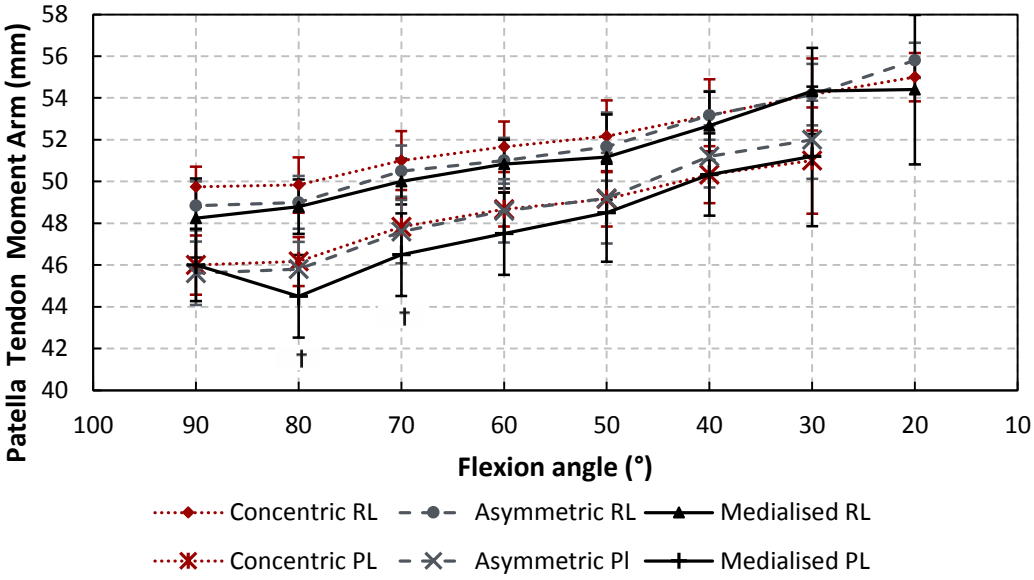

Figure 4-4: Variation in patella tendon moment arm with flexion angle for each patella configuration (mean ± SD). RL: Reduced Load; PL: Physiological Load. p < 0.05: * Concentric vs Asymmetric; † Concentric vs Medialised; ‡ Asymmetric vs Medialised

The normalised PTMA appeared to increase with extension at a greater rate under the physiological loading (Figure 4-5). This was, however, only significant in mid (70 - 50°) and deep flexion (90°) for the *Asymmetric* patella configuration.

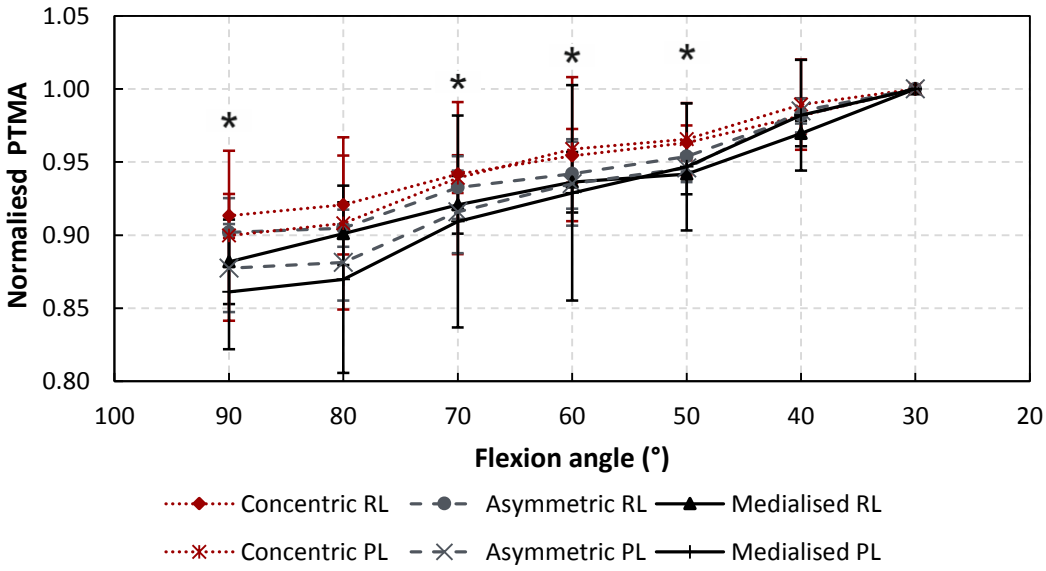

Figure 4-5: Variation in PTMA normalised relative to the PTMA at 30° of flexion angle for each patella configuration (mean ± SD). RL: Reduced Load; PL: Physiological Load. p < 0.05: * Reduced Load vs Physiological Load for the Asymmetric configuration

4.2.3.3. Patellofemoral Compressive Force

As observed with the measured quadriceps force, the patellofemoral compressive force also decreased non-linearly with extension under both levels of loading for all of the patella

configurations (Figure 4-6). In comparison to the quadriceps force, the patella compressive force decreased less in early extension (90 – 70°).

Irrespective of the patella configuration, the decrease in measured patella compressive force with extension was also more pronounced under the physiological load. Between 90° and 20° of flexion, the patella force decreased from 1247.3 ± 29.5 N to 84.6 ± 8.0 N under physiological loading and from 321.9 ± 17.4 N to 43.0 ± 5.4 N under reduced loading. This equated to a reduction by a factor of 14.9 ± 1.5 under physiological loading compared to only 7.6 ± 0.9 under reduced loading (Figure 4-3). The difference between the two loading levels was significant throughout the extension movement for the *Concentric* and *Medialised* patella configurations.

Under the reduced level of loading, the *Concentric* and the *Asymmetric* configurations demonstrated similar patellofemoral compressive force patterns. The *Medialised* configuration was however subjected to significantly higher loads in early extension and reduced contact forces at flexion angles below 50°. Conversely, under physiological loading, throughout the extension movement, the *Medialised* configuration was subjected to a higher compressive force than the *Asymmetric* configuration, which was in turn under greater compression than the *Concentric* configuration (Figure 4-6). These differences became increasingly significant in deeper flexion, reaching a peak difference of 56.5 N.

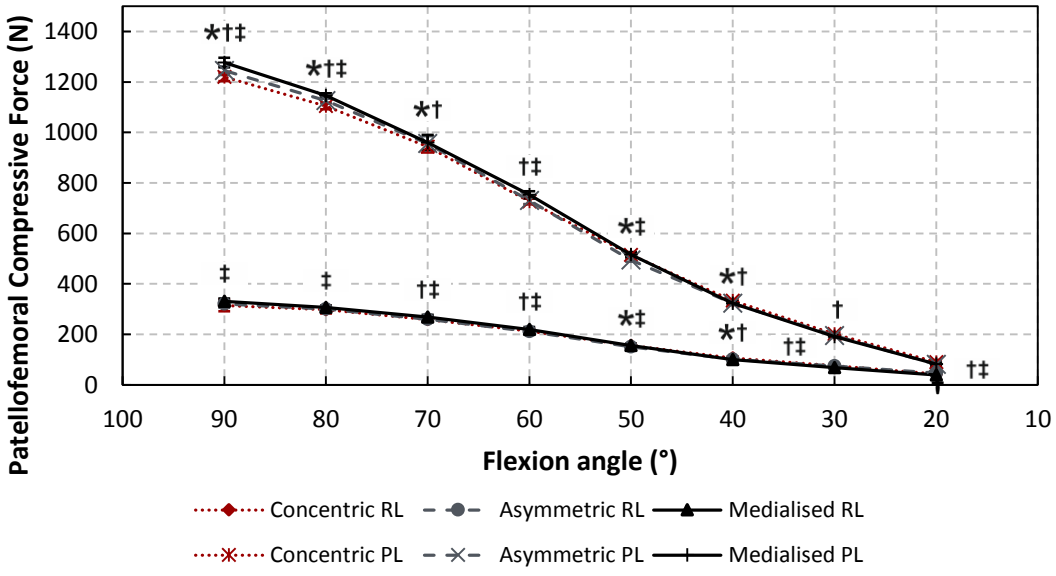

Figure 4-6: Variation in patellofemoral compressive forces with flexion angle for each patella configuration (mean ± SD). RL: Reduced Load; PL: Physiological Load. p < 0.05: * Concentric vs Asymmetric; † Concentric vs Medialised; ‡ Asymmetric vs Medialised

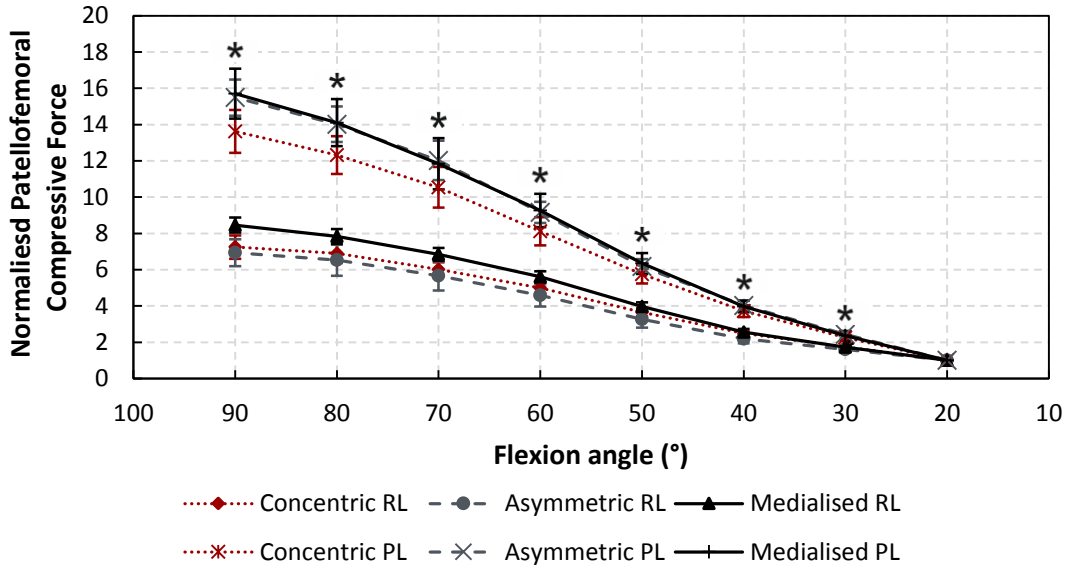

Figure 4-7: Variation in patellofemoral compressive force normalised relative to the values at 20° of flexion for each patella configuration (mean ± SD). RL: Reduced Load; PL: Physiological Load. $p < 0.05$: * Reduced Load vs Physiological Load for the Concentric and Medialised configurations

4.2.3.4. Ratio of Patella Compressive Force to Quadriceps Force

The ratio of patella compressive force to quadriceps force was fairly constant for all of the patella configurations under both levels of loading, at approximately 0.8 in extension from 90° to 70° of flexion. Under physiological loading, the ratio then fell with further extension to approximately 0.45 at 20° of flexion. Under the reduced loading the ratio levelled out at approximately 0.6 at 40° of flexion.

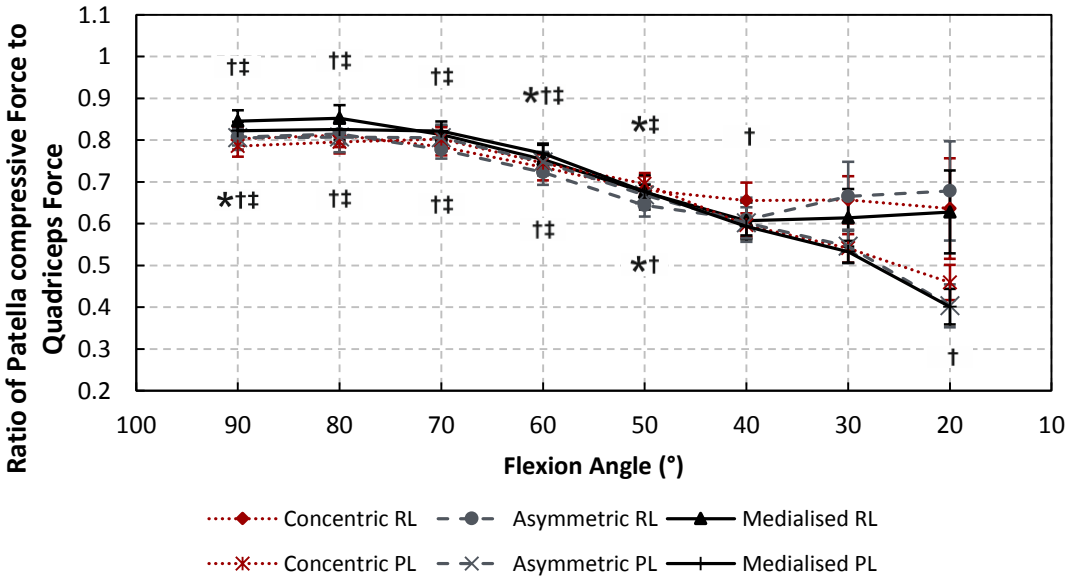

Figure 4-8: Variation in ratio of patella compressive force to quadriceps force with flexion angle for each patella configuration (mean ± SD). RL: Reduced Load; PL: Physiological Load. $p < 0.05$: * Concentric vs Asymmetric; † Concentric vs Medialised; ‡ Asymmetric vs Medialised

Under both levels of loading the different patella configurations demonstrated statistically different patella compressive force to quadriceps force ratios in mid to deep flexion. Under the physiological level of loading, at flexion angles greater than 50°, the *Medialised* configuration demonstrated a greater ratio than the *Concentric* or *Asymmetric* patella configurations. The ratio did not vary significantly with applied load.

4.2.3.5. Patellofemoral Contact Area

The patterns of recorded contact area were different under the two levels of loading (Figure 4-9). Under reduced loading the contact area for all the patella configurations fell slightly in early extension and then remained fairly constant in mid flexion, falling again near full extension. Under the reduced level of loading, few significant differences were seen between the different patella configurations.

When tested under physiological levels of loading, the contact area decreased consistently with extension. At flexion angles greater than 40°, the *Concentric* configuration resulted in a substantially lower contact area than the other patella configurations. This difference was more significant in deeper flexion and was seen visually on the contact area plots (Figure 4-11).

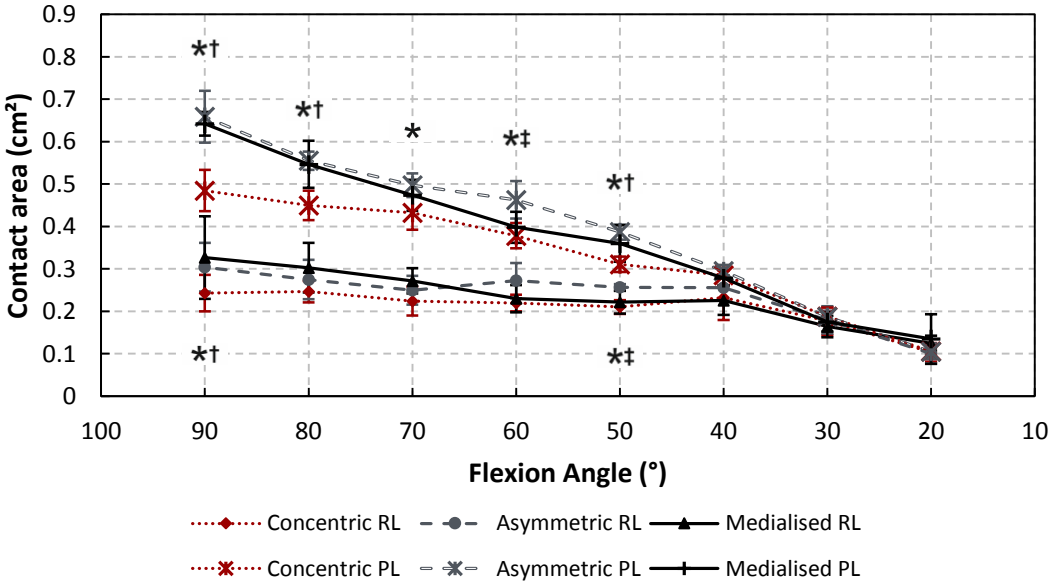

Figure 4-9: Variation in patellofemoral contact areas with flexion angle for each patella configuration (mean ± SD). RL: Reduced Load; PL: Physiological Load. p < 0.05: * Concentric vs Asymmetric; † Concentric vs Medialised; ‡ Asymmetric vs Medialised

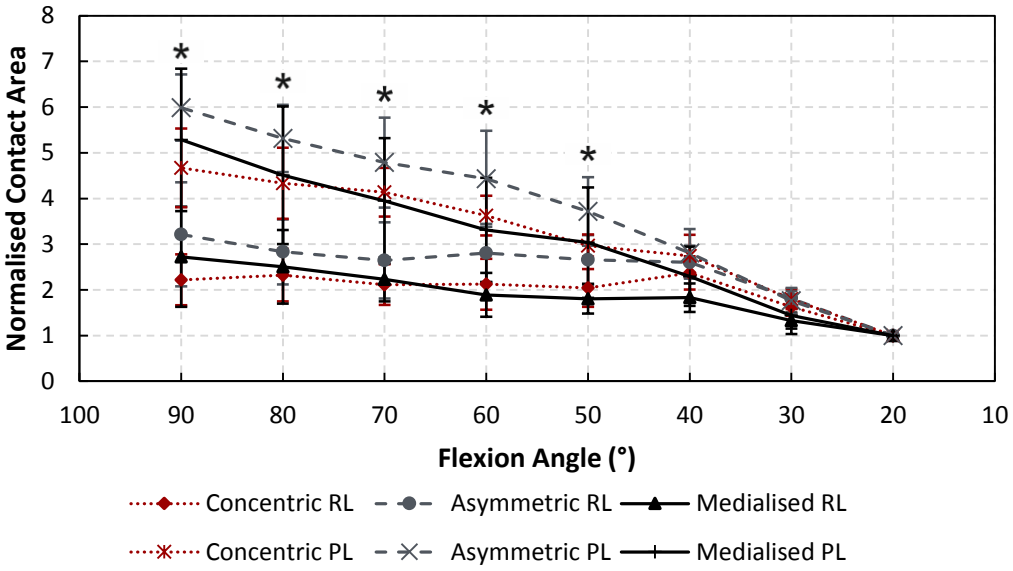

Figure 4-10: Variation in patellofemoral contact area normalised relative to the values at 20° of flexion for each patella configuration (mean ± SD). RL: Reduced Load; PL: Physiological Load. $p < 0.05$: * Reduced Load vs Physiological Load for the Concentric and Medialised configurations

In early extension (90° - 50°) the joint contact area fell at a much greater rate under physiological loading rather than under reduced loading. Between 90° and 20° of flexion the contact area reduced on average by a factor of 5.2 ± 1.2 under physiological loading compared to only 2.7 ± 1.0 under the reduced loading. At flexion angles greater than 40° the normalised contact area was significantly greater under the physiological loading compared to the reduced loading for the *Concentric* and *Medialised* configurations (Figure 4-10).

Throughout the extension cycle, under both levels of loading and for all of the assessed patella configurations, at least 65% of the recorded PFJ contact area was on the lateral aspect of the patella component (Figure 4-11, Figure 4-12). Irrespective of the loading level, the *Medialised* configuration was also loaded significantly more on the lateral aspect than either of the other two patella configurations throughout the extension motion. In deeper flexion (> 60°) the *Concentric* configuration demonstrated a similar level of lateral loading to the *Asymmetric* configuration. However, closer to full extension the *Asymmetric* configuration was loaded significantly more laterally than the *Concentric* configuration. For all of the patella configurations tested, when medial loading occurred, it appeared to be on the edge rather than on the dome of the patella component (Figure 4-11).

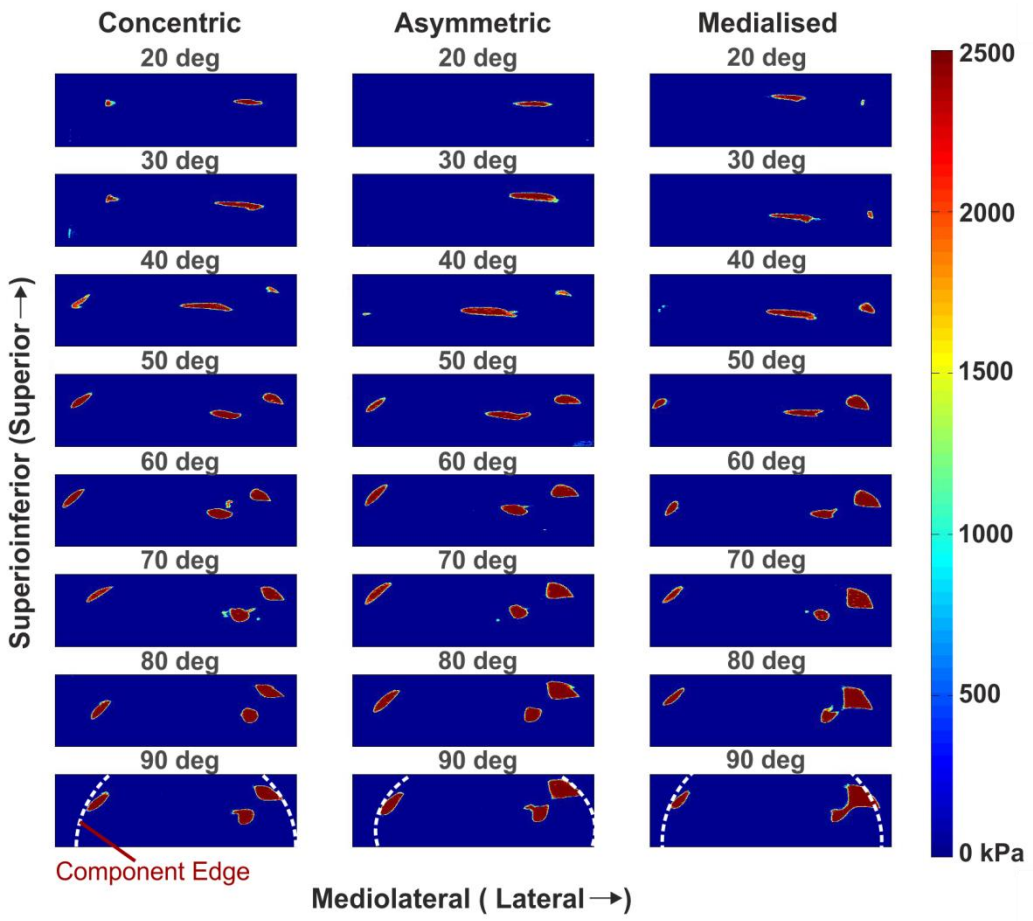

Figure 4-11: Example contact area plots for each patella configuration tested under physiological loading at 10° intervals

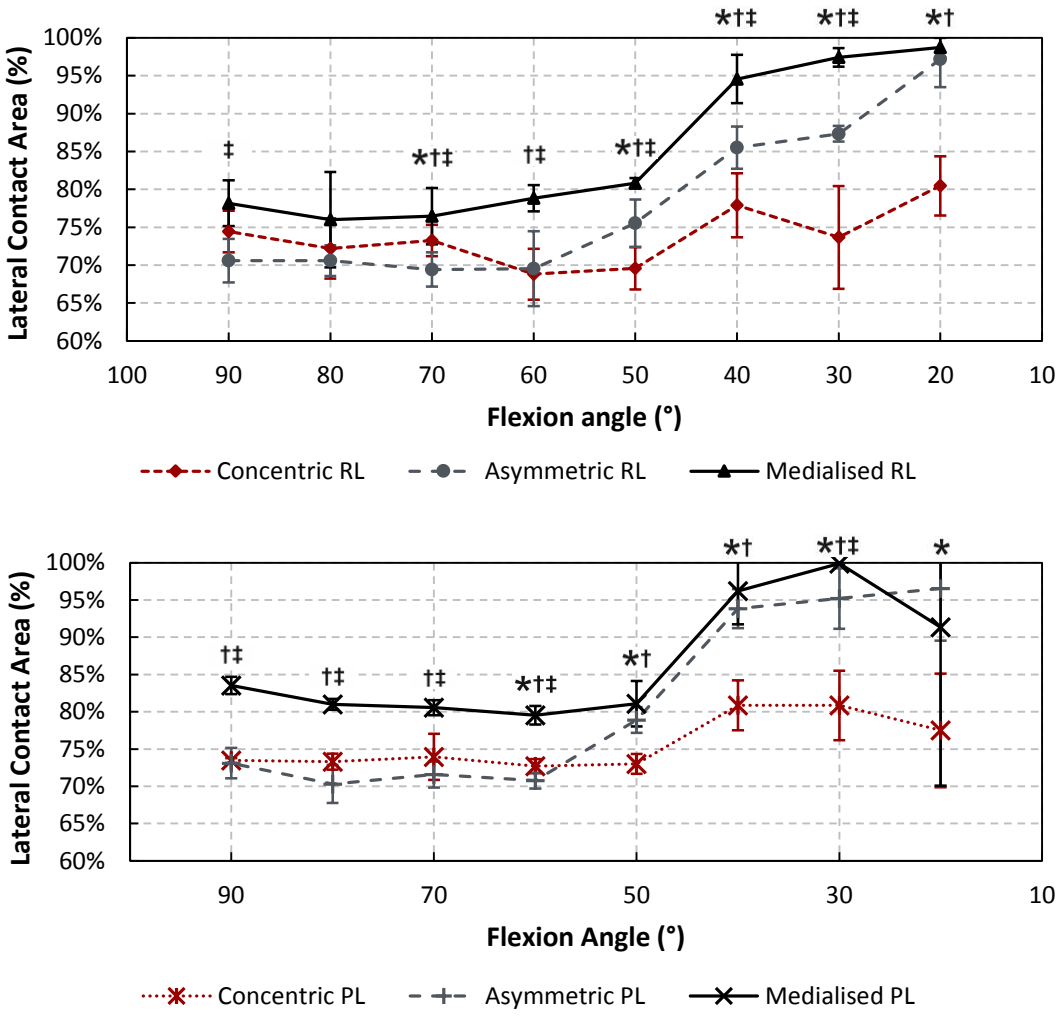

Figure 4-12: Variation in the percentage of lateral contact area with flexion angle for each patella configuration (mean ± SD (capped at 100%)). RL: Reduced Load; PL: Physiological Load. $p < 0.05$: * Concentric vs Asymmetric; † Concentric vs Medialised; ‡ Asymmetric vs Medialised

4.2.3.6. Patellofemoral Pressure

Under physiological loading, the calculated PFJ pressure fell with extension and demonstrated a slight levelling out at more than 70° of flexion for the *Asymmetric* and *Medialised* configurations, but not the *Concentric* configuration (Figure 4-13). Under the reduced loading, the contact pressure demonstrated no levelling out in deeper flexion. Under both loads the *Concentric* configuration demonstrated a significantly larger contact pressure in mid to deep flexion (50° - 90°) than the other patella configurations. All three configurations demonstrated calculated compressive pressures of greater than 13 MPa in deep flexion (> 60°) under physiological loading.

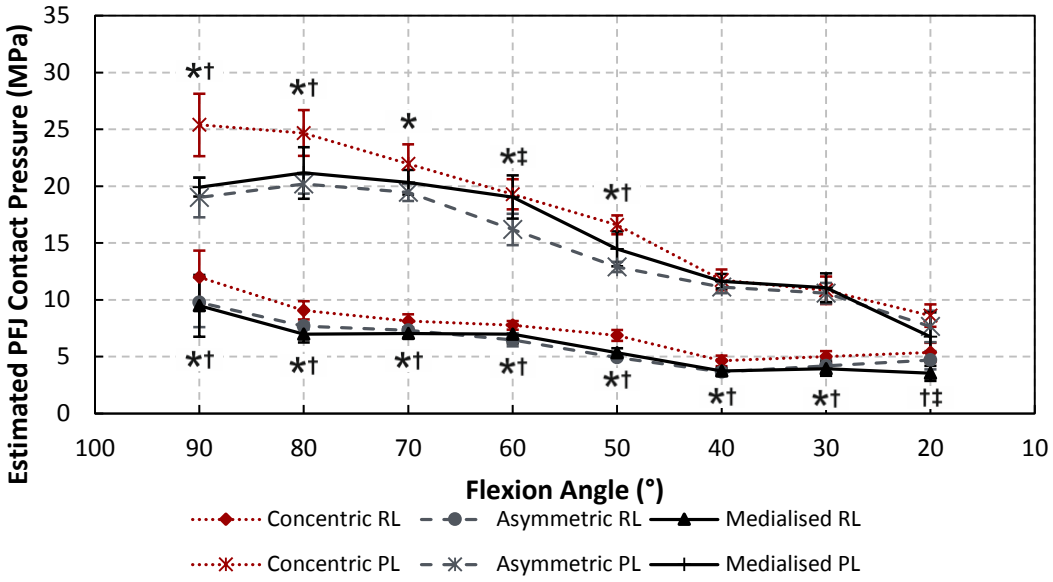

Figure 4-13: Variation in patellofemoral contact pressure with flexion angle for each patella configuration (mean ± SD). RL: Reduced Load; PL: Physiological Load. $p < 0.05$: * Concentric vs Asymmetric; † Concentric vs Medialised; ‡ Asymmetric vs Medialised

The centre of pressure was consistently concentrated on the lateral aspect and tracked inferiorly with extension for all of the patella configurations (Figure 4-14). No statistically relevant differences were demonstrated.

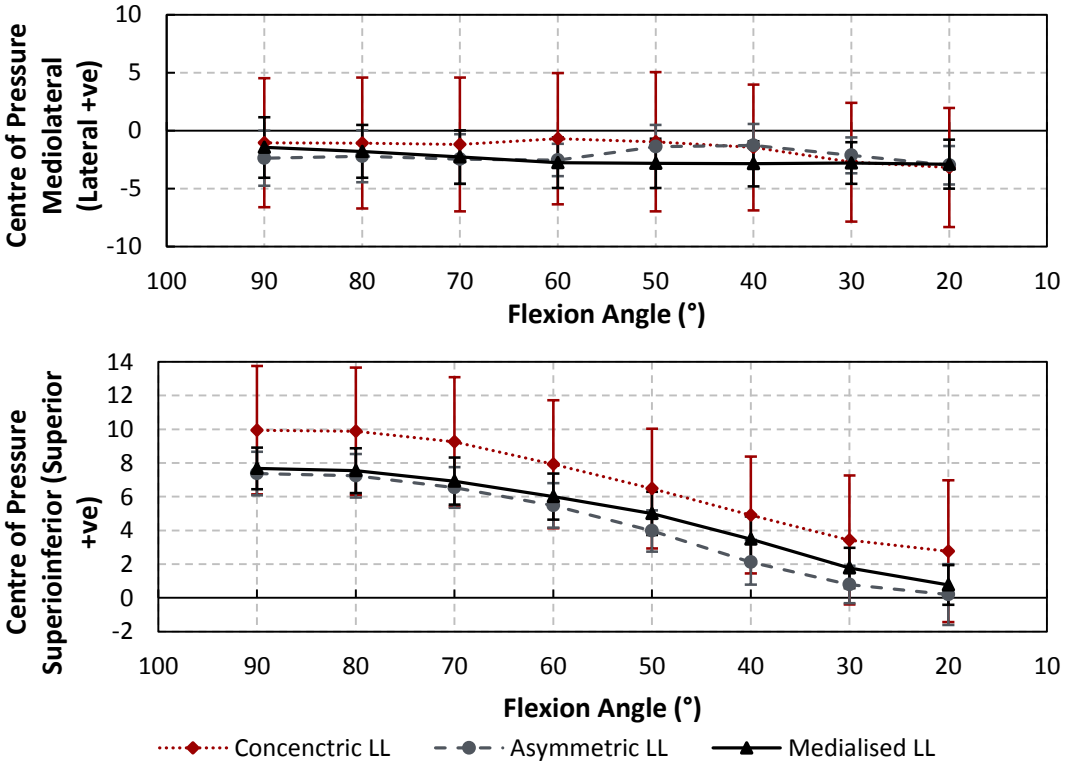

Figure 4-14: Variation in the centre of pressure relative to patella bone centre location with flexion angle for each patella configuration under reduced loading (mean ± SD). Top: Mediolateral; Bottom: Superioinferior.

4.2.3.7. Deformation

Cyclic loading caused permanent deformation on the edge of all of the tested patella components (Figure 4-15). Deformation occurred largely after the first repeat (Figure 4-15). After further repeats little change in the pattern of permanent deformation was seen. Only the data relating to the final repeat was available for the *Asymmetric* configuration. Qualitatively, the *Concentric* configuration demonstrated more lateral deformation than the other tested patella configurations. Lateral edge deformation appeared to be greatest for the *Medialised* configuration whereas, medial edge deformation was greater for the *Asymmetric* and *Concentric* configurations.

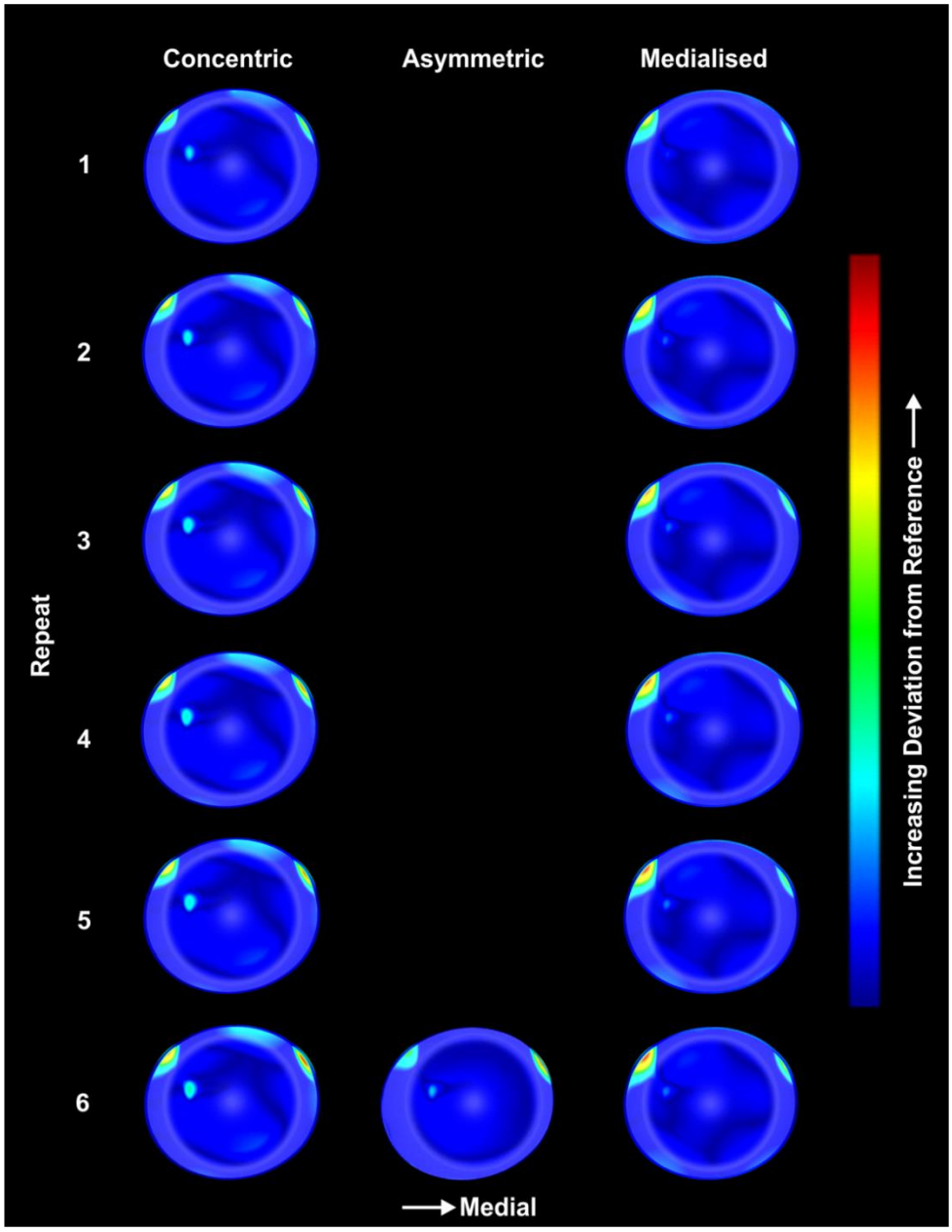

Figure 4-15: Patella surface plots demonstrating the level of permanent deformation, with respect to the implant pre-testing, which was measured for each patella configuration after each testing repetition

4.2.4. Discussion

4.2.4.1. Simulator Assessment

The simulator facilitated quadriceps force, patellofemoral compressive force and PFJ contact area measurements with a comparable, or in some cases a reduced, variability compared to cadaveric systems. The standard deviations of quadriceps and patellofemoral compressive force were substantially lower than those reported in the literature using cadaveric specimens (SD of peak QF 53 N vs 156 N [61]; SD of peak patellofemoral compressive force 17 N vs 278 N [61]). The reported contact area measurement standard deviations were comparable to those previously reported in the literature using cadaveric specimens (SD of peak contact area 0.06 cm^2 vs 0.02 - 0.03 cm^2 [37,188]). The demonstrated low measurement variability supported the assertion that the presented simulator would allow differences, in terms of PFJ biomechanics, between test conditions to be demonstrated using as many or fewer specimens than comparable cadaveric studies. In contrast, the COP measurements were associated with relatively large standard deviations because of the low sensor density of the Novel system.

Overall, in terms of PFJ forces and contact characteristics, the results reported in this thesis indicated that the simulator replicated physiological PFJ biomechanics. In line with the cadaveric study carried out by Browne *et al.* using the same implant and a similar simulator [61], under physiological loading, the measured QF decreased with extension (Figure 4-2). The recorded QF decreased with increasing extension as a result of the body weight moment arm falling, and a reduction in the effective patella moment arm. The recorded peak QF in this study, 1555 N ± 53 N at 90° of flexion, was higher than that reported by Browne *et al.* [61] because of the measurement of extension rather than flexion cycles. The magnitude of peak QF reported in this thesis was however consistent with values reported by Ostermeier *et al.*, who used a fixed femur simulator and a similar implant [23].

The patella compressive force also decreased with extension (Figure 4-6), but, compared to the quadriceps force, levelled out in deeper flexion. This levelling out was previously demonstrated in the literature using cadavers [31,61], and highlighted that the simulator was able to replicate the physiological contact of the quadriceps tendon with the distal femur in deep flexion, which reduced the load carried by the PFJ. The peak patellofemoral compressive force reported in this thesis was higher than that previously reported by Browne *et al.* for the same implant, using cadavers, again as a result of reporting extension rather

than flexion values [61]. The peak reported in this thesis was however consistent with *in vivo* estimates in the literature [1].

The ratio of the patella compressive force to the quadriceps force peaked at approximately 0.8 for all of the patella configurations. It remained fairly constant from 90° to 70° of flexion and then fell to approximately 0.45 at 20° of flexion. This pattern matched that reported in *in vivo* studies in the literature [1,291]. This suggested that the simulator modelled the natural changes in the relationship between the patella and quadriceps loads caused by changes in the superioinferior position of the patellofemoral contact and the sagittal plane orientation of the patella component [1,291].

Van Eijden *et al.'s* work on the natural knee indicated that the ratio of the patella compressive force to the quadriceps force reached approximately 1 at 90° of flexion [1,291]. Using a simple 2D model of the PFJ [89], it can be shown that the lower peak ratio reported in this thesis indicated that at 90° flexion of the TFJ the patellofemoral contact point was more superior and/or the patella was less flexed in this set up than in the natural knee. This change may be an artefact of the simulator design or a result of the implant patellofemoral design.

The measured PTMA, for all of the patella configurations, demonstrated a gradual increase (Figure 4-4) with increasing extension, which was related to the tracking of the patella component from above the trochlear groove, into the trochlear grove and ultimately into the intercondylar notch. This pattern did not correspond to data reported in the literature for the natural knee, but was in keeping with data reported for replaced knees [24,87,224,270]. The natural knee demonstrates a steeper increase in the PTMA in early extension, and a decrease close to full extension. The pattern reported here corresponded with previous work on hinged knee prostheses using the original rig design [196]. Ward *et al.* also demonstrated a similar increase in PTMA with increasing extension from 60° of flexion, but reported a decrease from 90° to 60° of flexion using the same implant [24]. The differences reported from 90° to 60° of flexion were most likely a result of the use of different loading simulations. Irrespective of loading method however, the Scorpio replacement system has been shown to confer a greater mechanical advantage to the extensor mechanism, near full extension, than the natural knee.

Throughout the extension movement, irrespective of the patella configuration, there was a significantly greater proportion of patellofemoral contact on the lateral aspect (Figure 4-12) and a consistently lateral location of the COP (Figure 4-14). Unreplaced knees have been reported in the literature to maintain approximately 60% lateral loading during normal daily

motion [78]. The results reported in this thesis therefore suggest that the Scorpio implant only replicates natural loading in mid flexion. The graphs of lateral loading in the present study (Figure 4-14) demonstrate a step change from approximately 75% lateral loading to almost 100% lateral loading at approximately 50° of flexion. Previous studies have not reported such a trend but have indicated similarly high levels lateral loading, which correlates with reports of significantly greater lateral rather than medial patella component wear on retrievals [29,292]. The sudden change in lateral contact area reported in this study is likely to be related to the implant geometry. The increased level of lateral loading in extension suggests a reduction in the constraint provided by the femoral geometry to overcome the lateral pull of the quadriceps mechanism and may indicate the point at which the patella exits the main portion of the trochlear groove. The patella COP was also consistently superior, but became more inferior with increasing extension. This was in keeping with Anglin *et al.'s* work on cadaveric specimens [31].

The contact area and pressure within the PFJ, following TKA with the Scorpio NRG system, or its predecessor the Scorpio system, have not previously been reported in the literature. The geometry of the femoral and patella components has been demonstrated in the literature to have a significant effect on the contact within the PFJ [205,256] and therefore comparisons to measurements made using different implant systems are not valid. The pattern of the recorded contact area under physiological loading was however consistent with modern kinematic understanding [44,101], showing a consistent reduction with tibiofemoral extension as the patella component traversed the intercondylar notch, moving through the trochlear groove and, closer to full extension, into a position superior to the groove.

The lack of consideration of many patellofemoral soft tissue structures in the present simulator could be considered to have resulted in an underestimation of the PFJ contact area as patellofemoral soft tissues, such as the retinaculum, restrain the patella and may therefore increase the forces within the PFJ in extension. However, as the knee flexes many patellofemoral soft tissues slacken as bone geometry becomes the primary mechanism of patella constraint [77-79]. The measured peak contact area values are therefore considered to be reasonable and the reported patellofemoral pressures appropriate estimates. The magnitude of PFJ pressure is related to the risk of developing functional limitations as a result of PFJ instability, pain and even component failure [21,248,293]. The simulator was therefore demonstrated to be appropriate not only for repeatable comparative studies but also for indicating the risk of the development of functional limitations relating to the PFJ under extended clinical use.

4.2.4.2. Effect of Loading Level

The results associated with the two loading conditions indicated that they were not comparable. The measurements of quadriceps force, patellofemoral compressive force and PFJ contact area all demonstrated distinctly different patterns when the two loading conditions were compared (Figure 4-2, Figure 4-6 & Figure 4-9).

The measured QF fell during extension, from 90° to 20° of flexion, by a factor of 7.8 ± 0.9 under physiological loading but only 5.9 ± 0.7 under the reduced loading (Figure 4-3). With regards to the *Concentric* configuration, the normalised values of QF were statistically different for the two loading conditions from 30° to 90° of flexion. For the other patella configurations a similar trend was demonstrated, but it did not reach statistical significance.

Similarly, the measured patella forces fell during extension, from 90° to 20° of flexion, by a factor of 14.9 ± 1.5 under physiological loading, but only 7.6 ± 0.9 under the reduced level of loading (Figure 4-7). The normalised values of patella compressive force were statistically different under the two levels of loading for the *Concentric* and *Medialised* configurations from 30° to 90° of flexion. For the *Asymmetric* configuration a similar trend was demonstrated, but did not reach statistical significance.

A comparable pattern was seen with respect to the contact area values. Under physiological loading, the contact area decreased on average by a factor of 5.2 ± 1.2 during extension. The decrease was only by a factor of 2.7 ± 1.0 under the reduced loading (Figure 4-10). There was a significant difference between the reported normalised values from 50° to 90° of flexion for the *Concentric* and *Medialised* configuration, but only a trend with respect to the *Asymmetric* configuration.

Lower rates of decrease in quadriceps force during knee extension, under reduced loading compared to physiological loading, have previously been reported using cadaveric specimens by Müller *et al*. [294], but corresponding trends in measured patella compressive forces or contact areas have never been reported. The increased level of hip load resulted in an increased frictional force within the PFJ. The QF required to overcome this force therefore increased correspondingly. In deeper flexion the required QF also increased due to the increased body weight moment, which exacerbated the differences, causing the increasingly divergent trends visible on Figure 4-2. This pattern was reflected for the PFJ compressive forces as the two are biomechanically linked (Figure 4-6, Figure 4-7). The significantly higher patella compressive force under the physiological loading caused both plastic and elastic

deformation of the relatively soft UHMWPE patella component, which resulted in the reported higher contact areas (Figure 4-9).

Differences between the rate of change of the PTMA for the two loading conditions were less substantial and demonstrated fewer significant differences (Figure 4-5). However, throughout the flexion range the PTMA was on average 3 mm larger under the reduced level of loading. The Pliance sensor array was 2 mm thick, which accounted for a proportion of the reported 3 mm reduction in PTMA under the physiological loading: when the sensor was not used. The remainder of the reduction may be attributed to compression of the UHMWPE patella component under the higher loading. The reduced PTMA reported under the physiological loading condition also contributed to the increased quadriceps force.

Many studies carry out testing under sub-physiological levels of loading to protect cadaveric soft tissues and, in some cases, sensor systems. These results suggest that it is important to carry out tests under physiological levels of load in order to achieve clinically relevant results and failing that to understand the limitations of studies carried out under reduced loading [29,31,38,188,189,191,194,210,295].

4.2.4.3. Effect of Patella Component Medialisation

Medialisation of the patella component by 5 mm did not substantially affect the forces within the PFJ. No significant differences were seen in the measured quadriceps force for the *Concentric* compared to the *Medialised* configuration. Conversely, under the physiological loading, at all flexion angles except 50°, the measured patellofemoral compressive force was significantly higher for the *Medialised* compared to the *Concentric* configuration. These differences were not mirrored under the reduced loading. The difference between the patellofemoral compressive forces for each patella configuration at the peak physiological load, which was probably a result of slight tracking differences, was less than 60 N. This was well within the level of variability which would be expected between patients [1]. The effect of medialising the patella component on the patella compressive forces was therefore significant, but probably not clinically relevant.

The differences seen with regards to the patella compressive forces were not replicated in the quadriceps forces. The largest component of the quadriceps force, the force required to move the joint against the body weight moment, was not significantly altered by medialisation, as the PTMA was not significantly affected (Figure 4-4). The use of grease within the PFJ resulted in a friction coefficient of approximately 0.03 [197]. The differences

in friction forces within the PFJ caused by the changes in patella compressive force were therefore less than 10 N, and within the error margin of the quadriceps load cell.

These results did not agree with cadaveric studies reported in the literature [31,33], which suggested that medialisation of the patella, by the same or even a smaller amount than that assessed here, caused a reduction in patella compressive forces. This difference may have related to the simulator design. However, given the previously demonstrated physiological relevance of the simulator, it was more likely a result of using a different implant system. Regardless, the differences reported here and in the literature are most likely too small to be of any clinical relevance.

In deep flexion (> 60°), under both levels of loading, the patella compressive force to quadriceps force ratio was statistically lower for the *Concentric* configuration compared to the *Medialised* configuration (Figure 4-10). This implied that the superioinferior position of the PFJ contact point and/or the degree of patella flexion was altered by medialisation. The latter was not measured by the current study design. However, the measured COP superioinferior position did demonstrate a trend towards a more superior position for the *Concentric* configuration (Figure 4-14). With respect to the effect of patella medialisation these parameters have not been measured in other published studies.

Medialisation of the concentric patella component significantly increased the joint contact area and reduced the pressure within the PFJ. Under physiological loading, at 80° and 90° of flexion, the *Concentric* configuration demonstrated a significantly reduced total contact area compared to the *Medialised* configuration. This was only replicated under the reduced level of loading at 90° of flexion. This suggested that the *Concentric* configuration did not settle as well within the trochlear groove and intercondylar notch as the *Medialised* configuration (Figure 4-11). At its peak, under physiological loading, this difference represented a 24% reduction in PFJ contact area.

Under reduced loading, the *Concentric* configuration also demonstrated significantly greater patellofemoral pressures than the *Medialised* configuration. This difference was mirrored under increased loading in deep flexion (80° - 90°) (Figure 4-13). At a peak, under physiological levels of loading, the *Concentric* configuration was subjected to a 28% higher contact pressure. The observation that the *Concentric* configuration was under greater pressure, correlates with the greater levels of permanent deformation seen compared to the *Medialised* configuration (Figure 4-15). The effect of medialisation on PFJ pressure or contact area has not previously been assessed using the Scorpio NRG system or any single radius

knee. However, Bronson *et al*. reported a reduction in PFJ pressure in mid flexion following medialisation by 4 mm of an alternative modern implant [35].

Whether it was medialised or not, the concentric patella component was subjected to significantly more contact on the lateral, rather than medial aspect, under both levels of loading (Figure 4-11 & Figure 4-12). However, throughout the extension motion, the *Medialised* configuration demonstrated a significant trend towards more lateral loading than the *Concentric* configuration. Anglin *et al*. also reported this pattern in their cadaveric study carried out using a multi radius implant [31]. If it is assumed that the apex of the patella component sat in the same mediolateral position within the trochlear grove for each configuration, the resultant patella compressive force would be more lateral when the patella component was medialised. This would have resulted in a lateral moment causing a lateral tilt of the patella, which has been noted in the literature [31,33-35,38,214], and hence the increasingly lateral contact.

The differences in reported pressures seen in this study indicate that the increased lateral tilt induced by medialisation improved the patella seating, resulting in an increased PFJ contact area. This had a greater effect than the minimal differences reported in the patella compressive force. These results suggested that medialisation of the concentric patella component by 5 mm may reduce the risk of the development of functional limitations as a result of instability and pain within the PFJ [21,293]. However, whether the patella component was medialised or not, at flexion angles greater than 50°, the calculated pressures on the symmetric patella component exceeded 13 MPa under physiological loading (Figure 4-13), and caused permanent deformation of the patella components (Figure 4-15). UHMWPE is commonly quoted to have an offset yield strength of 13 MPa [248]. Medialisation of 5 mm does not therefore appear to be sufficient to eliminate the risk of long term instability as a result of plastic deformation [16] or the delamination of non-cross-linked and the fracture of cross-linked UHMWPE components [21,248,293].

Irrespective of mediolateral position, the concentric patella component also demonstrated consistent lateral and medial edge loading and no superior or inferior loading, which caused permanent deformation of the UHMWPE patella components under relatively few cycles (Figure 4-11, Figure 4-15) and was consistent with a literature report of wear on a Scorpio retrieval [292]. Edge loading and deformation have also been reported in the literature for alternative implant systems [254,296] and may suggest that the sombrero design of the Scorpio patella component (Figure 4-1) is not congruent with the femoral component

geometry. The consecutive surface plots suggest that the deformation largely occurred during the first testing repetition. The amount of deformation then remained relatively constant. This may suggest that the system underwent an initial settling period. However, this was not sufficient to reduce the PFJ contact pressure to safe levels.

4.2.4.4. Effect of Patella Component Geometry

The use of an asymmetric patella component rather than a concentric patella component did not substantially affect the forces within the PFJ. No significant differences were seen between the recorded quadriceps force or the PTMA for each patella configuration under either level of loading (Figure 4-2, Figure 4-4). However, in deeper flexion (> 60°) under physiological loading only, the patella compressive force was greater for the *Asymmetric* configuration than the *Concentric* configuration (Figure 4-6). The peak difference between the patellofemoral compressive forces was less than 25 N, which was well within expected levels of patient variability [1] and therefore not clinically relevant. The differences reported in patellofemoral compressive force did not translate to the quadriceps force because of the low simulated PFJ coefficient of friction.

Few statistical differences, in terms of the ratio of patella compressive force to quadriceps force were demonstrated by this present study. However, at 90° of flexion, under physiological loading, the ratio of patella compressive force to QF for the *Concentric* configuration was statistically lower than that for the *Asymmetric* configuration (Figure 4-8). This implies that the superioinferior position of the PFJ contact and/or the degree of patella flexion was altered by the change in component design. The patella flexion angle was not assessed by the present study design. However, the measured superioinferior position of the COP did demonstrate a trend towards a more superior location for the *Concentric* option (Figure 4-14). Previous computational work by Fitzpatrick *et al*. has also indicated that the use of an asymmetric component may reduce patella flexion [256].

The use of the asymmetric patella component rather than the concentric component significantly increased the joint contact area and reduced the pressure within the PFJ. Under physiological levels of loading, the *Asymmetric* configuration demonstrated significantly increased values of contact area compared to the *Concentric* configuration in mid to deep flexion (50° - 90°) (Figure 4-9). Similarly, under both levels of loading, the PFJ contact pressure calculated for the *Asymmetric* configuration was significantly lower than that estimated for the *Concentric* configuration (Figure 4-13). This was corroborated by the reduced permanent deformation seen on the asymmetric component (Figure 4-15) and suggested that the use of

the asymmetric component with this TKA system may reduce the risk of the development of functional limitations relating to the PFJ [21,248,293].

Near full extension, the *Asymmetric* configuration demonstrated significantly greater lateral loading than the *Concentric* configuration (Figure 4-12). This was may have been a result of a lateral tilt induced by the medialised component apex and may have contributed to improved patella component seating and hence the reduced contact area. In deeper flexion however, under the physiological level of loading, the loading on the asymmetric dome became more balanced and began to approximate the lateral to medial contact area ratio of the *Concentric* configuration. This suggests a reduced lateral tilt compared to the *Medialised* configuration and corresponds with the reported trend towards an increased pressure (Figure 4-13).

Irrespective of the geometry of the patella component, at flexion angles greater than 50°, the calculated PFJ pressures again exceeded 13 MPa under physiological loading. This indicated that, similar to the introduction of 5 mm of medialisation, using an asymmetric component would not fully eliminate the potential risk of long term PFJ pain, instability and component failure [16,21,248]. This assertion was again supported by the visible permanent deformation demonstrated on both patella components (Figure 4-15).

4.2.4.5. Comparison of Medialised and Asymmetric Patella Configurations

There were no differences between the quadriceps force measured for the *Medialised* and *Asymmetric* configurations (Figure 4-2). However, the *Asymmetric* configuration was subjected to significantly less patellofemoral compressive force than the *Medialised* configuration in deeper flexion (> 70°) (Figure 4-6). The peak difference was less than 35 N and again within expected levels of patient variation [1] and therefore unlikely to have a clinically relevant impact.

The ratio of patella compressive force to quadriceps force was the same for both patella configurations under physiological loading (Figure 4-8). Similarly the superioinferior COP position did not change (Figure 4-14) and when measured under physiological loading, the values of contact area and pressure were comparable for the *Medialised* and *Asymmetric* configurations (Figure 4-9, Figure 4-13). *Medialisation* of the concentric dome component appeared to result in a comparable biomechanical situation to the use of the asymmetric component. However, the percentage of contact area on the lateral aspect and the patterns of edge loading were not the same for the two patella configurations.

Under physiological levels of loading, near full extension, the *Medialised* and *Asymmetric* configurations demonstrated similar percentages of contact area on the lateral aspect (Figure 4-12). They both demonstrated statistically more lateral contact than the *Concentric* configuration due to the medialisation of the component apex in both cases. However, in mid to deep flexion (> 50°) the *Asymmetric* configuration became relatively more balanced and began to approximate the lateral to medial contact area ratio of the *Concentric* configuration. The smoother lateral plateau of the wider asymmetric dome may have allowed it to settle further into the intercondylar notch than the sharper edge of the concentric dome which, when medialised, may have impinged on the lateral femoral condyle, causing the greater permanent lateral deformation seen qualitatively on the profile plots (Figure 4-15). The different patterns of deformation reported for the *Medialised* and *Asymmetrical* configurations highlighted that although both result in similar PFJ pressure reductions they were not identical situations and will be at risk of deformation in different areas.

4.2.4.6. Limitations

The present study was limited by not testing with the TKA implanted in cadaveric bone to provide a direct assessment of the physiological relevance of the simulator. However, comparisons to published studies using the same implant were possible and allowed a thorough examination of the physiological relevance of the simulator.

As discussed in detail in the previous section, the method was also limited by the need to combine single axis compressive force measurements with static contact area measurements to obtain an estimate of the pressure the PFJ was subjected to, rather than directly measuring the contact pressure or bone stress. The resultant force on the patella component was unlikely to correspond directly with the measurement axis of the single-axis load cell positioned behind the patella component. However, based on literature results [62], compression was assumed to be the largest component of force in the joint. Literature values for pressure within the PFJ following implantation with the Scorpio system were not available for comparison. The pattern of recorded contact area under physiological loading was however, consistent with modern kinematic understanding [44,101]. The estimated pressure values were therefore considered to give a good indication of the loading magnitude on the patella component during testing and the potential risk of long term functional limitations relating to the PFJ as a result of component failure and pain under cyclic loading [21,248,293].

The simulator may also have been limited by modelling only a small proportion of the soft tissue structures found in the knee. However, it is only feasible to account for more structures

using cadaveric specimens with intact soft tissues, which would increase the variability of the results and hence the required sample size and cost of all subsequent investigations. The primary PFJ stabilising soft tissue structures provide little restraint in deeper flexion when the risk of pain due to excessive loading is highest [77-79]. The simulator employed in this study has been shown to sufficiently replicate the physiological situation, and is therefore suitable for use in biomechanical studies.

There are a number of other limitations of this study. Only one TKA implant design (Scorpio NRG) and only the PS variant has been assessed. The results of this study cannot therefore, be extrapolated to other total knee joint designs. The same tibiofemoral components were also used for all tests and only one patella component was used for each configuration. However, the number of cycles the implants were subjected to were negligible compared to the expected life of a knee implant and grease was used to minimise friction within the tibiofemoral and patellofemoral joints. As a result, no tibial bearing wear was observed visually and an analysis of the patellofemoral contact area and quadriceps force results and deformation plots for consecutive repeats demonstrated no consistent effect of repetitive testing (Figure 4-15, Figure 4-16 & Figure 4-17). The assumption that the component conditions were comparable in each repeat was therefore reasonable.

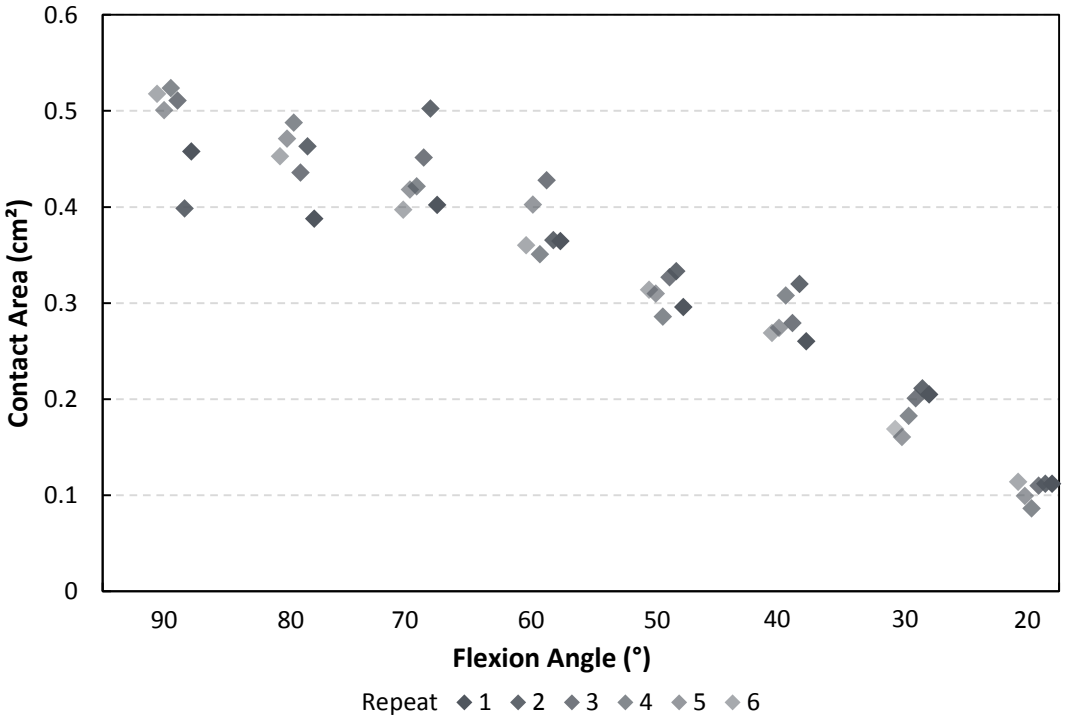

Figure 4-16: Contact area values recorded under physiological loading for each consecutive repeat (only Concentric data shown for clarity)

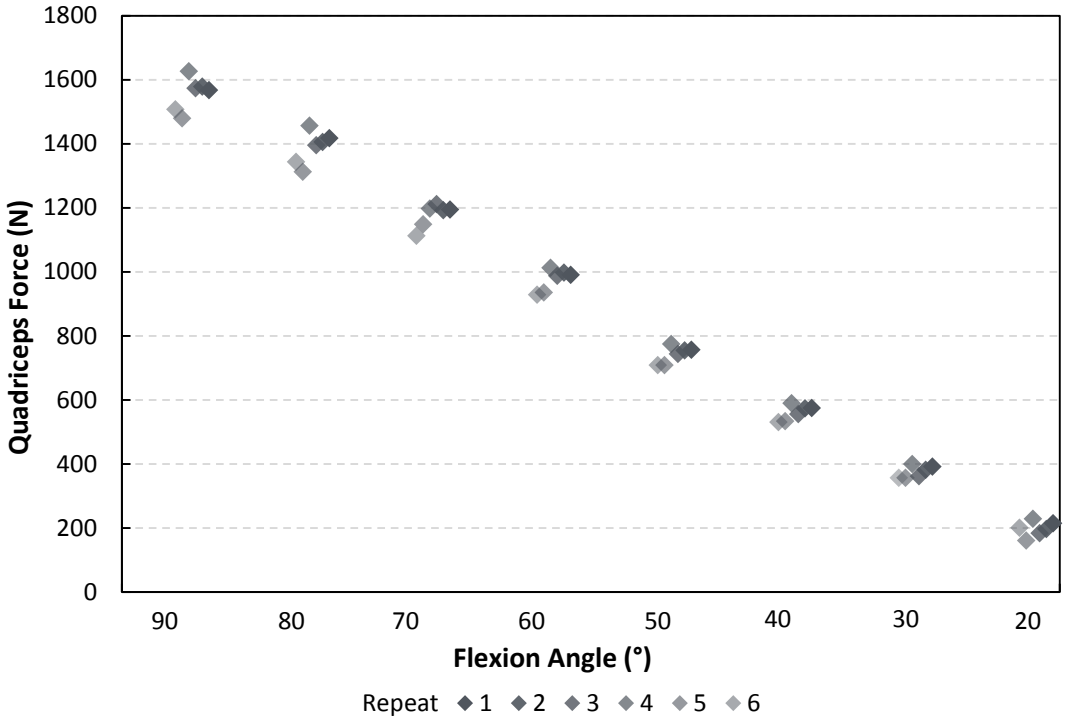

Figure 4-17: Quadriceps force values recorded under physiological loading for each consecutive repeat (only Concentric data shown for clarity)

4.2.5. Conclusions

The knee simulator employed in this study was able to model physiological knee motion and enabled the assessment of forces, areas and pressures, within the PFJ which were comparable with results published in the literature for studies using cadaveric knees. This study has also highlighted the effect of simulated body weight on PFJ biomechanics. The patterns of loads and contact areas reported at a reduced level of loading did not correspond to those reported under physiological loads. It is therefore important to carry out biomechanical evaluations under physiological levels of loading. The effect of multiple design or alignment factors on PFJ biomechanics can be assessed under physiological loads, using this protocol, with a relatively low number of samples and hence a reduced time and cost commitment.

The present study demonstrated that, for the prosthesis tested, medialisation of the apex of the patella component, either through component medialisation or use of an asymmetric geometry, reduced the relative potential risk of developing functional limitations relating to the PFJ as a result of instability, pain and/or patella component failure. The use of a concentric component medialised by 5 mm or an asymmetrical component increased the PFJ contact area by more than 20% and resulted in a corresponding reduction in joint pressures of more than 25%. However, the study also highlighted that there were differences between 5 mm medialisation of the concentric component and the use of an asymmetric component.

The medialised concentric component underwent significantly more lateral loading and a noticeably different pattern of deformation.

This study is the first to have assessed deformation of patella components during *in vitro* biomechanical testing and highlighted the substantial permanent edge deformation which occurred in all three patella configurations. This corresponds with a finding reported in the literature of a retrieval analysis [292]. It may be attributable to poor congruency between the patella and femoral components of the Scorpio NRG implant system and be related to the anecdotal reporting of long term complications [297]. The study also demonstrated that, although medialisation of the patella component apex may reduce PFJ pressures, in all cases, the reported joint pressures still exceeded the fatigue limit of UHMWPE in deeper flexion. Medialisation by 5 mm, or the use of an asymmetric geometry, did not therefore eliminate the potential risk of pain, and long term instability as a result of mechanical failure of the UHMWPE patella component [248,293].

4.2.5.1. Implications for Subsequent Studies

Given the clear benefits in terms of clinical relevance of testing under physiological loading, and the large variability associated with the COP measurements, it was concluded that only testing under physiological loads should be carried out for subsequent studies. This also limited the number of tests carried out on each patella component. Hence, for the following studies the previously detailed protocol was amended to exclude both the use of the Novel sensor, and completion of any testing under the reduced hip loading.

4.3.Study (ii) - The effect of Femoral Rotational Alignment Errors

4.3.1. Aim

This study aimed to evaluate the effect of femoral rotational alignment errors on the biomechanics of the PFJ during dynamic knee movements and hence their potential influence on the risk of the development of patellofemoral issues and pain after TKA.

4.3.2. Methods & Materials

This experiment was carried out using the protocol stages associated with physiological loading detailed in the previous chapter, and the Scorpio NRG PS fixed bearing implant. An asymmetric dome patella component was used for all tests.

Three femoral rotations were assessed: *Optimal* (as defined by the surgical operating guidelines), *5° internal rotation (IR),* and *5° external rotation (ER)* (Figure 4-18). Rotational malalignment of was achieved by rotating the femoral mount relative to the modelled femur. Internal and external rotations of 5° were modelled to simulate the maximum errors reported surgically [162,179].

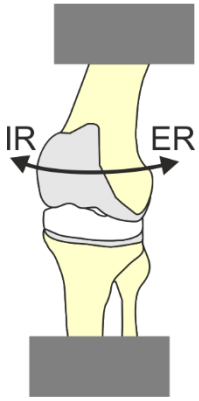

Figure 4-18: Three femoral rotations were assessed: *Optimal* (as defined by the surgical operating guidelines), *5° internal rotation (IR),* and *5° external rotation (ER)*

Each rotation was assessed six times, repositioning the Sawbone tibia and femur between each experimental repeat. The order of the tests for the three rotations was altered for each repeat. Only one new patella component was available for the tests.

4.3.2.1. Statistical Methods

For all of the tests the sample number was five. Data has been reported using mean ± standard deviation (SD) to give an indication of the variability. The standard deviation values for the reported percentage of lateral contact area were capped at 100% as this variable could not physically exceed 100%.

All data was assessed for statistical differences. The p values are not reported but when a difference was significant it has been highlighted on the appropriate graph. Non-parametric tests were used to assess differences between the configurations to reduce the threat of outliers within the relatively small sample. A paired Friedman test and then, where appropriate, Wilcoxon signed rank post hoc tests, were used to assess any differences for each variable between the three simulated femoral rotational configurations ($\alpha = 0.05$).

4.3.3. Results

4.3.3.1. Quadriceps Force

The measured QF decreased with extension for all of the femoral rotational configurations tested (Figure 4-19). Femoral rotation of ± 5° caused few statistically relevant changes to the recorded QF.

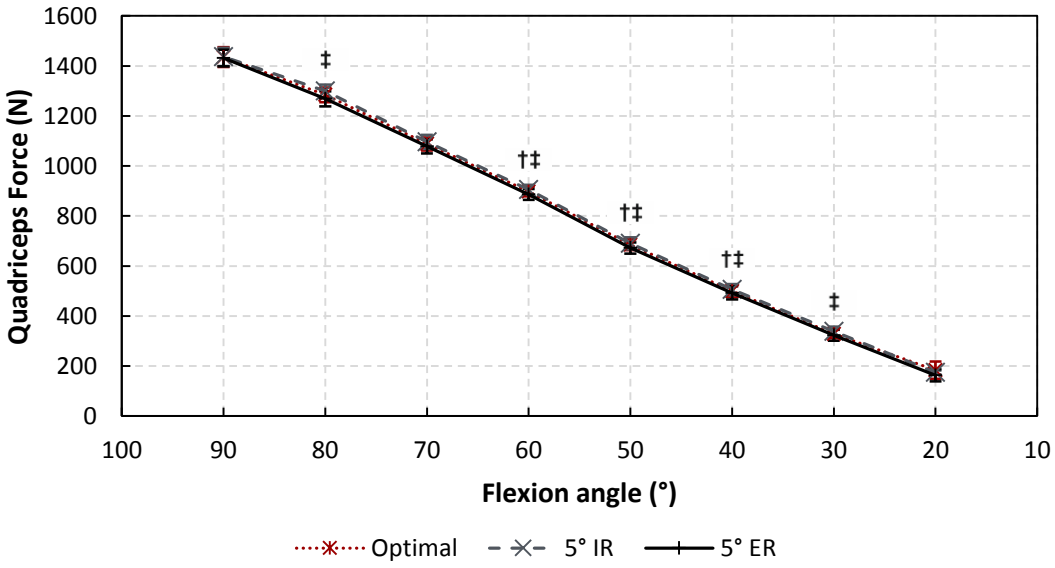

Figure 4-19: Variation in quadriceps force with flexion angle for each modelled femoral rotational position (mean ± SD). p < 0.05: * Optimal vs 5° IR; † Optimal vs 5° ER; ‡ 5° IR vs 5° ER;

4.3.3.2. Patella Tendon Moment Arm

For all of the assessed femoral rotations, the PTMA increased with extension (Figure 4-20) from 90° to 30° of flexion by, on average, 5.8 ± 2 mm. Measurements were not possible at 20° of flexion because of issues relating to measurements when the joint was close to full extension. During extension from 90° to 40° of flexion the PTMA was statistically significantly lower when the distal femur was rotated externally by 5° (Figure 4-20). This equated to an average difference of 5 ± 2 mm.

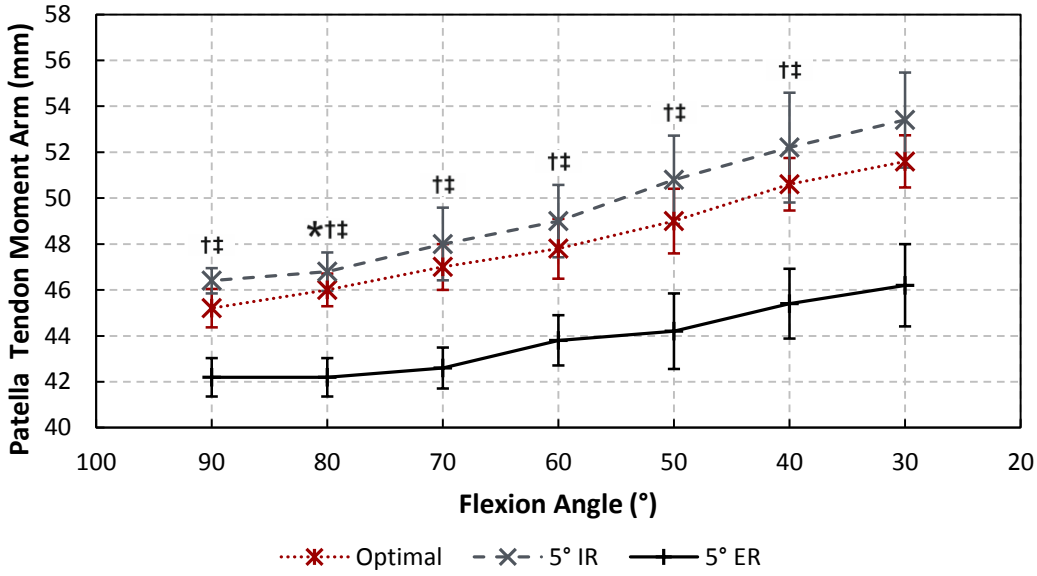

Figure 4-20: Variation in PTMA with flexion angle for each modelled femoral rotational position (mean ± SD). p < 0.05: * Optimal vs 5° IR; † Optimal vs 5° ER; ‡ 5° IR vs 5° ER;

No consistent statistically relevant difference was seen between the measured PTMA values when the distal femur was placed optimally or rotated 5° internally.

4.3.3.3. Patellofemoral Compressive Force

As was the case for the measurements of the quadriceps force, the patellofemoral compressive force fell with extension for all of the tested femoral rotations (Figure 4-22). However, the pattern was less linear, and demonstrated some degree of levelling out in deeper flexion.

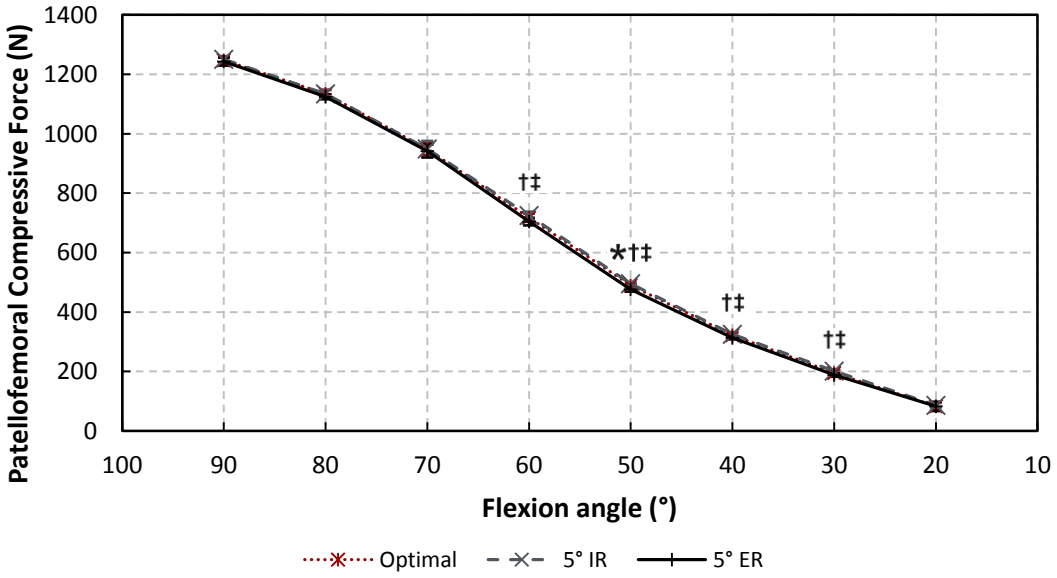

Figure 4-21: Variation in patellofemoral compressive force with flexion angle for each modelled femoral rotational position (mean ± SD). p < 0.05: * Optimal vs 5° IR; † Optimal vs 5° ER; ‡ 5° IR vs 5° ER;

External rotation resulted in statistically lower patellofemoral compressive forces in mid flexion (30° - 60°), but at all flexion angles this difference was less than 20 N. In deeper flexion (> 60°), distal femoral rotation of ± 5° had no statistically relevant effect on the measured patellofemoral compressive force.

4.3.3.4. Ratio of Patella Compressive Force to Quadriceps Force

The patella compressive force to quadriceps force ratio remained, for all of the assessed femoral rotations, constant at approximately 0.87 during knee extension from 90° to 70° (Figure 4-22). It then reduced fairly linearly to approximately 0.5 at 20° of flexion. Distal femoral rotation had little effect on the ratio.

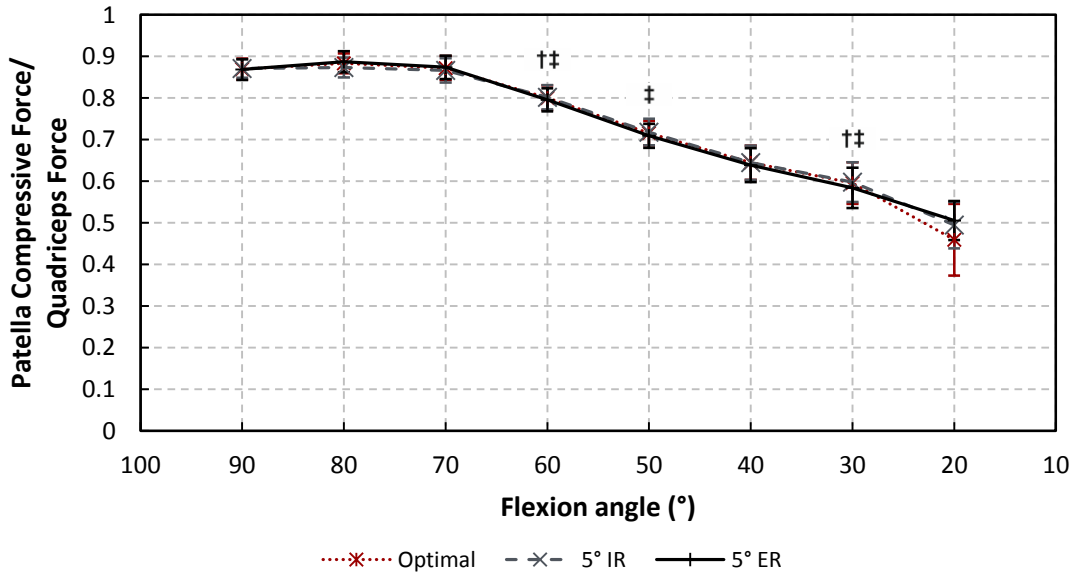

Figure 4-22: Variation in ratio of patella compressive force to quadriceps force ratio with flexion angle for each modelled femoral rotational position (mean ± SD). p < 0.05: * Optimal vs 5° IR; † Optimal vs 5° ER; ‡ 5° IR vs 5° ER;

4.3.3.5. Patellofemoral Contact Area

For all of the assessed femoral rotations, the PFJ contact area fell with extension from approximately 0.7 cm² at 90° to 0.1 cm² at 20° of flexion (Figure 4-23). Throughout the extension movement, the proportion of joint contact on the lateral aspect exceeded 65% (Figure 4-24, Figure 4-25), increasing sharply in mid flexion and approaching 100% in full extension.

Malrotation of the distal femur did not affect the total amount of PFJ contact area or the magnitude of contact on the lateral aspect of the patella component (Figure 4-23, Figure 4-24). All of the tested configurations demonstrated consistent lateral edge loading at all

flexion angles and when medial contact did occur it was purely on the edge of the patella components (Figure 4-25).

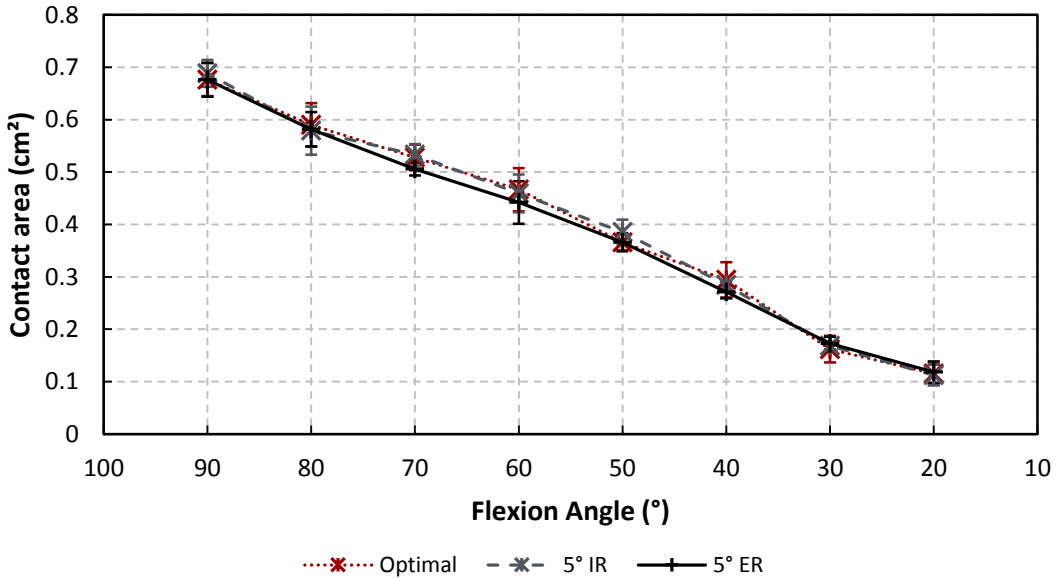

Figure 4-23: Variation in patella contact area with flexion angle for each modelled femoral rotational position (mean ± SD).

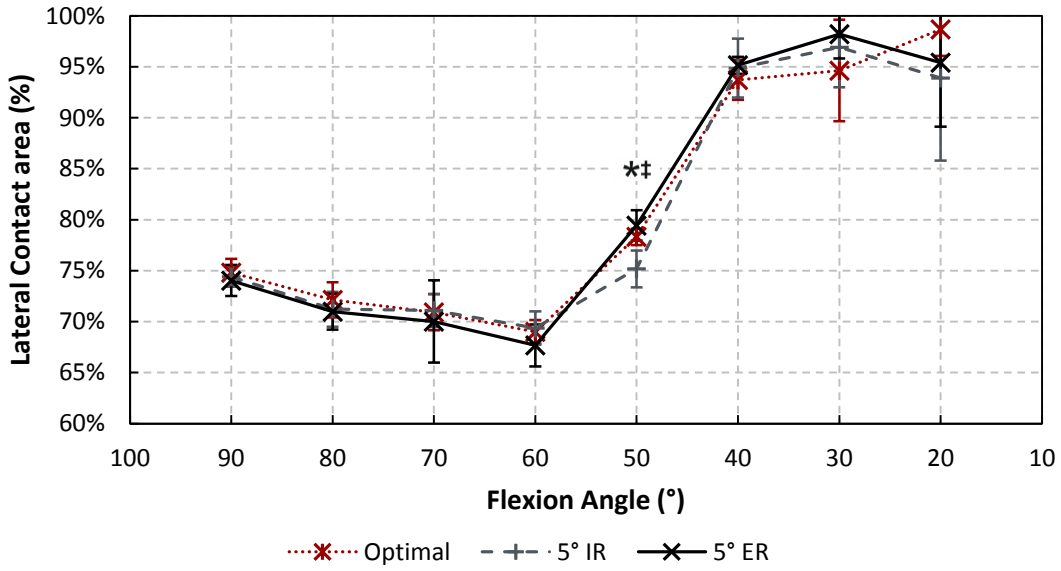

Figure 4-24: Variation in percentage of lateral contact area with flexion angle for each modelled femoral rotational position (mean ± SD (capped at 100%)). p < 0.05: * Optimal vs 5° IR; † Optimal vs 5° ER; ‡ 5° IR vs 5° ER;

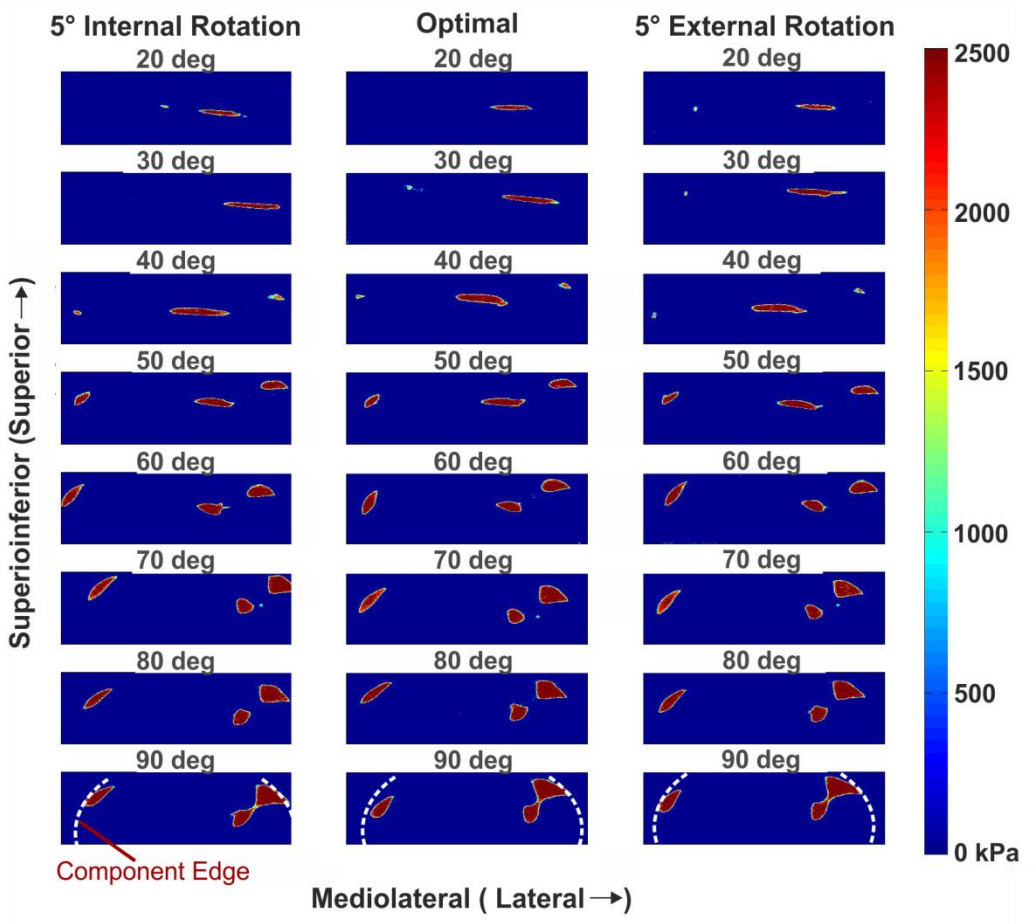

Figure 4-25: Example contact area plots

4.3.3.6. Patellofemoral Pressure

The calculated PFJ pressure followed a similar pattern to the patellofemoral compressive force, demonstrating a slight levelling out under more than 70° of flexion (Figure 4-26). Distal femoral rotation did not affect the amount of pressure that the PFJ was subjected to. For all of the assessed femoral rotations, in deep flexion (> 60°), the PFJ contact pressure exceeded 15 MPa.

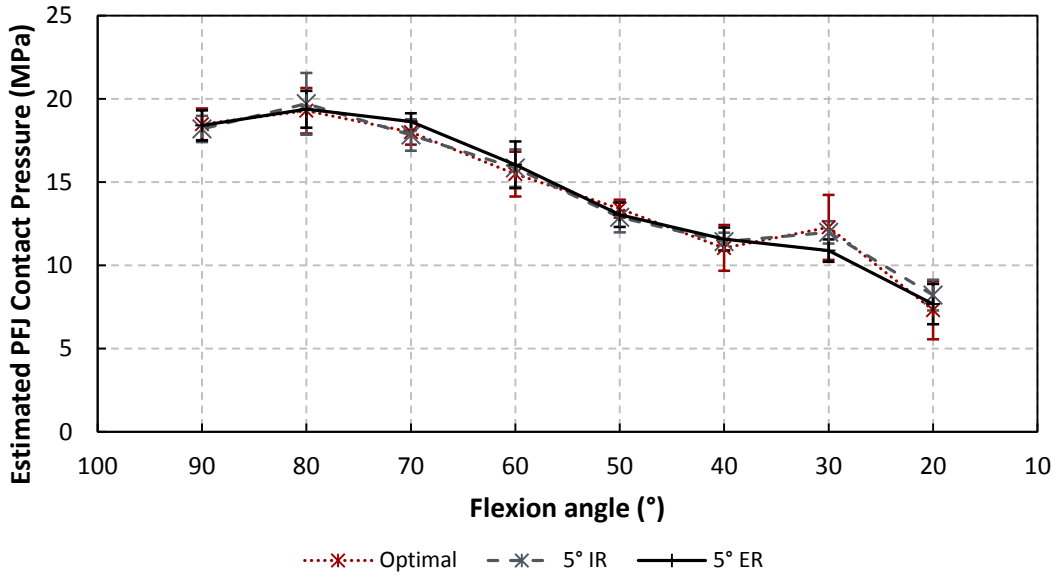

Figure 4-26: Variation in patellofemoral pressure with flexion angle for each modelled femoral rotation (mean ± SD).

4.3.4. Discussion

The general patterns of the measured contact area, forces, pressures and PTMA are comparable to those reported during Study (i). Therefore, discussion of these general patterns will not be repeated. The present discussion concentrates on the differences between the three test configurations.

External rotation did not have a clinically relevant impact on the forces associated with the extensor mechanism. In mid flexion (40 - 60°) 5° ER caused a statistically relevant reduction in the measured quadriceps and patellofemoral compressive forces (Figure 4-19 & Figure 4-21). At a peak, this difference was less than 20 N. This is well within the magnitude of variation which would be expected between patients [1] and therefore unlikely to be of any clinical relevance. No difference was seen in deep flexion when the patella was under most load. Internal rotation of 5° had no statistically or clinically relevant effect on the measured forces within the extensor mechanism (Figure 4-19 & Figure 4-21).

Two computational studies carried out under a variety of loading levels using the Scorpio system demonstrated similarly small reductions in contact force with 3° and 5° ER, and a negligible effect of IR by 3° [261,262]. In line with these literature studies, the Scorpio NRG implant, when matched with an asymmetric dome (Figure 4-1), has therefore been shown to be relatively forgiving, in terms of extensor mechanism forces, to femoral rotation.

External rotation of the distal femur by 5° caused a significant reduction in the PTMA, whereas IR only caused a trend towards an increased PTMA (Figure 4-20). External rotation

of the distal femur, relative to the quadriceps mechanism, will have resulted in a less prominent lateral condyle, which was the primary patella contact point throughout the tested flexion range (Figure 4-25). This caused the patella component to tilt and shift laterally, and sit deeper within the trochlear groove and intercondylar notch. This observation is supported by previous kinematic studies reported in the literature, with this and other implants, which demonstrated that *ER* causes an increase in lateral tilt and shift [33,216,262,263]. Internal rotation will have resulted in a more prominent lateral condyle and as previously reported [29,216,262,263], this caused a medial patella tilt and shift. However, the increase in PTMA caused by *IR* was substantially less than the decrease caused by ER. This suggests that the patellofemoral geometry of the system and the tension in the quadriceps tendon prevented the patella reaching an excessively anterior position.

This reported change in PTMA would have been expected, if the PFJ is modelled as a simple pulley, to cause a corresponding change in the quadriceps force, and hence the patella compressive force. The results from this study therefore support the theory that the PFJ acts as an amplifying lever and that the patella lever arm has a greater impact on the quadriceps force than the PTMA. This cannot be assessed further as the superioinferior position of the PFJ contact was not measured during this study. However, femoral rotation would not be expected to substantially affect the superioinferior joint contact position, and hence the patella lever arm, as it purely alters the femoral transverse plane geometry.

The ratio of patella compressive force to quadriceps force was also unaffected by distal femoral rotation (Figure 4-22), which again suggested the superioinferior position of the PFJ contact was unchanged. The lack of variation of the ratio of patella compressive force to quadriceps force also suggested that patella flexion was not effected by femoral rotation as has been demonstrated previously in the literature [29].

Rotation of the distal femur also had no significant effect on the PFJ contact area, the amount of lateral contact, or the PFJ pressure. Irrespective of femoral rotation, the asymmetric patella component demonstrated substantial edge loading and consistently greater lateral loading throughout the tested flexion range (Figure 4-25) which corresponds with literature reports of wear on retrieved implants [292]. Similarly, irrespective of femoral rotation, at flexion angles greater than 50°, the calculated pressures exceeded 15 MPa under physiological loading and resulted in permanent component deformation. This suggested that the sombrero patella component design (Figure 4-1) was not congruent with the femoral component. Femoral rotation may therefore have had little biomechanical impact because

the tested rotations (± 5°) were not sufficient to prevent edge loading (Figure 4-25). Previous studies using the same implant have not measured PFJ contact areas or pressures. One study in the literature which overly constrained the knee joint and used a different implant system indicated statistically significant reductions in contact area and increases in contact pressure with ± 5° rotation [28]. However, a computational study by Heegard *et al*, which used a set up more in line with the present work, also indicated few statistically relevant effects of ± 5° femoral rotation [29].

4.3.4.1. Limitations

In addition to the limitations discussed for the previous study, the present study was limited by the use of one patella component for all of the tests rather than one per configuration. This resulted in permanent deformation of the patella component, which caused a trend over consecutive cycles towards an increased contact area in deep flexion (Figure 4-27) and an increased quadriceps force throughout the flexion range (Figure 4-28). The alteration of the sequence of testing for each repeat and the relatively small maximum differences indicates however that this did not affect comparisons of the data for the different rotations.

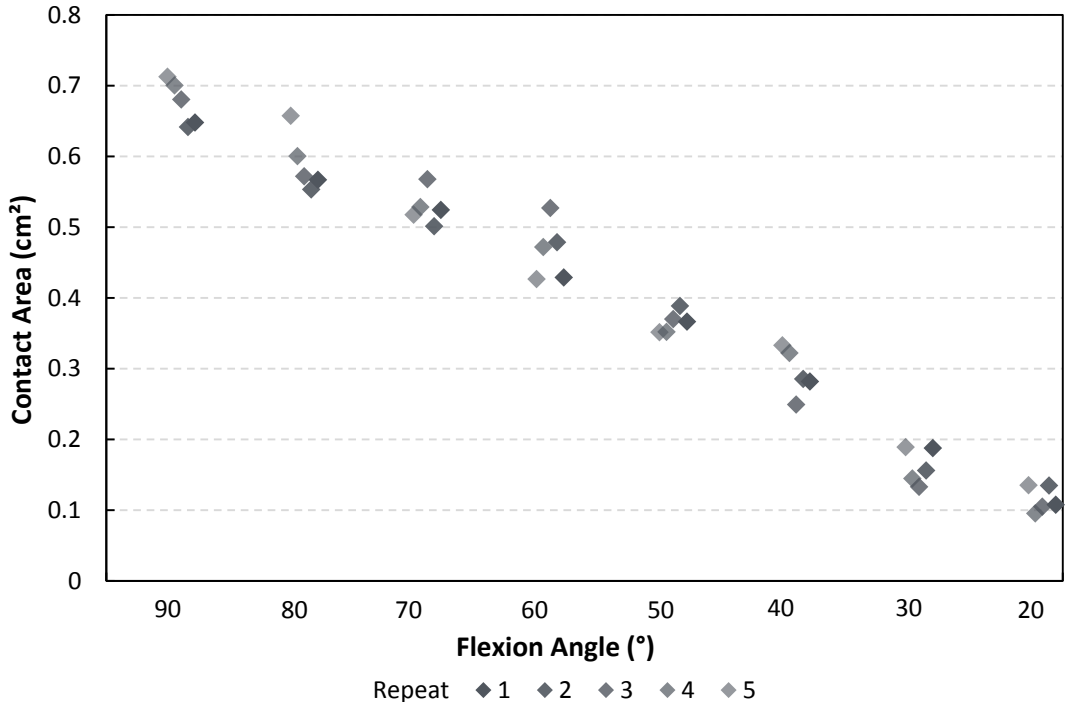

Figure 4-27: Contact area values recorded under physiological loading for each consecutive repeat (only Optimal data shown for clarity)

Femoral rotation was introduced by rotating the femoral component and the proximal insertion points of the collateral and politeofibular ligament models. Such a small change in the location of the approximated ligament attachment points is unlikely to have had a

significant effect on the joint kinematics, as the larger forces applied via the hamstring and quadriceps mechanisms dominate. This assertion was not tested but the agreement of the study results with cadaveric work reported in the literature could be considered to support it [262].

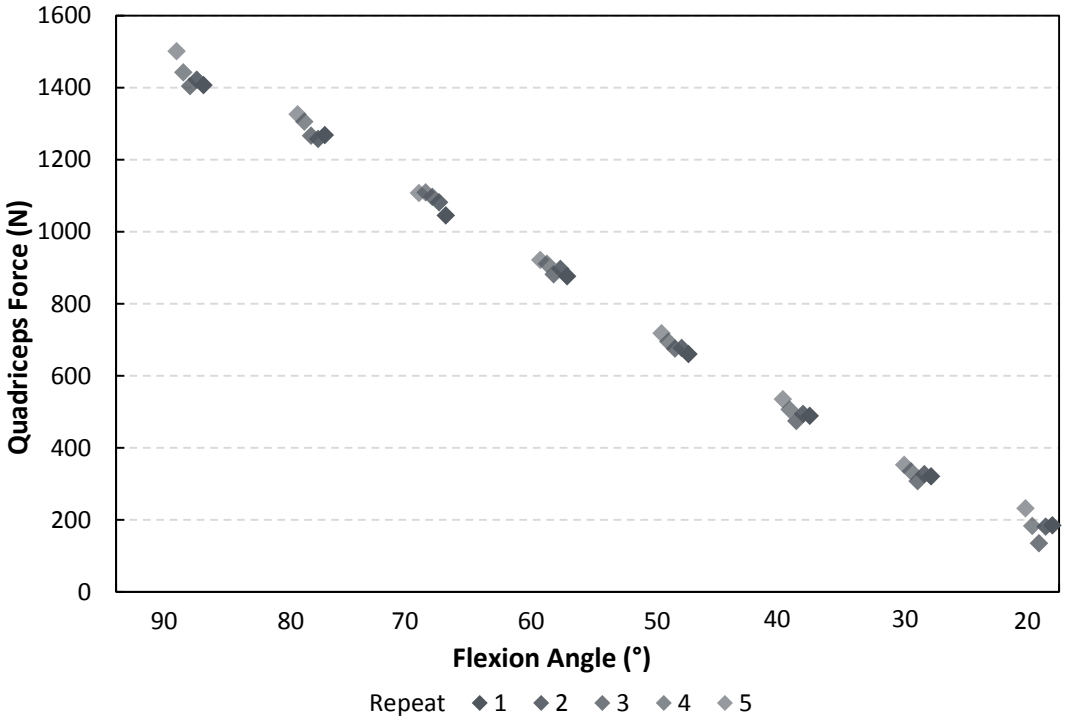

Figure 4-28: Quadriceps force values recorded under physiological loading for each consecutive repeat (only Optimal data shown for clarity)

4.3.5. Conclusions

The present study indicated that, for the prosthesis tested, femoral rotation of ± 5° had no effect on the forces, pressures or contact areas within the PFJ and did not therefore have an impact on the relative potential risk of developing functional limitations relating to the PFJ as a result of instability, pain and/or patella component failure. Irrespective of femoral rotation the estimated PFJ pressures exceeded the offset yield strength of UHMWPE in deeper flexion resulting in permanent deformation.

The study also demonstrated that 5° external femoral rotation significantly decreased the PTMA. However, the lack of corresponding effect on the forces within the PFJ leads to the secondary conclusion that PFJ biomechanics are dominated by the joint contact position, and hence the patella lever arm, rather than the PTMA.

4.4. Study (iii) - The effect of Femoral Sagittal Plane Alignment Errors

4.4.1. Aim

This study aimed to evaluate the effect of femoral component sagittal plane alignment errors on the biomechanics of the PFJ during dynamic knee movements and the associated potential risk of the development of functional limitation relating to patellofemoral instability and pain after TKA.

As a secondary aim, the longer term repeatability of the simulator was also assessed. This was achieved by comparing the results of the optimally placed asymmetric component configurations from this study (*Optimal*) and studies (i) (*Asymmetric*) and (ii) (*Optimal*).

4.4.2. Methods & Materials

This third study was carried out using the previously described protocol. An asymmetric dome patella component was used for all tests.

Three femoral component sagittal rotations were assessed: *Optimal* (as defined by the surgical operating guidelines), *5° Flexion*, and *5° Extension* (Figure 4-29). Rotation was modelled to occur around the femoral component flexion axis. Sagittal plane rotation of ± 5° was simulated based on the maximum errors reported surgically [172,177,179,180].

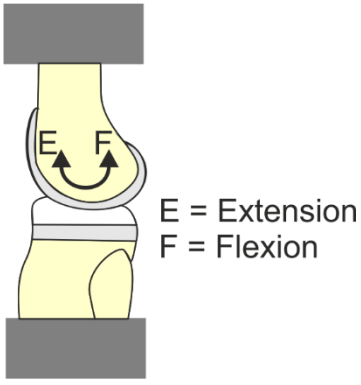

Figure 4-29: Three femoral component sagittal rotations were assessed: *Optimal* (as defined by the surgical operating guidelines), *5° Flexion*, and *5° Extension*

Each rotation in the sagittal plane was assessed five times, repositioning the Sawbone tibia and femur between each experimental repeat. The order of the tests for the three rotations was altered for each repeat. One new patella component was available for each condition and therefore tested five times. In order to assess the effect of repeated testing on the component geometry, the digitising protocol detailed in the previous chapter was used.

4.4.2.1. Statistical Methods

For all of the tests the sample number was five. Data has been reported using mean ± standard deviation (SD) to give an indication of the variability. The standard deviation values for the reported percentage of lateral contact area were capped at 100% as this variable could not physically exceed 100%.

All data was assessed for statistical differences. The p values are not reported but when a difference was significant it has been highlighted on the appropriate graph. Non-parametric tests were used to assess differences between the configurations to reduce the threat of outliers within the relatively small sample. A paired Friedman test and then, where appropriate, Wilcoxon signed rank post hoc tests, were used to assess any differences for each variable between the three femoral rotational configurations ($\alpha = 0.05$).

To assess differences between the optimally placed asymmetric component repeats from this study and studies (i) and (ii), Kruskal Wallis and where appropriate Mann-Whitney-U post hoc tests, were used.

4.4.3. Results

4.4.3.1. Quadriceps Force

The bespoke load cell used to measure the quadriceps force did not function reliably when the femoral component was positioned in the *5° Flexion* or *5° Extension* configurations. Quadriceps data was therefore only available for the *Optimal* situation. The effect of femoral component sagittal plane malalignment on the required quadriceps force could not therefore be assessed. Similarly, the ratios of patella compressive force to quadriceps force could not be computed.

4.4.3.2. Patella Tendon Moment Arm

For all of the assessed femoral sagittal malalignments the PTMA increased with extension of the knee (Figure 4-30). Throughout the extension movement femoral component extension and flexion caused a trend towards a decreased PTMA, which was significant in mid flexion (60° - 40°).

Measurements were not possible at 20° of flexion or at 90° for the flexed condition due to limitations of the rig. Data collection issues also resulted in some data sets being unattainable at 30° flexion of the TFJ (*Optimal*: N = 4; *5° Extension*: N = 3).

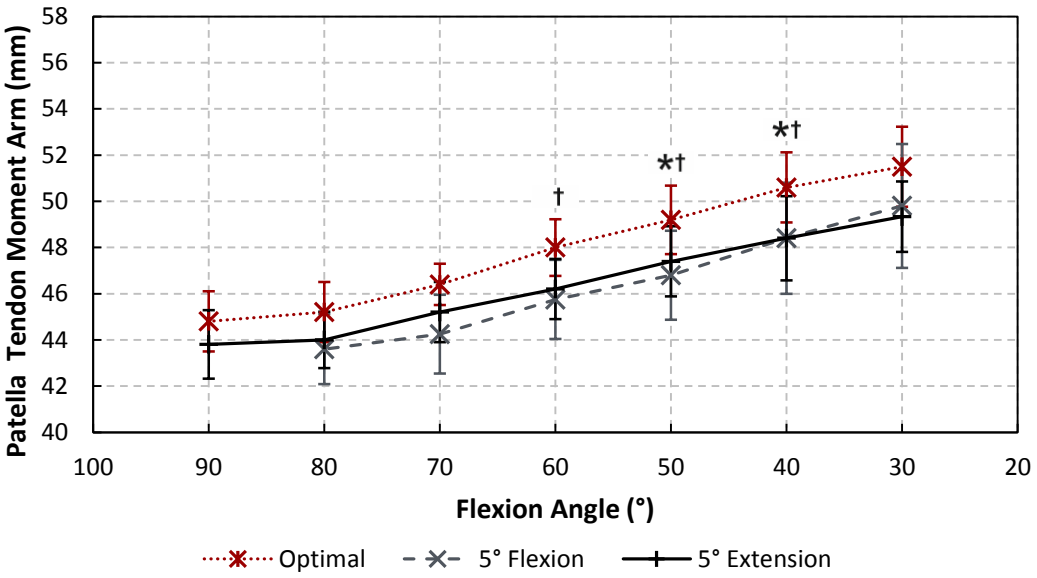

Figure 4-30: Variation in PTMA with flexion angle for each modelled femoral flexion position (mean ± SD). $p < 0.05$: * Optimal vs 5° Flexion; † Optimal vs 5° Extension; ‡ 5° Flexion vs 5° Extension;

4.4.3.3. *Patellofemoral Compressive Force*

The patellofemoral compressive force fell with extension for all of the assessed femoral rotational configurations (Figure 4-31). During extension from 90° to 30° of tibiofemoral flexion, 5° *Flexion* caused a significant reduction in the recorded patella compressive force. In deep flexion (90°)

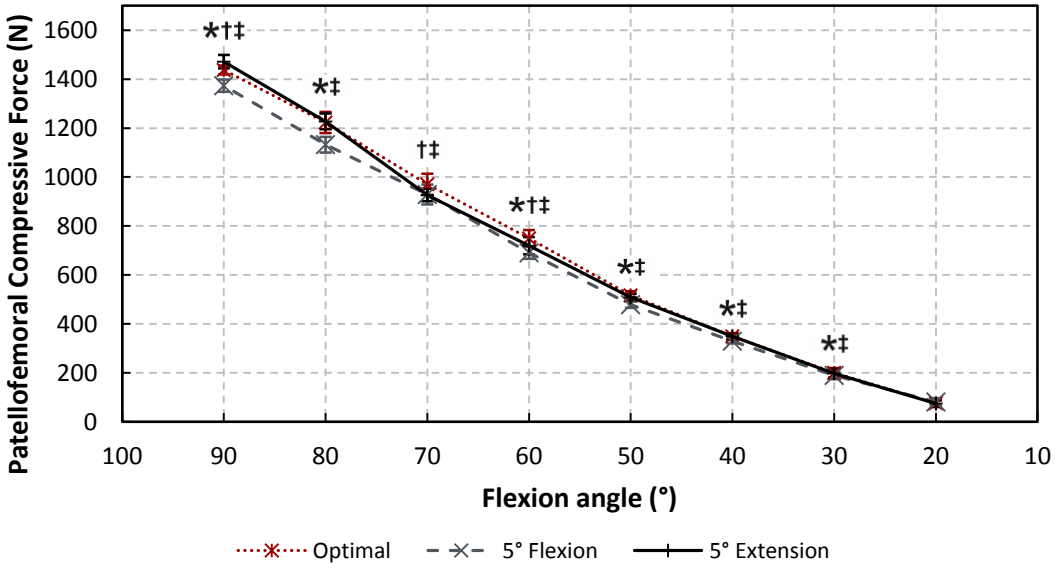

Figure 4-31: Variation in patellofemoral compressive force with flexion angle for each modelled femoral flexion position (mean ± SD). $p < 0.05$: * Optimal vs 5° Flexion; † Optimal vs 5° Extension; ‡ 5° Flexion vs 5° Extension;

5° Extension resulted in a significant increase in the patellofemoral compressive force. However, as the knee extended to 80° this increase disappeared and in mid flexion (70° - 60°) extension of the femoral component caused a significant reduction in the patellofemoral

compressive force. Near full extension, femoral component extension had no effect on the patellofemoral compressive force.

4.4.3.4. Patellofemoral Contact Area

For all of the assessed femoral sagittal plane rotations, the PFJ contact area fell with extension (Figure 4-32). In deep flexion (90°) *5° Extension* caused a significant increase in the PFJ contact area and *5° Flexion* a reduction. As the knee continued to extend the contact area values for the three configurations converged. However, from 60° to 20° of tibiofemoral flexion, *5° Flexion* caused a reduction in the contact area, which was significant at 30° and 50° of flexion. Nearing tibiofemoral extension, extension of the femoral component had little effect.

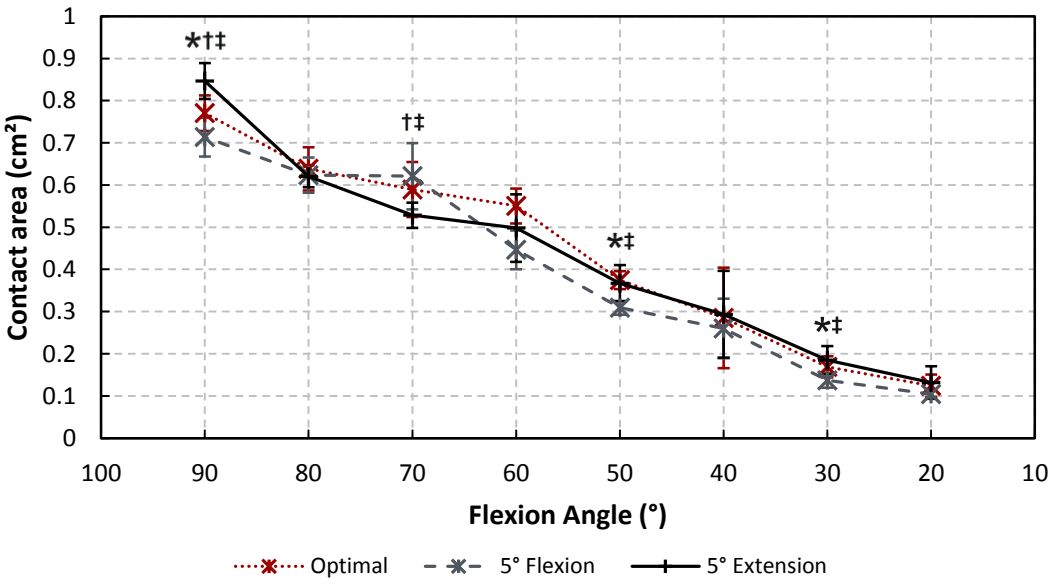

Figure 4-32: Variation in patella contact area with flexion angle for each modelled femoral flexion position (mean ± SD). p < 0.05: * Optimal vs 5° Flexion; † Optimal vs 5° Extension; ‡ 5° Flexion vs 5° Extension;

Throughout the extension movement, more than 70% of the joint contact was on the lateral aspect of the patella components (Figure 4-33, Figure 4-34). During an extension cycle, the amount of lateral contact increased sharply in mid flexion and approached 100% in full extension. This increase was steeper when the femoral component was in flexion.

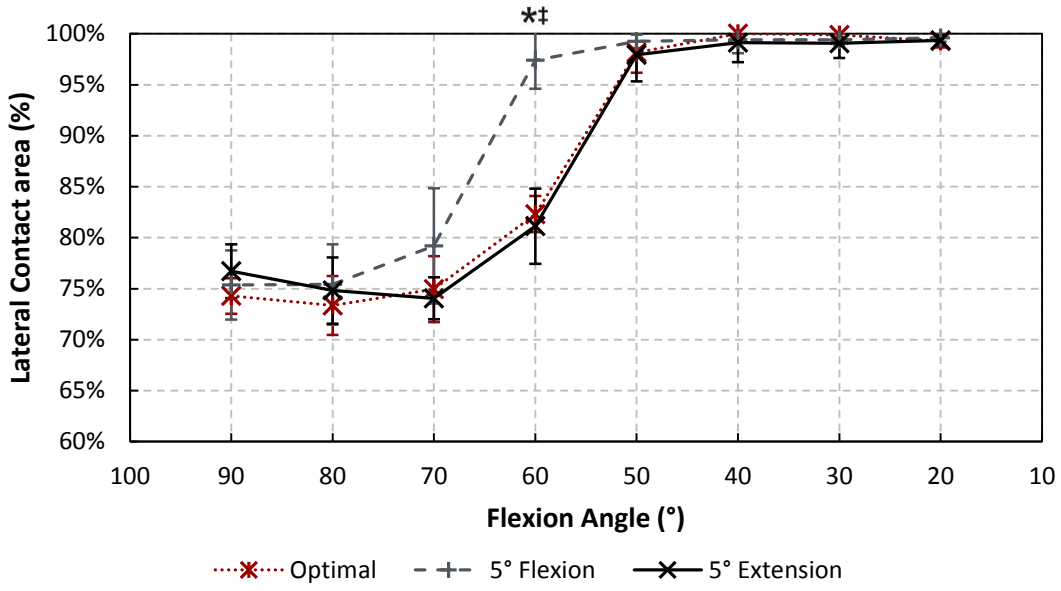

Figure 4-33: Variation in percentage of lateral contact area with flexion angle for each modelled femoral flexion position (mean ± SD (capped at 100%)). $p < 0.05$: * Optimal vs 5° Flexion; † Optimal vs 5° Extension; ‡ 5° Flexion vs 5° Extension;

Consistent lateral edge loading at all flexion angles was seen irrespective of the femoral component sagittal placement (Figure 4-34). Medial contact was only ever on the edge of the patella components.

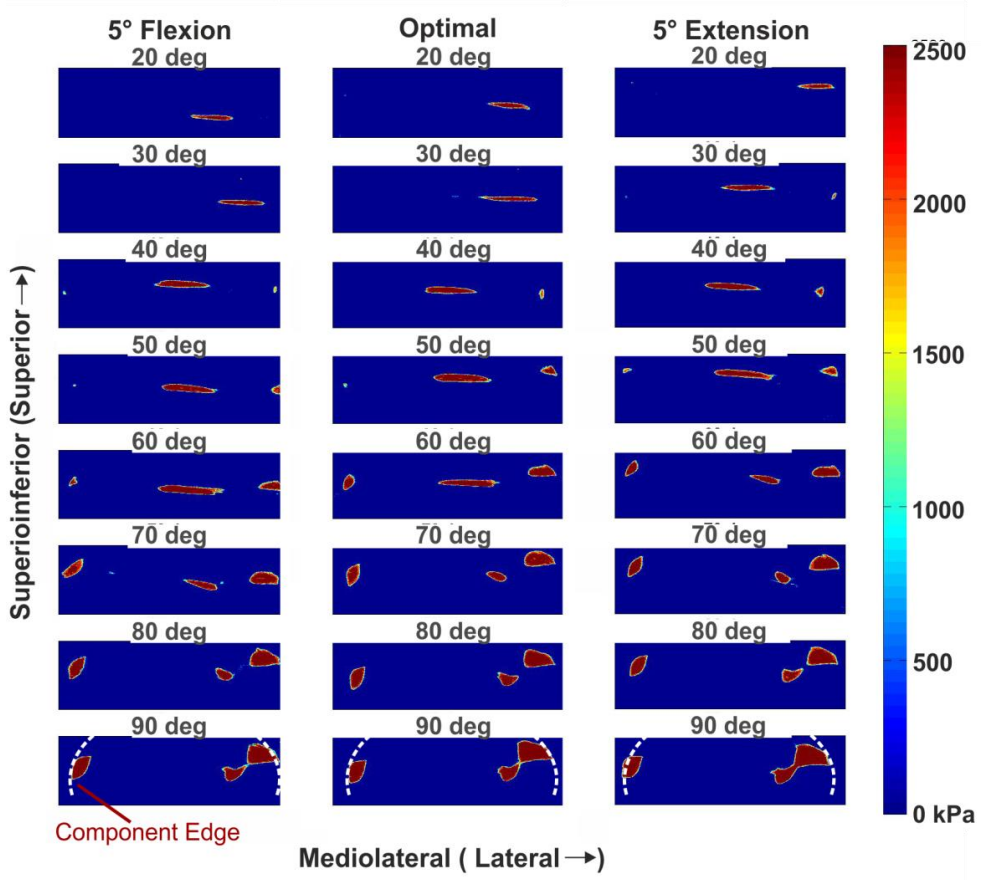

Figure 4-34: Example contact area plots

4.4.3.5. Patellofemoral Pressure

Femoral component flexion *(5° Flexion)* caused a trend towards an increased joint pressure and femoral component extension *(5° Extension)* a significant reduction in contact pressure in deep flexion (90°) (Figure 4-35). Throughout the remainder of the extension cycle femoral component sagittal alignment had little effect. For all of the tested femoral rotational configurations, in deep flexion (> 70°), the PFJ contact pressure exceeded 15 MPa.

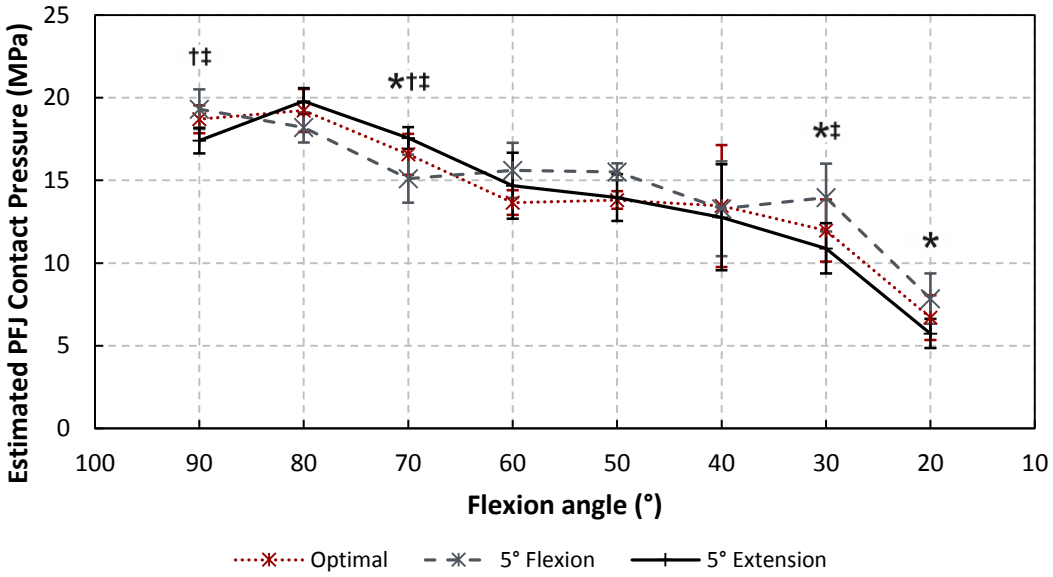

Figure 4-35: Variation in patellofemoral pressure with flexion angle for each modelled femoral flexion position (mean ± SD). p < 0.05: * Optimal vs 5° Flexion; † Optimal vs 5° Extension; ‡ 5° Flexion vs 5° Extension;

4.4.3.6. Deformation

The cyclic loading resulted in permanent deformation on the edge of all of the tested patella components and a small amount of lateral dome deformation (Figure 4-36). The deformation occurred largely after the first repeat (Figure 4-36). After further repeats little change in the pattern of permanent deformation was seen. The patella components were subjected to similar levels of deformation irrespective of the femoral component sagittal plane alignment.

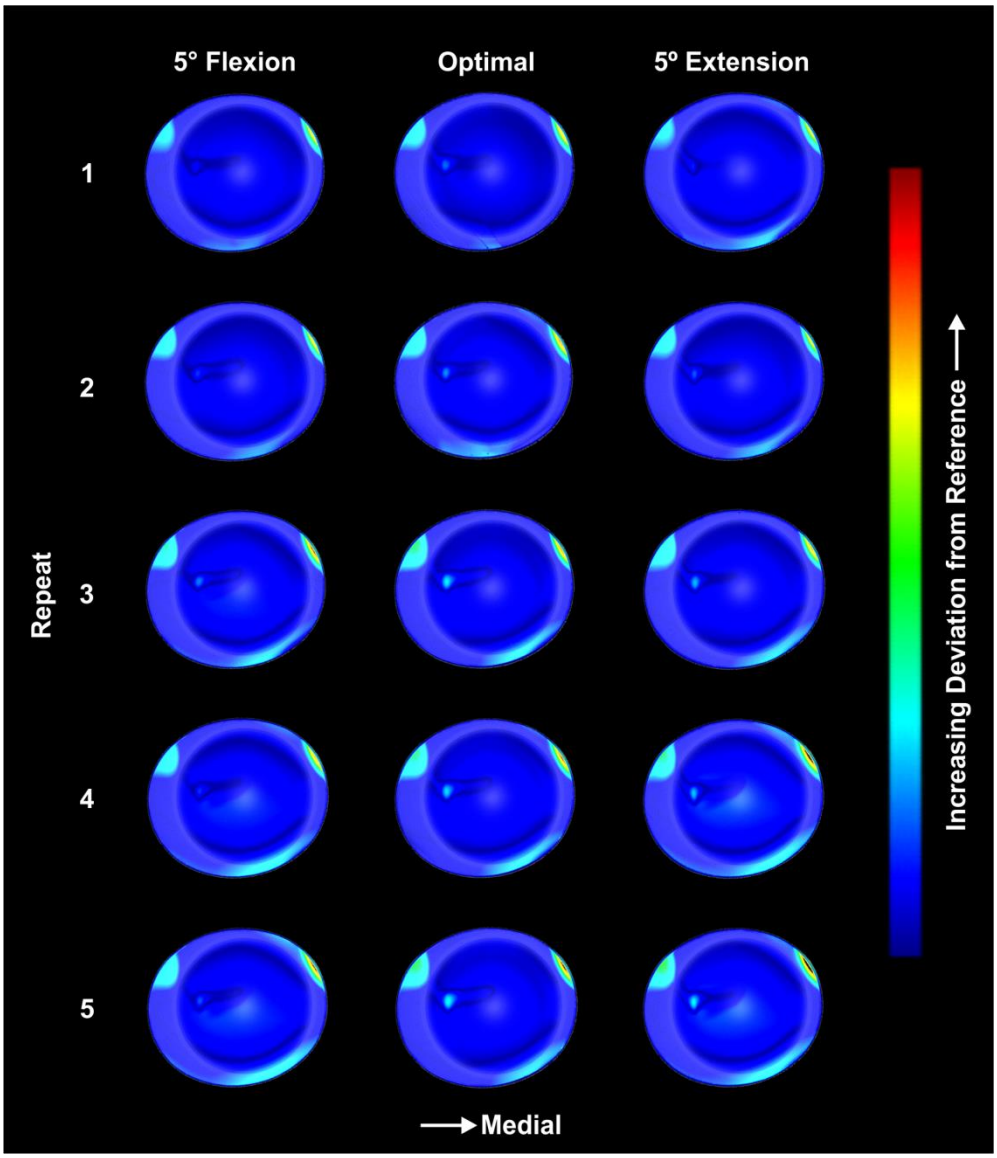

Figure 4-36: Patella surface plots demonstrating the level of permanent deformation, with respect to the implant pre-testing, which was measured for each patella configuration after each testing repitition

4.4.3.7. Simulator Repeatability

The PTMA recorded using the asymmetric dome with the femoral component optimally placed did not vary across the three studies ($p > 0.05$). However, the required quadriceps force was higher for Study (i) (Figure 4-37). This difference was significant in deeper flexion (>60°).

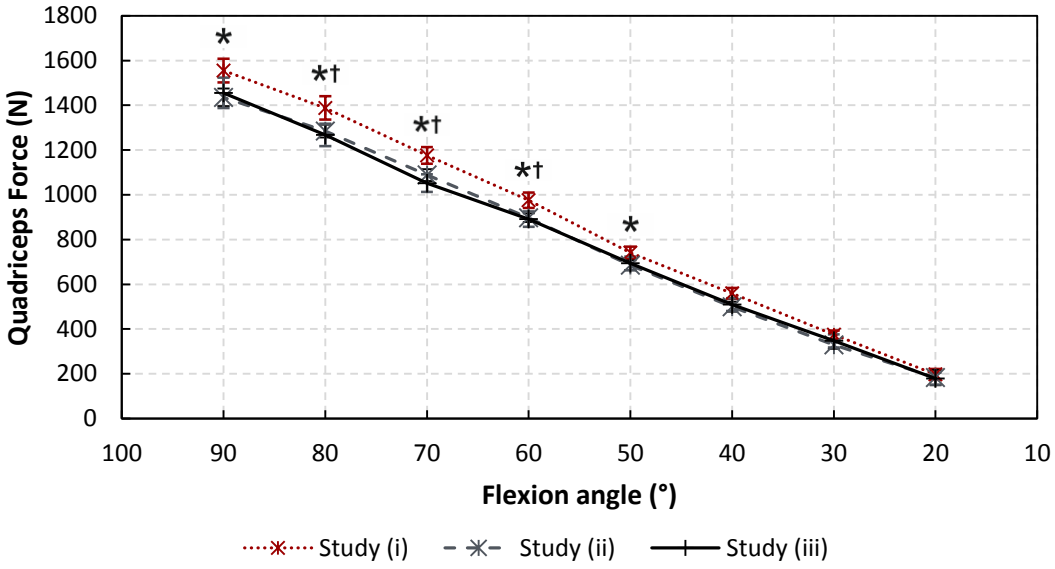

Figure 4-37: Variation in quadriceps force with flexion angle for the optimally placed asymmetric patella component (mean ± SD). $p < 0.05$: * Study (i) vs Study (ii); † Study (i) vs Study (iii); ‡ Study (ii) vs Study (iii);

The recorded patellofemoral compressive force also varied between the studies (Figure 4-38). The patellofemoral compressive force recorded for Study (iii) demonstrated less levelling out in deeper flexion and was significantly higher in mid and deep flexion. The measured PFJ contact area followed a similar pattern and was significantly higher for Study (iii) in deeper flexion (>50°) (Figure 4-39).

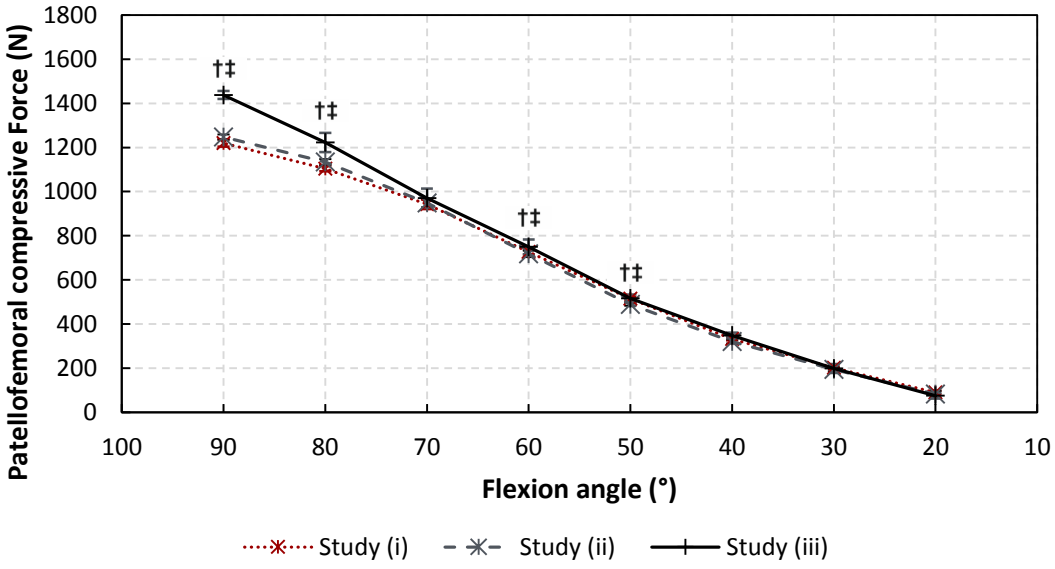

Figure 4-38: Variation in patellofemoral compressive force with flexion angle for the optimally placed asymmetric patella component (mean ± SD). $p < 0.05$: * Study (i) vs Study (ii); † Study (i) vs Study (iii); ‡ Study (ii) vs Study (iii);

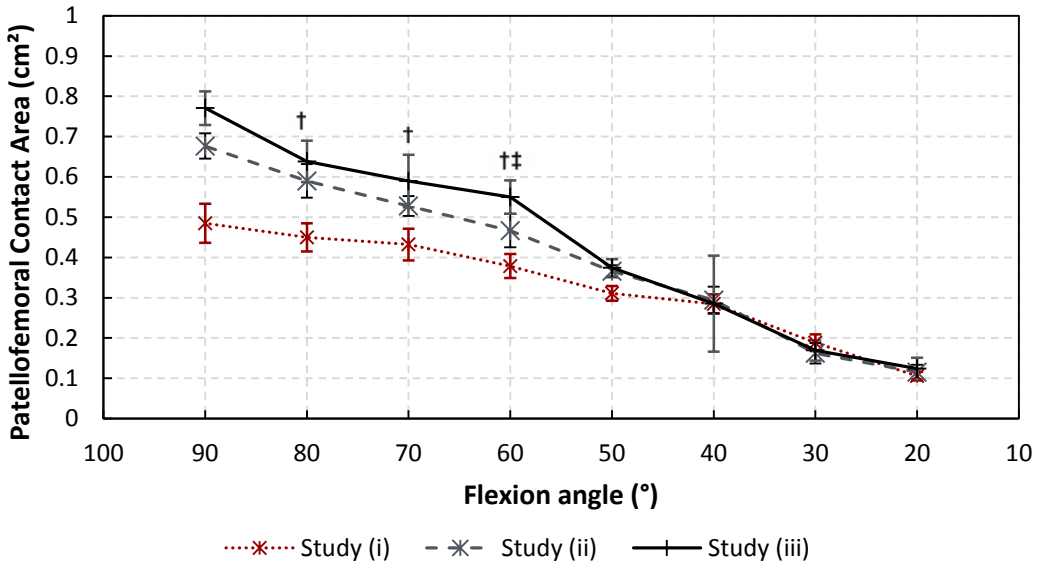

Figure 4-39: Variation in patellofemoral contact area with flexion angle for the optimally placed asymmetric patella component (mean ± SD). p < 0.05: * Study (i) vs Study (ii); † Study (i) vs Study (iii); ‡ Study (ii) vs Study (iii);

4.4.4. Discussion

4.4.4.1. Simulator Repeatability

The optimally placed asymmetric component configurations from this study (*Optimal*) and studies (i) (*Asymmetric*) and (ii) (*Optimal*) were nominally the same. All three configurations employed the same patella component and modelled the optimal surgical femoral component positioning. When these three configurations were compared it was demonstrated that the PTMA recorded for each was comparable but the measured quadriceps force, patellofemoral compressive forces and PFJ contact areas were not always equivalent.

The recorded quadriceps force was significantly higher in deeper flexion for Study (i) (Figure 4-37). No differences were seen between the recorded quadriceps forces for Studies (i) and (ii). This difference did not impact on any of the other measured variables, and was most likely a result of a change in the friction coefficient between the shafts and bearings which allowed the hip construct to move vertically. The bearings were greased at the beginning of the first study only. The results therefore suggested that there was a period of settling in, during which the bearings self-lubricated, before a constant friction force was reached. It may therefore be beneficial for a future study to be carried out to assess how many cycles are needed after greasing of the bearings before a constant friction force is achieved and additionally how many cycles can be carried out before further greasing is required.

In contrast to the measured quadriceps forces, the patella compressive force was significantly higher, in deeper flexion, for Study (iii) as opposed to Study (i) (Figure 4-39). Between Study (ii) and Study (iii) the quadriceps/patella tendon construct was replaced. Although the replacement steel cable was the same dimensions as the original, due to the reduced number of test cycles it had endured, it was straighter and less conformed to the femoral component geometry. The newer steel cable therefore did not contact the femoral component as much and therefore did not share the same proportion of the joint loading as the original construct. This resulted in the observed higher patellofemoral compressive forces in deeper flexion. It may also be beneficial for a future study to be carried out to assess how many cycles are needed to bed in the steel cable patella tendon construct. Alternatively, it may be appropriate to develop a similarly inextensible, but more compliant quadriceps/patella tendon model. The differences seen for the patella compressive forces were mirrored with respect to the PFJ contact area. The joint contact area was significantly higher for Study (iii) compared to Studies (i) and (ii). This was probably a result of increased elastic deformation caused by the increased patella compressive force.

The differences demonstrated did not impact on the conclusions drawn in this thesis as none relied on comparisons between the three separate studies. They purely highlighted potential improvements and further work.

4.4.4.2. Effect of Femoral Component Sagittal Plane Malalignment

With the exception of the patellofemoral compressive forces, which were discussed in the previous sub-section, the general patterns of the various measured and calculated outputs were similar to those reported for the previous two studies. This sub-section therefore concentrates on the differences induced by changes in the femoral component sagittal plane rotational position rather than the general measurement patterns.

Throughout the tibiofemoral extension cycle, *5° Flexion* or *5° Extension* caused a reduction in the PTMA (Figure 4-30). This difference was only significant in mid flexion. Placing the femoral component in extension altered the effective femoral geometry. During the extension movement, the patella component may therefore have tracked in the intercondylar notch for a greater range of flexion of the TFJ before traversing into the trochlear groove, and ultimately exiting the notch later when the femoral component was placed in extension compared to when it was optimally positioned. This caused the consistent shift towards a smaller PTMA which was seen for the *5° Extension* configuration throughout the extension motion (Figure 4-30).

Flexion of the femoral component *(5° Flexion)* was expected to have the opposite effect to component extension, but the results did not support this (Figure 4-30). Flexion of the femoral component could have been expected to cause an effective *"overstuffing of the PFJ"* and hence an increased joint moment arm. However, in the case of the current knee simulation, flexion of the femoral component caused a reduction of the PTMA, possibly because it induced a greater degree of posterior motion of the femoral component. Few other studies have assessed the biomechanical effects of femoral component flexion on the PFJ [29], and this study did not measure joint kinematics, therefore these theories cannot be assessed any further.

The experimental difficulties encountered with the use of the quadriceps load cell when the femoral component was placed in 5° flexion and extension *(5° Flexion* and *5° Extension)* meant that the effect of this change of PTMA on the required quadriceps force could not be assessed. The results of Studies (i) and (ii) do however suggest that the differences would not have been directly mirrored. Indeed the trends seen with regards to quadriceps force have in Studies (i) and (ii) been better aligned to the measured patella compressive force than the PTMA. During extension from 90° to 30°, *5° Flexion* resulted in a significant reduction in the patellofemoral compressive force compared to the *Optimal* rotation (Figure 4-31). At a peak this difference, which is obscured by the scale in Figure 4-32, was 101 N.

At 90° flexion of the TFJ, *5° Extension* caused a small, but significant, increase in the patellofemoral compressive force (Figure 4-31). In contrast, in mid flexion (70 - 60°), *5° Extension* caused a similarly small, but significant, reduction in the patellofemoral compressive force. At a peak, the difference between the compressive force for the *Optimal* and *5° Extension* configurations was 30 N which was within the levels of natural patient variability [1] and unlikely to have any clinical relevance.

If the patella is considered to act as a two dimensional amplifying lever, it can be deduced that the magnitude of the patellofemoral compressive force will primarily depend on the magnitude of the required quadriceps force, the degree of patella flexion and/or the superioinferior position of the PFJ contact position. These results therefore suggest that *5° Flexion* or *5° Extension* of the femoral component significantly alters one or more of these variables. None of these measurements were possible during the present study, but computation work reported in the literature has suggested that flexion of the femoral component caused a trend towards reduced patella flexion in deep tibiofemoral flexion [29].

In deep flexion (90°), and during extension from 60° to 20°, the changes in PFJ contact area mirrored the differences in patellofemoral compressive force (Figure 4-32) suggesting that the patella component was simply deformed by a greater amount when under a greater compressive force. A slight reduction in lateral deformation is demonstrated qualitatively by the surface plots (Figure 4-36) but this is by no means conclusive. Any differences in terms of contact area are therefore likely to have been due to excess elastic, not plastic, deformation.

In mid to late flexion (80 - 70°) however, the differences in PFJ contact area resulting from *5° Flexion* or *5° Extension* did not fully mirror the differences seen in the patellofemoral compressive force. The change in effective femoral geometry as a result of placing the femoral component in *5° Flexion* or *5° Extension* meant that at any nominal tibiofemoral flexion angle the position of the patella component along the trochlear groove or intercondylar notch for each condition would have been different. This may explain the conflicting differences seen in mid to late flexion and may have contributed to the differences reported during the remainder of the extension cycle.

Irrespective of the femoral component flexional position, the degree of lateral contact followed a similar pattern to that detailed previously: approximately 75% in early extension rising sharply to almost 100% in mid extension (Figure 4-33 and Figure 4-34), which is again in keeping with published retrieval data [292]. However, in contrast to the *Optimal* or *5° Extension* configurations, *5° Flexion* caused the shift to almost exclusively lateral loading to occur almost 10° earlier (Figure 4-33). This is likely to be a result of the patella exiting the intercondylar notch earlier in the tibiofemoral extension cycle. When released from the intercondylar notch the geometrical resistance to the lateral quadriceps force will have reduced, allowing the patella to tilt more laterally, hence increasing the proportion of lateral contact. The reverse may not have been true when the femoral component was placed in extension *(5° Extension)* due to changes in the PFJ kinematics or possibly because by 60° flexion of the TFJ the lateral quadriceps force vector was sufficient to tilt the patella irrespective of the femoral geometric constraints.

Only one study in the literature has previously assessed the effect of femoral component sagittal plane rotation on the contact within the PFJ [29]. This study suggested that femoral component flexion of 5° had no effect on the contact patterns. The difference between this study and the previous work is likely a combination of the use of a different implant and a substantially reduced level of loading in the previous work. Computational work by Heegard *et al*. [29], did however demonstrate a trend towards an increased patellofemoral pressure

with 5° femoral component flexion, which is in line with the results detailed here (Figure 4-35). The reported changes in estimated patellofemoral pressure followed corresponding patterns to the reported PFJ contact area.

Flexion of the femoral component has been proposed as an effective intra-operative method to reduce the risk of oversizing the femoral component [298]. However, in the case of the TKA system assessed in this study, 5° flexion of the femoral component has been demonstrated to increase the PFJ pressure by up to 2 MPa and should therefore be used with caution (Figure 4-35).

Irrespective of the degree of femoral component sagittal plane malalignment, at flexion angles greater than 60°, the calculated pressures exceeded 15 MPa under physiological loading. When the femoral component was flexed by 5° however, 15 MPa was exceeded at flexion angles greater than 40°. UHMWPE is commonly quoted to have an offset yield strength of 13 MPa [248]. Femoral component flexion of 5° may therefore increase further the already present potential risk of developing functional limitations in a clinical setting as a consequence of pain and PFJ instability [248,293]. The relatively low number of test cycles and the qualitative nature of the deformation assessment meant that the correlation of these pressure differences to the degree of permanent patella deformation could not be assessed. In line with the results of Studies (i) and (ii) however, the results clearly demonstrated consistent edge loading (Figure 4-34) which resulted in permanent patella component deformation (Figure 4-35).

4.4.4.3. Limitations

This third, and final, study was not subject to any limitations beyond those discussed with respect to Study (i).

4.4.5. Conclusions

The present study demonstrated that, for the prosthesis tested, femoral sagittal plane malalignment of ± 5° caused a reduction in the PTMA. Quadriceps forces could not be measured. It was however demonstrated that flexion of the femoral component by 5° caused a 9% reduction in the patella compressive force, but an increase of up to 2 MPa in the estimated calculated joint pressure. Flexion of the Scorpio NRG component may therefore increase the risk of long term instability as a result of plastic deformation [16], or delamination of non-cross-linked UHMWPE or fractures of cross-linked UHMWPE components [248]. The effect of extension of the femoral component was less pronounced.

Irrespective of the degree of femoral component flexion the patella component was subject to substantial edge loading, in excess of the yield strength of UHMPE, which, in line with the results of Studies (i) and (ii) and retrieval reports in the literature [292], caused permanent implant deformation. This sub-study has therefore once again demonstrated the lack of congruency of the patella component used with the Scorpio NRG implant system may have contributed to the anecdotal reporting of increased long term complications [297].

Chapter 5

Discussion

A review of the literature highlighted the significant role that PFJ complications play with regard to pain and functional limitations following TKA [15,126]. The causes of pain and other complications in the PFJ are not fully understood, but changes in the biomechanics, relating to loading and contact parameters within the joint, are thought to be contributing factors [20-22]. The biomechanics of the PFJ may be affected by a variety of factors, including, but not limited to; implant design and geometry, whether or not the patella is resurfaced, and component positioning.

Some of the factors which may affect the PFJ have been assessed in *in vitro* studies reported in the literature. However, a lack of standard test protocols, and the frequent introduction of multiple confounding factors, makes it difficult to draw conclusions on the clinical issues reported in the literature. The present study therefore aimed to improve understanding of the many factors which may contribute to high rates of PFJ complications and associated pain. This overall aim was achieved through the development of a reliable knee joint simulator and repeatable methods for assessing load and contact parameters within the PFJ. The simulator, was designed to provide an effective protocol and approach for investigating the parameters affecting the PFJ in TKA and to improve on the current approaches that are reported in the literature. The simulator was then used to assess the effect of a number of design and alignment factors on PFJ biomechanics following TKA with a specific implant system.

A table top knee simulator, which was based on the OKR philosophy and replicated human squatting [1,59], was developed. The OKR design constrains the hip, and hence the action of the body weight force component acts vertically above the ankle joint. This does not replicate many activities of daily living where the position of the upper body changes to reduce the body weight moment arm when flexing the knee [196]. In spite of this limitation, and as discussed in the literature [270], the OKR design does facilitate dynamic testing, and allows the simulation of a body weight component, whilst maintaining all six degrees of freedom at the knee joint.

The majority of work evaluating TKA systems reported in the literature has been carried out using implants fixed in cadaveric knees [37,38,188,189,205]. The use of cadaveric knees are however associated with high inter-specimen variability, can be costly and difficult to obtain and time consuming to work with. In addition, due to issues relating to tissue degradation, cadaveric materials can only be tested under limited loads. A knee model to replace a cadaveric knee was therefore developed to reduce the impact of inter-specimen variability,

facilitate extended testing at physiological loads, and limit the overall time and cost commitment.

To maintain a degree of similarity to published studies [23-26,61,190,192,193,201-204,217,218,223,225], and achieve an acceptable compromise between simplicity and physiological relevance, the quadriceps mechanism was modelled dynamically by a single actuator, and the hamstrings simulated as two compartments by constant force springs. In contrast to previously reported non-cadaveric studies [212], the collateral and popliteofibular ligaments were also modelled so as to replicate both the compressive joint force and the kinematic restraint that these structures have been reported to provide in the natural knee [65,67].

There are a number of variables relating to the loading and contact parameters within the PFJ which could be measured using the simulator. The quadriceps force required to carry out a specific task is commonly measured in the studies reported in the literature [23,24,61,96,199,202,236] as it directly impacts a patient's ability to carry out activities of daily living [283]. Similarly, the PTMA is frequently monitored as it gives an indication of the extensor mechanism efficiency [270]. The compressive force, contact area, and contact pressure within the PFJ are frequently measured in published studies [189,191,193,205,243] as they are indicators of the potential risk of pain and component failure following TKA [16,21,248].

Previous studies reported in the literature have also measured kinematics of the PFJ and TFJ [58,94,214]. An understanding of the joint kinematics can provide valuable information relating to the mechanisms contributing to the biomechanics of the PFJ. However, the direct link between kinematic changes and the development of knee pain and/or functional limitations is not clear. The measurement of joint kinematics was therefore not prioritised as a measurement in the present study. The deformation of the patella components over time was however assessed, as this provided an indication of the degree of excessive loading that occurred within the joint. This has not previously been monitored during *in vitro* kinematic studies.

Many studies using cadaveric knees in the literature are carried out under reduced loading to protect the cadaveric tissue [29,31,38,188,189,191,194,210,295]. The work presented in Section 5.2 (Study (i)) demonstrated, in line with the literature [294], that the rate of quadriceps force increase with flexion angle changed with applied load. Furthermore, differences in the rate of change of compressive forces in the patella, and the contact area

were seen when the simulator was subjected to a physiological load level (43 Nm peak flexion moment) compared to the tests at a reduced loading level (approximately 19 Nm peak moment). Measurements carried out under reduced levels of load may therefore significantly under estimate the parameters associated with loading at physiological levels. This result highlighted the importance of testing under physiological loads and therefore the benefit of using a system which did not include cadaveric tissue.

Comparisons with published studies [1,23,24,29,31,61,270,291,292] demonstrated that the simulator modelled physiological knee motion and therefore provided a good representation of the expected clinical scenario. The standard deviations of the force measurements were lower, and those of the contact area comparable, to studies with cadaveric knees in the literature [37,61,188]. The protocol developed therefore facilitated consistent measurements of the quadriceps force, patella compressive force, and PFJ contact area, which enabled the detection of statistically relevant differences at, and below, clinically relevant levels throughout the reported studies. The system therefore demonstrated high sensitivity with regards to PFJ biomechanical measurements, highlighting its suitability for use in comparative studies.

During the course of the study the knee simulator was assessed thoroughly. This highlighted a number of limitations and potential modifications, which were discussed in detail in the previous chapter and could be introduced in any future studies. These limitations however did not detract from any of the conclusions made in the present thesis. The PFJ contact pressure was not measured directly by the described system, but was reliably estimated using accurate measurements of contact area and patella compressive force.

A second limitation of the study was that the simulator did not include models for any soft tissues which stabilise the PFJ. This may be considered to limit the physiological relevance of the model. All of the three studies carried out demonstrated significant, and at some flexion angles, almost exclusive patella edge loading. This was most likely a result of the lack of congruency of the patella component with the trochlea groove of the femoral implant. A previous reported study has indicated that this concern is not unique to the Scorpio system [254]. The primary compressive and constraining action of the PFJ soft tissues occurs in early flexion of the TFJ [77-79]. As the joint flexes further these structures weaken and would be unlikely to provide sufficient force to substantially alter the tracking of the Scorpio patella component or potentially those of many other commercially available TKA implant designs. At most the patella retinaculum may be expected to provide a small additional compressive

force. The absence of any soft tissue constraints in the PFJ, which was considered necessary to preserve the simplicity of the system, should therefore have had a limited effect on the reported peak pressure and contact area measurements and no significant impact on the comparisons made.

Overall, the simulator was shown to provide a simplified but physiologically relevant model of the human knee which allowed effective assessment of PFJ biomechanics. The system eliminated the need for cadaveric tissue and therefore enabled a relatively low cost and timely assessment of the potential contribution of a number of design and alignment factors to the potential risk of long term functional limitations following TKA. However, despite the effectiveness of the developed simulator, only a small number of the factors hypothesised to effect PFJ biomechanics following TKA could be assessed in the present study. Initially, the effect of patella design, medialisation of the patella component, femoral component rotation and femoral component sagittal plane rotation were assessed using a specific TKA design. Patella design was highlighted as an important starting point as it has never been systematically assessed before [16]. Studies reported in the literature have indicated that the chosen alignment factors may be important contributors to the development of PFJ complications, but the evidence is sparse and sometimes conflicting [28-36].

The specific effect of each design and alignment and the consistency of the results with the literature were discussed in the previous chapter. This final discussion concentrates on evaluating the different modifications that had corresponding or opposing effects on different PFJ biomechanical measurements. Table 5-1 demonstrates the statistically relevant changes which were reported during the three experimental studies. The differences are simply reported in terms of an increase or decrease in a measured variable.

The experimental results suggested that, with respect to the Scorpio NRG PS implant system, the PTMA was sensitive to transverse and sagittal plane femoral component rotations. However, the clinical effect of this is not clear as, especially in deep flexion, the quadriceps force required to maintain a constant rate of motion was largely unaffected by any of the assessed changes.

The patellofemoral compressive force was much more sensitive to alignment and changes in the patella component design than the quadriceps force. Flexion of the femoral component, the use of a centrally placed patella component, and, in early flexion, femoral external rotation caused a significant reduction in the patella compressive force. To a lesser extent femoral component extension and the use of a medialised concentric patella component had

the converse effect. However, if the magnitude of change is considered it was only the introduction of femoral sagittal plane malrotation in deep flexion that had a clinically relevant impact on the measured compressive forces. It may therefore be hypothesised that the Scorpio knee is relatively forgiving, in terms of extensor mechanism forces, design and alignment changes and was only affected by the sagittal plane malalignments as this had an effect equivalent to placing the joint in more or less flexion.

Table 5-1: Table demonstrating the variations which had statistically significant effects on each measured or calculated variable. The datum was considered to be an asymmetric patella component placed in an optimal location (N.b. Quadriceps force data and ratio data not available for the sagittal plane error study (Study (iii))

Flexion Angle	90	80	70	60	50	40	30	20
Quadriceps Force								
Increased				ER	ER ◎ ◎	ER	◎	
Reduced								
PTMA								
Increased		IR						
Reduced	ER	ER	ER	ER Ext	ER Ext Flex	ER Ext Flex		
Patella Compressive Force								
Increased	Ext ◎	◎		◎	◎ IR			
Reduced	Flex ◎	Flex ◎	Ext ◎	ER Ext Flex	ER Flex ◎	ER Flex ◎	ER Flex	
Ratio of Patella Compressive Force to Quadriceps Force								
Increased	Ext ◎	◎	◎	◎	◎			
Reduced	Flex		Ext	ER	Flex		ER	
Patella Contact Area								
Increased				Flex				
Reduced	◎	◎	◎	◎	◎			
Lateral Patella Contact Area								
Increased	◎	◎	◎	◎				
Reduced					IR ◎	◎	◎	◎
Patellofemoral Pressure								
Increased	◎	◎	Ext ◎	◎ ◎	◎			Flex
Reduced	Ext		Flex				Flex	

IR **5° Femoral Component Internal Rotation** Flex **5° Femoral Component Flexion** ◎ **Concentric**

ER **5° Femoral Component External Rotation** Ext **5° Femoral Component Extension** ◎ **Medialised**

In contrast, the measured contact characteristics, PFJ contact area and joint pressure, were, for the most part, only sensitive to patella component changes. Medialisation of the patella component apex, either geometrically or through component medialisation, caused a significant, and most likely a clinically relevant, increase in PFJ contact area and a corresponding reduction in the joint pressure. With respect to the potential risk of functional limitations associated with PFJ complications, the Scorpio system therefore appears to be much more sensitive to patella component design than alignment alterations, which may be a consequence of a lack of congruency between the patella component and femoral implant.

With respect to the Scorpio NRG PS implant, these results could be used to advocate medialisation of the apex of the patella component, and potentially warn against excessive femoral component sagittal plane malalignment. However, the completed studies are only a start. In order to fully map the factors which affect PFJ biomechanics following TKA, and provide comprehensive advice to surgeons and implant designers, all potential alignment errors with respect to the femoral, patella, and tibial components must be assessed. The studies must then be repeated using a variety of implant systems to establish the effect of tibiofemoral design factors. It is also important to note that these factors may not act in isolation. The effect of compound errors must also be considered. The completion of such a significant body of work is a great undertaking, but the development of the present simulator will facilitate such a systematic investigation. The development of a validated, computational model of the present simulator could also be considered.

Irrespective of patella geometry, patella medialisation, and femoral alignment, in deep flexion, the offset yield strength of UHMWPE [248] was consistently exceeded under the physiological loading conditions used in this study. This resulted in permanent deformation where loading was greatest: on the edge of the patella components. This deformation, which was also observed visually, appeared to be a consequence of a lack of congruency between the femoral and patella components and corresponded with literature reports of wear scars on retrievals [292].

The prominent edges associated with the sombrero design of the Scorpio patella component appeared to be a primary point of contact with the femoral component throughout mid to deep flexion or once the patella component had entered or was approaching the intercondylar notch. The relatively high tolerance of the implant system to the range of clinically relevant alignment errors modelled during the present investigation may therefore be because the levels of rotations modelled were not sufficient to prevent this edge loading

and induce increased loading on the dome of the component. An alternative implant design, with a more congruent patella component may be much more sensitive to rotational errors. The long term effect of this excessive loading is not clear but it may cause chronic instability, result in failure of the patella component, or stimulate intraosseous nerve cells within the patella remnant resulting in AKP and functional limitations [16,21,248].

Chapter 7

Conclusions & Further Work

6.1. Conclusions

The overall aim of this research study was to improve current understanding of factors contributing to high rates of PFJ complications. This was addressed through the investigation of the effect of TKA component alignment and design on the biomechanics of the PFJ. In order to achieve this aim three objectives were detailed:

1. *Develop an in vitro human knee simulator, which enables the dynamic assessment of the PFJ after primary TKA.*
2. *Develop in vitro test methods to measure pressures, contact areas, and forces in the PFJ, as well as the quadriceps force and patella tendon moment arm during a dynamic knee movement.*
3. *Evaluate the effect of design and component alignment on the variables detailed in Objective 2.*
    - *3.1. Evaluate the effect of patella component design.*
    - *3.2. Evaluate the effect of patella component mediolateral placement.*
    - *3.3. Evaluate the effect of femoral component transverse plane rotation.*
    - *3.4. Evaluate the effect of femoral sagittal component plane rotation.*

To address *Objective 1*, a knee simulator which modelled a human squatting motion was developed. Methods to assess PFJ pressure, PFJ contact area, patellofemoral compressive force, PTMA and the quadriceps force were developed to address *Objective 2* and facilitate the assessment of the relative potential risk of the development of functional limitations relating to the PFJ after TKA. Comparisons with previous *in vivo* and *in vitro* results demonstrated that the simulator provided a good representation of the natural knee. In addition, as the system did not use cadaveric specimens, it facilitated testing at physiological load levels, the importance of which was demonstrated during the experimental testing. The measured results using the simulator also had substantially lower standard deviations than those associated with the use of cadaveric specimens reported in the literature. This enabled the assessment of clinically relevant differences between the various tested configurations with fewer repeats.

The results obtained in this study were specific to one type of implant design: the Scorpio NRG. For this TKA design, the study demonstrated that the use of an asymmetric patella component, as opposed to a symmetric component, or medialisation of a symmetric component by 5 mm significantly increased the PFJ contact area and reduced the joint

contact pressure. The use of an asymmetric component or medialisation could therefore be considered to reduce the relative potential risk of instability, pain and patella component failure.

The study also indicated that the Scorpio NRG system, in terms of PFJ biomechanics, was relatively forgiving to clinically reported maximum errors in femoral transverse plane alignment. Femoral rotation of ± 5° had no effect on the forces, pressures or contact areas within the PFJ. External rotation of 5° significantly decreased the PTMA. However, the lack of corresponding effect on the forces within the PFJ draws the clinical relevance of this finding into doubt. In contrast 5° flexion of the femoral component, a relatively large surgical error, resulted in a 9% reduction in the patella compressive force but an increase of up to 2 MPa in the estimated calculated joint pressure. Flexion of the Scorpio NRG component may therefore increase the risk of long term PFJ complications. The effect of extension of the femoral component on the patella compressive force was less pronounced, but 5° extension did result in a significant reduction in the PFJ contact pressure at 90° flexion of the TFJ.

In addition, the three studies which were carried out to address *Objective 3* all concluded that neither the symmetric nor the asymmetric patella components available with the Scorpio NRG system are congruent with the femoral trochlea geometry. Irrespective of alignment, the patella components were subject to substantial edge loading, in excess of the yield strength of UHMPE in deep flexion, which caused permanent implant deformation. None of the alignment or design changes assessed in the present study were sufficient to eliminate the potential risk of deformation and pain, which appeared to be associated with the patellofemoral design of the system.

With respect to the Scorpio NRG PS implant system, the results highlighted the importance of considering PFJ placement carefully, and could be used to advocate medialisation of the apex of the patella component, and warn against excessive femoral component sagittal plane malalignment. The investigations carried out as part of this initial work are however only a first step. Further investigations assessing the effect of all possible component malalignments, utilising a number of different implant systems must be carried out before a comprehensive understanding of the effect of each change on the PFJ is achieved. The results detailed in the present study demonstrate that the investigations required to achieve this can be carried out accurately and relatively swiftly using the developed simulator.

6.2. Further Work

6.2.1. Simulator Developments

Before carrying out further testing using the simulator a few issues could be addressed. The vertical bearing arrangement could be replaced by a self-lubricated arrangement to eliminate the need for periodic lubrication and reduce the sensitivity of the rig to the level of bearing lubrication.

Secondly, a more physiological quadriceps tendon model could be developed to allow both the consistent transfer of load to the patella and the natural wrapping of the tendon onto the femur in deeper flexion. Thirdly, the bespoke load-cell used to measure the quadriceps force should be redesigned to allow the assessment of a greater number of malalignments and, if feasible, the compressive patella load cell could be replaced by a three axis load cell to measure the resultant PFJ vector.

6.2.2. Future Investigations

In order to develop a more comprehensive understanding of the factors which may contribute to the potential risk of functional limitations associated with pain and failure in the PFJ after TKA further investigations should primarily focus on the continued assessment of the effect of individual design and alignment factors. For example, the effect of femoral geometry should be considered, as should the effect of changes in the tibiofemoral joint line. The effect of changes in more than one factor at the same time should also be explored.

The completion of such a body of work, through experimental studies using the developed simulator or perhaps utilising a validated computational model of the described method, would allow the full population of a matrix such as that detailed in the discussion (Table 6-1). The knowledge gained from the understanding of the effect of each specific alignment factor could inform future surgical and design practice. It may also provide a matrix which could be used to interpret future cadaveric studies assessing a new implant design or an assessment of the biomechanical effect of a new surgical philosophy such as kinematic alignment.

References

1. Mason, J. J., Leszko, F., Johnson, T. and Komistek, R. D., 2008. Patellofemoral joint forces. *Journal of Biomechanics,* 41 (11), pp.2337-2348.

2. Iorio, R., Robb, W. J., Healy, W. L., Berry, D. J., Hozack, W., Kyle, R. F., Lewallen, D. G., Trousdale, R. T., Jiranek, W. A., Stamos, V. P. and Parsley, B. S., 2008. Orthopaedic surgeon workforce and volume assessment for total hip and knee replacement in the United States: preparing for an epidemic. *The Journal of Bone & Joint Surgery. American Volume,* 90 pp.1598-1605.

3. Lotke and Lonner ed, 2004. *Master Techniques in Orthopaedic Surgery: Knee Arthroplsty.* Philadelphia:Lippincott Williams & Wilkins.

4. Callaghan, J. J. ed, 2003. *The adult knee.* Philidelphia:Lippincott Williams & Wilkins.

5. Kurtz, S., Ong, K., Lau, E., Mowat, F. and Halpern, M., 2007. Projections of primary and revision hip and knee arthroplasty in the United States from 2005 to 2030. *The Journal of Bone & Joint Surgery. American Volume,* 89 pp.780-785.

6. Swedish Joint Registry, 2012. *Annual Report 2012.*

7. Behrend, H., Giesinger, K., Giesinger, J. M. and Kuster, M. S., 2012. The "forgotton joint" as the ultimate goal in joint arthroplasty. *The Journal of Arthroplasty,* 27 (3), pp.430-436.

8. Lygre, S. H. L., Espehaug, B., Havelin, L. I., Vollset, S. E. and Furnes, O., 2011. Failure of total knee arthroplasty with or without patella resurfacing. *Acta Orthopaedica,* 82 (3), pp.282-292.

9. Clements, W. J., Miller, L., Whitehouse, S. L., Graves, S. E., Ryan, P. and Crawford, R. W., 2010. Early outcomes of patella resurfacing in total knee arthroplasty. *Acta Orthopaedica,* 81 (1), pp.108-113.

10. Calvisi, V., Camillieri, G. and Lupparelli, S., 2009. Resurfacing versus nonresurfacing the patella in total knee arthroplasty: a critical appraisal of the available evidence. *Archives of Orthopaedic and Trauma Surgery,* 129 (9), pp.1261-1270.

11. Pavlou, G., Meyer, C., Leonidou, A., As-Sultany, M., West, R. and Tsiridis, E., 2011. Patellar Resurfacing in Total Knee Arthroplasty: Does Design Matter? *The Journal of Bone & Joint Surgery. American Volume,* 93 (14), pp.1301.

12. Forster, M. C., 2004. Patellar resurfacing in total knee arthroplasty for osteoarthritis: a systematic review. *The Knee,* 11 pp.427-430.

13. Sensi, L., Buzzi, R., Giron, F., De Luca, L. and Aglietti, P., 2011. Patellofemoral Function After Total Knee Arthroplasty. *The Journal of Arthroplasty,* 26 (8), pp.1475-1480.

14. Arbuthnot, J. E., Mcnicholas, M. J., Mcgurty, D. W. and Rowley, D. I., 2004. Total knee replacement and patellofemoral pain. *Surgeon-journal of The Royal Colleges of Surgeons of Edinburgh and Ireland,* 2 (4), pp.230-233.

15. Hsin-Nun, S., Lih-Yuann Shih, Yon-Cheong Wong and Hsu, R. W.-W., 2004. Long-term changes of the nonresurfaced patella after total knee arthroplasty. *The Journal of Bone & Joint Surgery. American Volume,* 86 (5), pp.935.

16. Seil, R. and Pape, D., 2011. Causes of failure and etiology of painful primary total knee arthroplasty. *Knee Surgery, Sports Traumatology, Arthroscopy,* 19 (9), pp.1418-1432.

17. Berend, K. R., Parvizi, J., Nunley, R. M., Lombardi, A. V., Ruh, E. L., Clohisy, J. C., Hamilton, W. G., Della Valle, C. J. and Barrack, R. L., 2013. High level of residual symptoms in young patients with TKA. *In: AAOS,* March 19-23 2013, Chicago, USA.

18. National Joint Registry for England & Wales, 2011. *8th Annual Report 2011.* Hemel Hempstead:National Joint Registry for England & Wales.

19. Petersen, W., Rembitzki, I., Brüggemann, G.-P., Ellermann, A., Best, R., Koppenburg, A. and Liebau, C., 2013. Anterior knee pain after total knee arthroplasty: a narrative review. *International Orthopaedics,* pp.1-10.

20. Biedert, R. M. and Sanchis-Alfonso, V., 2002. Sources of Anterior Knee Pain. *Clinical Sports Medicine,* 21 pp.335-347.

21. Dye, S. F., 2005. The Pathophysiology of Patellofemoral Pain. *Clinical Orthopaedics and Related Research,* 436 pp.100-110.

22. Barton, R. S., Ostrowski, M. L., Anderson, T. D., Ilahi, O. A. and Heggeness, M. H., 2007. Intraosseous innervation of the human patella. *The American Journal of Sports Medicine,* 35 (2), pp.307-311.

23. Ostermeier, S. and Stukenborg-Colsman, C., 2011. Quadriceps force after TKA with femoral single radius. *Acta Orthopaedica,* 82 (3), pp.339-343.

24. Ward, T. R., Pandit, H., Hollinghurst, D., Moolgavkar, P., Zavatsky, A. B., Gill, H. S., Thomas, N. P. and Murray, D. W., 2012. Improved quadriceps mechanical advantage in single radius tkrs is not due to increased patella tendon moment arm. *The Knee,* 19 (5), pp.564-570.

25. Becher, C., Heyse, T. J., Kron, N., Ostermeier, S., Hurschler, C., Schofer, M. D., Fuchs-Winkelmann, S. and Tibesku, C. O., 2009. Posterior stabilized TKA reduce patellofemoral contact pressure compared with cruciate retaining TKA in vitro. *Knee Surgery, Sports Traumatology, Arthroscopy,* 17 (10), pp.1159-1165.

26. Heyse, T. J., Becher, C., Kron, N., Ostermeier, S., Hurschler, C., Schofer, M. D., Tibesku, C. O. and Fuchs-Winkelmann, S., 2009. Patellofemoral pressure after TKA in vitro: highly conforming vs. posterior stabilized inlays. *Archives of Orthopaedic and Trauma Surgery,* 130 (2), pp.191-196.

27. Heinert, G., Kendoff, D., Gehrke, T., Preiss, S. and Sussmann, P., 2012. Patellar tracking in mobile bearing and fixed bearing total knee replacements, a cadaveric study. *The Journal of Bone & Joint Surgery. British Volume,* 94 (S IX), pp.11.

28. Verlinden, C., P Uvin, L Labey, J. P Luyckx, J Bellemans and Vandenneucker, H., 2010. The influence of malrotation of the femoral component in total knee replacement on the mechanics of patellofemoral contact during gait. *The Journal of Bone & Joint Surgery. British Volume,* 92 (5), pp.737.

29. Heegaard, J. H., Leyvraz, P. F. and Hovey, C. B., 2001. A computer model to simulate patella biomechanics following tkr. *Clinical Biomechanics,* 16 pp.415-423.

30. Luyckx, J., Verlinden, C., Vanbiervliet, J., Labey, L., Innocenti, B., Bellemans, J. and Vandenneucker, H., 2012. The influence of malrotation and material of the femoral component on patellofemoral contact mechanics and wear during gait. *In: ORS 2012 Annual Meeting,* San Fransisco.

31. Anglin, C., Brimacombe, J. M., Wilson, D. R., Masri, B. A., Greidanus, N. V., Tonetti, J. and Hodgson, A. J., 2010. Biomechanical Consequences of Patellar Component Medialization in Total Knee Arthroplasty. *The Journal of Arthroplasty,* 25 (5), pp.793-802.

32. Mane, A. M., Clary, C. W. and Maletsky, L. P., 2005. The effects of patellar misalignment on patello-femoral kinematics for fixed and mobile bearing knees. *In: Summer Bioengineering Conference,* June 22-26, Vail, Colorado.

33. Miller, M. C., Zhang, A. X., Petrella, A. J., Berger, R. A. and Rubash, H., 2001. The effect of component placement on knee kinetics after arthroplasty with an unconstrained prosthesis. *Journal of Orthopaedic Research,* 19 pp.614-620.

34. Yoshii, I., Whiteside, L. A. and Anouchi, Y. S., 1992. The effect of patella button placement and femoral component design on patella tracking in total knee arthroplasty. *Clinical Orthopaedics and Related Research,* 275 pp.211.

35. Bronson, F., Halloran, J. P., Laz, P. J., Petrella, A. J. and Rullkoetter, P. J., 2005. Sensitivity of patellofemoral mechanics to patella component position. *In: 51st Annual Meeting of the Orthopaedic Research Society,* Washington.

36. Korbuda, L. A., Klein, R. and Essner, A., 2011. Development of a malaligned patella testing model. *In: ORS 2011 Annual Meeting,* San Fransisco.

37. Fornalski, S., Mcgarry, M. H., Bui, C. N. H., Kim, W. and Lee, 2012. Biomechanical effects of joint line elevation in TKA. *Clinical Biomechanics,* 27 (8), pp.824-829.

38. Lee, T. Q., Budoff, J. E. and Glaster, F. E., 1999. Patella component positioning in total knee arthroplasty. *Clinical Orthopaedics and Related Research,* 366 pp.274-281.

39. Hsu, H. C., Luo, Z. P., Rand, J. A. and An, K. N., 1996. Influence of patellar thickness on patellar tracking and patellofemoral contact characteristics after total knee arthroplasty. *The Journal of Arthroplasty,* 11 (1), pp.69-80.

40. Oishi, C. S., Kaufman, K. R., Irby, S. E. and Colwell, C. W., 1996. Effects of patellar thickness on compression and shear forces in total knee arthroplasty. *Clinical Orthopaedics and Related Research,* 331 pp.283-291.

41. Star, M. J., Kaufman, K. R., Irby, S. E. and Colwell, C. W., 1996. The effects of patellar thickness on patellofemoral forces after resurfacing. *Clinical Orthopaedics and Related Research,* 322 pp.279-285.

42. Anderson, K., Buehler, K. and Markel, D., 2005. Computer Assisted Navigation in Total Knee ArthroplastyComparison With Conventional Methods. *The Journal of Arthroplasty,* 20 pp.132-138.

43. Robinson, R. P., 2005. The early inovators of totay's resurfacing condylar knees. *The Journal of Arthroplasty,* 20 (1 S1), pp.2.

44. Schindler, O. S., 2012. Basic kinematics and biomechanics of the patellofemoral joint Part 2: the patella in total knee arthroplasty. *Acta Orthopaedica Belgium,* 78 pp.11-29.

45. Brick, G. W. and Scott, R. D., 1988. The patellofemoral component of total knee arthroplasty. *Clinical Orthopaedics and Related Research,* 231 pp.163.

46. Wylde, V., Blom, A., Whitehouse, S., Taylor, A., Pattison, G. and Bannister, G., 2009. Patient-Reported Outcomes After Total Hip and Knee Arthroplasty: Comparison of Midterm Results. *The Journal of Arthroplasty,* 24 (2), pp.210-216.

47. Palastanga, Field and Soames, 2002. *Anatomy & Human Movement.* 4th. Oxford:Butterworth-Heinemann.

48. Rand, J. A., 2004. Extensor Mechanism Complications Following Total Knee Arthroplasty. *The Journal of Bone & Joint Surgery. American Volume,* 86 (9), pp.2061.

49. Elias, S. G., Freeman, M. A. and Gokcay, E. I., 1990. A correlative study of the geometry and anatomy of the distal femur. *Clinical Orthopaedics and Related Research,* 260 pp.98.

50. Eckhoff, D. G., Dwyer, T. F., Bach, J. M., Spitzer, V. M. and Reinig, K. D., 2001. 3D morphology of the distal part of the femur viewed in virtual reality. *The Journal of Bone & Joint Surgery. British Volume,* 83 (S2P1), pp.43.

51. Stiehl, J. B., 2005. A Clinical overview patellofemoral joint and application to total knee arthroplasty. *Journal of Biomechanics,* 38 pp.209-214.

52. Churchill, D. J., Incavo, S. J., Johnson, C. C. and Beynnon, B. D., 1998. The transepicondylar axis approximates the optimal flexion axis of the knee. *Clinical Orthopaedics and Related Research,* 356 pp.111-118.

53. Iwaki, H., Piskerova, V. and Freeman, M. A., 2000. Tibiofemoral movement 1: the shapes and relative movements of the femur and tibia in the unloaded cadaver knee. *The Journal of Bone & Joint Surgery. British Volume,* 82 pp.1189.

54. Freeman, M. A., 2003. The movement of the knee studied by MRI. *Clinical Orthopaedics and Related Research,* 410 pp.35-43.

55. Standring ed, 2005. *Grey's Anatomy.* 29th. London:Elsevier Churchill Livingstone.

56. Johnson, A. J., Harwin, S. F., Howell, A. M., Banjerjee, A. and Mont, M. A., 2013. Alignment in TKA: where have we come from and where are we going? *In: AAOS,* Chicago.

57. Cox, A. J., 1990. Biomechanics of the patello-femoral joint. *Clinical Biomechanics,* 5 pp.123-130.

58. Andriacchi, T. P., Yoder, D., Conley, A., Rosenberg, A., Sum, J. and Galante, J., 1997. Patellofemoral design influences function following total knee arthroplasty. *The Journal of Arthroplasty,* 12 (3), pp.243.

59. Peebles and Norris, 1998. *Adult Data.* London:Department of Trade and Industry.

60. Stiehl, J., 2001. Kinematics of the patellofemoral joint in total knee arthroplasty. *The Journal of Arthroplasty,* 16 (6), pp.706-714.

61. Browne, C., Hermida, J., Bergula, A., Colwelljr, C. and Dlima, D., 2005. Patellofemoral forces after total knee arthroplasty: effect of extensor moment arm. *The Knee,* 12 (2), pp.81-88.

62. D'lima, D. D., Chen, P. C., Kester, M. A. and Colwell, C. W., 2003. Impact of PF design on PF forces and polyethelyne stresses. *The Journal of Bone & Joint Surgery. American Volume,* 85 pp.85-93.

63. Johanson, N. A., Cerynik, D. L. and Pasquale, M., 2011. Measuring patellofemoral forces and pressures in a simulated operating room environment. *The Journal of Arthroplasty,* 26 (1), pp.137.

64. Robinson, J. R., Bull, A. M. J., Thomas, R. R. D. and Amis, A. A., 2006. The Role of the Medial Collateral Ligament and Posteromedial Capsule in Controlling Knee Laxity. *The American Journal of Sports Medicine,* 34 (11), pp.1815-1823.

65. Robinson, J. R., Bull, A. M. J. and Amis, A. A., 2005. Structural properties of the medial collateral ligament complex of the human knee. *Journal of Biomechanics,* 38 (5), pp.1067-1074.

66. Victor, J., Wong, P., Witvrouw, E., Sloten, J. V. and Bellemans, J., 2009. How Isometric Are the Medial Patellofemoral, Superficial Medial Collateral, and Lateral Collateral Ligaments of the Knee? *The American Journal of Sports Medicine,* 37 (10), pp.2028-2036.

67. Sugita, T. and Amis, A. A., 2001. Anatomic and Biomechanical Study of the Lateral Collateral and Popliteofibular Ligaments. *The American Journal of Sports Medicine,* 29 (4), pp.466.

68. Meister, B. R., Michael, S. P., Moyer, R. A., Kelly, J. D. and Schneck, C. D., 2000. Anatomy and kinematics of the lateral collateral ligament of the knee. *The American Journal of Sports Medicine,* 28 (6), pp.869.

69. Laprade, R. F., Ly, T. V., Wentorf, F. A. and Engebretsen, L., 2003. The Posterolateral Attachments of the Knee. *The American Journal of Sports Medicine,* 31 (6), pp.854.

70. Shahane, S., Ibbotson, C., Strachan, R. and Bickerstaff, D. R., 1999. The popliteofibular ligament. An anatomical study of the posterolateral corner of the knee. *The Journal of Bone & Joint Surgery. British Volume,* 81 (4), pp.636-642.

71. Veltri, D. M., Deng, X.-H., Torzilli, P. A., Maynard, M. J. and Warren, R. F., 1996. The Role of the Popliteofibular Ligament in Stability of the Human Knee. *The American Journal of Sports Medicine,* 24 (1), pp.19-27.

72. Pasque, C., Noyes, F. R., Gibbons, M., Levy, M. and Grood, E., 2003. The role of the popliteofibular ligament and the tendon of popliteus in providing stability in the human knee. *The Journal of Bone & Joint Surgery. British Volume,* 85 (2), pp.292-298.

73. Nau, T., Chevalier, Y., Hagemeister, N., Deguise, J. A. and Duval, N., 2005. Comparison of 2 surgical techniques of posterolateral corner reconstruction of the knee. *The American Journal of Sports Medicine,* 33 (12), pp.1838-1845.

74. Chun, Y. M., Kim, S. J. and Kim, H. S., 2008. Evaluation of the mechanical properties of posterolateral structures and supporting posterolateral instability of the knee. *Journal of Orthopaedic Research,* 26 (10), pp.1371-1376.

75. Miyatake, S., Kondo, E., Tsai, T. Y., Hirschmann, M., Halewood, C., Jakobsen, B. W., Yasuda, K. and Amis, A. A., 2011. Biomechanical comparisons between 4-strand and modified Larson 2-strand procedures for reconstruction of the posterolateral corner of the knee. *The American Journal of Sports Medicine,* 39 (7), pp.1462-1469.

76. Rand, J. A., 1994. The Patellofemoral Joint in Total Knee Arthroplasty. *The Journal of Bone & Joint Surgery. American Volume,* 76 (4), pp.612.

77. Bicos, J., Fulkerson, J. P. and Amis, A., 2007. Current Concepts Review: The Medial Patellofemoral Ligament. *The American Journal of Sports Medicine,* 35 (3), pp.484-492.

78. Amis, A. A., 2007. Current concepts on anatomy and biomechanics of patellar stability. *Journal of Sports Medicine Arthroscopy Review,* 15 (2), pp.48-56.

79. Sandmeier, R. H., Burks, R. T., Bachus, K. N. and Billings, A., 2000. The effect of reconstruction of the medial patellofemoral ligament on patellar tracking. *The American Journal of Sports Medicine,* 28 (3), pp.345-349.

80. Merican, A. M., Sanghavi, S., Iranpour, F. and Amis, A. A., 2009. The structural properties of the lateral retinaculum and capsular complex of the knee. *Journal of Biomechanics,* 42 (14), pp.2323-2329.

81. Weber, W., And Weber, E., (Translated By: Maquet, P., and Furlong, R.), 1992. *Mechanics of the human walking apparatus.* Berlin:Springer-Verlag.

82. Pinskerova, V., Maquet, P. and Freeman, M. a. R., 2000. Writings on the knee between 1836 and 1917. *The Journal of Bone & Joint Surgery. British Volume,* 82-B (8), pp.1100-1102.

83. Lengsfeld, M., Ahlers, J. and Ritter, G., 1990. Kinematics of the patellofemoral joint. *Archives of Orthopaedic and Trauma Surgery,* 109 (5), pp.280-283.

84. Morrey, 2003. *Total joint arthroplasty.* 3rd. Philadelphia:Churchill-Livingstone.

85. Soudan, K., Van Audekercke, R. and Martens, M., 1979. Methods, difficulties and inaccuracies in the study of human joint kinematics and pathokinematics by the instant axis concept. Example: The knee joint. *Journal of Biomechanics,* 12 (1), pp.27-33.

86. Frankel, V. H., Burstein, A. H. and Brooks, D. B., 1971. Biomechanics of Internal Derangement of the Knee Pathomechanics as determined by analysis of the instant centers of motion. *The Journal of Bone & Joint Surgery. American Volume,* 53 (5), pp.945-977.

87. Smidt, G. L., 1973. Biomechanical analysis of knee flexion and extension. *Journal of Biomechanics,* 6 (1), pp.79-92.

88. Goodfellow, J. and O'connor, J., 1978. The mechanics of the knee and prosthesis design. *The Journal of Bone & Joint Surgery. British Volume,* 60-B (3), pp.358-369.

89. Ellis, M. I., Seedhom, B. B., Wright, V. and Dowson, D., 1980. An Evaluation of the Ratio between the Tensions along the Quadriceps Tendon and the Patellar Ligament. *Engineering in Medicine,* 9 (4), pp.189-194.

90. Kurosawa, H., Walker, P. S., Abe, S., Garg, A. and Hunter, T., 1985. Geometry and motion of the knee for implant and orthotic design. *Journal of Biomechanics,* 18 (7), pp.487-499.

91. Hollister, A. M., Jatana, S., Singh, A. K., Sullivan, W. W. and Lupichuk, A. G., 1993. The axes of rotation of the knee. *Clinical Orthopaedics and Related Research,* (290), pp.259-268.

92. Eckhoff, D. G., Bach, J. M., Spitzer, V. M., Reinig, K. D., Baqur, M. M., Baldini, T. H. and Flannery, N. M., 2005. Three-Dimensional Mechanics, Kinematics, and Morphology of the Knee Viewed in Virtual Reality. *The Journal of Bone & Joint Surgery. American Volume,* 87 (Supplement 2), pp.71-80.

93. Eckhoff, D. G., Dwyer, T. F., Bach, J. M., Spitzer, V. M. and Reining, K. D., 2003. 3D morphology and kinematics of the distal part of the femur viewed in virtual reality part 2. *The Journal of Bone & Joint Surgery. British Volume,* 85 pp.97-104.

94. Asano, T., Akagi, M., Tanaka, K., Tamura, J. and Nakamura, T., 2001. In vivo 3D knee kinematics using a biplanar imaging technique. *Clinical Orthopaedics and Related Research,* 388 pp.157-166.

95. Eckhoff, D., Hogan, C., Dimatteo, L., Robinson, M. and Bach, J., 2007. Abjs Best Papers. *Clinical Orthopaedics and Related Research,* PAP

96. Luyckx, T., Didden, K., Vandenneucker, H., Labey, L., Innocenti, B. and Bellemans, J., 2009. Is there a biomechanical explanation for anterior knee pain in patients with patella alta? *The Journal of Bone & Joint Surgery. British Volume,* 91 pp.344-350.

97. Freeman, M. R. and Pinskerova, V., 2005. The movement of the normal tibio-femoral joint. *Journal of Biomechanics,* 38 (2), pp.197-208.

98. Brantigan, O. C. and Voshell, A. F., 1941. The mechanics of the ligaments and menisci of the knee joint. *The Journal of Bone & Joint Surgery. American Volume,* 23 (1), pp.44-66.

99. Komistek, R. D., 2003. In vivo fluroscopic analysis of the normal human knee. *Clinical Orthopaedics and Related Research,* 410 pp.69-81.

100. Leszko, F., Hovinga, K. R., Lerner, A. L., Komistek, R. D. and Mahfouz, M. R., 2010. In Vivo Normal Knee Kinematics: Is Ethnicity or Gender an Influencing Factor? *Clinical Orthopaedics and Related Research,* 469 (1), pp.95-106.

101. Barink, M., Meijerink, H., Verdonschot, N., Kampen, A. and Waal Malefijt, M., 2006. Asymmetrical total knee arthroplasty does not improve patella tracking: a study without patella resurfacing. *Knee Surgery, Sports Traumatology, Arthroscopy,* 15 (2), pp.184-191.

102. Komistek, R. D., Mahfouz, M. R., Bertin, K. C., Rosenberg, A. and Kennedy, W., 2008. In Vivo Determination of Total Knee Arthroplasty Kinematics. *The Journal of Arthroplasty,* 23 (1), pp.41-50.

103. Hill, P. F., 2000. Tibialfemoral movement 2: the loaded and unloaded living knee studied by MRI. *The Journal of Bone & Joint Surgery. British Volume,* 82 pp.1196.

104. Karrholm, J., Brandsson, S. and Freeman, M. A., 2000. Tibialfemoral movement 4: Changes of axial tibial rotation caused by forced rotation at the weight bearing knee studied by RSA. *The Journal of Bone & Joint Surgery. British Volume,* 82 pp.1201-1203.

105. Massin, P., Boyer, P., Hajage, D., Kilian, P. and Tubach, F., 2011. Intra-operative navigation of knee kinematics and the influence of osteoarthritis. *The Knee,* 18 (4), pp.259-264.

106. Nakagawa, S., Kadoya, Y., Todo, S., Kobayashi, A., Sakamoto, H., Freeman, M. A. and Yamano, Y., 2000. Tibiofemoral movement 3: Full flexion in the living knee studied by MRI. *The Journal of Bone & Joint Surgery. British Volume,* 82 pp.1199-2000.

107. Wyss, U., Kim, I. Y., Cooke, D. and Amiri, S., 2007. Mechanics of the passive knee joint. Part 2: interaction between the ligaments and the articular surfaces in guiding the joint motion. *Proceedings of the Institution of Mechanical Engineers. Part H, Journal of engineering in medicine,* 221 (8), pp.821-832.

108. Wilson, D. R., Feikes, J. D., Zavatsky, A. B. and O'connor, J. J., 2000. The components of passive knee movement are coupled to flexion angle. *Journal of Biomechanics,* 33 (4), pp.465-473.

109. Heller, M. O., Konig, C., Graichen, H., Hinterwimmer, S., Ehrig, R. M., Duda, G. N. and Taylor, W. R., 2007. A new model to predict in vivo human knee kinematics under physiological-like muscle activation. *Journal of Biomechanics,* 40 Suppl 1 pp.S45-53.

110. Belvedere, C., Leardini, A., Ensini, A., Bianchi, L., Catani, F. and Giannini, S., 2009. Three-dimensional patellar motion at the natural knee during passive flexion/extension. An in vitro study. *Journal of Orthopaedic Research,* 27 (11), pp.1426-1431.

111. Belvedere, C., Catani, F., Ensini, A., Moctezuma De La Barrera, J. L. and Leardini, A., 2007. Patellar tracking during total knee arthroplasty: an in vitro feasibility study. *Knee Surgery, Sports Traumatology, Arthroscopy,* 15 (8), pp.985-993.

112. Von Eisenhart-Rothe, R., Vogl, T., Englmeier, K. H. and Graichen, H., 2007. A new in vivo technique for determination of femoro-tibial and femoro-patellar 3D kinematics in total knee arthroplasty. *Journal of Biomechanics,* 40 (14), pp.3079-3088.

113. Iranpour, F., Merican, A. M., Baena, F. R. Y., Cobb, J. P. and Amis, A. A., 2010. Patellofemoral joint kinematics: The circular path of the patella around the trochlear axis. *Journal of Orthopaedic Research,* 28 (5), pp.589-594.

114. Amis, A. A., Senavongse, W. and Bull, A. M. J., 2006. Patellofemoral kinematics during knee flexion-extension: An in vitro study. *Journal of Orthopaedic Research,* 24 (12), pp.2201-2211.

115. Katchburian, M. V., Bull, A., Shih, Y. F., Heatley, F. W. and Amis, A., 2003. Measurement of patella tracking: assessment and analysis of the literature. *Clinical Orthopaedics and Related Research,* 412 pp.241-259.

116. Merican, A. M., Ghosh, K. M., Iranpour, F., Deehan, D. J. and Amis, A. A., 2011. The effect of femoral component rotation on the kinematics of the tibiofemoral and patellofemoral joints after total knee arthroplasty. *Knee Surgery, Sports Traumatology, Arthroscopy,* 19 (9), pp.1479-1487.

117. Sheehan, F. T., Zajac, F. E. and Drace, J. E., 1999. In vivo tracking of the human patella using cine phase contrast magnetic resonance imaging. *Journal of Biomechanical Engineering,* 121 (6), pp.650-656.

118. Suzuki, T., Hosseini, A., Li, J. S., Gill, T. J. T. and Li, G., 2012. In vivo patellar tracking and patellofemoral cartilage contacts during dynamic stair ascending. *Journal of Biomechanics,* 45 (14), pp.2432-2437.

119. Heinert, G., Kendoff, D., Preiss, S., Gehrke, T. and Sussmann, P., 2010. Patellofemoral kinematics in mobile-bearing and fixed-bearing posterior stabilised total knee replacements: a cadaveric study. *Knee Surgery, Sports Traumatology, Arthroscopy,* 19 (6), pp.967-972.

120. Baldwin, M. A., Clary, C., Maletsky, L. P. and Rullkoetter, P. J., 2009. Verification of predicted specimen-specific natural and implanted patellofemoral kinematics during simulated deep knee bend. *Journal of Biomechanics,* 42 (14), pp.2341-2348.

121. Mow, V., 2005. *Basic Orthopaedic Biomechanics and Mechano-Biology.* 3rd. Philadelphia:Lippincott Williams & Wilkins.

122. National Joint Registry for England & Wales, 2012. *9th Annual Report 2012.* Hemel Hempstead:National Joint Registry for England & Wales.

123. Williams, D. H., Garbuz, D. S. and Masri, B. A., 2010. Total Knee Arthroplasty: Techniques and results. *Bristish columbia Medical Journal,* 52 (9), pp.447-454.

124. Swedish Joint Registry, 2011. *Annual Report 2011.* Swedish National Joint Registry.

125. Weinstein, A. M., Rome, B. N., Reichmann, W. M., Collins, J. E., Burbine, S. A., Thornhill, T. S., Wright, J., Katz, J. N. and Losina, E., 2013. Estimating the Burden of TKR in the US. *J Bone Joint Surg Am,* 95 (5), pp.385-392.

126. Sharkey, P. F., Hozack, W., Rothman, R. H., Shastri, S. and Jacoby, S. M., 2002. Why are total knee arthroplasties failing today? *Clinical Orthopaedics and Related Research,* 404 pp.7-13.

127. Dakin, H., Gray, A., Fitzpatrick, R., Maclennan, G. and Murray, D., 2012. Rationing of total knee replacement: a cost-effectiveness analysis on a large trial data set. *British Medical Journal Open,* 2 (1),

128. J., D. B., Petruccelli, D., Adili, A., Piccirillo, L., Wismer, D. and Winemaker, M., 2012. Patient perspective survey of total hip vs total knee arthroplasty surgery. *The Journal of Arthroplasty,* 27 (6), pp.865.

129. Bourne, R. B., Chesworth, B. M., Davis, A. M., Mahomed, N. N. and Charron, K. D. J., 2009. Patient Satisfaction after Total Knee Arthroplasty: Who is Satisfied and Who is Not? *Clinical Orthopaedics and Related Research,* 468 (1), pp.57-63.

130. Amendola, L., Tigani, D., Fosco, M. and Dallari, D., 2012. *History of Condylar Total Knee Arthroplasty.* InTech.

131. Ranawat, C. S., 2002. History of total knee replacement. *Journal of the Southern Orthopaedic Association,* 11 (4), pp.218-226.

132. Clary, C. W., Fitzpatrick, C. K., Maletsky, L. P. and Rullkoetter, P. J., The influence of total knee arthroplasty geometry on mid-flexion stability: An experimental and finite element study. *Journal of Biomechanics,* 46 (7), pp.1351-1357.

133. Hamilton, D. F., Simpson, A. H., Burnett, R., Patton, J. T., Moran, M., Clement, N. D., Howie, C. R. and Gaston, P., 2013. Lengthening the moment arm of the patella confers enhanced extensor mechanism power following total knee arthroplasty. *Journal of Orthopaedic Research,* 31 (8), pp.1201-1207.

134. Hamilton, D., Gaston, P. and Simpson, A., 2012. Single radius of curvature implant design enhances patient lowerlimb output following total knee arthroplasty. *In: ORS 2012 Annual Meeting,*

135. Barbella, M., *The Right Fit* [online]. ODT: Rodman Media. Available from: http://www.odtmag.com/articles/2010/09/the-right-fit. [Accessed 10/07/2013].

136. *Mobile-bearing three-compartment knee prosthesis* [online]. Medical Expo. Available from: http://www.medicalexpo.com/prod/fh-orthopedics/mobile-bearing-three-compartment-knee-prostheses-68487-460450.html. [Accessed 10/07/2013].

137. *Fixed-bearing three-compartment knee prosthesis* [online]. Medical Expo. Available from: http://www.medicalexpo.com/prod/fh-orthopedics/fixed-bearing-three-compartment-knee-prostheses-68487-460446.html. [Accessed 10/07/2013].

138. Fraser, A., 2006. *REMINDER: OR-Live.com Presents: Triathlon MIS Total Knee Arthroplasty Procedure* [online]. Market Wired. Available from: http://www.marketwire.com/press-release/reminder-or-livecom-presents-triathlon-mis-total-knee-arthroplasty-procedure-685924.htm. [Accessed 10/07/2013].

139. *Vanguard System Summary* [online]. Biomet. Available from: http://biomet.co.uk/resource/1848/System%20Summary.pdf. [Accessed 17/07/2014].

140. Sathasivam, S. and Walker, P. S., 2000. Design forms of total knee replacement. *Proc IMechE Part H Journal of Engineering in Medicine,* 214 (1), pp.101-119.

141. Shelburne, K. B., Pandy, M. G. and Torry, M. R., 2004. Comparison of shear forces and ligament loading in the healthy and ACL-deficient knee during gait. *Journal of Biomechanics,* 37 (3), pp.313-319.

142. National Joint Registry for England & Wales, 2008. *5th Annual Report 2007.* Hemel Hempstead:National Joint Registry for England & Wales.

143. Australian National Joint Registry, 2011. *Annual Report 2011.* Australian National Joint Registry.

144. New Zealand National Joint Registry, 2010. *Annual Report 2010.* New Zealand National Joint Registry.

145. Australian Joint Registry, 2012. 2012 Annual Report.

146. Norwegian National Joint Registry, 2010. *Annual Report.* Norwegian National Joint Registry.

147. Norwegian National Joint Registry, 2010. *Annual Report 2010.* Norwegian National Joint Registry.

148. Canadian National Joint Registry, 2008. *Annual Report 2008.* Canadian National Joint Registry.

149. *Sigma CR 150 Fixed Reference Surgical Technique with High Performance Instruments* [online]. DePuy. Available from: http://www.depuy.com/sites/default/files/products/files/Sigma%20CR150%20Final%20ST.pdf. [Accessed 25/07/2013].

150. *NexGen LEGACY ® KNEE LPS - FLEX* [online]. Zimmer. Available from: http://www.zimmer.co.uk/content/pdf/en-US/NexGen_LPS_Flex-Fixed_Brochure_(97-5964-101).pdf. [Accessed 25/07/2013].

151. 2006. *Triathlon Knee System Surgical Protocol.* Stryker.

152. *AGC Premier Instrumentation CR or PS Surgical Technique* [online]. Biomet. Available from: http://www.biomet.co.uk/userfiles/files/Knees/AGC/FLK214%20AGC%20Premier%20ST.pdf. [Accessed 25/07/2013].

153. *Vanguard Instrumentation Options* [online]. Biomet. Available from: http://www.biomet.co.uk/resource/1848/System%20Summary.pdf. [Accessed 25/07/2013].

154. 2009. *Scorpio NRG CR & PS Surgical Protocol.* Stryker.

155. *LCS® RPS Flexion Product Rationale* [online]. DePuy. Available from: http://www.depuy.com/sites/default/files/products/files/9075-16-000-v1-LCS-RPS-PR_EN.pdf. [Accessed 25/07/2013].

156. *Knee Arthroplasty* [online]. B Braun. Available from: http://www.bbraun.com/cps/rde/xchg/bbraun-com/hs.xsl/knee-arthroplasty.html. [Accessed 25/07/2013].

157. *Legion* [online]. Smith & Nephew. Available from: http://www.smith-nephew.com/uk/products/orthopaedic-reconstruction/legion/. [Accessed 24/07/2013].

158. *LINK® Patella Components* [online]. Link. Available from: https://www.linkorthopaedics.com/en/for-the-physician/products/knie/patella/. [Accessed 24/07/2013].

159. Collier, M. B., Engh, C. A., Mcauley, J. P. and Engh, G. A., 2007. Factors Associated with the Loss of Thickness of Polyethylene Tibial Bearings After Knee Arthroplasty. *The Journal of Bone & Joint Surgery. British Volume,* 89 (6), pp.1306-1314.

160. Desai, A. S., Dramis, A., Kendoff, D. and Board, T. N., 2011. Critical review of the current practice for computer-assisted navigation in total knee replacement surgery: cost-effectiveness and clinical outcome. *Current Reviews in Musculoskeletal Medicine,* 4 (1), pp.11-15.

161. Spencer, J. M., Chauhan, S. K., Sloan, K., Taylor, A. and Beaver, R. J., 2007. Computer navigation versus conventional total knee replacement. *The Journal of Bone & Joint Surgery. British Volume,* 89-B pp.477-480.

162. Matziolis, G., Krocker, D., Weiss, U., Tohtz, S. and Perka, C., 2007. A Prospective, Randomized Study of Computer-Assisted and Conventional Total Knee Arthroplasty. *The Journal of Bone & Joint Surgery. American Volume,* 89 (2), pp.236.

163. Jeffery, R. S., Morris., R. W. and Denham, R. A., 1991. Coronal alignment after total knee replacement. *The Journal of Bone & Joint Surgery. British Volume,* 73 pp.709-714.

164. Fang, D. M., Ritter, M. A. and Davis, K. E., 2009. Coronal Alignment in Total Knee ArthroplastyJust How Important is it? *The Journal of Arthroplasty,* 24 (6), pp.39-43.

165. Parratte, S., Pagnano, M. W., Trousdale, R. T. and Berry, D. J., 2010. Effect of Postoperative Mechanical Axis Alignment on the Fifteen-Year Survival of Modern, Cemented Total Knee Replacements. *The Journal of Bone & Joint Surgery. American Volume,* 92 (12), pp.2143-2149.

166. Tanamas, S., Hanna, F. S., Cicuttini, F. M., Wluka, A. E., Berry, P. and Urquhart, D. M., 2009. Does knee malalignment increase the risk of development and progression of knee osteoarthritis? A systematic review. *Arthritis & Rheumatism,* 61 (4), pp.459-467.

167. T. J. Bonner, W. G. P. Eardley, P. Patterson and Gregg, P. J., 2011. The effect of post-operative mechanical axis alignment on the survival of primary total knee replacements after a follow-up of 15 years. *The Journal of Bone & Joint Surgery. British Volume,* 93 pp.1217-1222.

168. Morgan, S. S., Bonshahi, A., Pradhan, N., Gregory, A., Gambhir, A. and Porter, M. L., 2008. The influence of postoperative coronal alignment on revision surgery in total knee arthroplasty. *International Orthopaedics,* 32 pp.639-642.

169. Bellemans, J., Colyn, W., H Vandenneucker, H. and Victor, J., 2012. Is Neutral Mechanical Alignment Normal for All Patients? *Clinical Orthopaedics and Related Research,* 470 pp.45-53.

170. Jenny, J.-Y., Boeri, C. and Ballonzoli, L., 2005. Coronal alignment of the lower limb. *Acta Ortopaedica,* 76 (3), pp.403-407.

171. Nam, D., Shah, R. R., Nunley, R. M. and Barrack, R. L., 2014. Evaluation of the 3-dimensional, weight-bearing orientation of the normal adult knee. *The Journal of Arthroplasty,* 29 (5), pp.906-911.

172. Yau, W. P. and Chiu, K. Y., 2008. Cutting errors in total knee replacement: assessment by computer assisted surgery. *Knee Surgery Sports Traumatology Arthroscopy,* 16 (7), pp.670-673.

173. Plaskos, C., Hodgson, A. J., Inkpen, K. and Mcgraw, R. W., 2002. Bone cutting errors in total knee arthroplasty. *The Journal of Arthroplasty,* 17 (6), pp.698-705.

174. Longstaff, L. M., Sloan, K., Stamp, N., Scaddan, M. and Beaver, R., 2009. Good Alignment After Total Knee Arthroplasty Leads to Faster Rehabilitation and Better Function. *The Journal of Arthroplasty,* 24 (4), pp.570-578.

175. Mahaluxmivala, J., Bankes, M. J. K., Nicolai, P., Aldam, C. H. and Allen, P. W., 2001. The effect of surgeon experience on component positioning in 673 press fit condylar posterior cruciate-sacrificing total knee arthroplasties. *The Journal of Arthroplasty,* 16 (5), pp.635-640.

176. Molli, R. G., Anderson, K. C., Buehler, K. C. and Markel, D. C., 2011. Computer-Assisted Navigation Software Advancements Improve the Accuracy of Total Knee Arthroplasty. *The Journal of Arthroplasty,* 26 (3), pp.432-438.

177. Sparmann, M., Wolke, B., Czupalla, H., Banzer, D. and Zink, A., 2003. Positioning of total knee arthroplasty with and without navigation support. *The Journal of Bone & Joint Surgery. British Volume,* 85 pp.830-835.

178. Jeffcote, B. and Shakespeare, D., 2003. Varus/valgus alignment of the tibial component in total knee arthroplasty. *The Knee,* 10 (3), pp.243-247.

179. Belvedere, C., Ensini, A., Leardini, A., Bianchi, L., Catani, F. and Giannini, S., 2007. Alignment of resection planes in total knee replacement obtained with the conventional technique, as assessed by a modern computer-based navigation system. *International Journal of Medcial Robotics,* 3 (2), pp.117-124.

180. Bathis, H., Perlick, L., Tingart, M., Perlick, C., Lring, C. and Grifka, J., 2004. Intraoperative cutting errors in total knee arthroplasty. *Archives of Orthopaedic and Trauma Surgery,* 125 (1), pp.16-20.

181. Siston, R. A., Goodman, S. B., Patel, J. J., Delp, S. L. and Giori, N. J., 2006. The high variability of tibial rotational alignment in TKA. *Clinical Orthopaedics and Related Research,* 452 pp.65-69.

182. Şahin, N., Atıcı, T., Öztürk, A., Özkaya, G., Özkan, Y. and Avcu, B., 2011. Accuracy of anatomical references used for rotational alignment of tibial component in total knee arthroplasty. *Knee Surgery, Sports Traumatology, Arthroscopy,* 20 (3), pp.565-570.

183. Howell, S. M., Chen, J. and Hull, M. L., 2013. Variability of the location of the tibial tubercle affects the rotational alignment of the tibial component in kinematically aligned total knee arthroplasty. *Knee Surgery Sports Traumatology Arthroscopy,* 21 (10), pp.2288-2295.

184. Indelli, P. F., Marcacci, M., Cariello, D., Poli, P. and Innocenti, M., 2011. Contemporary femoral designs in total knee arthroplasty: effects on patello-femoral congruence. *International Orthopaedics,* 36 (6), pp.1167-1173.

185. Anglin, C., Fu, C., Hodgson, A. J., Helmy, N., Greidanus, N. V. and Masri, B. A., 2009. Finding and defining the ideal patellar resection plane in total knee arthroplasty. *Journal of Biomechanics,* 42 (14), pp.2307-2312.

186. Ledger, M., Shakespeare, D. and Scaddan, M., 2005. Accuracy of patellar resection in total knee replacement. *The Knee,* 12 (1), pp.13-19.

187. Belvedere, C., Ensini, A., Leardini, A., Feliciangeli, A., Boschert, H. and Giannini, S., 2012. Does patella resurfacing affect patello-femoral kinematics in total knee replacement? An in-vitro study. *In: ORS 2012 Annual Meeting,* San Fransisco.

188. Lee, T., Gerken, A., Glaser, F., Kim, W. and Anzel, S., 1997. Patellofemoral joint kinematics and contact pressures in TKA. *Clinical Orthopaedics and Related Research,* 340 pp.257-266.

189. Matsuda, S., Ishinishi, T., White, S. E. and Whiteside, L. A., 1997. Patellofemoral joint after total knee arthroplasty. *The Journal of Arthroplasty,* 12 (7), pp.790.

190. Xu, C., Chu, X. and Wu, H., 2007. Effects of patellar resurfacing on contact area and contact stress in total knee arthroplasty. *The Knee,* 14 (3), pp.183-187.

191. Leichtle, U. G., Wunschel, M., Leichtle, C. I., Muller, O., Kohler, P., Wulker, N. and Lorenz, A., 2013. Increased patellofemoral pressure after TKA: an in vitro study. *Knee Surgery, Sports Traumatology, Arthroscopy,* 22 (3), pp.500-508.

192. Didden, K., Luyckx, T., Bellemans, J., Labey, L., Innocenti, B. and Vandenneucker, H., 2010. Anteroposterior positioning of the tibial component and its effect on the mechanics of patellofemoral contact. *The Journal of Bone & Joint Surgery. British Volume,* 92 pp.1466-1470.

193. Skwara, A., Tibesku, C. O., Ostermeier, S., Stukenborg-Colsman, C. and Fuchs-Winkelmann, S., 2008. Differences in patellofemoral contact stresses between mobile-bearing and fixed-bearing total knee arthroplasties: a dynamic in vitro measurement. *Archives of Orthopaedic and Trauma Surgery,* 129 (7), pp.901-907.

194. Kainz, H., Reng, W., Augat, P. and Wurm, S., 2011. Influence of total knee arthroplasty on patellar kinematics and contact characteristics. *International Orthopaedics,* 36 (1), pp.73-78.

195. Perry, J., Antonelli, D. and Ford, W., 1975. Analysis of knee joint forces during flexed knee stance. *The Journal of Bone & Joint Surgery. American Volume,* 57 (7), pp.961.

196. Long, R., 2011. *The Biomechanics of Hinged Total Knee Replacements: An In Vitro Comparative Evaluation of Five Prostheses*. Thesis (PhD). Univeristy of Bath, Bath.

197. Yildirim, G., Walker, P. S. and Boyer, J., 2009. Total knees designed for normal kinematics evaluated in an up-and-down crouching machine. *Journal of Orthopaedic Research,* 27 (8), pp.1022-1027.

198. Wünschel, M., Lo, J., Dilger, T., Wülker, N. and Müller, O., 2011. Influence of bi- and tri-compartmental knee arthroplasty on the kinematics of the knee joint. *BMC Musculoskeletal Disorders,* 12 (1), pp.29.

199. Halloran, J. P., Clary, C. W., Maletsky, L. P., Taylor, M., Petrella, A. J. and Rullkoetter, P. J., 2010. Verification of Predicted Knee Replacement Kinematics During Simulated Gait in the Kansas Knee Simulator. *Journal of Biomedical Engineering,* 132 (8), pp.081010.

200. Maletsky, L. P. and Hillberry, B. M., 2005. Simulating Dynamic Activities Using a Five-Axis Knee Simulator. *Journal of Biomedical Engineering,* 127 (1), pp.123.

201. Coughlin, K. M., Incavo, S. J., Churchill, D. L. and Beynnon, B. D., 2003. Tibial axis and patellar position relative to the femoral epicondylar axis during squatting. *The Journal of Arthroplasty,* 18 (8), pp.1048-1055.

202. Heyse, T. J., Becher, C., Kron, N., Ostermeier, S., Hurschler, C., Schofer, M. D., Fuchs-Winkelmann, S. and Tibesku, C. O., 2009. Quadriceps force in relation of intrinsic anteroposterior stability of TKA design. *Archives of Orthopaedic and Trauma Surgery,* 130 (1), pp.1-9.

203. Ostermeier, S., Buhrmester, O., Hurschler, C. and Stukenborg-Colsman, C., 2005. Dynamic in vitro measurement of patellar movement after total knee arthroplasty: an in vitro study. *BMC Musculoskeletal Disorders,* 6 (1), pp.30.

204. Ostermeier, S., Stein, C., Hurschler, C., Windhagen, H. and Stukenborg-Colsman, C., 2007. Measurement of the effect of hamstring muscle force on knee cruciate ligament loading patterns during simulated extension motions. *Isokinetics and Exercise Science,* 15 pp.83-90.

205. Matsuda, S., Ishinishi, T. and Whiteside, L. A., 2000. Contact stresses with an unresurfaced patella in total knee arthroplasty: the effect of femoral component design. *Orthopedics,* 23 (3), pp.213-218.

206. Fuchs, S., Skwara, A., Tibesku, C. and Rosenbaum, D., 2005. Retropatellar contact characteristics before and after total knee arthroplasty. *The Knee,* 12 (1), pp.9-12.

207. Wilke, H.-J., Werner, K., Häussler, K., Reinehr, M. and Böckers, T. M., 2011. Thiel-fixation preserves the non-linear load–deformation characteristic of spinal motion segments, but increases their flexibility. *Journal of the Mechanical Behavior of Biomedical Materials,* 4 (8), pp.2133-2137.

208. Park, J. and Lakes, R. S., 2007. *Biomaterials An Introduction.* New York:Springer Science+Business Media, LLC

209. Marinozzi, G., Pappalardo, S. and Steindler, R., 1983. Human knee ligaments: mechanical tests and ultrasonic observations. *Italian Journal of Orthoapedic Trauma,* 9 (2), pp.231-240.

210. Peretz, J. L., Driftmier, K. R., Cerynik, D. L., Kumar, N. S. and Johanson, N. A., 2012. Does lateral release change patellofemoral forces and pressures. *Clinical Orthopaedics and Related Research,* 470 pp.903-909.

211. Walker, P. S., Yildirim, G., Sussman-Fort, J., Roth, J., White, B. and Klein, G. R., 2007. Factors Affecting the Impingement Angle of Fixed- and Mobile-Bearing Total Knee Replacements. *The Journal of Arthroplasty,* 22 (5), pp.745-752.

212. Walker, P. S., Heller, Y., Cleary, D. J. and Yildirim, G., 2011. Preclinical Evaluation Method for Total Knees Designed to Restore Normal Knee Mechanics. *The Journal of Arthroplasty,* 26 (1), pp.152-160.

213. Heiner, A. D., 2008. Structural properties of fourth-generation composite femurs and tibias. *Journal of Biomechanics,* 41 (15), pp.3282-3284.

214. Anglin, C., Brimacombe, J. M., Hodgson, A. J., Masri, B. A., Greidanus, N. V., Tonetti, J. and Wilson, D. R., 2008. Determinants of patellar tracking in total knee arthroplasty. *Clinical Biomechanics,* 23 (7), pp.900-910.

215. Anglin, C., Brimacombe, J. M., Wilson, D. R., Masri, B. A., Greidanus, N. V., Tonetti, J. and Hodgson, A. J., 2008. Intraoperative vs. weightbearing patellar kinematics in total knee arthroplasty: A cadaveric study. *Clinical Biomechanics,* 23 (1), pp.60-70.

216. Colwell, C. W., Chen, P. C. and D'lima, D., 2011. Extensor malalignment arising from femoral component malrotation in knee arthroplasty: Effect of rotating–bearing. *Clinical Biomechanics,* 26 (1), pp.52-57.

217. D'lima, D. D., Poole, C., Chadha, H., Hermida, J., Mahar, A. and Colwell, C. W., 2001. Quadriceps moment arm and quadriceps forces after TKA. *Clinical Orthopaedics and Related Research,* 392 pp.213-220.

218. Macwilliams, B. A., Wilson, D. R., Desjardins, J. D., Romero, J. and Chao, E. Y., 1999. Hamstrings Cocontraction reduces internal rotatio, anterior translation, and anterior cruciate ligamant load in weight bearing flexion. *Journal of Orthopaedic Research,* 17 pp.817-822.

219. Singerman, R., Heiple, K. G., Davy, D. T. and Goldberg, V. M., 1995. Effect of tibial component position on patellar strain following total knee arthroplasty. *The Journal of Arthroplasty,* 10 (5), pp.651.

220. Lorenz, A., Muller, O., Kholer, P., Wunschel, M., Wulker, N. and Leichtle, U. G., 2012. The influence of asymmetric quadriceps loading on patellar tracking - An *in vitro* study. *The Knee,* 19 pp.818-822.

221. Cappozzo, A., Della Croce, U., Leardini, A. and Chiari, L., 2005. Human movement analysis using stereophotogrammetry. Part 1: theoretical background. *Gait & Posture,* 21 (2), pp.186-196.

222. Woltring, H. J., 1991. Representation and calculation of 3-D joint movement. *Human Movement Science,* 10 (5), pp.603-616.

223. Ostermeier, S., Friesecke, C., Fricke, S., Hurschler, C. and Stukenborg-Colsman, C., 2008. Quadriceps force during knee extension after non-hinged and hinged TKA: An in vitro study. *Acta Orthopaedica,* 79 (1), pp.34-38.

224. Krevolin, J. L., Pandy, M. G. and Pearce, J. C., 2004. Moment arm of the patellar tendon in the human knee. *Journal of Biomechanics,* 37 (5), pp.785-788.

225. Steinbruck, A., Schroder, C., Woiczinski, M., Fottner, A., Muller, P. and Jansson, V., 2013. Patellofemoral contact patterns before and after total knee arthroplasty: an in vitro measurement. *BioMedical Engineering OnLine,* 12 (1), pp.58.

226. Lumpaopong, P., Stephen, J., Amis, A. and Hansen, U., 2012. Computational assessment of patellofemoral joint force under various loading conditions. *Journal of Biomechanics,* 45 (S1), pp.S392.

227. Westphal, C. J., Schmitz, A., Reeder, S. B. and Thelen, D. G., 2013. Load-dependent variations in knee kinematics measured with dynamic MRI. *Journal of Biomechanics,* 46 (12), pp.2045-2052.

228. Lorenz, A., Blange, Herzog, Y., Schnauffer, P., Wünschel, M., Wülker, N. and Leichtle, U., 2012. The influence of the patellofemoral groove design on patella kinematics and pressure in TKA. *Journal of Biomechanics,* 45 (S1), pp.S385.

229. Walker, P. S., Heller, Y., Yildirim, G. and Immerman, I., 2011. Reference axes for comparing the motion of knee replacements with the anatomic knee. *The Knee,* 18 (5), pp.312-316.

230. Kessler, O., Bull, A. M. J. and Amis, A. A., 2009. A method to quantify alteration of knee kinematics caused by changes of TKR positioning. *Journal of Biomechanics,* 42 (6), pp.665-670.

231. Takano, 2008. Development of a Knee Joint Motion Simulator to Evaluate Deep Knee Flexion of Artificial Knee Joints. *In: IEE EMBS,* Vancouver.

232. Haider, H. and Walker, P. S., 2005. Measurements of constraint of total knee replacement. *Journal of Biomechanics,* 38 (2), pp.341-348.

233. Mesfar, W. and Shiraziadl, A., 2006. Knee joint mechanics under quadriceps–hamstrings muscle forces are influenced by tibial restraint. *Clinical Biomechanics,* 21 (8), pp.841-848.

234. Kwak, S. D., Ahmad, C. S., Gardner, T. R., Grelsamer, R. P., Henry, J. H., Blankevoort, L., Ateshian, G. A. and Mow, V., 2000. Hamstrings and iliotibial band forces affect knee kinematics and contact pattern. *Journal of Orthopaedic Research,* 18 pp.101-108.

235. Li, G., Defrate, L. E., Zayontz, S., Park, S. E. and Gill, T. J., 2004. The effect of tibiofemoral joint kinematics on patellofemoral contact pressures under simulated muscle loads. *Journal of Orthopaedic Research,* 22 (4), pp.801-806.

236. Victor, J., 2009. *A Comparative Study on the Biomechanics of the native human knee joint & TKA*. Thesis (M.D.). Katholieke Universiteit Leuven, Leuven.

237. Yildirim, G., Walker, P. S., Sussman-Fort, J., Aggarwal, G., White, B. and Klein, G. R., 2007. The contact locations in the knee during high flexion. *The Knee,* 14 (5), pp.379-384.

238. Gryzlo, S. M., Patek, R. M., Pink, M. and Perry, J., 1994. Electromyographic analysis of knee rehabilitation exercises. *Journal of Orthopaedic Sports Physical Therapy,* 20 (1), pp.36-43.

239. Wijdicks, C. A., Ewart, D. T., Nuckley, D. J., Johansen, S., Engebretsen, L. and Laprade, R. F., 2010. Structural Properties of the Primary Medial Knee Ligaments. *The American Journal of Sports Medicine,* 38 (8), pp.1638-1646.

240. Kennedy, J., 1976. Tension studies of human knee ligaments. *The Journal of Bone & Joint Surgery. American Volume,* 62 pp.350-355.

241. Bellemans, J., 2003. Biomechanics of anterior knee pain. *The Knee,* 10 pp.123-126.

242. Fitzpatrick, C. K. and Rullkoetter, P. J., 2012. Influence of patellofemoral articular geometry and materials on mechanics of the unresurfaced patella. *Journal of Biomechanics,* 45 (11), pp.1909-1915.

243. Martinelli, L., Hurschler, C. and Rosenbaum, D., 2006. Comparison of capacitive versus resistive joint contact stress sensors. *Clinical Orthopaedics and Related Research,* 447 pp.214-220.

244. Landinez-Parra, N. S., Garzon-Alvarado, D. A. and Vanegas-Acosta, J. C., 2011. A phenomenological mathematical model of the articular cartilage damage. *Computer Methods and Programs in Biomedicine,* 104 pp.e58-74.

245. Wurm, S., Kainz, H., Reng, W. and Augat, P., 2012. The influence of patellar resurfacing on patellar kinetics and retropatellar contact characteristics. *Journal of Orthopaedic Science,* 18 (1), pp.61-69.

246. *Genesis II* [online]. Smith & Nephew. Available from: http://www.smith-nephew.com/professional/products/all-products/genesis-ii-total-knee-replacement-system/. [Accessed 26th Jan 2012].

247. Kurtz, S. M. and Knovel ed, 2009. *UHMWPE biomaterials handbook ultra high molecular weight polyethylene in total joint replacement and medical devices.* Boston:Elsevier/Academic Press.

248. Kurtz, S. M., Villarraga, M. L., Herr, M. P., Bergström, J. S., Rimnac, C. M. and Edidin, A. A., 2002. Thermomechanical behavior of virgin and highly crosslinked ultra-high molecular weight polyethylene used in total joint replacements. *Biomaterials,* 23 (17), pp.3681-3697.

249. Katta, J., Jin, Z., Ingham, E. and Fisher, J., 2008. Biotribology of articular cartilage—A review of the recent advances. *Medical Engineering & Physics,* 30 (10), pp.1349-1363.

250. Forster, H. and Fisher, J., 1999. The influence of continuous sliding and subsequent surface wear on the friction of articular cartilage. *Proceedings of the Institution of Mechanical Engineers, Part H: Journal of Engineering in Medicine,* 213 (4), pp.329-345.

251. Forster, H. and Fisher, J., 1996. The Influence of Loading Time and Lubricant on the Friction of Articular Cartilage. *Proceedings of the Institution of Mechanical Engineers, Part H: Journal of Engineering in Medicine,* 210 (2), pp.109-119.

252. Fitzpatrick, C. K., Clary, C. W., Laz, P. J. and Rullkoetter, P. J., 2012. Relative contributions of design, alignment, and loading variability in knee replacement mechanics. *Journal of Orthopaedic Research,* 30 (12), pp.2015-2024.

253. Varadarajan, K. M., Rubash, H. E. and Li, G., 2011. Are Current Total Knee Arthroplasty Implants Designed to Restore Normal Trochlear Groove Anatomy? *The Journal of Arthroplasty,* 26 (2), pp.274-281.

254. Glaser, F. E., Gorab, R. S. and Lee, T. Q., 1999. Edge loading of patella components after total knee arthroplasty. *The Journal of Arthroplasty,* 14 (4), pp.493.

255. Sculco and Martucci, 2001. *Knee Arthroplasty.* New York:Springer.

256. Fitzpatrick, C. K., Baldwin, M. A., Clary, C. W., Wright, A., Laz, P. J. and Rullkoetter, P. J., 2012. Identifying alignment parameters affecting implanted patellofemoral mechanics. *Journal of Orthopaedic Research,* 30 (7), pp.1167-1175.

257. Hsu, H. P. and Walker, P. S., 1989. Wear and deformation of patella components in total knee arthroplasty. *Clinical Biomechanics,* 246 pp.261.

258. Nicoll, D. and Rowley, D. I., 2010. Internal rotational error of the tibial component is a major cause of pain after total knee replacement. *The Journal of Bone & Joint Surgery. British Volume,* 92 pp.1238-1244.

259. Zihlmann, M. S., Stacoff, A., Romero, J., Quervain, I. K.-D. and Stüssi, E., 2005. Biomechanical background and clinical observations of rotational malalignment in TKA. *Clinical Biomechanics,* 20 (7), pp.661-668.

260. Terashima, T., Onodera, T., Sawaguchi, N., Kasahara, Y. and Majima, T., 2014. External rotation of the femoral component decreases patellofemoral contact stress in total knee arthroplasty. *Knee Surgery, Sports Traumatology, Arthroscopy,* pp.1-7.

261. Thompson, J. A., Hast, M. W., Granger, J. F., Piazza, S. J. and Siston, R. A., 2011. Biomechanical effects of total knee arthroplasty component malrotation: A computational simulation. *Journal of Orthopaedic Research,* 29 (7), pp.969-975.

262. Kessler, O., Patil, S., Colwell, C. W. and D'lima, D. D., 2008. The effect of femoral component malrotation on patellar biomechanics. *Journal of Biomechanics,* 41 (16), pp.3332-3339.

263. Miller, M. C., Berger, R. A., Petrella, A. J., Karmas, A. and Rubash, H., 2001. Optomizing femoral component rotation in total knee arthroplasty. *Clinical Orthopaedics and Related Research,* 392 pp.38-45.

264. Sherwood, C. P., Zhang, A. X., Petrella, A. J., Miller, M. C., Berger, R. A. and Rubash, H., 1996. The effect of femoral component external rotation on tibial rotation in total knee arthroplasty. *In: Biomedical Engineering Conference,* Ohio.

265. Nagamine, R., Whiteside, L. A., White, S. E. and Mccarthy, D. S., 1994. Patella Tracking after total knee arthroplasty. *Clinical Orthopaedics and Related Research,* 304 pp.263-271.

266. Kawano, T., Miura, H., Nagamine, R., Urabe, K., Matsuda, S., Mawatari, T., Moro-Oka, T. and Iwamoto, Y., 2002. Factors affecting patellar tracking after total knee arthroplasty. *J Arthro,* 17 (7), pp.942-947.

267. Hofmann, A. A., Tkach, T. K., Evanich, C. J., Camargo, M. P. and Zhang, Y., 1997. Patellar component medialization in total knee arthroplasty. *The Journal of Arthroplasty,* 12 (2), pp.155-160.

268. Mane, A. M., Clary, C. W. and Maletsky, L. P., 2005. Effects of distal-proximal patella malpositioning on patellofemoral kinematics and quadriceps load during a deep squat. *In: 51st Annual Meeting of the Orthopaedic Research Society,* Washington.

269. Coles, L. G., Gheduzzi, S. and Miles, A. W., 2014. In vitro method for assessing the biomechanics of the patellofemoral joint following total knee arthroplasty. *Proc IMechE Part H J Eng in Med,* In Press

270. Long, R., Gheduzzi, S., Bucher, T. A., Toms, A. D. and Miles, A. W., 2013. A biomechanical evaluation of hinged total knee replacement prostheses. *Proceedings of the Institution of Mechanical Engineers. Part H, Journal of engineering in medicine,* 227 (8), pp.875-883.

271. Ali, S. A., Helmer, R. and Terk, M. R., 2009. Patella Alta: Lack of Correlation Between Patellotrochlear Cartilage Congruence and Commonly Used Patellar Height Ratios. *AJR American Journal of Roentgenology,* 193 (5), pp.1361-1366.

272. Schiedel, F., Probst, A., Buller, T. C. and Rödl, R., 2009. The postoperative patella height: a comparison of additive and subtractive high tibial osteotomy in correcting the genu varum. *Archives of Orthopaedic and Trauma Surgery,* 129 (9), pp.1271-1277.

273. Nemeth, G. and Ohlsen, H., 1985. In vivo moment arm lengths for hip extensor muscles at different angles of hip flexion. *Journal of Biomechanics,* 18 (2), pp.129-140.

274. Wretenberg, P., Nemeth, G., Lamontagne, M. and Lundin, B., 1996. Passive knee muscle moment arms measured in vivo with MRI. *Clinical Biomechanics,* 11 (8), pp.439-446.

275. Herzog, W. and Read, L. J., 1993. Lines of action and moment arms of the major force-carrying structures crossing the human knee joint. *Journal of Anatomy,* 182 pp.213-230.

276. Miller, S. L., Gill, J. and Webb, G. R., 2007. The Proximal Origin of the Hamstrings and Surrounding Anatomy Encountered During Repair. *The Journal of Bone & Joint Surgery. American Volume,* 89 (1), pp.44.

277. Fitzgerald, L., Gheduzzi, S. and Miles, A. W., 2014. Development of a synthetic collateral ligament model for use in an in vitro kinematic knee simulator. *The Bone and Joint Journal,* 96 B pp.156.

278. Germscheid, N. M., Thornton, G. M., Hart, D. A. and Hildebrand, K. A., 2011. A Biomechanical assessment to evaluate breed differences in normal porcine medial collateral ligaments. *Journal of Biomechanics,* 44 pp.725-731.

279. Riemersa, D. J. and Schamhardt, H. C., 1982. The cryo-jaw, a clamp designed for in vitro rheology studies of horse digital flexor tendons. *Journal of Biomechanics,* 15 (8), pp.619-620.

280. Drayton, P., 2008. *Biomechanical Investigation of Tendon Repair*. Thesis (Masters of Philosophy). University of Bath, Bath.

281. Laprade, R. F., Engebretsen, A. H., Ly, T. V., Johansen, S., Wentorf, F. A. and Engebretsen, L., 2007. The Anatomy of the Medial Part of the Knee. *The Journal of Bone & Joint Surgery. American Volume,* 89 (9), pp.2000-2010.

282. Liu, F., Yue, B., Gadikota, H. R., Kozanek, M., Liu, W., Gill, T. J., Rubash, H. E. and Li, G., 2010. Morphology of the medial collateral ligament of the knee. *Journal of Orthoapedic Surgical Research,* 5 pp.69.

283. Yoshida, Y., Mizner, R. L., Ramsey, D. K. and Snyder-Mackler, L., 2008. Examining outcomes from total knee arthroplasty and the relationship between quadriceps strength and knee function over time. *Clinical Biomechanics,* 23 (3), pp.320-328.

284. Silva, M., Shepherd, E. F., Jackson, W. O., Pratt, J. A., Mcclung, C. D. and Schmalzried, T. P., 2003. Knee strength after total knee arthroplasty. *J Arthroplasty,* 18 (5), pp.605-611.

285. Catani, F., Belvedere, C., Ensini, A., Feliciangeli, A., Giannini, S. and Leardini, A., 2011. In-Vivo knee kinematics in rotationally unconstrained total knee arthroplasty. *Journal of Orthopaedic Research,* 29 (10), pp.1484-1490.

286. Taylor, J. R., 1997. *An Introduction to Error Analysis.* 2nd. California:University Science books.

287. Harris, M. L., Morberg, P., Bruce, W. J. and Walsh, W. R., 1999. An improved method for measuring tibiofemoral contact areas in total knee arthroplasty: a comparison of K-scan sensor and Fuji film. *Journal of Biomechanics,* 32 (9), pp.951-958.

288. Industrial Products Division Fujifilm Europe, 2007. *Prescale Measurement Film* [online]. Online: Fujifilm Europe. Available from: http://www.fujifilm.eu/eu/products/industrial-products/prescale/prescale-measurement-film/. [Accessed 18/07/2014].

289. Wilharm, A., Hurschler, C., Dermitas, T. and Bohnsack, M., 2013. Use of Tekscan K-Scan Sensors for Retropatellar Pressure Measurement Avoiding Errors during Implantation and the Effects of Shear Forces on the Measurement Precision. *BioMed Research International,* 2013 pp.7.

290. Saevarsson, S. K., Romeo, C. I. and Anglin, C., 2013. Are static and dynamic kinematics comparable after TKA? *Journal of Biomechanics,* 46 (6), pp.1169-1175.

291. Van Eijden, T. M. G. J., Kouwenhoven, E., Verburg, J. and Weijs, W. A., 1986. A mathematical model of the patellofemoral joint. *Journal of Biomechanics,* 19 (3), pp.219-229.

292. Lindsey, J. A., Conner, D., Godleski, P., Perkinson, B., Mihalko, W. M. and Williams, J. L., 2010. Patellar button wear patterns in well-functioning total knee arthroplasty retrievals. *Journal of long-term effects of medical implants,* 20 (1), pp.73-79.

293. Burroughs, B. R., Rubash, H. E., Estok, D., Jasty, M., Krevolin, J. and Muratoglu, O. K., 2006. Comparison of conventional and highly crosslinked UHMWPE patellae evaluated by a new in vitro patellofemoral joint simulator. *Journal of Biomedical Materials Research Part B: Applied Biomaterials,* 79B (2), pp.268-274.

294. Müller, O., Lo, J., Wünschel, M., Obloh, C. and Wülker, N., 2009. Simulation of force loaded knee movement in a newly developed in vitro knee simulator / Simulation von belastungsabhängigen Kniebewegungen in einem neuartigen Knie-Simulator für In-vitro-Studien. *Biomedizinische Technik/Biomedical Engineering,* 54 (3), pp.142.

295. Fuchs, S., Schuette, G., Witte, H. and Tibesku, C., 2004. Patellofemoral contact characteristics in total knee prostheses with and without anterior flange. *Journal of Applied Biomechanics,* 20 pp.144-152.

296. Conditt, M. A., Noble, P. C., Allen, B., Shen, M., Parsley, B. S. and Mathis, K. B., 2005. Surface damage of patellar components used in total knee arthroplasty. *The Journal of Bone & Joint Surgery. American Volume,* 87 (6), pp.1265.

297. Martin, A., Quah, C., Syme, G., Segaren, N. and Pickering, S., Long term survivorship following Scorpio total knee replacement. *International Journal of Surgery,* 11 (8), pp.659.

298. Tsukeoka, T. and Lee, T. H., 2012. Sagittal flexion of the femoral component affects flexion gap and sizing in total knee arthroplasty. *The Journal of Arthroplasty,* 27 (6), pp.1094-1099.

Appendix A: Publications Arising from this Study

Article In Press

Coles, L. G., Gheduzi, S., Miles, A.W., 2014. *In vitro method for assessing the biomechanics of the patellofemoral joint following total knee arthroplasty*. Proc IMechE Part H J Eng in Med.

WCB 2014, Boston, USA, 6-11th July 2014

The Effect of Femoral Rotation During Total Knee Arthroplasty on Patellofemoral Contact Characteristics

L.G. Coles*, S. Gheduzzi*, T.P. Holsgrove*, A.W. Miles*
*Centre of Orthopaedic Biomechanics, Dept. Mech. Eng., Uni. Of Bath;
[Podium Presentation by L.G. Coles]

Patellofemoral joint (PFJ) complications are a common cause of dissatisfaction leading to revision total knee arthroplasty (TKA) due to wear and/or pain. It is thought that increased contact pressures and forces within the PFJ contribute to increased incidences of pain and wear of the patella button. Previous work suggests that this may be associated with femoral component rotation and hence this should be controlled tightly during surgery; but the available data are limited. This study aimed to assess the influence of femoral component rotation on the quadriceps forces, and the contact areas and compressive forces within the PFJ using an *in vitro*, non-cadaveric, TKA model.

Static and dynamic tests were carried out using a six degrees of freedom vertical knee simulator designed to replicate motion of an average UK woman. The movement at the knee is driven by actuation of the quadriceps model. The hamstrings are modelled physiologically by two cables each with a constant tension of 50N. Scorpio PS size 7 (Stryker, NJ) components were implanted in composite bones by an orthopaedic surgeon and primary ligaments were modelled using synthetic cords.

The required quadriceps force to achieve extension during a squat and the associated patella compressive forces were assessed using single axis load cells. The PFJ centre of pressure (COP) was measured using a pressure array (Novel, Munich) and the contact areas assessed using pressure film (FujiFilm). Three femoral positions were assessed (neutral, 5° internal and

5° external rotation) each with a 5 mm medialised patella dome and a centrally placed asymmetric patella button. Six repeats were carried out.

Irrespective of patella button type, femoral external rotation caused an increase of up to 10% in the required quadriceps force and compressive PFJ forces, likely due to the alteration of the Q angle caused by the component rotation. Internal rotation caused corresponding reductions. These trends are only significant in mid-flexion and are masked by increased loading. The patella button geometry also appeared to influence the degree to which femoral rotation affected the PFJ. Fewer differences were demonstrated with the medialised dome, which was associated with increasing lateral COP measurements post-TKA with external rotation. In contrast, the asymmetric dome demonstrated medial COP shifts with external rotation.

In conclusion, PFJ forces and pressures are influenced by a complex combination of prosthesis geometry and component positioning. As little as 5° of femoral rotation may have an implant specific, detrimental effect on the PFJ.

Femoral component rotation of a modern TKA implant does not affect PFJ biomechanics

L.G. Coles*, S. Gheduzzi*, A.W. Miles*

*Centre of Orthopaedic Biomechanics, Dept. Mech. Eng., Uni. Of Bath;

[Podium Presentation by L.G. Coles] Awarded Young Investigator Award

Research Summary

Patellofemoral joint (PFJ) complications, such as anterior knee pain, are a common complaint among knee arthroplasty patients and femoral rotational mal-alignment is thought to be a contributing factor. However, no studies have assessed the effect of femoral internal and external rotation on PFJ biomechanics using simulated physiological loading cycles. The present study aimed to assess the effect of surgical femoral rotational alignment errors on the forces, moment arms and contact areas within the PFJ.

Testing was carried out under physiological loading, with a quasi-static kinematic knee joint simulator, using Scorpio NRG prostheses implanted on synthetic bones. Three scenarios were simulated, to replicate the worst case in terms of surgical error; neutral placement was compared to 5° internal and 5° external femoral rotation.

External rotation caused a significant reduction in the patella moment arm. However, femoral rotational mal-alignments of ± 5° had no clinically relevant effect on the quadriceps force, patella compressive force, or PFJ contact areas. For all scenarios, the PFJ was subjected to over 65% lateral loading and consistent edge loading of the patella button. This study demonstrates that, in terms of PFJ biomechanics, the Scorpio NRG implant used was tolerant of surgically relevant levels of femoral rotational mal-alignment.

Introduction

The patellofemoral joint (PFJ) is implicated in many revision cases following total knee arthroplasty (TKA), with many patients reporting anterior knee pain (AKP). Changes in PFJ loading magnitudes and patterns are thought to contribute to AKP [1]. Femoral component rotational alignment has been demonstrated to affect the kinematics of the PFJ. However, no in vitro studies have assessed the effect of femoral rotational mal-alignment on PFJ biomechanics using a simulated physiological loading cycle.

This study aimed to assess whether femoral component mal-rotation, due to surgeon error, may be a significant contributor to the development of patellofemoral issues and pain following TKA.

Hypothesis

Femoral component mal-rotation will cause an increase in the forces within the PFJ and a decrease in contact areas after TKA.

Methods

Scorpio NRG PS size 7 implants (Stryker, NJ, USA), and an asymmetrical patella button, were implanted on Sawbones. Three scenarios were simulated; neutral femoral rotational placement was compared to 5° internal (IR) and 5° external rotation (ER) of the femoral component with respect to the cylindrical axis of the knee.

A quasi-static kinematic knee joint simulator, a derivative of the Oxford Knee Rig, was used to cycle the knee through flexion/extension via a single quadriceps actuator against a physiological peak flexion moment of 43 Nm. The joint was stabilised using synthetic ligaments and by two constant force springs simulating the action of the hamstrings. The quadriceps tendon load and the compressive force applied to the patella were measured using single axis load cells. The patella moment arm was measured with an optical technique, while the PFJ contact area was assessed using Prescale pressure films. Five repeats were carried out for each alignment scenario. Differences between the groups were evaluated with the Friedman test and post-hoc Wilcoxon signed ranked test; significance was assumed for $p < 0.05$.

Results

In mid flexion ER resulted in a statistically significant reduction in quadriceps and patella forces amounting in either case to no more than 20N. This finding is unlikely to be of clinical relevance given that it is comparable to the levels of variation expected between patients. No differences were observed in high flexion when the PFJ was under the highest loading condition.

ER resulted in a significant reduction in the patella moment arm throughout the flexion range compared to neutral alignment, while IR exhibited the opposite trend (Fig 1). The joint contact area was unaffected by mal-rotation. Throughout the tested flexion range at least 65% of the loading was on the lateral side. Both lateral and medial edge loading occurred.

Discussion and Conclusion

This study demonstrated that femoral rotational mal-alignment altered the patella moment arm. This affect is attributable to changes in the Q angle as a result of induced tibial varus/valgus. However, possibly due to the geometry of the patella button used, this did not ultimately result in clinically relevant changes to the quadriceps force, PFJ compressive force, or PFJ contact area. The hypothesis can therefore be rejected.

Femoral rotational mal-alignment of ± 5° is considered the worst case in terms of surgical error, and may affect ligament forces, but has been demonstrated, with the exception of varus/valgus rotations, to have a limited effect on Scorpio tibiofemoral kinematics [3, 4]. This in vitro study indicates that the Scorpio implant is also tolerant of commonly reported levels of femoral rotational alignment errors with regards to PFJ biomechanics.

Significance

The results of this study suggest that the Scorpio NGR knee replacement can tolerate, in terms of PFJ biomechanics, femoral rotational mal-alignment.

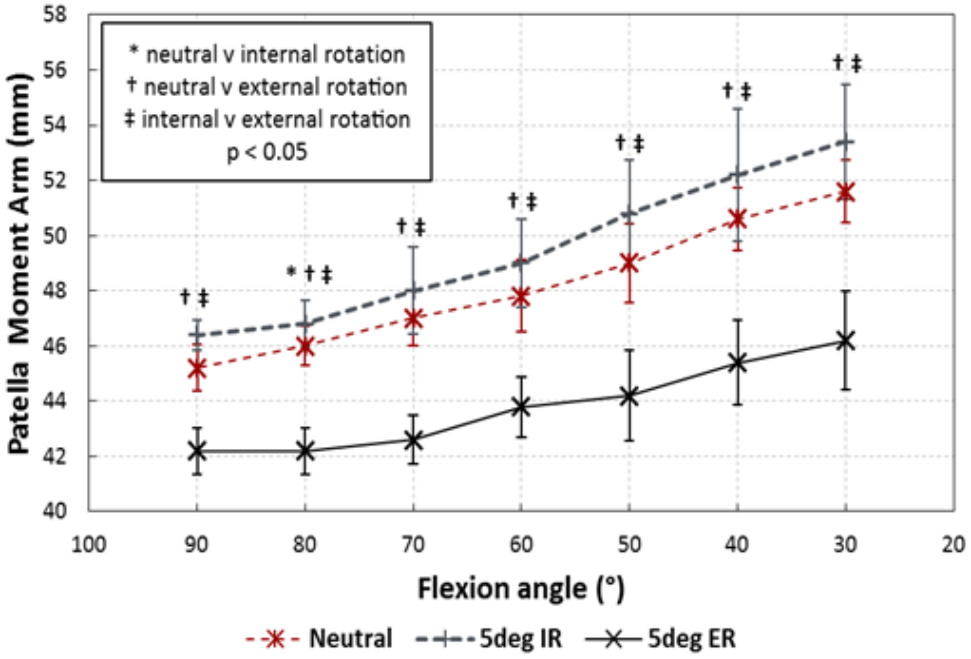

Figure 1: Variation in patella moment arm with flexion angle (mean ± standard deviation).

References

1. Dye, S.F., CORR, 2005. 436 pp 100-110.
2. Saevarsson, S.K.,et al., J Biomech, 2013. 46 (6) pp 1169-1175.
3. Matziolis, G., et al, JBJS. Am, 2007. 89(2).
4. Thompson, J.A., et al., JOR, 2011. 29(7) pp 969-975.

The effect of medialisation of the patella button during total knee arthroplasty on patellofemoral contact characteristics

L.G. Coles*, S. Gheduzzi*, A.W. Miles*
*Centre of Orthopaedic Biomechanics, Dept. Mech. Eng., Uni. Of Bath;
[Poster Presentation by L.G. Coles]

Introduction

The patellofemoral joint (PFJ) has been implicated as a contributing factor in around 20% of total knee arthroplasty (TKA) revisions [126] and up to 25% of un-revised patients report pain within the joint [15]. The source(s) of pain within the anterior region of the knee is not fully understood but it is thought that increased contact pressures and forces within the PFJ contribute to increased incidences of pain and wear of the patella button. It has been advocated by some that medialisation of the standard symmetrical dome button or the use of a medialised dome asymmetric patella may reduce patellofemoral contact pressures and forces and hence improve outcomes.

Objectives

The primary objective was to assess if medialisation of the patella button or prosthetic geometrical differences may have an effect on the required quadriceps forces, or the contact areas, compressive forces and pressures within the PFJ using an *in vitro*, non-cadaveric, TKA model.

Methods

Static and dynamic tests were carried out using a six degrees of freedom vertical knee simulator designed to replicate motion of an average UK woman. The movement at the knee is driven by actuation of the quadriceps model. The hamstrings are modelled physiologically by two cables each with a constant tension of 50N. Scorpio PS size 7 (Stryker, NJ) components were implanted on to composite bones by an orthopaedic surgeon and primary ligaments were modelled using synthetic cords.

The required quadriceps force to achieve extension during a squat and the associated patella compressive forces were assessed using single axis load cells. The PFJ centre of pressure (COP) was measured using a pressure array (Novel, Munich) and the contact areas assessed

using pressure film (FujiFilm). The contact pressures were estimated using the compressive force and area data and Hertzian contact theory.

Three patella conditions were assessed: a symmetrically placed dome button, 5 mm medialisation of the dome and a centrally placed asymmetric patella button. Six repeats were carried out.

Results

No effects were recorded regarding the required quadriceps forces. However, medialisation and the use of an asymmetric dome resulted in 4% and 2% reductions respectively in compressive forces in deep flexion. Neither medialisation nor the use of an asymmetric patella reduced the peak pressures developed in the PFJ, which remained in the range of UHMWPE fatigue (> 10 MPa).

All patella conditions demonstrated two distinctly separate loading areas throughout the flexion range. However, the medialised dome demonstrated a significantly more lateral COP than the asymmetrical dome which was significantly more lateral than the central dome throughout the flexion range. This is likely due to the lateral tilt the medialisation causes and will increase the uneven loading in the joint post-TKA, which may have implications for joint wear and pain. All three conditions also demonstrated edge loading throughout the range of motion which casts doubt over the congruence of the patella and femoral geometry.

Conclusions

In contrast to popular belief, in the case of the modern, patella friendly, single-radius Scorpio knee, medialisation of the patella button peak does not appear to substantially reduce PFJ forces or pressures. However, medialisation of the dome peak does appear to increase the lateral position of the joint COP.

References

Hsin-Nun, S., LIH-YUANN SHIH, YON-CHEONG WONG,HSU, R.W.-W., 2004. Long-term changes of the nonresurfaced patella after total knee arthroplasty. J. Bone Joint Surg. Am. 86.

Sharkey, P.F., Hozack, W., Rothman, R.H., Shastri, S.,Jacoby, S.M., 2002. Why are total knee arthroplasties failing today? Clin. Orthop. Relat. Res. 404**,** 7-13.

Development of a Synthetic Collateral Ligament Model for use in an In Vitro Kinematic Knee Simulator

L.G. Fitzgerald†, A Titchener‡, A.W. Miles†

†Centre of Orthopaedic Biomechanics, Dept. Mech. Eng., Uni. Of Bath; ‡ Nottingham University Hospitals

[Podium Presentation by L.G. Fitzgerald (now known as L.G. Coles)]

Summary Statement

The tensile properties of a number of synthetic fibre constructs and porcine MCLs were experimentally determined and compared to allow the selection of an appropriate synthetic collateral ligament model for use in a kinematic knee simulator.

Introduction

As patient expectations regarding functional outcomes of total knee arthroplasty rise the need to assess the kinematics of new implants in vitro has increased. This has traditionally been done using cadaveric models, which can demonstrate high physiological relevance but also substantial inter-specimen variability. More recently there has been a shift towards the use of *in silico* and non-cadaveric methods. Such methods require significant simplifications of the joint and the modelling of soft tissue structures such as the collateral ligaments. Collateral ligaments are often modelled in *in silico* studies but have not, in the published literature, been modelled in *in vitro* knee kinematic simulators.

Tensile testing of ligament tissue, to provide reference data, and the subsequent analysis of potential synthetic analogues was carried out. The overall aim of the study was to develop a synthetic ligament analogue for use in kinematic knee simulators.

Methods

Porcine MCLs were chosen as these are of a similar size and are a readily available alternative to human ligaments. Six porcine knee specimens were sourced and the MCLs dissected by an orthopaedic registrar. Testing was carried out on an Instron MTS fitted with a 5kN load cell. Each specimen was subjected to 5 pre-conditioning loading cycles before cross-sectional and length measurements were made. Each specimen was then cyclically loaded from 0-200N for 30 cycles before being loaded to failure at a rate of 100mm/min. (Figure 1)

Ten potential synthetic analogues were also assessed using the same procedure: the Lars 80 (Corin Ltd) synthetic ligament reconstruction system and a selection of readily available synthetic constructs.

Results

The porcine specimens demonstrated 6% ± 1% strain (mean ± standard error) after 30 cycles of loading, and a tensile stiffness of 100 N/mm ± 8.9 N/mm. The results of the load to failure tests also indicated a substantial toe region and highlighted the substantial variability associated with cadaveric specimens (Figure 2).

The Lars system demonstrated a tensile stiffness of nearly 9 times that of the porcine specimens. However, non-parametric Mann-Whitney U analyses indicated that three of the synthetic samples did not have statistically significantly different tensile stiffness values compared to the porcine specimens ($p < 0.05$) (Figure 3). Of these samples, the polyester braided cord demonstrated the longest and most physiologically relevant toe region (Figure 2). All of the polyester load-displacement traces fell within the range demonstrated by the porcine specimens.

Discussion/Conclusion

The tensile properties of the porcine specimens analysed were similar to those reported in in the literature for human ligaments[1]. Porcine MCLs are thus a fair model of human collateral ligaments and were a suitable reference material for the selection of a synthetic analogue. The tensile testing carried out in the present study indicated that commercially available synthetic ligaments are over engineered in terms of strength and inappropriate for use in kinematic analysis. However, a polyester braided cord did demonstrate appropriate basic mechanical properties and would be appropriate as an analogue model on kinematic knee rigs.

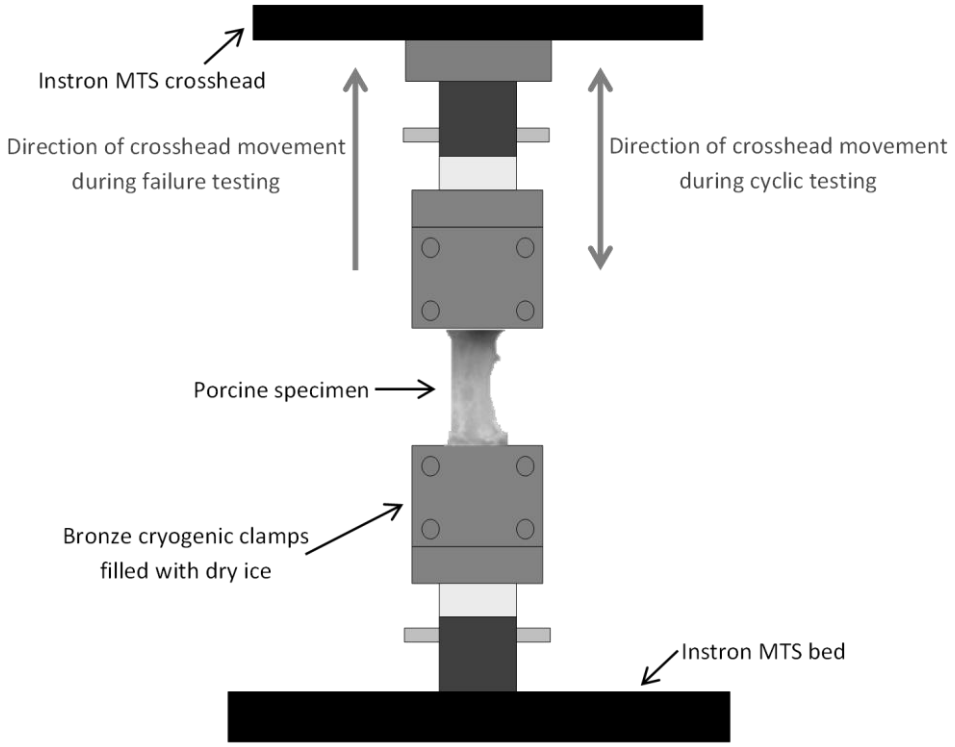

Figure 1: Diagrammatic representation of experimental method.

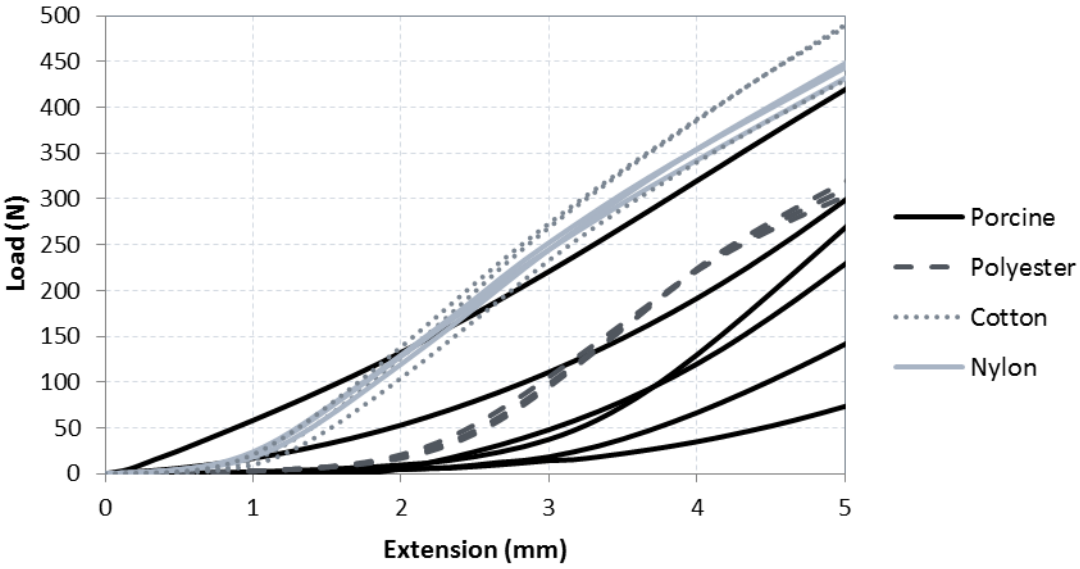

Figure 2: Load deformation curves generated from failure testing of each porcine specimen and each synthetic material which did not show a statistically significantly different tensile stiffness to the porcine mean ($p > 0.05$).

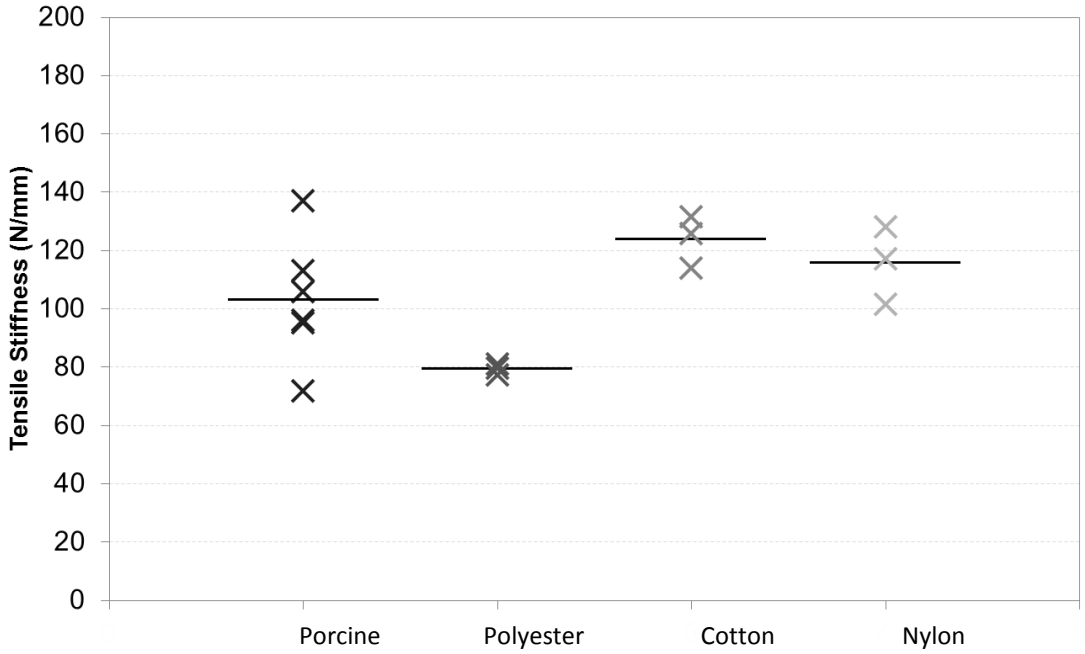

Figure 3: Tensile stiffness values for each porcine specimen and each synthetic material which did not show a statistically significantly difference to the porcine mean ($p > 0.05$) shown with average values.

References

1. Robinson, J.R., *et. al.* J Biomech, 2005. **38**(5): 1067-1074.

Appendix B: Component Implantation

Scorpio NRG tibial and femoral components were implanted onto composite Sawbones by an orthopaedic fellow, as detailed in Figure B-1. An experienced Stryker representative, an orthopaedic consultant and an orthopaedic engineering professor were also present. The implantation was carried out using Stryker Series 5 power tools and a Stryker Scorpio demo surgical kit.

Figure B-1: Implantation of Scorpio NRG tibial and femoral components

Alignment pegs were added to the Sawbones to allow accurate and secure placement in the alignment rig (Figure B-2). The alignment pin locations were defined (Table B-1), using CAD models so as to ensure anatomical kinematic alignment of both components within the rig.

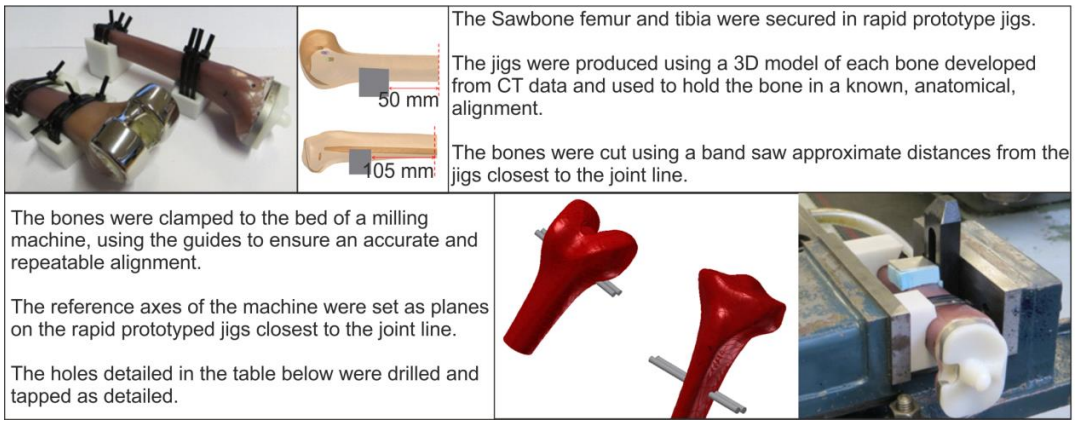

Figure B-2: Accurate addition of alignment pegs to Sawbone models

Table B-1: Positioning of Sawbone alignment pegs

Bone	Side	Proximodistal Reference Plane	Proximo-distal Distance	Anterio-posterior Positioning	Depth Reference Plane	Depth
Tibia	Medial	Distal surface of most proximal jig	10 mm distal	2 holes 10 mm apart as central as feasible	Medial surface	22 mm
	Lateral				Distal surface	22 mm
Femur	Medial		15 mm distal		Medial surface	16.5 mm
	Lateral				Distal surface	24.5 mm

The tibial attachment of the patella tendon was also simulated. As Figure B-3 depicts, a hole was drilled through the tibia in the anterioposterior direction at the approximate location of the tibial tuberosity. A bolt, locating a pulley, was placed through this hole and secured on the posterior end using a nut. The force on the posterior side was spread out through the use of a thick rubber washer. The pulley connects to the wire patella tendon model to mimic the anatomical tendon-bone attachment.

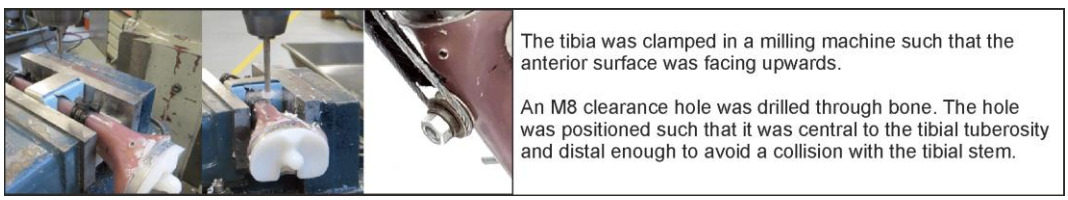

Figure B-3: Patella tendon tibial attachment

Appendix C: Alignment Rig

1. Adjust rig position arms: Consult table of jig settings (4) for the prosthesis being mounted and set the mediolateral (1), proximodistal (2) and anteroposterior (3) positioning arms at the appropriate positions for the tibial component.
2. Bolt tibial mounting block to base of jig (4) and place tibial component in holders (6) ensuring it is flush with the anteroposterior positioning plate (7). Fill tibial mounting block with molten Wood‟s metal and allow to cool and set.
3. Remove the tibial block from the jig.
4. Adjust rig position arms: consult table of jig settings for the prosthesis being mounted and set the mediolateral (1), proximodistal (2) and anteroposterior (3) positioning arms at the appropriate positions for the femoral component.
5. Bolt femoral mounting block to base of jig(4) and place femoral component in holders (6) ensuring it is flush with the anteroposterior positioning plate (7). Fill femoral mounting block with molten Woods Metal and allow to cool and set.

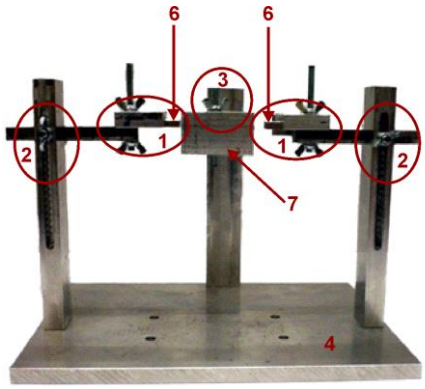

Figure C-1: Alignment rig

Table C-1: Mounting jig settings for implanted Scorpio NRG components

Alignment Setting	Femur	Tibia
Proximodistal 1	3.6	5.05
Proximodistal 2	3.2	4.7
Mediolateral 1	1.6	1.5
Mediolateral 2	1.7	1.55
Anterioposterior	2	2.75

Appendix D: Alignment Rig Assessment

Methodology

All tests were carried out using Long's protocol [196,270], the only exception being the use of the dynamic method (detailed in Chapter 4) to measure the patella tendon moment arm and extensor mechanism angle. Five repeats were carried out for each group. Tests were carried out using the Zimmer NexGen hinge (Zimmer, Warsaw, IN, USA).

Test Groups

- Dependant Alignment (DA): positioned using Long's rig, which is based on aligning the tibial component and relying on the joints congruency for alignment of the femoral component
- Independent Alignment (IA): positioned using the new alignment rig, which aligns the tibial and femoral components independently

Results and Discussion

The results achieved using the two different alignment methods follow consistent patterns, but are not identical (Figure D-1 and Figure D-2). The most notable changes are demonstrated in the tibial rotation and patella tendon moment arm measurements, suggesting that prosthesis alignment has a greater influence on these variables.

A difference between the results achieved using the two different methods would be expected as the alignment arm positions for each rig were calculated and measured independently by two different researchers. This process is by no means faultless, making it impossible to determine which the correct alignment is. However, as all variables indicate relatively small differences, it can be assumed that both are sufficiently close to the ideal situation. Slight variations from ideal alignment will not affect comparisons between tests, or the suitability of the method for comparative testing, if the variations are constant across all of the tests. It is therefore important to analyse the relative standard deviations associated with each of the alignment methods.

The quadriceps force errors are comparable between the methods, but the variability is substantially reduced when assessing tibial rotation, patella tendon moment arm and the extensor mechanism angle using the new method (Figure D-3 and Figure D-4). This indicates that the IA method is more repeatable and results in less user error.

Tibial rotational variability is relatively high, at an average of 0.6° which equates to 28% of the measured value, even using the IA method. This indicates that the zeroing method may not be consistent. Following alterations to the rig, detailed in Section 6, tibial rotation measurement was removed from the protocol.

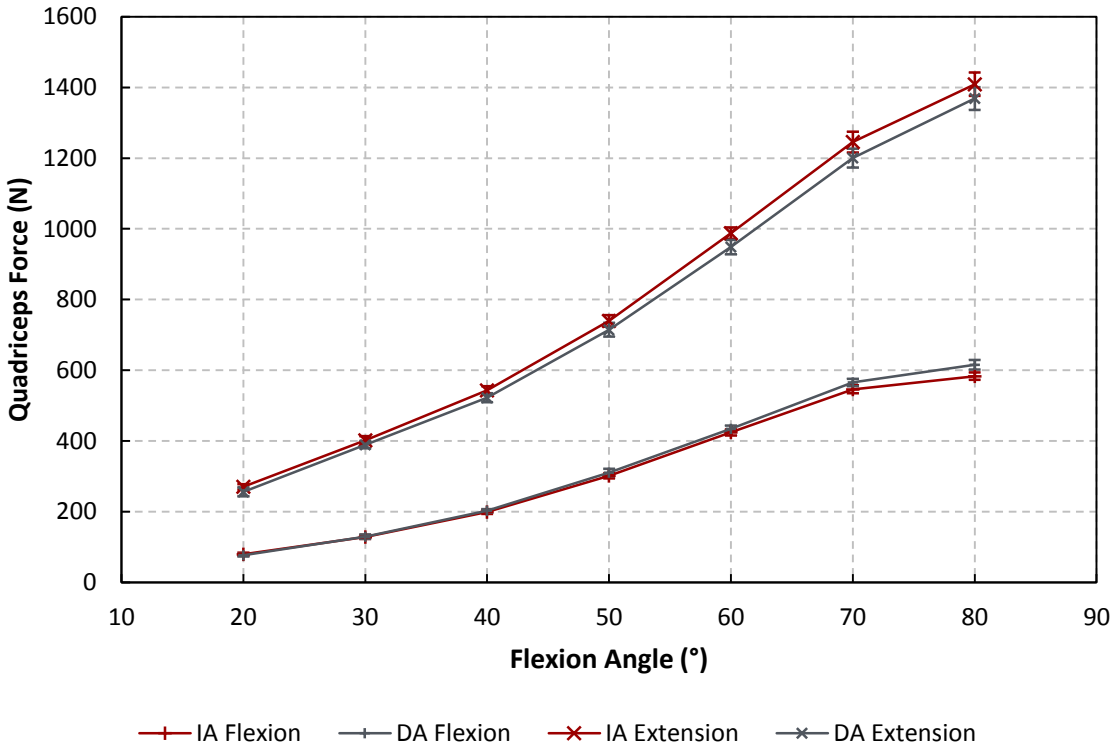

Figure D-1: Average quadriceps force measured in flexion and extension of joints mounted using independent (IA) and dependent (DA) alignment methods. Error bars represent 1 standard deviation.

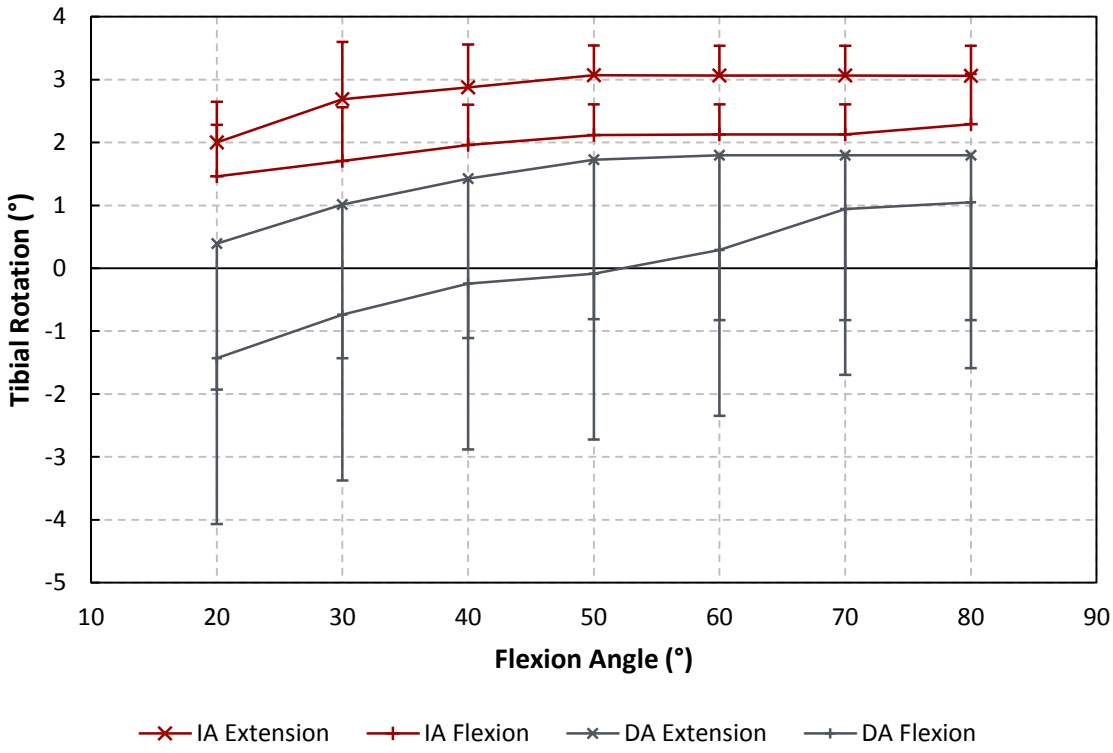

Figure D-2: Average tibial rotation measured in flexion and extension of joints mounted using independent and dependent alignment methods. Error bars represent 1 standard deviation only one half is shown for clarity.

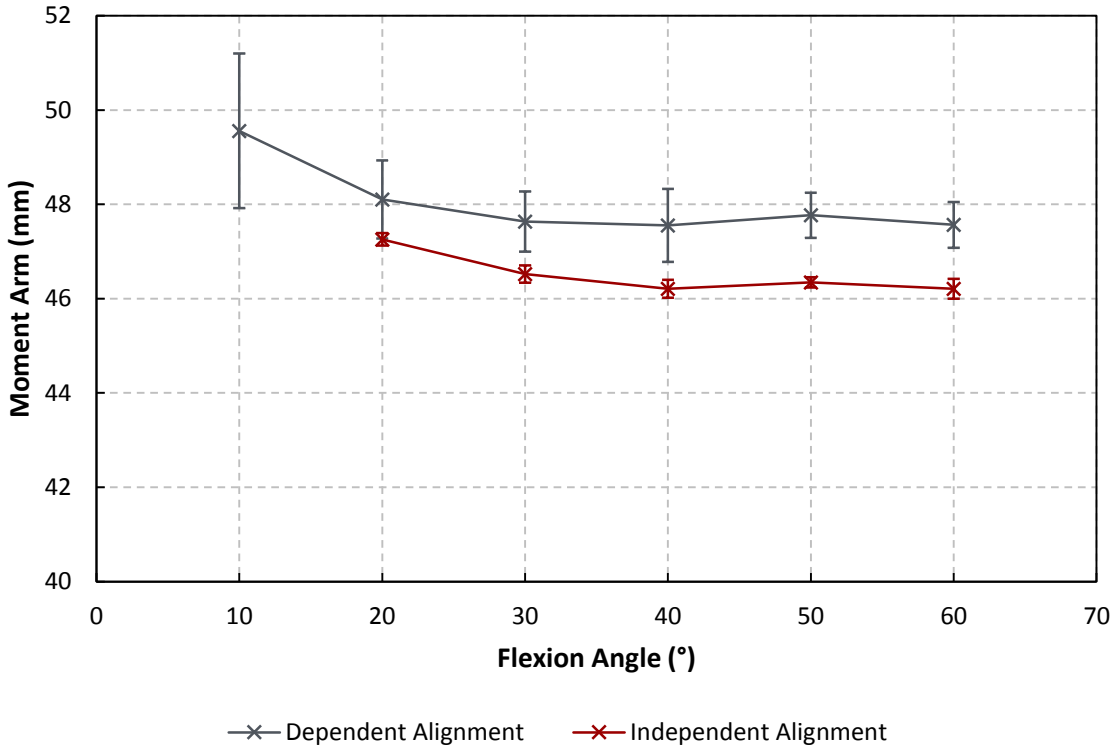

Figure D-3: Average patella tendon moment arm measured in flexion of joints mounted using independent and dependent alignment methods. Error bars represent 1 standard deviation.

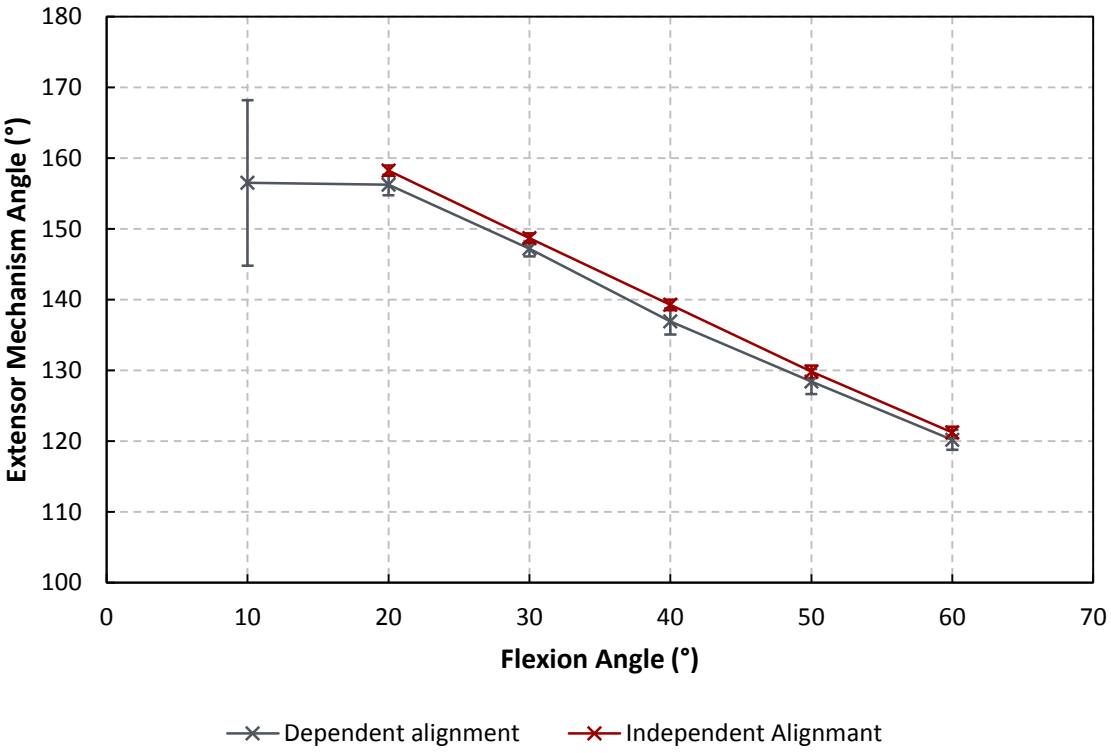

Figure D-4: Average extensor mechanism angle measured in flexion of joints mounted using independent and dependent alignment methods. Error bars represent 1 standard deviation.

Appendix E: Joint Flexion Angle Calculation

The following method was developed by R. Long as part of the PhD he completed at the University of Bath [196,270].

The joint angle, with respect to the joint centre of rotation can be calculated using trigonometry as Figure E-1 and Equation 1 detail.

$$\alpha = cos^{-1}\left(\frac{H^2 - (F^2 + T^2)}{-2FT}\right)$$

Equation 1

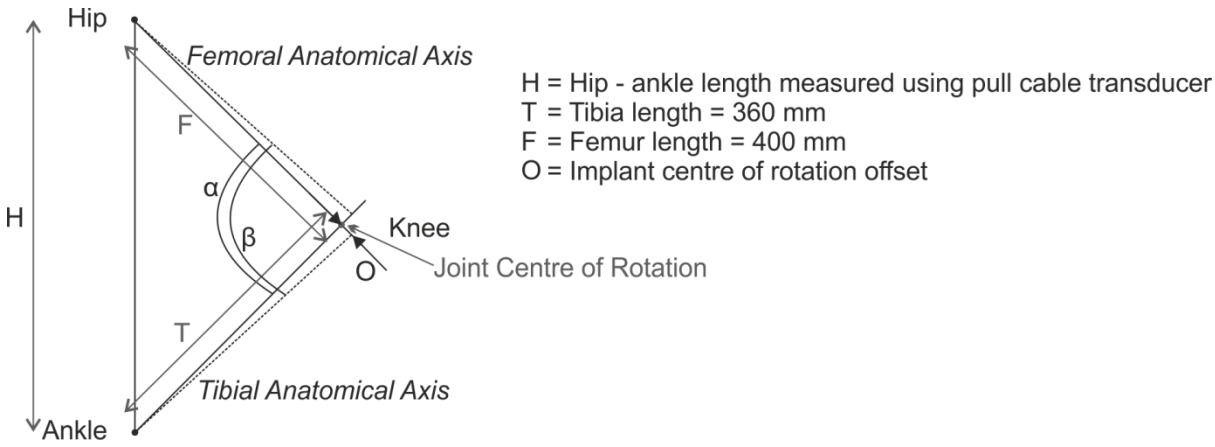

Figure E-1: Flexion Angle Calculation (Adapted from: [196])

However, it is more common to report the joint angle in terms of the tibial and femoral anatomical axes. This value for joint angle can be calculated if the implant centre of rotation offset is known (Figure E-1). For the single radius implants used in the present study this value can be measured as the joint centre of rotation will be constant, and equal to the centre of the sagittal condylar arc, in the functional flexion range. The measured values for the tested prostheses are detailed in Table E-1.

Table E-1: Implant centre of rotation offset for tested prosthesis

Implant	Offset (O) (mm)	Angle Offset (ϒ) (°)
Scorpio	11.15	3.20

The flexion angle offset (ϒ = β – α) will be constant throughout the flexion range and can be assessed for each prosthesis using Solid edge (Siemens PLM Software Inc, Camberly, UK). The calculated values are detailed in Table E-1.

The joint angle relative to the anatomical axes can therefore be calculated using Equation 2.

$$\beta = \alpha + \gamma$$

Equation 2

By convention the flexion angle is reported relative to the vertical. The flexion angle (θ) can therefore be calculated using Equation 3

$$\theta = 180 - \beta$$

Equation 3

Appendix F: Matlab Routine for PMA Calculations

The Matlab image toolbox was used to develop a set of functions to locate the markers in an image, compute their positions, generate the required measurements, and analyse the data. The highlights of the method are detailed in Figure F-1. The full code is on the following pages.

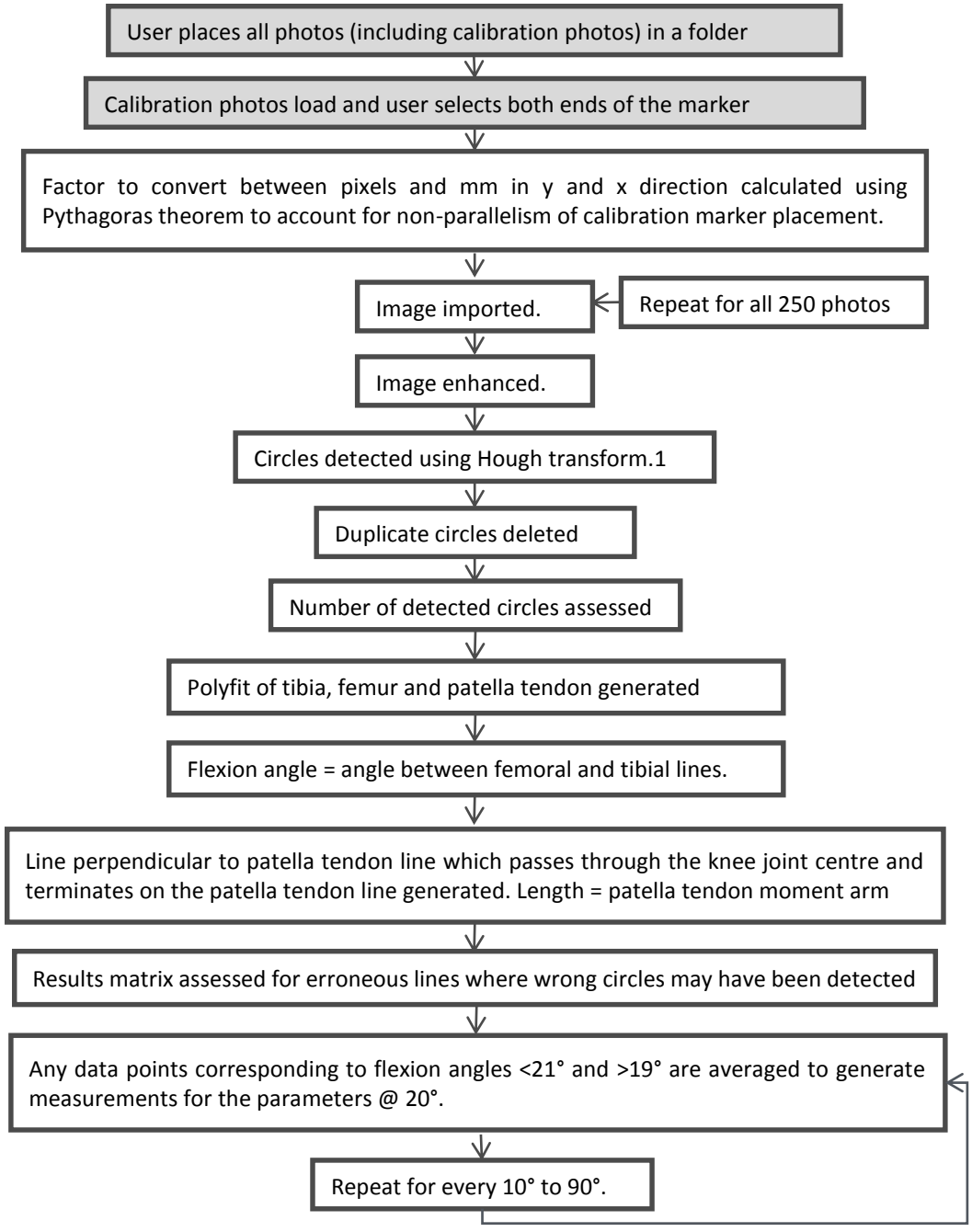

Figure F-1: High speed image analysis method

[1] The matlab code utilised in this stage was written by Tao Peng, Copyright (c) 2006. Author gives permission for its use

```
function [comdata, results, A] = TwoDPhoto_AnalysisNOMANUAL (~)
% 2D Photo_Analysis analyses a set of images of a single dynamic experiment
% to cacluate values at 10deg intervals for patella moment arm & extensor mechanicsm angle and prints them to a results file.
%Lisa Fitzgerald
%Uni Bath
%12/12/13

tic

% user selects photofolder to be analysed
folder_name=uigetdir;
cd (folder_name);
filenames = dir('*.jpg');

% calibration files identified
cal1=filenames(1).name;
cal2=filenames(2).name;

% Calibration function called
[scaley, scalex] = Calibration(cal1,152,cal2,152);

% number of photos to be analysed assessed
s=size(filenames,1);
s=s-4;
comdata = zeros(s,2);


% program loops through each photo in turn
for i=3:size(filenames,1);
   j=i-2;

   % locates correct file in sequence
   fname = filenames(i).name;

   % checks if file extension is jpg
   if strcmp( fname(size(fname,2)-3:size(fname,2)) ,'.jpg'  ) == 1

      %indicates to user which file is being analysed
      disp([fname ' loaded']);
      image=fullfile(folder_name, fname);

      %image is opened and processed
      im=imread(image);
      [img]=Convert_im(im);
      [tmp] = Im_Process(img);

      %hough transform performed
      [~, circen, ~] = CircularHough_Grd(tmp, [round(2.5*scalex - 4) round(2.5*scalex +4)], 5, 3);
    % identified circles sorted in terms of ascending x
      [z,k]=sort(circen(:,1));
      circen=circen(k,:);

      %remove circles which are within 1 pixle of each other i.e. duplicates
      if length(circen)>=3;
         for n=1:length(circen)-1;
            if abs(circen(n, 1)-circen(n+1, 1))<1;
               circen(n,:)=[0 0];
            end
         end

         circen = circen(any(circen,2),:);

         %checks that corect number of circles have been identified
         if length(circen) == 8

         circen(8,:)=[];

            [data]= Centre_AnalysisNOMANUAL_mod(circen, scaley, scalex, tmp, fname);
            comdata(j,:)=data;

         elseif length(circen) == 7

            [data]= Centre_AnalysisNOMANUAL_mod(circen, scaley, scalex, tmp, fname);
            comdata(j,:)=data;

         else

            comdata(j,:)=[0 0];

         end


      else
```

```
        comdata(j,:)=[0 0];

      end

   else
      disp 'error'

   end

end

   % remove data relating to unprocessed
images
   comdata(all(comdata==0,2),:)=[]

   % sort processed data to remove
erronous lines (i.e. ones which have
identified the
   % the wrong circles
   for l=1:10;
      if comdata(l,1) < 90 && comdata(l,1)
> 80

      else
         comdata(l,:)=[];
      end
   end

   for j=7: length(comdata);
      k=j-1;

      a1=comdata(j,1);
      a2=comdata((k),1);
      m1=comdata(j,2);
      m2=comdata((k),2);
      if m1<=40

         comdata(j,:)=[a2 m2];

      else

      end

      if abs(m1-m2)>=5

         comdata(j,:)=[a2 m2];

      else

      end

   end

comdata=unique(comdata,'rows');

% compute values at 10deg intervals
[results] = ten_deg_int (comdata);

%Create output file and print results
ofile=fullfile(folder_name,
'ImageResults.txt');
fid = fopen(ofile, 'wt');
fprintf(fid, date);
fprintf (fid, '\n flexion angle \t moment
arm \n');
fprintf (fid, '%6.0f\t  %6.0f\n', results);
fclose (fid);

toc
```

```
function [scaley, scalex] = Calibration(cal1,
v, cal2, h)
% Calibration caries out the calibration,
with user input, required to
% produce the calibration scales for the
given experimental set up
%Inputs: cal1=vertical calibration image;
v= vertical height of calibration
%object; cal2=horrizontal calibration
image; h= horrizontal length of calibration
%object;
%Output: scaley=pixles to mm scale factor
in y direction; scalex=pixles to mm scale
factor in x direction;
%Lisa Fitzgerald
%Uni Bath
%13/09/12

% Display calibration photo - user
manually selects calibration points
disp 'Vertical Calibration (152mm)'
imshow (cal1)
a=ginput(1);
b=ginput(1);

% scale factor calculated using pythag to
account for position errors
%does not account for errors due to
positioning at an angle into the plane
```

```
%of the image
scaley=sqrt((a(1, 1)-b(1, 1))^2+(a(1, 2)-b(1, 2))^2)/v;
close

% Display calibration photo - user manually selects calibration points
disp 'Horizontal Calibration (152mm)'
imshow (cal2)
c=ginput(1);
d=ginput(1);

% scale factor calculated using pythag to account for position errors
%does not account for errors due to positioning at an angle into the plane
%of the image
scalex=sqrt((c(1, 1)-d(1, 1))^2+(c(1, 2)-d(1, 2))^2)/h;
close
```

```
function [img]=Convert_im(im)
%Conver_im checks if an image is in greyscale and converts it to greyscale if not

%Input: im=image
%Output: img=output image
%lisa Fitzgerald
%Uni Bath
%13/09/12

if ndims(im) ~= 2;
   img=rgb2grey;

else
   img=im;
end
```

```
function [tmp] = Im_Process(img)
%Im_Process process a greyscale image to make it suitable for circular
%hough analysis.
%Inputs: img = greyscale image
%Output: tmp=processed image
%Lisa Fitzgerald
%Uni Bath
%13/09/12

%remove background to increase contrast
tmp=imadjust(img,[0 1], [0 1], 1);
 tmp = 255-tmp;
 background=imopen(tmp,strel('disk',7));
 tmp=imsubtract(tmp,background);
```

```
THIS SOFTWARE IS PROVIDED BY THE COPYRIGHT HOLDERS AND CONTRIBUTORS "AS IS"
AND ANY EXPRESS OR IMPLIED WARRANTIES, INCLUDING, BUT NOT LIMITED TO, THE
IMPLIED WARRANTIES OF MERCHANTABILITY AND FITNESS FOR A PARTICULAR PURPOSE
ARE DISCLAIMED. IN NO EVENT SHALL THE COPYRIGHT OWNER OR CONTRIBUTORS BE
LIABLE FOR ANY DIRECT, INDIRECT, INCIDENTAL, SPECIAL, EXEMPLARY, OR
CONSEQUENTIAL DAMAGES (INCLUDING, BUT NOT LIMITED TO, PROCUREMENT OF
SUBSTITUTE GOODS OR SERVICES; LOSS OF USE, DATA, OR PROFITS; OR BUSINESS
INTERRUPTION) HOWEVER CAUSED AND ON ANY THEORY OF LIABILITY, WHETHER IN
CONTRACT, STRICT LIABILITY, OR TORT (INCLUDING NEGLIGENCE OR OTHERWISE)
ARISING IN ANY WAY OUT OF THE USE OF THIS SOFTWARE, EVEN IF ADVISED OF THE
POSSIBILITY OF SUCH DAMAGE.

function [accum, varargout] = CircularHough_Grd(img, radrange, varargin)

%Detect circular shapes in a grayscale image. Resolve their center
%positions and radii.
%

% Author: Tao Peng
% Department of Mechanical Engineering
```

```
%           University of Maryland, College
Park, Maryland 20742, USA
%         pengtao@glue.umd.edu
%  Version: Beta          Revision: Mar. 07,
2007

% Validation of arguments
if ndims(img) ~= 2 || ~isnumeric(img),
   error('CircularHough_Grd: ''img'' has to
be 2 dimensional');
end
if ~all(size(img) >= 32),
   error('CircularHough_Grd: ''img'' has to
be larger than 32-by-32');
end

if      numel(radrange)      ~=      2      ||
~isnumeric(radrange),
   error(['CircularHough_Grd:  ''radrange''
has to be ', ...
      'a two-element vector']);
end
prm_r_range            =            sort(max(
[0,0;radrange(1),radrange(2)] ));

% Parameters (default values)
prm_grdthres = 10;
prm_fltrLM_R = 8;
prm_multirad = 0.5;
func_compu_cen = true;
func_compu_radii = true;

% Validation of arguments
vap_grdthres = 1;
if nargin > (1 + vap_grdthres),
   if      isnumeric(varargin{vap_grdthres})
&& ...
         varargin{vap_grdthres}(1) >= 0,
      prm_grdthres                          =
varargin{vap_grdthres}(1);
   else
      error(['CircularHough_Grd:
''grdthres'' has to be ', ...
         'a non-negative number']);
   end
end

vap_fltr4LM = 2;   % filter for the search of
local maxima
if nargin > (1 + vap_fltr4LM),
   if  isnumeric(varargin{vap_fltr4LM})  &&
varargin{vap_fltr4LM}(1) >= 3,
      prm_fltrLM_R                          =
varargin{vap_fltr4LM}(1);
   else
      error(['CircularHough_Grd:
''fltr4LM_R'' has to be ', ...
         'larger than or equal to 3']);
   end
end

vap_multirad = 3;
if nargin > (1 + vap_multirad),
   if      isnumeric(varargin{vap_multirad})
&& ...
      varargin{vap_multirad}(1)  >=  0.1  &&
...
      varargin{vap_multirad}(1) <= 1,
   prm_multirad                             =
varargin{vap_multirad}(1);
   else
      error(['CircularHough_Grd:
''multirad'' has to be ', ...
         'within the range [0.1, 1]']);
   end
end

vap_fltr4accum = 4; % filter for smoothing
the accumulation array
if nargin > (1 + vap_fltr4accum),
   if   isnumeric(varargin{vap_fltr4accum})
&& ...
         ndims(varargin{vap_fltr4accum})
== 2 && ...
         all(size(varargin{vap_fltr4accum})
>= 3),
      fltr4accum                            =
varargin{vap_fltr4accum};
   else
      error(['CircularHough_Grd:
''fltr4accum'' has to be ', ...
         'a 2-D matrix with a minimum size
of 3-by-3']);
   end
else
   % Default filter (5-by-5)
         fltr4accum = ones(5,5);
         fltr4accum(2:4,2:4) = 2;
         fltr4accum(3,3) = 6;
end

func_compu_cen = ( nargout > 1 );
func_compu_radii = ( nargout > 2 );
```

```
% Reserved parameters
dbg_on = false;      % debug information
dbg_bfigno = 4;
if nargout > 3,  dbg_on = true;  end


%%%%%%%% Building accumulation array
%%%%%%%%%%%%%%%%%%%%%%%%%%%%%%%%%

% Convert the image to single if it is not of
% class float (single or double)
img_is_double = isa(img, 'double');
if ~(img_is_double || isa(img, 'single')),
   imgf = single(img);
end

% Compute the gradient and the magnitude of gradient
if img_is_double,
   [grdx, grdy] = gradient(img);
else
   [grdx, grdy] = gradient(imgf);
end
grdmag = sqrt(grdx.^2 + grdy.^2);

% Get the linear indices, as well as the subscripts, of the pixels
% whose gradient magnitudes are larger than the given threshold
grdmasklin = find(grdmag > prm_grdthres);
[grdmask_IdxI, grdmask_IdxJ] = ind2sub(size(grdmag), grdmasklin);

% Compute the linear indices (as well as the subscripts) of
% all the votings to the accumulation array.
% The Matlab function 'accumarray' accepts only double variable,
% so all indices are forced into double at this point.
% A row in matrix 'lin2accum_aJ' contains the J indices (into the
% accumulation array) of all the votings that are introduced by a
% same pixel in the image. Similarly with matrix 'lin2accum_aI'.
rr_4linaccum = double( prm_r_range );
linaccum_dr = [ (-rr_4linaccum(2) + 0.5) : -rr_4linaccum(1) , ...
   (rr_4linaccum(1) + 0.5) : rr_4linaccum(2) ];

lin2accum_aJ = floor( ...
        double(grdx(grdmasklin)./grdmag(grdmasklin)) * linaccum_dr + ...
        repmat( double(grdmask_IdxJ)+0.5 , [1,length(linaccum_dr)] ) ...
);
lin2accum_aI = floor( ...
        double(grdy(grdmasklin)./grdmag(grdmasklin)) * linaccum_dr + ...
        repmat( double(grdmask_IdxI)+0.5 , [1,length(linaccum_dr)] ) ...
);

% Clip the votings that are out of the accumulation array
mask_valid_aJaI = ...
        lin2accum_aJ > 0 & lin2accum_aJ < (size(grdmag,2) + 1) & ...
        lin2accum_aI > 0 & lin2accum_aI < (size(grdmag,1) + 1);

mask_valid_aJaI_reverse = ~ mask_valid_aJaI;
lin2accum_aJ = lin2accum_aJ .* mask_valid_aJaI + mask_valid_aJaI_reverse;
lin2accum_aI = lin2accum_aI .* mask_valid_aJaI + mask_valid_aJaI_reverse;
clear mask_valid_aJaI_reverse;

% Linear indices (of the votings) into the accumulation array
lin2accum = sub2ind( size(grdmag), lin2accum_aI, lin2accum_aJ );

lin2accum_size = size( lin2accum );
lin2accum = reshape( lin2accum, [numel(lin2accum),1] );
clear lin2accum_aI lin2accum_aJ;

% Weights of the votings, currently using the gradient maginitudes
% but in fact any scheme can be used (application dependent)
```

```
weight4accum = ...
  repmat( double(grdmag(grdmasklin)) , [lin2accum_size(2),1] ) .* ...
  mask_valid_aJaI(:);
clear mask_valid_aJaI;

% Build the accumulation array using Matlab function 'accumarray'
accum = accumarray( lin2accum , weight4accum );
accum = [ accum ; zeros( numel(grdmag) - numel(accum) , 1 ) ];
accum = reshape( accum, size(grdmag) );


%%%%%%%% Locating local maxima in the accumulation array %%%%%%%%%%%%

% Stop if no need to locate the center positions of circles
if ~func_compu_cen,
  return;
end
clear lin2accum weight4accum;

% Parameters to locate the local maxima in the accumulation array
% -- Segmentation of 'accum' before locating LM
prm_useaoi = true;
prm_aoithres_s = 2;
prm_aoiminsize = floor(min([ min(size(accum)) * 0.25, ...
  prm_r_range(2) * 1.5 ]));

% -- Filter for searching for local maxima
prm_fltrLM_s = 1.35;
prm_fltrLM_r = ceil( prm_fltrLM_R * 0.6 );
prm_fltrLM_npix = max([ 6, ceil((prm_fltrLM_R/2)^1.8) ]);

% -- Lower bound of the intensity of local maxima
prm_LM_LoBndRa = 0.2;  % minimum ratio of LM to the max of 'accum'

% Smooth the accumulation array
fltr4accum = fltr4accum / sum(fltr4accum(:));
accum = filter2( fltr4accum, accum );

% Select a number of Areas-Of-Interest from the accumulation array
if prm_useaoi,
  % Threshold value for 'accum'
  prm_llm_thres1 = prm_grdthres * prm_aoithres_s;

  % Thresholding over the accumulation array
  accummask = ( accum > prm_llm_thres1 );

  % Segmentation over the mask
  [accumlabel, accum_nRgn] = bwlabel( accummask, 8 );

  % Select AOIs from segmented regions
  accumAOI = ones(0,4);
  for k = 1 : accum_nRgn,
    accumrgn_lin = find( accumlabel == k );
    [accumrgn_IdxI, accumrgn_IdxJ] = ...
      ind2sub( size(accumlabel), accumrgn_lin );
    rgn_top = min( accumrgn_IdxI );
    rgn_bottom = max( accumrgn_IdxI );
    rgn_left = min( accumrgn_IdxJ );
    rgn_right = max( accumrgn_IdxJ );
    % The AOIs selected must satisfy a minimum size
    if ( (rgn_right - rgn_left + 1) >= prm_aoiminsize && ...
        (rgn_bottom - rgn_top + 1) >= prm_aoiminsize ),
      accumAOI = [ accumAOI; ...
        rgn_top, rgn_bottom, rgn_left, rgn_right ];
    end
  end
else
  % Whole accumulation array as the one AOI
  accumAOI = [1, size(accum,1), 1, size(accum,2)];
end

% Thresholding of 'accum' by a lower bound
prm_LM_LoBnd = max(accum(:)) * prm_LM_LoBndRa;
```

```
% Build the filter for searching for local maxima
fltr4LM = zeros(2 * prm_fltrLM_R + 1);

[mesh4fLM_x, mesh4fLM_y] = meshgrid(-prm_fltrLM_R : prm_fltrLM_R);
mesh4fLM_r = sqrt( mesh4fLM_x.^2 + mesh4fLM_y.^2 );
fltr4LM_mask = ...
        ( mesh4fLM_r > prm_fltrLM_r & mesh4fLM_r <= prm_fltrLM_R );
fltr4LM = fltr4LM - ...
        fltr4LM_mask * (prm_fltrLM_s / sum(fltr4LM_mask(:)));

if prm_fltrLM_R >= 4,
        fltr4LM_mask = ( mesh4fLM_r < (prm_fltrLM_r - 1) );
else
        fltr4LM_mask = ( mesh4fLM_r < prm_fltrLM_r );
end
fltr4LM = fltr4LM + fltr4LM_mask / sum(fltr4LM_mask(:));

% **** Debug code (begin)
if dbg_on,
  dbg_LMmask = zeros(size(accum));
end
% **** Debug code (end)

% For each of the AOIs selected, locate the local maxima
circen = zeros(0,2);
for k = 1 : size(accumAOI, 1),
  aoi = accumAOI(k,:);      % just for referencing convenience

  % Thresholding of 'accum' by a lower bound
  accumaoi_LBMask = ...
    ( accum(aoi(1):aoi(2), aoi(3):aoi(4)) > prm_LM_LoBnd );

  % Apply the local maxima filter
  candLM = conv2( accum(aoi(1):aoi(2), aoi(3):aoi(4)) , ...
    fltr4LM , 'same' );
  candLM_mask = ( candLM > 0 );

  % Clear the margins of 'candLM_mask'
  candLM_mask([1:prm_fltrLM_R, (end-prm_fltrLM_R+1):end], :) = 0;
  candLM_mask(:, [1:prm_fltrLM_R, (end-prm_fltrLM_R+1):end]) = 0;

  % **** Debug code (begin)
  if dbg_on,
    dbg_LMmask(aoi(1):aoi(2), aoi(3):aoi(4)) = ...
      dbg_LMmask(aoi(1):aoi(2), aoi(3):aoi(4)) + ...
      accumaoi_LBMask + 2 * candLM_mask;
  end
  % **** Debug code (end)

  % Group the local maxima candidates by adjacency, compute the
  % centroid position for each group and take that as the center
  % of one circle detected
  [candLM_label, candLM_nRgn] = bwlabel( candLM_mask, 8 );

  for ilabel = 1 : candLM_nRgn,
    % Indices (to current AOI) of the pixels in the group
    candgrp_masklin = find( candLM_label == ilabel );
    [candgrp_IdxI, candgrp_IdxJ] = ...
      ind2sub( size(candLM_label) , candgrp_masklin );

    % Indices (to 'accum') of the pixels in the group
    candgrp_IdxI = candgrp_IdxI + ( aoi(1) - 1 );
    candgrp_IdxJ = candgrp_IdxJ + ( aoi(3) - 1 );
    candgrp_idx2acm = ...
      sub2ind( size(accum) , candgrp_IdxI , candgrp_IdxJ );

    % Minimum number of qulified pixels in the group
    if sum(accumaoi_LBMask(candgrp_masklin) ) < prm_fltrLM_npix,
      continue;
    end

    % Compute the centroid position
```

```
      candgrp_acmsum = sum(
accum(candgrp_idx2acm) );
      cc_x = sum( candgrp_IdxJ .*
accum(candgrp_idx2acm) ) / ...
         candgrp_acmsum;
      cc_y = sum( candgrp_IdxI .*
accum(candgrp_idx2acm) ) / ...
         candgrp_acmsum;
      circen = [circen; cc_x, cc_y];
   end
end

% **** Debug code (begin)
if dbg_on,
   figure(dbg_bfigno);
imagesc(dbg_LMmask); axis image;
   title('Generated map of local maxima');
   if size(accumAOI, 1) == 1,
      figure(dbg_bfigno+1);
      surf(candLM, 'EdgeColor', 'none');
axis ij;
      title('Accumulation array after local
maximum filtering');
   end
end
% **** Debug code (end)


%%%%%%%% Estimation of the Radii of
Circles %%%%%%%%%%%%

% Stop if no need to estimate the radii of
circles
if ~func_compu_radii,
   varargout{1} = circen;
   return;
end

% Parameters for the estimation of the
radii of circles
fltr4SgnCv = [2 1 1];
fltr4SgnCv = fltr4SgnCv / sum(fltr4SgnCv);

% Find circle's radius using its signature
curve
cirrad = zeros( size(circen,1), 1 );

for k = 1 : size(circen,1),
   % Neighborhood region of the circle for
building the sgn. curve
   circen_round = round( circen(k,:) );
   SCvR_I0 = circen_round(2) -
prm_r_range(2) - 1;
   if SCvR_I0 < 1,
      SCvR_I0 = 1;
   end
   SCvR_I1 = circen_round(2) +
prm_r_range(2) + 1;
   if SCvR_I1 > size(grdx,1),
      SCvR_I1 = size(grdx,1);
   end
   SCvR_J0 = circen_round(1) -
prm_r_range(2) - 1;
   if SCvR_J0 < 1,
      SCvR_J0 = 1;
   end
   SCvR_J1 = circen_round(1) +
prm_r_range(2) + 1;
   if SCvR_J1 > size(grdx,2),
      SCvR_J1 = size(grdx,2);
   end

   % Build the sgn. curve
   SgnCvMat_dx = repmat(
(SCvR_J0:SCvR_J1) - circen(k,1) , ...
      [SCvR_I1 - SCvR_I0 + 1 , 1] );
   SgnCvMat_dy = repmat(
(SCvR_I0:SCvR_I1)' - circen(k,2) , ...
      [1 , SCvR_J1 - SCvR_J0 + 1] );
   SgnCvMat_r = sqrt( SgnCvMat_dx .^2 +
SgnCvMat_dy .^2 );
   SgnCvMat_rp1 = round(SgnCvMat_r) +
1;

   f4SgnCv = abs( ...
      double(grdx(SCvR_I0:SCvR_I1,
SCvR_J0:SCvR_J1)) .* SgnCvMat_dx + ...
      double(grdy(SCvR_I0:SCvR_I1,
SCvR_J0:SCvR_J1)) .* SgnCvMat_dy ...
      ) ./ SgnCvMat_r;
   SgnCv = accumarray( SgnCvMat_rp1(:) ,
f4SgnCv(:) );

   SgnCv_Cnt = accumarray(
SgnCvMat_rp1(:) ,
ones(numel(f4SgnCv),1) );
   SgnCv_Cnt = SgnCv_Cnt + (SgnCv_Cnt ==
0);
   SgnCv = SgnCv ./ SgnCv_Cnt;

   % Suppress the undesired entries in the
sgn. curve
   % -- Radii that correspond to short arcs
```

```
  SgnCv = SgnCv .* ( SgnCv_Cnt >= (pi/4 * [0:(numel(SgnCv_Cnt)-1)]') );
  % -- Radii that are out of the given range
  SgnCv( 1 : (round(prm_r_range(1))+1) ) = 0;
  SgnCv( (round(prm_r_range(2))+1) : end ) = 0;

  % Get rid of the zero radius entry in the array
  SgnCv = SgnCv(2:end);
  % Smooth the sgn. curve
  SgnCv = filtfilt( fltr4SgnCv , [1] , SgnCv );

  % Get the maximum value in the sgn. curve
  SgnCv_max = max(SgnCv);
  if SgnCv_max <= 0,
    cirrad(k) = 0;
    continue;
  end

  % Find the local maxima in sgn. curve by 1st order derivatives
  % -- Mark the ascending edges in the sgn. curve as 1s and
  % -- descending edges as 0s
  SgnCv_AscEdg = ( SgnCv(2:end) - SgnCv(1:(end-1)) ) > 0;
  % -- Mark the transition (ascending to descending) regions
  SgnCv_LMmask = [ 0; 0; SgnCv_AscEdg(1:(end-2)) ] & (~SgnCv_AscEdg);
  SgnCv_LMmask = SgnCv_LMmask & [ SgnCv_LMmask(2:end) ; 0 ];

  % Incorporate the minimum value requirement
  SgnCv_LMmask = SgnCv_LMmask & ...
    ( SgnCv(1:(end-1)) >= (prm_multirad * SgnCv_max) );
  % Get the positions of the peaks
  SgnCv_LMPos = sort( find(SgnCv_LMmask) );

  % Save the detected radii
  if isempty(SgnCv_LMPos),
    cirrad(k) = 0;
  else
    cirrad(k) = SgnCv_LMPos(end);
    for i_radii = (length(SgnCv_LMPos) - 1) : -1 : 1,
      circen = [ circen; circen(k,:) ];
      cirrad = [ cirrad; SgnCv_LMPos(i_radii) ];
    end
  end
end

% Output
varargout{1} = circen;
varargout{2} = cirrad;
if nargout > 3,
  varargout{3} = dbg_LMmask;
end
```

```
function [data]= Centre_AnalysisNOMANUAL_mod(circen, scaley, scalex, tmp, fname)
% Centre_Analysis calculates the patella moment arm and the
% extensormechanism angle
%Input: circen: matrix containing circle centre x & y points; scaley: scale
%factor in y direction; scalex: scale factor in x direction; tmp = image;
%fname = file name of image being analysed
%Output: data = horrizontal vector containing measured flexion angle,
%moment arm and extensor mechanism angle error: 1 or 0 indicating whether
%success was achieved
%Lisa fitzgerald
%Uni Bath
%13/09/12

%generate polyfit for tibial and femoral lines and calculate angle between
%them
a1=circen (1,1);
a2=circen (2,1);
b1=circen (1,2);



b2=circen (2,2);


A=[a1 a2];
```

```
B=[b1 b2];

p1=polyfit(A,B,1);
m1=p1(1);
c1=circen (6,1);
c2=circen (7,1);
d1=circen (6,2);
d2=circen (7,2);

C=[c1 c2];
D=[d1 d2];

p2=polyfit(C,D,1);
m2=p2(1);

q=atan((m1-m2)/(1+(m1*m2)));
qd=radtodeg(q);
qd=abs(qd);

%generate polyfit for quad tendon and patella tendon lines and calculate angle between
%them
e1=circen (3,1);
e2=circen (4,1);

f1=circen (3,2);
f2=circen (4,2)
```

```
function [results] = ten_deg_int (comdata)

% ten_deg_int calcualtes the average moment arm and extensor mechanism
% angle at 10deg flexion intervals
%Input: com_data= all results;
%Output: results= average values and number of values included in average
%calculation for each 10 deg increment
%Lisa Fitzgerald
%Uni Bath
%13/09/12

momarm10=[];
%extang10=[];
momarm20=[];
%extang20=[];
momarm30=[];
%extang30=[];
momarm40=[];
%extang40=[];
momarm50=[];
%extang50=[];
momarm60=[];
%extang60=[];
momarm70=[];
%extang70=[];
momarm80=[];
%extang80=[];
momarm90=[];
%extang90=[];

n10 = 1;
n20 = 1;
n30 = 1;
n40 = 1;
n50 = 1;
n60 = 1;
n70 = 1;
n80 = 1;
n90 = 1;

for i = 1 : length(comdata)

   if (comdata(i,1) > 9) && (comdata(i,1) < 11)
      momarm10(i) = comdata(i,2);
      %extang10(n10) = comdata(i,3);
      n10 = n10 + 1;

 elseif (comdata(i,1) > 19) && (comdata(i,1) < 21)
      momarm20(i) = comdata(i,2);

      %extang20(n20) = comdata(i,3);
      n20 = n20 + 1;

 elseif (comdata(i,1) > 29) && (comdata(i,1) < 31)
      momarm30(i) = comdata(i,2);
      %extang30(n30) = comdata(i,3);
      n30 = n30 + 1;

   elseif (comdata(i,1) > 39) && (comdata(i,1) < 41)
      momarm40(i) = comdata(i,2);
      %extang40(n40) = comdata(i,3);
```

```
      n40 = n40 + 1;

   elseif (comdata(i,1) > 49) &&
(comdata(i,1) < 51)
      momarm50(i) = comdata(i,2);
      %extang10(n50) = comdata(i,3);
      n50 = n50 + 1;

   elseif (comdata(i,1) > 59) &&
(comdata(i,1) < 61)
      momarm60(i) = comdata(i,2);
      %extang10(n60) = comdata(i,3);
      n60 = n60 + 1;

   elseif (comdata(i,1) > 69) &&
(comdata(i,1) < 71)
      momarm70(i) = comdata(i,2);
      %extang70(n70) = comdata(i,3);
      n70 = n70 + 1;

   elseif (comdata(i,1) > 79) &&
(comdata(i,1) < 81)
      momarm80(i) = comdata(i,2);
      %extang80(n80) = comdata(i,3);
      n80 = n80 + 1;

   elseif (comdata(i,1) > 89) &&
(comdata(i,1) < 91)
      momarm90(i) = comdata(i,2);
      %extang90(n90) = comdata(i,3);
      n90 = n90 + 1;

   end

end

momarm10(momarm10==0) =[];
momarm20(momarm20==0) =[];
momarm30(momarm30==0) =[];
momarm40(momarm40==0) =[];
momarm50(momarm50==0) =[];
momarm60(momarm60==0) =[];
momarm70(momarm70==0) =[];
momarm80(momarm80==0) =[];
momarm90(momarm90==0) =[];

if (n10 > 1)

   mma10 = mean(momarm10);
   %mea10 = mean(extang10);

else

   mma10 = 0;
   %mea10 = 0;

end

if (n20 > 1)

   mma20 = mean(momarm20);
   %mea20 = mean(extang20);

else

   mma20 = 0;
   %mea20 = 0;

end

if (n30 > 1)

   mma30 = mean(momarm30);
   %mea30 = mean(extang30);

else

   mma30 = 0;
   %mea30 = 0;

end

if (n40 > 1)

   mma40 = mean(momarm40);
   %mea40 = mean(extang40);

else

   mma40 = 0;
   %mea40 = 0;

end

if (n50 > 1)

   mma50 = mean(momarm50);
   %mea50 = mean(extang50);

else

   mma50 = 0;
   %mea50 = 0;
```

```
end

if (n60 > 1)

   mma60 = mean(momarm60);
   %mea60 = mean(extang60);

else

   mma60 = 0;
   %mea60 = 0;

end

if (n70 > 1)

   mma70 = mean(momarm70);
   %mea70 = mean(extang70);

else

   mma70 = 0;
   %mea70 = 0;

end

if (n80 > 1)

   mma80 = mean(momarm80);
   %mea80 = mean(extang80);

else

   mma80 = 0;
  %mea80 = 0;

end

if (n90 > 1)

   mma90 = mean(momarm90);
   %mea90 = mean(extang90);

else

   mma90 = 0;
   %mea90 = 0;

end
```

Appendix G: Matlab Routine for Fujifilm Prescale Film Analysis

The Matlab image toolbox was used to develop a series of scripts to take scans of developed Prescale film and analyse the data to produce values for PFJ contact area at 10° flexion increments. The highlights of the method are detailed in Figure G-1. The full code follows.

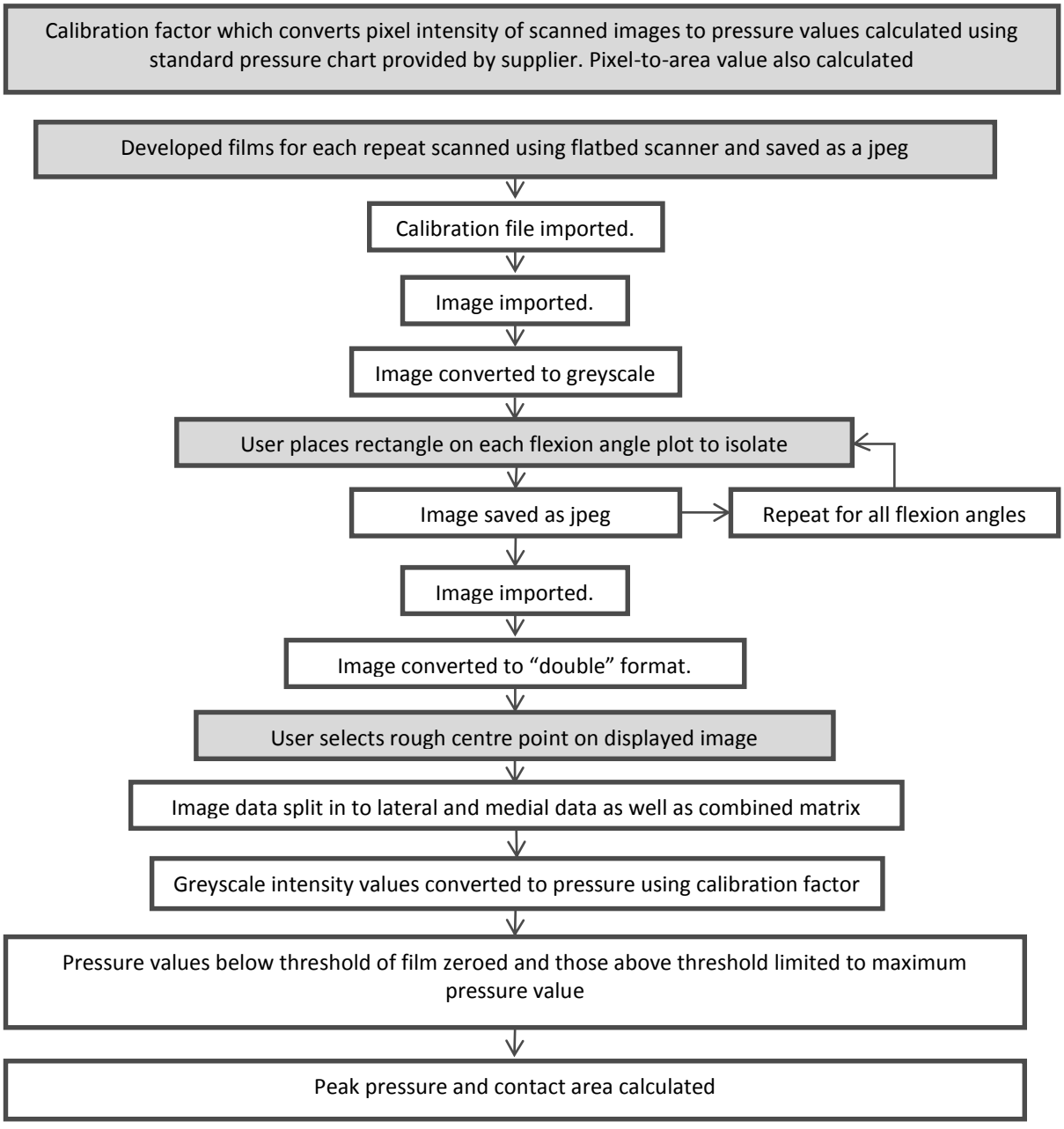

Figure G-1: Fujifilm analysis method

```
function [call]=PrescaleCalibration(~)

clc
clear all

% for i=1:3

%user selects calibration image file
disp 'select 1st calibration image'
[filename, folder_name] = uigetfile('.jpg')
file=strcat(folder_name,filename)

%read in image
I=imread(file);

%convert image to grayscale
% G=rgb2gray(I);

G=I;

%open image
figure, imshow(G);

disp 'select 1.1 box'
h=imrect;
H=getPosition(h);
x1=H(1);
x2=H(1)+H(3);
y1=H(2);
y2=H(2)+H(4);
C=G(y1:y2,:);
C=C(:,x1:x2);
clear x1 x2 y1 y2 h H
c=mean(mean(C));

disp 'select 0.9 box'
h=imrect;
H=getPosition(h);
x1=H(1);
x2=H(1)+H(3);
y1=H(2);
y2=H(2)+H(4);
D=G(y1:y2,:);
D=D(:,x1:x2);
clear x1 x2 y1 y2 h H
d=mean(mean(D));

disp 'select 0.7 box'
h=imrect;
H=getPosition(h);
x1=H(1);
x2=H(1)+H(3);
y1=H(2);
y2=H(2)+H(4);
E=G(y1:y2,:);
E=E(:,x1:x2);
clear x1 x2 y1 y2 h H
e=mean(mean(E));

disp 'select 0.5 box'
h=imrect;
H=getPosition(h);
x1=H(1);
x2=H(1)+H(3);
y1=H(2);
y2=H(2)+H(4);
F=G(y1:y2,:);
F=F(:,x1:x2);
clear x1 x2 y1 y2 h H
f=mean(mean(F));

disp 'select 0.3 box'
h=imrect;
H=getPosition(h);
x1=H(1);
x2=H(1)+H(3);
y1=H(2);
y2=H(2)+H(4);
I=I(y1:y2,:);
I=I(:,x1:x2);
clear x1 x2 y1 y2 h H
i=mean(mean(I));

% disp 'select 0.1 box'
% h=imrect;
% H=getPosition(h);
% x1=H(1);
% x2=H(1)+H(3);
% y1=H(2);
% y2=H(2)+H(4);
% J=G(y1:y2,:);
% J=J(:,x1:x2);
% clear x1 x2 y1 y2 h H
% j=mean(mean(J));

close all

%Y values corresponding to intensity values of
each box combined
X=[c d e f i];

Y=[2.525 2.05 1.625 1.225 0.775];

%quadratic polyfit carried out
[p3 S3] = polyfit(X,Y,3);

% p(i).data= p3;
call = p3;

% end

% call= [0 0 0 0];
%  call(1,1)=(p(1).data(1,1)  +  p(2).data(1,1)  +
p(3).data(1,1))/3;
```

```
% call(1,2)=(p(1).data(1,2) + p(2).data(1,2) + p(3).data(1,2))/3;
% call(1,3)=(p(1).data(1,3) + p(2).data(1,3) + p(3).data(1,3))/3;
% call(1,4)=(p(1).data(1,4) + p(2).data(1,4) + p(3).data(1,4))/3;

figure, imshow(G)

a=ginput(1);
b=ginput(1);
scale=sqrt(((a(1, 1)-b(1, 1))^2+(a(1, 2)-b(1, 2))^2))/48;
pixA=scale^2;

close all
```

```
%chose folder to save results in
folder_name=uigetdir('','chose folder to save results in');
cd=folder_name;

%create output file
ofile=fullfile(folder_name, 'PrescaleCalibration.txt');

%print date and polynomial coefficients
fid=fopen(ofile, 'wt');
fprintf(fid, date);
fprintf(fid, '\n');
fprintf(fid, '%2i\t', call);
fprintf(fid, '%2i\t', pixA);

fclose(fid);
```

---

function [Output] = Prescale (~)

```
clear all

%user selects calibration file
disp 'select calibration file'
[filename, folder_name] = uigetfile('.txt')
file=strcat(folder_name,filename)
p = importdata(file,'\t',1);
pp = p.data;
pixA=pp(5);
pp(5)=[];

[SplitScans]=PrescaleSacnSplit(1);


[Pressures]=PrescaleAnalysis(SplitScans, pixA, pp);

UserResponse=questdlg('Analyses another set?', '', 'Yes', 'No', 'Yes');

% Handle response
switch UserResponse
   case 'No'
```

```
 Y=0;
   case 'Yes'
      Y=1;
end

while Y == 1

[SplitScans]=PrescaleSacnSplit(1);

[Pressures]=PrescaleAnalysis(SplitScans, pixA, pp);

UserResponse=questdlg('Analyses another set?', '', 'Yes', 'No', 'Yes');

% Handle response
switch UserResponse
   case 'No'
      Y=0;
   case 'Yes'
      Y=1;
end

end
```

---

function [Pressures]=PrescaleAnalysis(SplitScans, pixA, pp)

```
%Select folder with images in
folder_name=SplitScans;
cd (folder_name);
filenames = dir('*.jpg');

%loop through each image file
```

```
results = [30 0 0 0 0 0 0 ; 40 0 0 0 0 0 0; 50 0 0 0 0 0 0; 60 0 0 0 0 0 0; 70 0 0 0 0 0 0; 80 0 0 0 0 0 0; 90 0 0 0 0 0 0];

for k=1:7

   datafile = filenames(k).name;
```

```
%open image
I=imread(datafile);
Pressures(k).rawI=I;

%convert image to grayscale
%G=rgb2gray(I);
G=I;
class(G);
Pressures(k).rawG=G;

%convert image to double
D=im2double(G);
%    figure, contourf(D);
D=D.*255;
D=flipud(D);
Pressures(k).rawD=D;

%open image
figure(1), imagesc(D);

[x,y]=ginput(1)

%split medial and lateral data
M=D;
M(:,x:end)=[];
Pressures(k).rawM=M;

L=D;
L(:,1:x)=[];
Pressures(k).rawL=L;

%convert grayscale intensity values to
pressure values
P=polyval(pp,D);
Pressures(k).rawP=P;
PL=polyval(pp,L);
Pressures(k).rawPL=PL;
PM=polyval(pp,M);
Pressures(k).rawPM=PM;

%zero values below threshold i.e. pressures
less than 0.5MPa
P(P<=0.5) = 0;
Pressures(k).Pz=P;
PL(PL<=0.5) = 0;
Pressures(k).PLz=PL;
PM(PM<=0.5) = 0;
Pressures(k).PMz=PM;

%limit vales above threshold (2.5MPa)
P(P>=2.5) = 2.5;
Pressures(k).P=P;
PL(PL>=2.5) = 2.5;
Pressures(k).PL=PL;
PM(PM>=2.5) = 2.5;
Pressures(k).PM=PM;

%calculate peak pressure
Pv=P;
PPmax=max(Pv);
PP=max(PPmax)
PLv=PL;
PPLmax=max(PLv);
PPL=max(PPLmax)
PMv=PM;
PPMmax=max(PMv);
PPM=max(PPMmax)

%calculate contact area
Av=find(P);
An=length(Av);
CA= An/pixA;
CA=CA/(10*10);

ALv=find(PL);
ALn=length(ALv);
CAL= ALn/pixA;
CAL=CAL/(10*10);

AMv=find(PM);
AMn=length(AMv);
CAM= AMn/pixA;
CAM=CAM/(10*10);

%identify flexion angle
if datafile(1)=='8';

   results(7,2)=PP;
   results(7,3)=CA;
   results(7,4)=PPL;
   results(7,5)=CAL;
   results(7,6)=PPM;
   results(7,7)=CAM;

   PressuresR(7).angle='80';
   PressuresR(7).P=Pressures(k).P;

elseif datafile(1)=='9';

   results(8,2)=PP;
   results(8,3)=CA;
   results(8,4)=PPL;
   results(8,5)=CAL;
   results(8,6)=PPM;
   results(8,7)=CAM;

   PressuresR(8).angle='90';
   PressuresR(8).P=Pressures(k).P;

elseif datafile(1)=='7';

   results(6,2)=PP;
   results(6,3)=CA;
   results(6,4)=PPL;
```

```
    results(6,5)=CAL;
    results(6,6)=PPM;
    results(6,7)=CAM;

    PressuresR(6).angle='70';
    PressuresR(6).P=Pressures(k).P;

    elseif datafile(1)=='6';

    results(5,2)=PP;
    results(5,3)=CA;
    results(5,4)=PPL;
    results(5,5)=CAL;
    results(5,6)=PPM;
    results(5,7)=CAM;

    PressuresR(5).angle='60';
    PressuresR(5).P=Pressures(k).P;

     elseif datafile(1)=='5';

    results(4,2)=PP;
    results(4,3)=CA;
    results(4,4)=PPL;
    results(4,5)=CAL;
    results(4,6)=PPM;
    results(4,7)=CAM;

    PressuresR(4).angle='50';
    PressuresR(4).P=Pressures(k).P;

elseif datafile(1)=='4';

    results(3,2)=PP;
    results(3,3)=CA;
    results(3,4)=PPL;
    results(3,5)=CAL;
    results(3,6)=PPM;
    results(3,7)=CAM;

    PressuresR(3).angle='40';
    PressuresR(3).P=Pressures(k).P;

elseif datafile(1)=='3';

    results(2,2)=PP;
    results(2,3)=CA;
    results(2,4)=PPL;
    results(2,5)=CAL;
    results(2,6)=PPM;
    results(2,7)=CAM;

    PressuresR(2).angle='30';
    PressuresR(2).P=Pressures(k).P;

else
        error

    end

    clear I D M L G angle P Pl PM CA CAL CAM Av
ALv AMv An ALn AMn PP PPL PPM Pv PLv PMv
a b x y datafile

    close all

end

%create output file containing data
ofile=fullfile(folder_name, 'Results.txt');

fid=fopen(ofile, 'wt');
fprintf(fid, date);
fprintf(fid, '\n');
fprintf(fid, folder_name);
fprintf(fid, '\n');
fprintf (fid, ' \t 20deg \t 30deg \t 40deg \t
50deg \t 60deg \t 70deg \t 80deg  \t90deg\n');
fprintf (fid, 'Contact Area cm^2 \t');
fprintf(fid, '%2i\t', results(:,3));
fprintf(fid, '\n');
fprintf (fid, 'Contact Area Lateral cm^2 \t');
fprintf(fid, '%2i\t', results(:,5));
fprintf(fid, '\n');
fprintf (fid, 'Contact Area Medial cm^2 \t');
fprintf(fid, '%2i\t', results(:,7));
fprintf(fid, '\n');

fclose (fid);

%generate pressure plots
figure('units', 'centimeters', 'position', [1 1 12
30]);
set(gcf, 'PaperPositionMode','auto');
%axes('Position', [0.05 0.05 0.6 0.95]);
hold on

s=[1 5 9 13 17 21 25];

for i=1:7

    j=1+i;

    k=s(i);
    l=k+2;

    Pd=PressuresR(j).P;
    Pd=Pd .*1000;
    PressuresR(j).Pd=Pd;

    subplot(7,4,k:l);
    contourf(Pd,'LineStyle','none');
    colormap 'jet';
```

```
   set(gca,'xtick',[])
   set(gca,'xticklabel',[])
   set(gca,'ytick',[])
   set(gca,'yticklabel',[])
   grid off;
   t=strcat(PressuresR(j).angle, ' deg');
   title(t, 'Fontsize', 10, 'FontWeight', 'bold',
'FontName', 'Ariel');

   if i == 4
    ylabel('Proximodistal (Superior ->)',
'Fontsize', 12, 'FontWeight', 'bold',
'FontName', 'Ariel');
   end

   if i == 7
   xlabel('Mediolateral (Lateral ->)', 'Fontsize',
12, 'FontWeight', 'bold', 'FontName', 'Ariel');
   end
end
   hold off
   axes('Position', [0.05 0.1 0.85 0.85], 'Visible',
'off');
   c=colorbar('Fontsize', 10, 'FontName',
'Ariel');
   ylabel(c,'(kPa)', 'Fontsize', 10, 'FontWeight',
'bold', 'Rotation',0.0, 'Position', [7 30],
'FontName', 'Ariel' );
   caxis([0 2500]);
   set(gca,'xtick',[])
   set(gca,'xticklabel',[])
   set(gca,'ytick',[])
   set(gca,'yticklabel',[])

saveas(gcf, 'plots.jpg');

%close all
```

Function [SplitScans]=PrescaleSacnSplit(a)

```
%user selects scan image file
disp 'select scan image'
[filename, folder_name] = uigetfile('.jpg')
file=strcat(folder_name,filename)

%read in image
I=imread(file);

%convert image to grayscale
%G=rgb2gray(I);

G=I;

% create folder to save split images in
cd (folder_name);
mkdir ('SplitScan');
folder_name = strcat (folder_name,
'SplitScan');
cd (folder_name);
SplitScans=folder_name;

%open image
figure, imshow(G)
hold on

%user draws rectangle selection for each
flecion angle on image

D ={'select 30deg box', 'select 40deg box',
'select 50deg box', 'select 60deg box', 'select
70deg box', 'select 80deg box', 'select 90deg
box'};

F = {'30deg.jpg', '40deg.jpg', '50deg.jpg',
'60deg.jpg', '70deg.jpg', '80deg.jpg',
'90deg.jpg'};


for i = 1:7;

d = D{1, i};

disp d

[x1 y1]=ginput(1);
x2=x1+300;
y2=y1+500;

rectangle( 'Position', [x1, y1, 300, 500])

UserResponse=questdlg('Rectangle OK?', '',
'Yes', 'No', 'Yes');


% Handle response
switch UserResponse
   case 'No'
      Y=0;
   case 'Yes'
      Y=1;
end

while Y == 0

clear h x1 x2 y1 y2

[x1 y1]=ginput(1);
```

```
x2=x1+300;
y2=y1+500;

rectangle( 'Position', [x1, y1, 300, 500])

UserResponse=questdlg('Rectangle    OK?',    '',
'Yes', 'No', 'Yes');

% Handle response
switch UserResponse
   case 'No'
      Y=0;
   case 'Yes'
      Y=1;
end
```

```
end

A=G(y1:y2,:);
A=A(:,x1:x2);

A = rot90(A,-1);

f = F{1, i};

imwrite(A, f);

clear x1 x2 y1 y2 h d f A

end

hold off
```